



FINAL REPORT
VOLUME 1: MAIN REPORT
October 2005

DYNAMIC STABILITY ANALYSIS OF CHABOT DAM

Alameda County, California



Prepared for
East Bay Municipal Utility District
375 Eleventh Street
Oakland, CA 94607



URS

URS Corporation
1333 Broadway, Suite 800
Oakland, CA 94612

26814536.G0000



October 4, 2005

Mr. Atta B. Yiadom, Project Manager
East Bay Municipal Utility District
375 – 11th Street
Oakland, CA 94607-4240

**Subject: Dynamic Stability of Chabot Dam
Final Engineering Report**

Dear Mr. Yiadom:

In accordance with the requirements of our contract with the District, dated 13 January 2004, we are pleased to submit herewith our final engineering report on the dynamic stability analysis of Chabot Dam. We previously submitted the report in draft final form on May 27, 2005, for review by the District. The District's comments have been addressed and incorporated into the final report.

The report is submitted in two volumes as follows:

Volume 1 - Main report
Volume 2 - Appendices

The study was carried out by URS with support from our subconsultants Robert Y. Chew Geotechnical Inc., John Wakabayashi, William Lettis and Associates, HQE Inc., and DotDat.inc.

It has been a pleasure working with you on this interesting assignment and we look forward to continuing to serve the District on future projects. If you have any questions regarding the report or if we can be of any other service, please do not hesitate to contact the undersigned.

Yours truly,

URS Corporation

Lelio H. Mejia, PhD, GE
Project Manager



Enclosures: Final Engineering Report, Volumes 1 and 2 (15 copies)

URS Corporation
1333 Broadway, Suite 800
Oakland, CA 94612-1924
Tel: 510.893.3600
Fax: 510.874.3268

FINAL REPORT

VOLUME 1

**DYNAMIC STABILITY ANALYSIS
OF CHABOT DAM**

ALAMEDA COUNTY, CALIFORNIA

Prepared for

East Bay Municipal Utility District
375 Eleventh Street
Oakland, California 94607

October 2005

URS

URS Corporation
1333 Broadway, Suite 800
Oakland, California 94612

26814536.G0000

TABLE OF CONTENTS

Executive Summary.....	ES-1
Section 1 Introduction.....	1-1
1.1 Background.....	1-1
1.2 Purpose and Objectives.....	1-1
1.3 Previous Investigations.....	1-1
1.4 Report Organization.....	1-2
Section 2 Scope of Work	2-1
Section 3 Project Description.....	3-1
3.1 Site Setting.....	3-1
3.2 Description of Dam.....	3-1
3.3 Appurtenant Facilities.....	3-1
3.4 Construction History.....	3-1
3.5 Performance and Monitoring.....	3-2
Section 4 Field and Laboratory Investigations	4-1
4.1 Field Investigations.....	4-1
4.1.1 Rotary Wash Drilling.....	4-1
4.1.2 Becker Penetration Testing.....	4-2
4.1.3 Hammer Energy Measurements.....	4-2
4.1.4 Downhole Geophysical Surveys.....	4-2
4.2 Laboratory Testing.....	4-3
Section 5 Geological Setting.....	5-1
5.1 Regional Geology	5-1
5.2 Site Geology.....	5-1
5.3 Fault Rupture	5-2
Section 6 Site - Specific Earthquake Ground Motions	6-1
6.1 General Approach.....	6-1
6.2 Seismic Sources	6-1
6.3 Design Response Spectra.....	6-2
6.3.1 Site Conditions.....	6-2
6.3.2 Attenuation Relationships.....	6-2
6.3.3 Deterministic Ground Motion Analysis.....	6-2
6.3.4 Fault Rupture Directivity Effects.....	6-3
6.3.5 Design Response Spectra.....	6-3
6.4 Spectrum-Compatible Acceleration Time Histories.....	6-4

TABLE OF CONTENTS

Section 7	Embankment and Foundation Conditions.....	7-1
7.1	Dam Materials and Zonation	7-1
7.2	Embankment Conditions.....	7-2
7.2.1	Wagon Fill	7-2
7.2.2	Sluiced Fill.....	7-4
7.2.3	Modern Fill	7-6
7.2.4	Random Fill	7-6
7.3	Foundation Conditions.....	7-6
7.3.1	Foundation Soils	7-6
7.3.2	Bedrock.....	7-7
7.4	Groundwater Conditions.....	7-8
Section 8	General Analysis Approach.....	8-1
Section 9	Limit Equilibrium Stability Analyses.....	9-1
9.1	Analytical Procedures	9-1
9.2	Cross Sections.....	9-1
9.3	Material Properties.....	9-1
9.4	Analysis Results.....	9-2
Section 10	Dynamic Response Analyses.....	10-1
10.1	Methodology	10-1
10.2	Dynamic Material Properties	10-2
10.2.1	Shear Wave Velocities.....	10-2
10.2.2	Modulus Reduction and Damping Relationships	10-2
10.3	Analysis Results.....	10-3
10.3.1	1989 Loma Prieta Earthquake.....	10-3
10.3.2	Hayward-Rogers Creek Fault MCE.....	10-3
10.3.3	San Andreas Fault MCE	10-4
Section 11	Seismic Stability Analyses	11-1
11.1	Approach.....	11-1
11.2	Evaluation of Liquefaction Potential In Sluiced Fill	11-1
11.2.1	Evaluation Procedures	11-1
11.2.2	SPT Blow Count Evaluation.....	11-2
11.2.3	BPT Blow Count Evaluation	11-2
11.2.4	Liquefaction Potential.....	11-3
11.2.5	Residual Strength Evaluation.....	11-3
11.3	Evaluation of Potential Strength Loss in Wagon Fill and Foundation Soils	11-3
11.3.1	Evaluation Procedures	11-3
11.3.2	Potential for Strength Loss.....	11-5
11.4	Post-Earthquake Slope Stability	11-5

TABLE OF CONTENTS

11.5	Deformation Analyses	11-6
11.5.1	Methodology	11-6
11.5.2	Yield Acceleration Evaluation.....	11-6
11.5.3	Analysis Results.....	11-6
11.5.4	Analyses of Alternative Cross-Sections.....	11-7
Section 12	Nonlinear Analyses	12-1
12.1	Methodology.....	12-1
12.2	Material Properties.....	12-1
12.3	Analysis Results.....	12-2
12.3.1	1989 Loma Prieta Earthquake.....	12-2
12.3.2	Hayward-Rogers Creek Fault MCE.....	12-2
Section 13	Expected Dam Performance	13-1
Section 14	Conclusions	14-1
Section 15	References	15-1

Tables

Table 3-1	Existing Piezometers at Chabot Dam
Table 4-1	Summary of Borings
Table 6-1	Earthquake Sources Affecting Chabot Dam
Table 6-2	Selected Attenuation Relationships
Table 6-3	Calculated Horizontal Peak Ground Acceleration
Table 6-4	Recommended Design Response Spectral Values
Table 6-5	Earthquake Records Used to Develop Time Histories for Hayward-Rodgers Creek Fault and San Andreas Fault MCEs
Table 7-1	Representative Index Properties of Embankment and Foundation Materials(1)
Table 7-2	Strength Parameters for Embankment and Foundation Soils
Table 7-3	Comparison of Effective Stress Strength Parameters Between This and Previous Studies
Table 7-4	Comparison of Total Stress Strength Parameters Between This and Previous Studies
Table 9-1	UTEXAS3 Input Parameters for Static Stability Analysis - Long Term Condition
Table 9-2	UTEXAS3 Input Parameters for Seismic Stability Analysis - Pre-Earthquake Condition
Table 10-1	Material Parameters for Dynamic Response Analysis
Table 11-1	Post-Earthquake Factors of Safety for Hayward Fault MCE
Table 11-2	Yield Acceleration Coefficients of Selected Sliding Blocks for Various Levels of Post-cyclic Strength Reduction in Embankment and Foundation Materials
Table 11-3	Calculated Horizontal Displacement in Newmark-type Analyses
Table 11-4	Sensitivity Analysis of Calculated Horizontal displacement to Uncertainties in Embankment and Foundation Conditions - Hayward Fault MCE
Table 12-1	Material Properties for Seepage Analysis
Table 12-2	Material Properties for Static Stress Analysis
Table 12-3	Material Properties for Dynamic Analysis

Figures

Figure 1-1	Site Location Map
Figure 3-1	Location of Chabot Dam
Figure 3-2	Site Plan
Figure 3-3	Instrument Locations

List of Tables, Figures and Appendices

Figure 4-1	Location of Borings From Previous Studies
Figure 4-2	Boring Locations
Figure 5-1	Site Geological Map
Figure 6-1	Seismic Sources Map
Figure 6-2	Calculated 84th-percentile Acceleration Response Spectra for Hayward-Rodgers Creek Fault MCE
Figure 6-3	Calculated 84th-percentile Acceleration Response Spectra for San Andreas Fault MCE
Figure 6-4	Design Acceleration Response Spectra for Hayward-Rodgers Creek Fault MCE
Figure 6-5	Design Acceleration Response Spectra for San Andreas Fault MCE
Figure 6-6	Recorded Time History, 1992 Landers, CA, Earthquake at Lucerne Valley Station, Horizontal Component, 000 deg.
Figure 6-7	Acceleration Response Spectra, 1992 Landers, CA, Earthquake at Lucerne Valley Station, Horizontal Component 000 deg.
Figure 6-8	Recorded Time History, 1992 Landers, CA, Earthquake at Lucerne Valley Station, Horizontal Component, 270 deg.
Figure 6-9	Acceleration Response Spectra, 1992 Landers, CA, Earthquake at Lucerne Valley Station, Horizontal Component 270 deg.
Figure 6-10	Recorded Time History, 2002 Denali, Alaska, Earthquake at Carlo, Alaska Station, Horizontal Component, 360 deg.
Figure 6-11	Acceleration Response Spectra, 2002 Denali, Alaska, Earthquake at Carlo, Alaska Station, Horizontal Component 360 deg.
Figure 6-12	Hayward-Rodgers Creek Fault MCE, Recommended Time History No. 1
Figure 6-13	Hayward-Rodgers Creek Fault MCE, Recommended Time History No. 2
Figure 6-14	Comparison of Acceleration Response Spectra for Hayward-Rodgers Creek Fault MCE
Figure 6-15	San Andreas Fault MCE, Recommended Time History
Figure 6-16	Comparison of Acceleration Response Spectra for San Andreas Fault MCE
Figure 7-1	Plan View of Dam and Cross-Sections
Figure 7-2	GIS Model – Distribution of Soil Types in Embankment and Foundation
Figure 7-3	Cross Section A-A'
Figure 7-4	Cross Section B-B'
Figure 7-5	Cross Section C-C'
Figure 7-6	Gradation of Wagon Fill in Downstream Shell Borings
Figure 7-7	Gradation of Wagon Fill in Upstream Shell Borings

List of Tables, Figures and Appendices

- Figure 7-8 Gradation of Wagon Fill in Crest Borings
- Figure 7-9 Gravel Content From Borings WI-59, 61, 62, 64, 66 and 67, Wagon Fill Zone
- Figure 7-10 Gravel Content From Previous Borings in Wagon Fill Zone
- Figure 7-11 Fines Content From Borings WI-59, 61, 62, 64, 66 and 67, Wagon Fill Zone
- Figure 7-12 Fines Content From Previous Borings in Wagon Fill Zone
- Figure 7-13 Plasticity From Borings WI-59, 61, 62, 64, 66 and 67, Wagon Fill Zone (by Material Zone)
- Figure 7-14 Plasticity From Previous Borings in Wagon Fill Zone
- Figure 7-15 Plasticity From Borings WI-59, 61, 62, 64, 66 and 67, Wagon Fill Zone (By Soil Classification)
- Figure 7-16 Plasticity Index From Borings WI-59, 61, 62, 64, 66 and 67, Wagon Fill Zone
- Figure 7-17 Liquid Limit From Borings WI-59, 61, 62, 64, 66 and 67, Wagon Fill Zone
- Figure 7-18 Dry Unit Weight From Borings WI-59, 61, 62, 64, 66 and 67, Wagon Fill Zone
- Figure 7-19 Dry Unit Weight From Previous Borings in Wagon Fill Zone
- Figure 7-20 Moisture Content From Borings WI-59, 61, 62, 64, 66 and 67, Wagon Fill Zone
- Figure 7-21 Moisture Content From Previous Borings in Wagon Fill Zone
- Figure 7-22 Total Unit Weight From Borings WI-59, 61, 62, 64, 66 and 67, Wagon Fill Zone
- Figure 7-23 Wagon Fill, Effective Shear Strength from CIU Triaxial Compression Tests
- Figure 7-24 Wagon Fill, Total Shear Strength From CIU Triaxial Compression Tests
- Figure 7-25 Wagon Fill, Effective Shear Strength From CIU Triaxial Compression Tests, Comparison with Prior Data
- Figure 7-26 Wagon Fill, Total Shear Strength From CIU Triaxial Compression Tests, Comparison with Prior Data
- Figure 7-27 Wagon Fill, Total Shear Strength From S&W CU Triaxial Compression Tests on Modified California Samples
- Figure 7-28 Liquefaction Susceptibility Chart, WI-59, 61, 62, 64, 66 and 67, Wagon Fill Zone
- Figure 7-29 Gradation of Sluiced Fill in Downstream Toe Borings
- Figure 7-30 Fines Content From Borings WI-60, 63 and 65, Sluiced Fill Zone
- Figure 7-31 Fines Content From Previous Borings in Sluiced Fill Zone
- Figure 7-32 Gravel Content From Borings WI-60, 63 and 65, Sluiced Fill Zone
- Figure 7-33 Gravel Content From Previous Borings in Sluiced Fill Zone
- Figure 7-34 Plasticity From Borings WI-60, 63 and 65, Sluiced Fill Zone
- Figure 7-35 Plasticity From Previous Borings in Sluiced Fill Zone
- Figure 7-36 Dry Unit Weight From Previous Borings in Sluiced Fill Zone

List of Tables, Figures and Appendices

- Figure 7-37 Moisture Content From Previous Borings in Sluiced Fill Zone
- Figure 7-38 Total Unit Weight From Previous Borings in Sluiced Fill Zone
- Figure 7-39 Gradation of Foundation Soil
- Figure 9-1 Plan View of Dam and Analysis Cross-sections
- Figure 9-2 Idealized Cross Section A-A' for Stability Analysis
- Figure 9-3 Idealized Cross Section B-B' for Stability Analysis
- Figure 9-4 Modified Cross Section A-A' for Stability Analysis
- Figure 9-5 Composite Downstream Section A-A'' for Stability Analysis
- Figure 9-6 Static Stability Analysis, Long-Term Condition, Cross Section A-A'
- Figure 9-7 Static Stability Analysis, Long-Term Condition, Modified Cross Section A-A'
- Figure 9-8 Seismic Stability Analysis, Pre-Earthquake Condition, Cross Section A-A'
- Figure 9-9 Seismic Stability Analysis, Pre-Earthquake Condition, Modified Cross Section A-A'
- Figure 9-10 Seismic Stability Analysis, Pseudo-Static Loading, (Pre-Earthquake Strengths), Cross Section A-A'
- Figure 9-11 Seismic Stability Analysis, Pseudo-Static Loading, (Pre-Earthquake Strengths), Modified Cross Section A-A'
- Figure 9-12 Static Stability Analysis, Long-Term Condition, Cross Section B-B'
- Figure 9-13 Seismic Stability Analysis, Pre-Earthquake Condition, Cross Section B-B'
- Figure 9-14 Seismic Stability Analysis, Pre-Earthquake Condition, Downstream Section A-A''
- Figure 10-1 Finite Element/Difference Mesh Cross, Section A-A'
- Figure 10-2 1989 Loma Prieta Earthquake, Acceleration Time History, (CSUH Stadium A3E000)
- Figure 10-3 Seismic Wave Velocity Profiles and Stratigraphy of Boring WI-61
- Figure 10-4 Seismic Wave Velocity Profiles and Stratigraphy of Boring WI-59
- Figure 10-5 Seismic Wave Velocity Profiles and Stratigraphy of Boring WI-62
- Figure 10-6 Seismic Wave Velocity Profiles and Stratigraphy of Boring WI-60
- Figure 10-7 Selected Element Locations for Stress Time-History Plots, QUAD4M Analysis
- Figure 10-8 Selected Nodal Points for Acceleration Outputs, QUAD4M Analysis
- Figure 10-9 Sliding Blocks for Newmark Deformation Analyses, Cross Section A-A'
- Figure 10-10 Peak Horizontal Acceleration, QUAD4M Analysis, 1989 Loma Prieta Earthquake
- Figure 10-11 Cyclic Stress Ratio, QUAD4M Analysis, 1989 Loma Prieta Earthquake
- Figure 10-12 Average Mass Acceleration, Upstream Sliding Blocks, QUAD4M Analysis, 1989 Loma Prieta Earthquake

List of Tables, Figures and Appendices

- Figure 10-13 Average Mass Acceleration, Downstream Sliding Blocks, QUAD4M Analysis, 1989 Loma Prieta Earthquake
- Figure 10-14 Average Mass Acceleration, Downstream Sliding Block #4, QUAD4M Analysis, 1989 Loma Prieta Earthquake
- Figure 10-15 Peak Horizontal Acceleration, QUAD4M Analysis, Hayward Fault MCE TH #1
- Figure 10-16 Acceleration Time History Beneath Crest Nodes 1145, 1147 and 1149, Hayward Fault MCE TH #1
- Figure 10-17 Acceleration Time History Beneath Crest Nodes 1160 and 1179, Hayward Fault MCE TH #1
- Figure 10-18 Peak Shear Stress, QUAD4M Analysis, Hayward Fault MCE TH #1
- Figure 10-19 Shear Stress Time History, Beneath Crest Elements 1095, 1101, and 1106, Hayward Fault MCE TH #1
- Figure 10-20 Shear Stress Time History, Beneath Crest Elements 1112 and 1117, Hayward Fault MCE TH #1
- Figure 10-21 Cyclic Stress Ratio, QUAD4M Analysis, Hayward Fault MCE TH #1
- Figure 10-22 Peak Horizontal Acceleration, QUAD4M Analysis, San Andreas Fault MCE
- Figure 10-23 Peak Shear Stress, QUAD4M Analysis, San Andreas Fault MCE
- Figure 10-24 Cyclic Stress Ratio, QUAD4M Analysis, San Andreas Fault MCE
- Figure 11-1 SPT-Based Liquefaction Triggering Correlations for Mw 7.5 Earthquakes (1996 and 1998 NCEER/NSF Workshops)
- Figure 11-2 SPT Blow Counts N60 From Borings in Sluiced Fill Zone
- Figure 11-3 Adjustment of Nbc for Casing Friction on BPT-1, 2 and 3
- Figure 11-4 Becker Penetration Test BPT-1
- Figure 11-5 SPT Resistance N60 From Borings WI-60 and BPT-1
- Figure 11-6 SPT Resistance N60 From Borings WI-63 and BPT-2
- Figure 11-7 SPT Resistance N60 From Borings WI-65 and BPT-3
- Figure 11-8 Equivalent SPT N1,60 and Stratigraphy From Boring BPT-1
- Figure 11-9 Equivalent SPT N1,60 and Stratigraphy From Boring BPT-2
- Figure 11-10 Equivalent SPT N1,60 and Stratigraphy From Boring BPT-3
- Figure 11-11 Factors of Safety Against Liquefaction in Sluiced Fill, 1989 Loma Prieta Earthquake
- Figure 11-12 Factors of Safety Against Liquefaction in Sluiced Fill, Hayward Fault MCE TH #1
- Figure 11-13 Factors of Safety Against Liquefaction in Sluiced Fill, San Andreas Fault MCE
- Figure 11-14 Correlations Between Undrained Residual Strength and Equivalent Clean Sand, SPT Corrected Blow Counts (Idriss, 2002)

List of Tables, Figures and Appendices

- Figure 11-15 Cyclic Strength and Undrained Strength Degradation of Saturated Wagon Fill and Foundation Soils
- Figure 11-16 Excess Pore Pressure Ratio in Wagon Fill and Foundation Soils, 1989 Loma Prieta Earthquake
- Figure 11-17 Excess Pore Pressure Ratio in Wagon Fill and Foundation Soils, Hayward Fault MCE TH #1
- Figure 11-18 Excess Pore Pressure Ratio in Wagon Fill and Foundation Soils, San Andreas Fault MCE
- Figure 11-19 Seismic Stability Analysis, Post-Earthquake Condition, Downstream Section A-A”, Hayward Fault MCE
- Figure 11-20 Newmark Deformation Analysis, Calculated Displacement, U/S Block #1, Hayward Fault MCE TH #1
- Figure 11-21 Newmark Deformation Analysis, Calculated Displacement, U/S Block #2, Hayward Fault MCE TH #1
- Figure 11-22 Newmark Deformation Analysis, Calculated Displacement, U/S Block #3 Hayward Fault MCE TH #1
- Figure 11-23 Newmark Deformation Analysis, Calculated Displacement, D/S Block #1, Hayward Fault MCE TH #1
- Figure 11-24 Newmark Deformation Analysis, Calculated Displacement, D/S Block #2, Hayward Fault MCE TH #1
- Figure 11-25 Newmark Deformation Analysis, Calculated Displacement, D/S Block #3, Hayward Fault MCE TH #1
- Figure 11-26 Newmark Deformation Analysis, Calculated Displacement, D/S Block #4, Hayward Fault MCE TH #1
- Figure 11-27 Newmark Deformation Analysis, Calculated Displacement, U/S Block #1, Hayward Fault MCE TH #1 (10% Max. Strength Reduction)
- Figure 11-28 Newmark Deformation Analysis, Calculated Displacement, U/S Block #3, Hayward Fault MCE TH #1 (10% Max. Strength Reduction)
- Figure 11-29 Newmark Deformation Analysis, Calculated Displacement, D/S Block #1, Hayward Fault MCE TH #1 (10% Max. Strength Reduction)
- Figure 11-30 Newmark Deformation Analysis, Calculated Displacement, U/S Block #1, San Andreas Fault MCE
- Figure 11-31 Newmark Deformation Analysis, Calculated Displacement, U/S Block #3, San Andreas Fault MCE
- Figure 11-32 Newmark Deformation Analysis, Calculated Displacement, D/S Block #4, San Andreas Fault MCE
- Figure 11-33 Newmark Deformation Analysis, Calculated Displacement, U/S Block #1, San Andreas Fault MCE (10% Max. Strength Reduction)

List of Tables, Figures and Appendices

- Figure 11-34 Newmark Deformation Analysis, Calculated Displacement, U/S Block #3, San Andreas Fault MCE (10% Max. Strength Reduction)
- Figure 11-35 Newmark Deformation Analysis, Calculated Displacement, D/S Block #1 (Modified Section A-A'), Hayward Fault MCE TH #1
- Figure 11-36 Newmark Deformation Analysis, Calculated Displacement, D/S Block #3 (Modified Section A-A'), Hayward Fault MCE TH #1
- Figure 11-37 Alternative Cross Section A-A' for Stability Analysis
- Figure 11-38 Seismic Stability Analysis, Pre-Earthquake Condition, Alternative Cross Section A-A'
- Figure 11-39 Seismic Stability Analysis, Condition with 20% Strength Reduction, Alternative Cross Section A-A'
- Figure 11-40 Alternative Cross Section A-A', Calculated Displacement, U/S Block #2, Hayward MCE Time-History #1
- Figure 11-41 Seismic Stability Analysis, Pre-Earthquake Condition, Alternative Modified Section A-A'
- Figure 11-42 Seismic Stability Analysis, Condition with 20% Strength Reduction, Alternative Modified Section A-A'
- Figure 11-43 Alternative Cross Section A-A', Calculated Displacement, D/S Block #2, Hayward MCE Time-History #1
- Figure 11-44 Alternative Modified Section A-A', Calculated Displacement, D/S Block #2, Hayward MCE Time-History #1
- Figure 12-1 FLAC Analysis, Pore Pressure Generation Model
- Figure 12-2 Mohr-Coulomb and Residual Strength Envelope
- Figure 12-3 Cyclic Strength of Saturated Sluiced Fill
- Figure 12-4 Cyclic Strength and Undrained Strength Degradation of Saturated Wagon Fill and Foundation Soils
- Figure 12-5 Acceleration at Dam Crest and Rock Outcrop, 1989 Loma Prieta Earthquake
- Figure 12-6 Excess Pore Pressure Ratio in Sluiced Fill, 1989 Loma Prieta Earthquake
- Figure 12-7 Cyclic Degradation of Wagon Fill and Foundation Soils, 1989 Loma Prieta Earthquake
- Figure 12-8 Calculated Displacement Vectors, 1989 Loma Prieta Earthquake
- Figure 12-9 Acceleration at Dam Crest and Rock Outcrop, Hayward Fault MCE TH #1
- Figure 12-10 Time Histories of Cyclic Degradation and Pore Pressure Ratio, Hayward Fault MCE TH #1
- Figure 12-11 Cyclic Degradation of Saturated Wagon Fill and Foundation Soils, Hayward Fault MCE TH #1
- Figure 12-12 Calculated Displacement Vectors, Hayward Fault MCE TH #1

List of Tables, Figures and Appendices

- Figure 12-13 Calculated Horizontal Displacement, Time Histories, Hayward Fault MCE TH #1
Figure 12-14 Calculated Vertical Displacement, Time Histories, Hayward Fault MCE TH #1
Figure 12-15 Post-Earthquake Stability of Downstream Slope, Hayward Fault MCE TH #1
Figure 12-16 Post-Earthquake Stability of Upstream Slope, Hayward Fault MCE TH #1

Appendices

- Appendix A Exploratory Drilling
Appendix B Becker Penetration Testing
Appendix C SPT Energy Measurements
Appendix D BPT Energy Measurements
Appendix E Downhole Geophysical Survey
Appendix F Laboratory Testing
Appendix G Site Geology
Appendix H Seismotectonic Setting and Seismic Sources
Appendix I 3-D GIS Model – Existing Boring Data

This report presents the results of a dynamic stability study of Chabot Dam. The dam is located near the city of San Leandro in Alameda County, California, within the East Bay hills, approximately 0.5 kilometers (km) east of the Hayward fault. Chabot Dam is owned and operated by the East Bay Municipal Utility District (EBMUD).

The dam is approximately 135 feet high and 500 feet long and has a 30-foot-wide crest. The main body of the dam (referred to as “wagon fill”) was placed and compacted by teams of horses and wagons to a crest elevation of 233¹ during 1874 and 1875. A hydraulic fill buttress (referred to as “sluiced fill”) was placed at the downstream toe of the embankment between 1875 and 1888. Additional fill was placed along the upstream and downstream slopes and the crest was raised to elevation 243 between 1890 and 1892. During further dam modifications in 1980, engineered fill was placed along the downstream slope to raise the crest to the current elevation 250. A new spillway was also constructed as part of the 1980 modifications. Random fill consisting of excess materials from the new spillway excavation and from demolition of the old spillway was placed near the downstream toe.

In March 2003, the California Department of Water Resources, Division of Safety of Dams (DSOD) conducted a simplified dynamic analysis of Chabot Dam, as part of a reevaluation of dams located near active faults. The study presented herein was conducted in response to a directive from DSOD to EBMUD to evaluate the dynamic stability of the dam. The purpose of the study was to evaluate the seismic hazard at the site and to re-evaluate the seismic stability of the dam using current state-of-the-practice techniques. The scope of work included reviewing the existing project data, performing field and laboratory investigations, developing site-specific earthquake design criteria, evaluating the dynamic stability and deformations of the dam, and preparing a report summarizing the analysis results and conclusions.

A comprehensive field exploration was carried out including geologic mapping, exploratory drilling, Becker Penetration testing (BPT), and downhole geophysical surveys. Samples retrieved from the field were subsequently examined in the URS Pleasant Hill Laboratory and tested for engineering properties and strengths. The subsurface data obtained from this study and from previous investigations were entered into a 3-dimensional Geographic Information System (GIS) database and were used to develop representative embankment cross-sections.

The study included development of site-specific earthquake ground motions for use in the dam stability analysis. The controlling sources were determined to be the Hayward-Rodgers Creek and San Andreas faults. The maximum credible earthquake (MCE) on the Hayward-Rodgers Creek fault was determined to be a magnitude 7.25 earthquake with a peak horizontal ground acceleration (PGA) of 1.05 g. The MCE on the San Andreas fault was found to be a magnitude 8 event with a PGA of 0.33 g. Two acceleration time-histories were developed to represent the earthquake ground motions for dynamic stability analysis under the Hayward fault MCE, and one time history was developed for the San Andreas fault MCE.

Based on its index properties including gradation, plasticity and moisture content, the wagon fill is judged not to be susceptible to liquefaction. Similarly, the foundation soils are judged not to be susceptible to liquefaction. However, the sluiced fill, which consists of primarily gravelly clayey sand, is liquefaction-susceptible due to its loose state and relatively low fines content.

¹ Unless otherwise noted, all elevations in this report are given in feet and refer to USGS datum.

The cyclic strength of the wagon fill and foundation soils were evaluated based on the results of laboratory cyclic triaxial tests previously performed by others. The post-cyclic strength of the materials was evaluated from published data for similar materials. The liquefaction resistance and post-liquefaction residual strength of the sluiced fill were evaluated based on its standard penetration test (SPT) blow count.

The seismic stability of the dam was evaluated using the Seed-Lee-Idriss approach (Seed, 1979). This approach consists of evaluating the dynamic response of the dam to the design earthquake motions, evaluating the potential for strength loss of the embankment and foundation materials under the earthquake shaking, estimating the deformations likely to be induced by the earthquake, and assessing the post-earthquake stability of the dam and its overall condition after the earthquake. The seismic response and deformations of the dam were also evaluated using a nonlinear analysis approach in which the above steps are coupled in a single analysis. The nonlinear analyses were performed with the computer program FLAC.

The design earthquake was defined as the MCE on the Hayward-Rodgers Creek fault since this earthquake is likely to generate the strongest ground motions at the site. Because the MCE on the San Andreas fault could result in strong shaking of long duration, the seismic stability of the dam was also evaluated for that earthquake. As a check of the analysis procedures, the dynamic response and deformations of the dam were also analyzed for motions representative of the 1989 Loma Prieta earthquake, for which the general performance of the dam is known.

The analyses indicate that the dam will experience deformations during the MCE on the Hayward fault, but will remain stable. No liquefaction of the wagon fill is expected because of its overall clayey nature, but the earthquake is likely to induce high excess pore pressures in these materials with accompanying strength reduction. Likewise, no widespread liquefaction of the foundation soils is expected, except possibly in interspersed pockets of sands and gravels. However, such pockets appear to be confined primarily to near the stream channel and are unlikely to affect the overall stability of the dam. The sluiced fill at the downstream toe of the dam is expected to liquefy early in the strong shaking phase of the earthquake and to deform subsequently.

The analyses for the Hayward fault MCE result in calculated downward vertical displacements of the crest between 1 and 6 feet. Considering the limitations of the methods of analysis, the best estimate of the maximum crest settlements is between 1.5 and 3.5 feet. These settlements correspond to about 1.1% to 2.5% of the structural dam height and are generally consistent with the past seismic performance of embankment dams, considering the age of Chabot Dam and the methods used for its construction.

The best estimate of horizontal displacements of the upstream slope is less than 5 feet. Progressive sliding of the dam and instability of the crest are not expected to occur. Except for the sluiced fill, horizontal displacements of the downstream slope are expected to be less than 2 feet. Displacements of several feet may occur in the sluiced fill in the direction of the downstream channel. The stability analyses indicate that such displacements, however, are unlikely to lead to instability of the main body of the embankment.

Because the dam has a freeboard of about 23 feet, the estimated crest settlements will not lead to overtopping of the embankment. However, the expected settlements and horizontal deformations will likely result in longitudinal and transverse cracking of the embankment crest and may require drawdown of the reservoir immediately after the earthquake. The estimated

dam deformations are not expected to affect the structural integrity of the spillway or outlet works. A separate study has been undertaken by EBMUD to evaluate the seismic stability of the outlet tower.

Transverse cracking of the embankment is most likely to develop near the abutments because of their steep nature. Transverse cracking is of particular concern as it could provide a mechanism for leakage, if it were to extend below the reservoir level and to be continuous across the dam crest or to be interconnected by longitudinal cracking.

The potential for developing through-going transverse cracks will be tempered by the width of the embankment. In addition, the likelihood of leakage will be a function of the reservoir level at the time of the earthquake. Nonetheless, transverse cracking that extends below the reservoir elevation, even if not continuous across the embankment, would increase seepage and the potential for leakage immediately after the earthquake. On this basis and given that the dam lacks an internal filter and drainage system to safely control possible leakage and its consequent effects, it may be concluded that the potential for transverse cracking represents a risk regarding the safety of the structure. The significance of this risk is to be further considered by EBMUD.

The analyses for the San Andreas fault MCE result in a dynamic response of the embankment lower than that calculated for the Hayward fault MCE. Nonetheless, liquefaction and deformations of the sluiced fill are also expected to occur during the San Andreas fault MCE. The calculated dam deformations for the San Andreas event are lower than those for the Hayward event. Thus, the results of the analyses indicate that the San Andreas event is less critical than the Hayward event regarding the seismic stability of the dam.

1.1 BACKGROUND

This report presents the results of a dynamic stability study of Chabot Dam, located near the City of San Leandro in Alameda County, California (Figure 1-1). The dam and reservoir were initially constructed between 1874 and 1892. Chabot Dam is owned and operated by the East Bay Municipal Utility District (EBMUD).

1.2 PURPOSE AND OBJECTIVES

The stability of Chabot Dam has been the subject of several previous investigations, including those by Shannon and Wilson (S&W) (1965), Woodward-Lundgren & Associates (WLA) (1974), and Woodward-Clyde Consultants (WCC) (1977). Those studies are briefly described below.

In 2003, the California Department of Water Resources, Division of Safety of Dams (DSOD) conducted a simplified dynamic analysis of the dam as part of a statewide reevaluation of dams located near high-slip rate faults. On that basis, they asked EBMUD to perform a more detailed dynamic stability study of the dam. The study presented herein was conducted in response to DSOD's request. The purpose of the study was to evaluate the seismic hazard at the site based on the current understanding of the tectonic and geologic setting of the region, evaluate the strengths of the embankment and foundation materials, and reevaluate the seismic stability of the dam using current state-of-practice analytical techniques.

1.3 PREVIOUS INVESTIGATIONS

Shannon and Wilson investigated the dam and performed stability analyses in 1965. EBMUD and S&W drilled 19 borings in the crest and downstream slope of the dam to identify the materials and retrieve samples for testing. The slope stability of the dam was analyzed under steady seepage conditions, pseudo-static conditions, and rapid drawdown conditions, using limit-equilibrium methods. The study concluded that the dam had adequate factors of safety, but made recommendations for minor improvements. Following the S&W study, EBMUD placed a fillet fill on the downstream slope of the dam and installed a subdrain system at the downstream toe.

Woodward-Lundgren and Associates performed an evaluation of the seismic stability of the dam in 1974. EBMUD and WLA drilled 15 borings in the upstream and downstream shells of the dam. The soil samples were tested by EBMUD and WLA for index properties and cyclic strength. The dynamic response of the dam was evaluated using the finite element method. The investigation predicted limited overall deformation of the dam during San Andreas and Hayward earthquake events, but indicated the possibility of surface sloughing of the upstream slope and accompanying crest settlement.

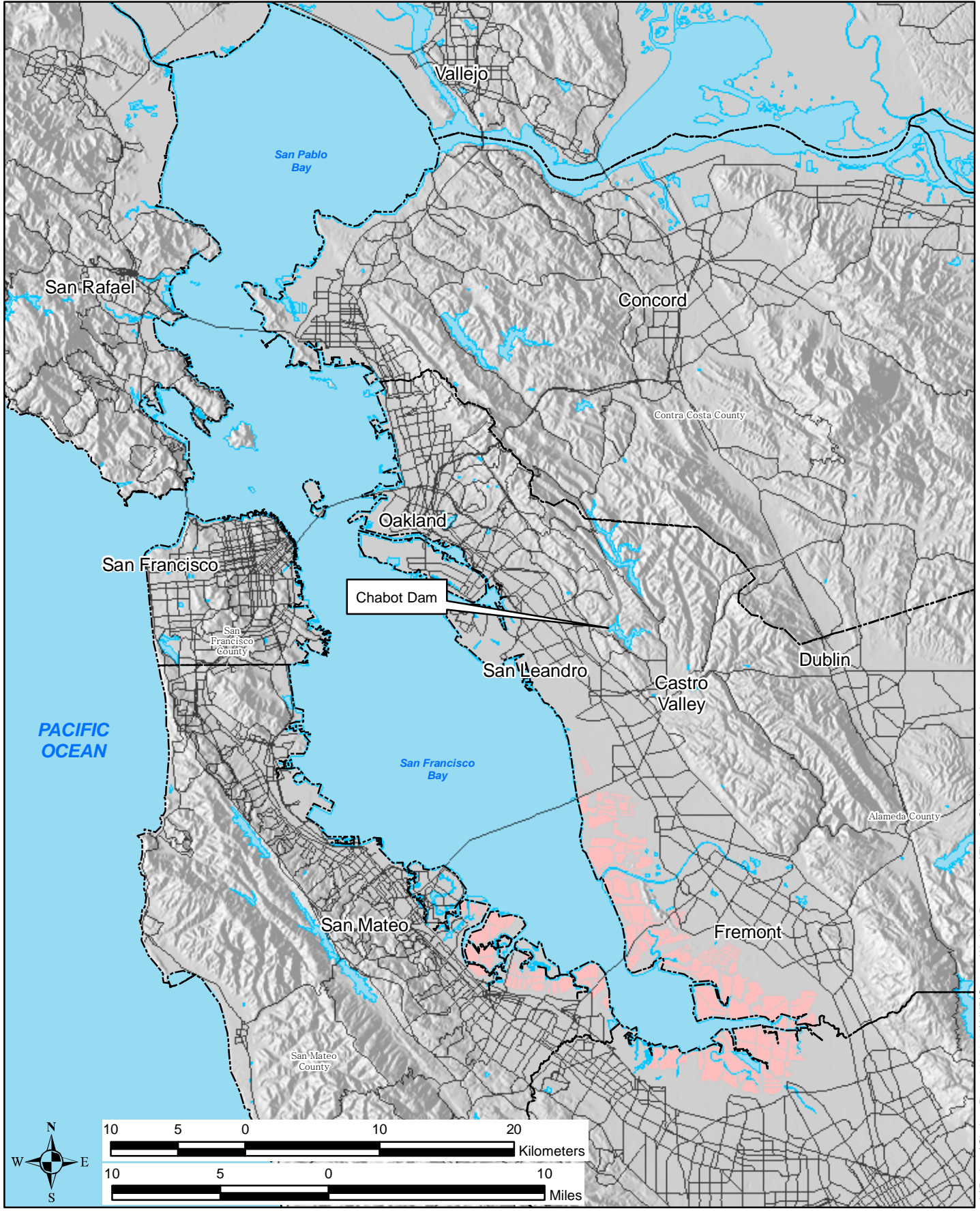
Woodward-Clyde Consultants re-evaluated the seismic stability of the dam in 1977. Three additional borings were drilled in the crest and downstream embankment and samples were retrieved and tested. The study predicted maximum crest settlements of about 3 to 5 feet. On that basis, an increase in crest elevation of 5 feet was recommended. EBMUD subsequently

placed compacted fill on the downstream slope of the dam and raised the crest from elevation 243² to 250. As part of the project, EBMUD also constructed a new spillway.

1.4 REPORT ORGANIZATION

This report is organized into fifteen sections and eight appendices. After this introductory section, Section 2 presents the scope of work of the study. A brief description of the project and information on the construction and performance of the dam are summarized in Section 3. Section 4 summarizes the field and laboratory investigations performed for the present study. The geological setting of the dam is discussed in Section 5, followed by a discussion of site-specific earthquake ground motions in Section 6. Characterizations of the embankment and foundation conditions are presented in Section 7. Section 8 discusses the general analysis approach. The details of the limit-equilibrium stability analyses, dynamic response analyses, seismic stability analyses, and non-linear analyses are presented in Sections 9 through 12. Section 13 summarizes the expected seismic performance of the dam whereas Section 14 summarizes the main conclusions and recommendations from the study. The references cited in the report are listed in Section 15. Appendices A through I present supporting documentation including field and laboratory data as well as geologic and seismologic reports produced for the study.

² Unless otherwise noted, all elevations in this report are given in feet and refer to USGS datum.



L:\Projects\Chabot_Dam_26814536\MXD\Current Working Documents\Fig 1-1 Site Location Map.mxd



Chabot Dam
Seismic Stability
26814536

Site Location Map

Figure 1-1

This study was performed in accordance with the Agreement between URS and EBMUD dated January 13, 2004. The main technical tasks of the scope of work are summarized below.

Data Review

This task consisted of reviewing existing information on the reservoir site geology and on the design, construction, and instrumentation monitoring of the dam.

Geologic Mapping

This task included developing an understanding of the site geology and the stratigraphy of the dam foundation. The existing boring data was incorporated into a geographic information system (GIS) database to help assess the distribution of soils and their characteristics within the embankment and the foundation.

Field Exploration and Laboratory Testing

This task included drilling rotary-wash borings through the embankment and foundation soils and into bedrock. Samples were retrieved with a Standard Penetration Test (SPT) sampler and other types of samplers for laboratory testing. Geophysical surveys were performed in selected borings to measure the shear wave velocity of the embankment and foundation materials. Becker Penetration Test (BPT) soundings were performed at locations adjacent to the toe borings. The hammer energy efficiencies were measured and calibrated during the SPT and BPT sampling. Laboratory tests were performed to characterize and evaluate the geotechnical properties of the materials for use in dynamic stability analyses.

Develop Site-Specific Earthquake Ground Motions

This task included reviewing recent information on the regional seismic environment and the characteristics of faults that could affect the dam to determine the maximum credible earthquake (MCE) on the controlling faults. Site-specific acceleration response spectra were developed using well-established attenuation relationships and up-to-date procedures that account for near-field and directivity effects. Acceleration time histories were developed for use in analysis of the dam.

Analysis of Dam Stability and Deformations

This task included developing representative cross-sections and material properties for analysis of dam stability. The potential for liquefaction of cohesionless soils and of strength degradation of cohesive soils were evaluated using state-of-the-practice procedures. The critical section of the dam was established using limit-equilibrium slope stability analyses. The seismic stability and deformations of the dam were evaluated using up-to-date two-dimensional finite element analysis and Newmark-type deformation analysis procedures. In addition, non-linear analyses were performed with the two-dimensional finite difference computer code FLAC. The overall performance and seismic stability of the dam were evaluated and assessed based on the results of the analyses.

3.1 SITE SETTING

The dam and reservoir are situated on San Leandro Creek in a narrow canyon in the East Bay hills, approximately nine miles southeast of Oakland and about two miles northeast of San Leandro. The site location is shown on Figure 3-1.

3.2 DESCRIPTION OF DAM

The dam is approximately 135 feet high and 500 feet long and has a 30-foot-wide crest. The dam crest elevation is 250 and the spillway crest elevation is 227.25 (per EBMUD as-built drawings). The current downstream slope is 3:1 (H:V) with a 15-foot-wide bench at elevation 210. The upstream slope is approximately 2:1 and is protected by a layer of riprap. The main body of the dam is composed of so-called “wagon fill,” which is a clayey sandy material placed and compacted by teams of horses and wagons. On the crest and downstream slope, the wagon fill is overlain by engineered fill. The downstream toe of the embankment is composed of sluiced fill and random fill zones. The dam layout is shown in Figure 3-2.

3.3 APPURTENANT FACILITIES

The project appurtenant facilities include three outlet tunnels and a spillway. The locations of the spillway and of outlet tunnels Nos. 1 and 2 are shown in Figure 3-2. The location of tunnel No. 3 is shown in Figure 3-1. The intake tower for tunnel No. 2 is located on the west shore of the lake near the spillway. The tower consists of a brick and stone masonry structure with a one-story reinforced concrete pavilion on top. Tunnel No. 2 is a masonry-lined conduit in rock through the west abutment, and is connected to a 36-inch raw water line, which in turn connects to a 30-inch blow-off pipe and an outlet structure. Tunnel No. 3, about 1,500 feet in length, is located at the northwest end of the lake and connects to San Leandro Creek, as shown in Figure 3-1. Tunnel No. 1 is to the west of tunnel No. 2 and is no longer in service. The spillway is an uncontrolled chute type, founded on rock on the west abutment. It consists of a concrete approach, weir, chute, and stilling basin. The spillway crest and approach are about 70 feet wide. The stilling basin is about 100 feet long.

3.4 CONSTRUCTION HISTORY

Construction of the dam started in early 1874. The dam footprint area was reportedly stripped to a depth of up to 3 feet to remove vegetation, roots, and loose topsoil. A core trench 10 to 30 feet deep and 40 to 90 feet wide was excavated to bedrock along the dam axis. Wagon fill was placed during 1874 and 1875 to elevation 233 to form the main body of the dam. The materials were selected from nearby sources so as to have sufficient clay to “bind and pack”. The fill was placed in one-foot layers, sprinkled with water, and compacted by horses and wagons. Reportedly, the materials were placed selectively to form a clay core. Between 1875 and 1888, the downstream slope was flattened by the addition of a sluiced (i.e. hydraulically-placed) fill buttress up to elevation 185. The wagon fill was raised to a crest elevation of 243 between 1891 and 1892. Around that same time, a berm was placed on the upstream face where a slide had apparently occurred during construction.

A fillet fill was placed on the downstream slope against the right abutment following recommendations of the 1965 stability evaluation by Shannon and Wilson. A substantial program of dam modifications was undertaken in 1980, after the 1977 stability evaluation by Woodward-Clyde Consultants. Engineered fill (referred to as “modern fill”) was placed along the downstream slope to raise the crest to the current elevation 250. A new spillway was also constructed during the dam modifications. Unsorted material from required excavations and construction demolition (referred to as “random fill”) was placed near the downstream toe and covered with topsoil.

3.5 PERFORMANCE AND MONITORING

The performance of Chabot Dam is monitored with piezometers, seepage measurement points, and survey monuments. The instruments are maintained and periodically read by EBMUD personnel. The piezometers are listed in Table 3-1. Some installations include two or three piezometers in a single boring. Seepage through the embankment is monitored at two locations. The spillway drain reading is typically between 0 and 2 gallons per minute (gpm). The toe drain readings are typically between 2 to 4 gpm. Nine survey monuments have been installed on the embankment: five on the crest, three on the downstream bench, and one at the downstream toe. The locations of the piezometers and survey monuments are shown in Figure 3-3.

Overall, the dam has performed very well since its construction. No evidence of instability or apparent damage was reported after the great 1906 San Francisco earthquake. Monitoring data before and after the 1989 Loma Prieta earthquake showed no signs of excessive seepage, phreatic level changes within the dam, or permanent displacement of the embankment. The dam has also performed satisfactorily during several instances of complete drawdown of the reservoir.

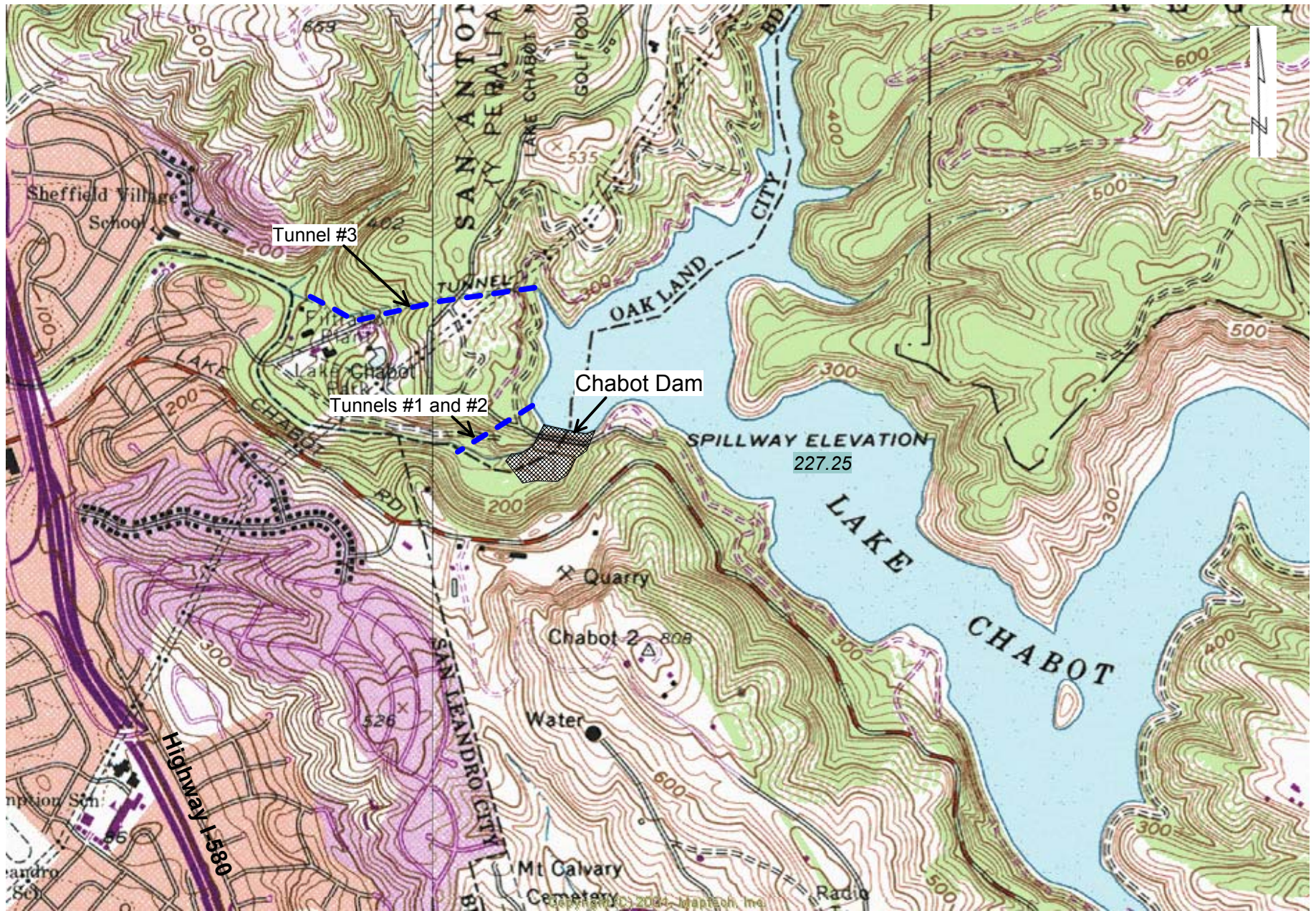
There is some indication that upstream slope instability may have occurred during construction in the 1890s, but it appears that the slope was reinforced and/or flattened afterwards and no subsequent instability has been reported.

**Table 3-1
Existing Piezometers at Chabot Dam**

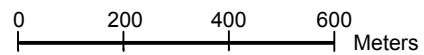
Boring No.	Ground Surface Elevation, ft	Piezometer A Tip Elevation, ft	Piezometer B Tip Elevation, ft	Piezometer C Tip Elevation, ft
WI-15	181.9	128.9	-	-
WI-18	188.8	165.8	-	-
WI-25	250.0	201.2	166.3	146.0
WI-28	250.5	186.9	129.2	101.2
WI-51	250.4	235.0	-	-
WI-52	250.4	137.0	122.0	-
WI-53	212.0	192.0	-	-
WI-54	211.5	186.5	169.5	-
WI-55	210.1	129.0	104.0	-
WI-56	210.7	113.7	97.7	-
WI-57	169.7	125.7	102.7	-
WI-58	162.1	106.8	80.3	-

Note:

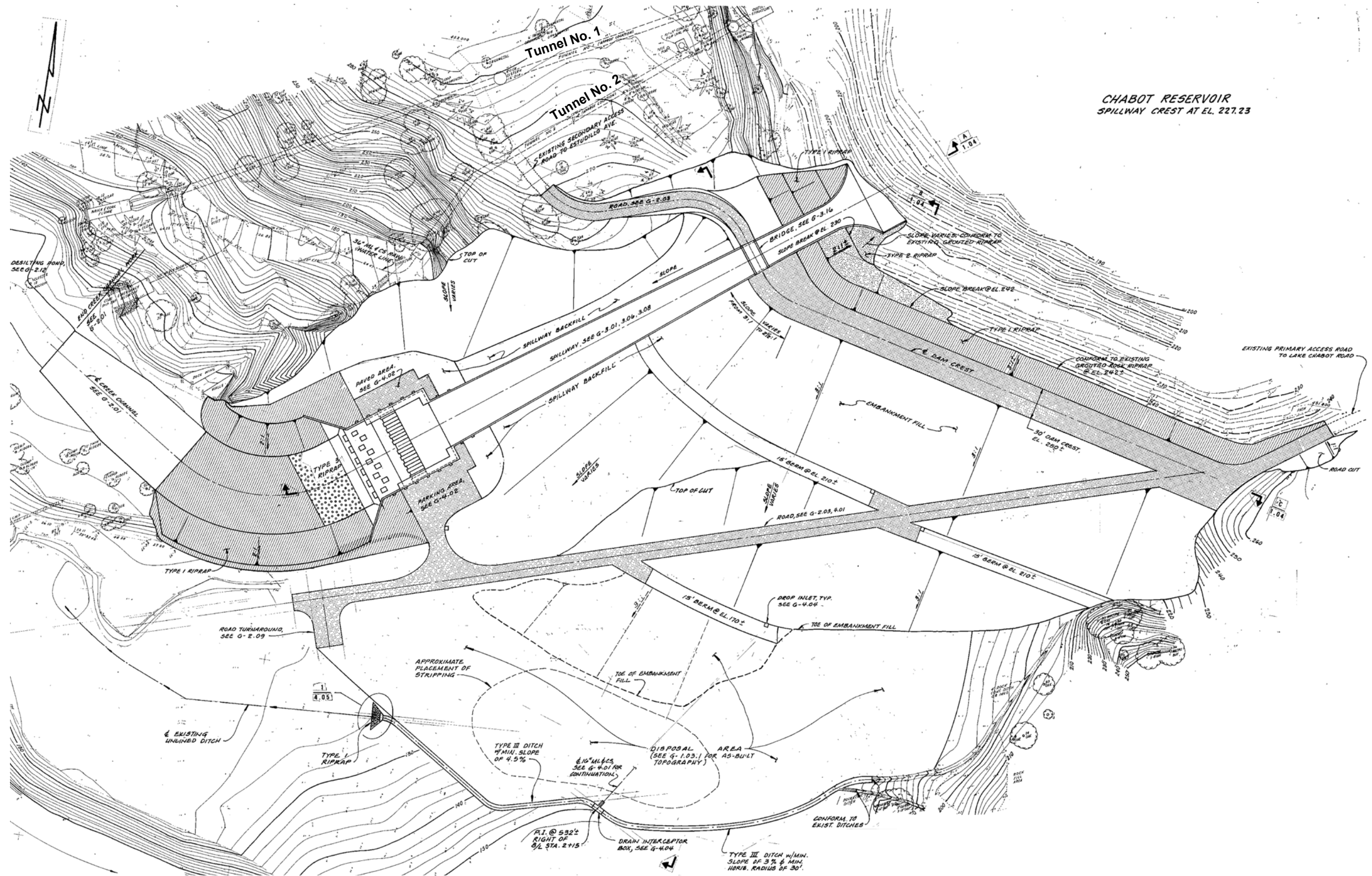
All piezometers are manually read open standpipes.



Source: Terrain Navigator, Maptech Inc., 2001



Project No. 26814536	Chabot Dam Seismic Stability	Location of Chabot Dam	Figure 3-1
URS			



Source:

EBMUD Drawing No. 6948-G-1.03, Chabot Dam & Spillway Modifications General Plan, dated May 14, 1979, last revised on December 7, 1982

Project No.
26814536

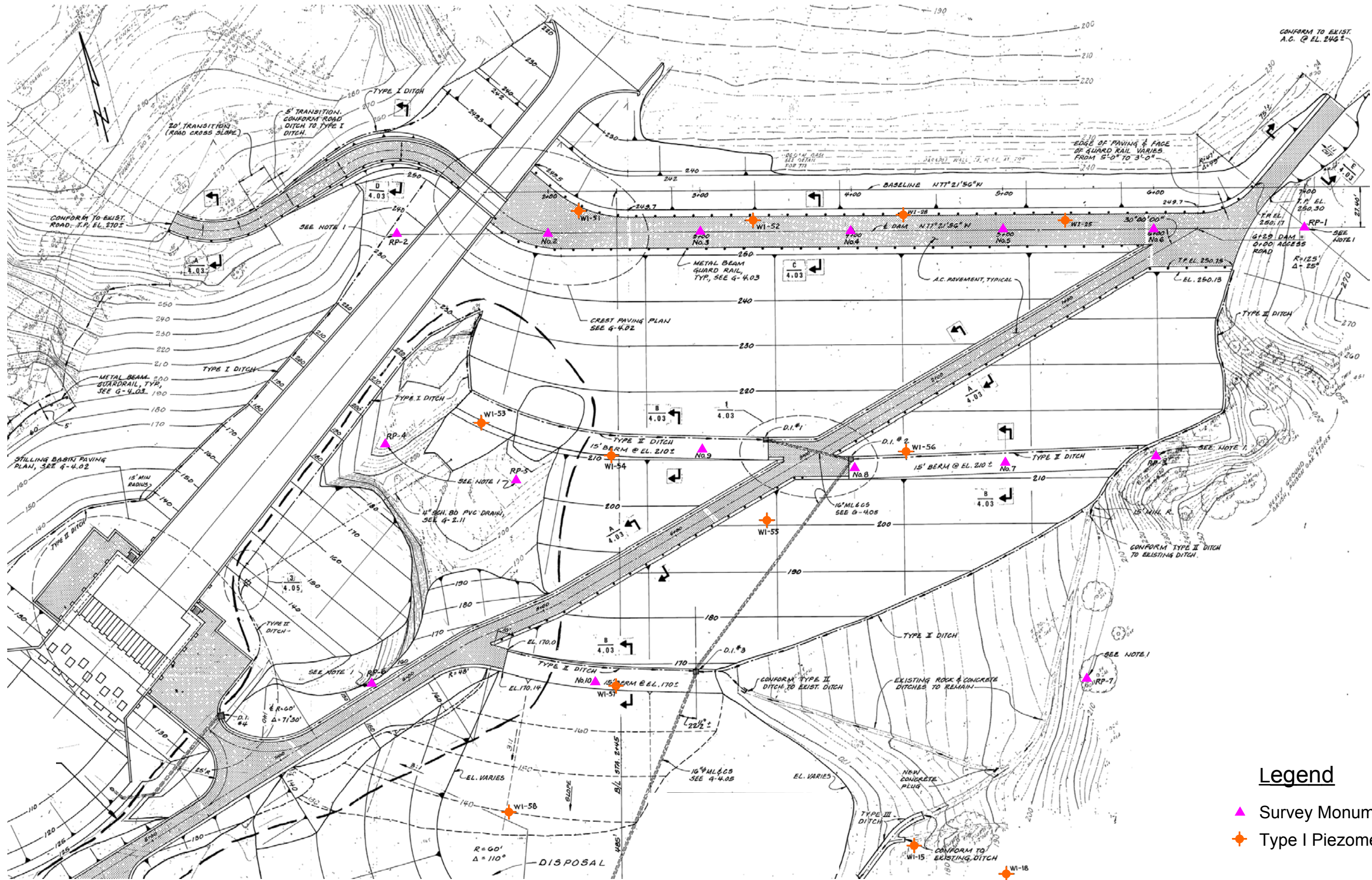
Chabot Dam
Seismic Stability

Site Plan

FIGURE

3-2





- Legend**
- ▲ Survey Monument
 - ◆ Type I Piezometer

Source:
 EBMUD Drawing No. 6948-G-4.01, Chabot Dam & Spillway Modifications Paving, Drainage & Instrumentation Plan, dated May 14, 1979, last revised on September 10, 1999

Project No. 26814536	Chabot Dam Seismic Stability	Instrument Locations	FIGURE 3-3
URS			

The objective of the field and laboratory investigations was to supplement the available geotechnical data, to support the seismic stability re-evaluation of the dam. Previous studies of the dam's stability have also included field and laboratory investigations. The locations of the borings from previous studies are shown in Figure 4-1. Whereas a relatively extensive body of data is available from the previous investigations, it was concluded that a reliable and robust dynamic stability study required additional high quality data and use of improved testing techniques to better characterize the materials in the dam. The investigation program that was carried out for this purpose is described below.

4.1 FIELD INVESTIGATIONS

The field investigation program included exploratory borings, Becker penetration testing, hammer energy measurements, and downhole geophysical surveys. The details of these elements of work are described in the following sections. The boring logs and data reports are presented in Appendices A through E. The boring depths and materials encountered are summarized in Table 4-1. The locations of the borings drilled for this study are shown in Figure 4-2, along with the locations of previous borings.

The field investigations were carried out between May 3 and June 8, 2004. The drilling program included 9 rotary wash borings and 3 Becker hammer penetration test soundings. The rotary wash borings were drilled by Taber Consultants of Sacramento, California. The Becker hammer soundings were performed by Great West Drilling of Fontana, California. Downhole geophysical measurements were obtained by GEOVision Geophysical Services of Corona, California. Energy transfer measurements of hammer efficiency during SPT and BPT testing were obtained by Abe Engineering, Inc. of Walnut Creek, California. Robert Y. Chew Geotechnical supervised the drilling and logged the borings, under the direction of URS. URS reviewed the samples, conducted the laboratory testing, and prepared the final boring logs with assistance from Dot Dat, Inc.

4.1.1 Rotary Wash Drilling

Nine rotary-wash borings were drilled at selected locations between May 3 and May 29, 2004. These borings (designated WI-59 through 67) were numbered in the order drilled, using nomenclature consistent with borings previously drilled by the District at the site. Borings WI-61 and WI-64 were drilled from the crest of the dam. Borings WI-59 and WI-62 were drilled from the downstream bench and sloping access road. Borings WI-60, WI-63, and WI-65 were drilled in the downstream toe area. Borings WI-66 and WI-67 were drilled in the reservoir near the upstream toe of the dam. The land borings were drilled with a truck-mounted Diedrich D-128 drill rig and the reservoir borings were drilled with a CME-45 drill rig mounted on a barge. Both rigs used the same SPT hammer.

The borings were initially located in the field by URS from available reference points. After drilling, a hand-held Trimble GPS receiver with built-in differential correction capability was used to record coordinates for each boring location. Comparison measurements taken at known reference points indicate a horizontal accuracy range for the GPS coordinates of about 5 feet. For the reservoir borings drilled from the barge, the GPS unit was first used to navigate the barge to within a few feet of the target boring locations. The boring coordinates were then recorded once the barge anchors and borehole casing were set in place.

The boring logs are presented in Appendix A. SPT blow counts were obtained using a Diedrich automatic hammer. Energy measurements were performed to calibrate the efficiency of the hammer.

4.1.2 Becker Penetration Testing

Based on the results of the drilling program, the potential effects of gravel on the measured SPT blow counts were determined to be significant. It was determined that such effects could introduce significant uncertainty in the evaluation of residual strength of the sluiced fill. Therefore, three BPT soundings (BPT-1 through 3) were performed in the downstream toe area, in close proximity to the SPT borings. The BPT soundings were advanced through the random fill and sluiced fill until they reached refusal.

The soundings were performed on June 7 and 8, 2004 using the procedures recommended by Harder and Seed (1986). The Becker hammer drill is essentially a steel pipe casing driven by a diesel hammer. A truck-mounted AP-1000 drill rig and a 6.5-inch-OD closed crowd-out bit were used. The hammer was an ICE model 180 double acting hammer. Blow counts and bounce chamber pressures were recorded for every foot of penetration. Re-drive tests were performed at about 20 foot intervals to monitor casing friction during the tests. Logs of the BPT soundings are presented in Appendix B. Energy measurements were performed to calibrate the efficiency of the Becker hammer during drilling.

4.1.3 Hammer Energy Measurements

The energy transferred from the hammer to the SPT sampler is an important factor in evaluating the liquefaction resistance of soils. The efficiency of energy transfer is measured by the energy ratio (ER), which is defined as the ratio of energy transferred to the drill rod to the theoretical “free fall” energy. Using the energy correction factor ($C_E = ER/60$), the field SPT blow counts (N) are adjusted to standardized blow counts (N_{60}) corresponding to an average energy ratio of 60 percent.

The SPT hammer energy measurements were obtained during sampling in boring WI-59 on May 3, 2004. The measurements were obtained with a Pile Driving Analyzer. The measured average ER was 84%. The complete results of the SPT hammer energy measurements are presented in Appendix C.

The BPT hammer energy measurements were obtained in all three BPT soundings. The energy measurements were digitally recorded for each foot of penetration. The measured average ER values were between 37 and 43%. The complete results of the BPT hammer energy measurements are presented in Appendix D.

4.1.4 Downhole Geophysical Surveys

Downhole seismic wave velocity measurements were made in borings WI-59 through 62 immediately after drilling each boring. An OYO Model 170 suspension logging recorder and suspension logging probe were used to measure shear and compression wave (S- and P-wave) velocities at 0.5-meter (m) intervals (1.64 feet). The main purpose of the surveys was to obtain shear wave velocity data for the embankment and foundation materials for use in dynamic

analysis of the dam. A more detailed description of the geophysical survey program and results is presented in Appendix E.

4.2 LABORATORY TESTING

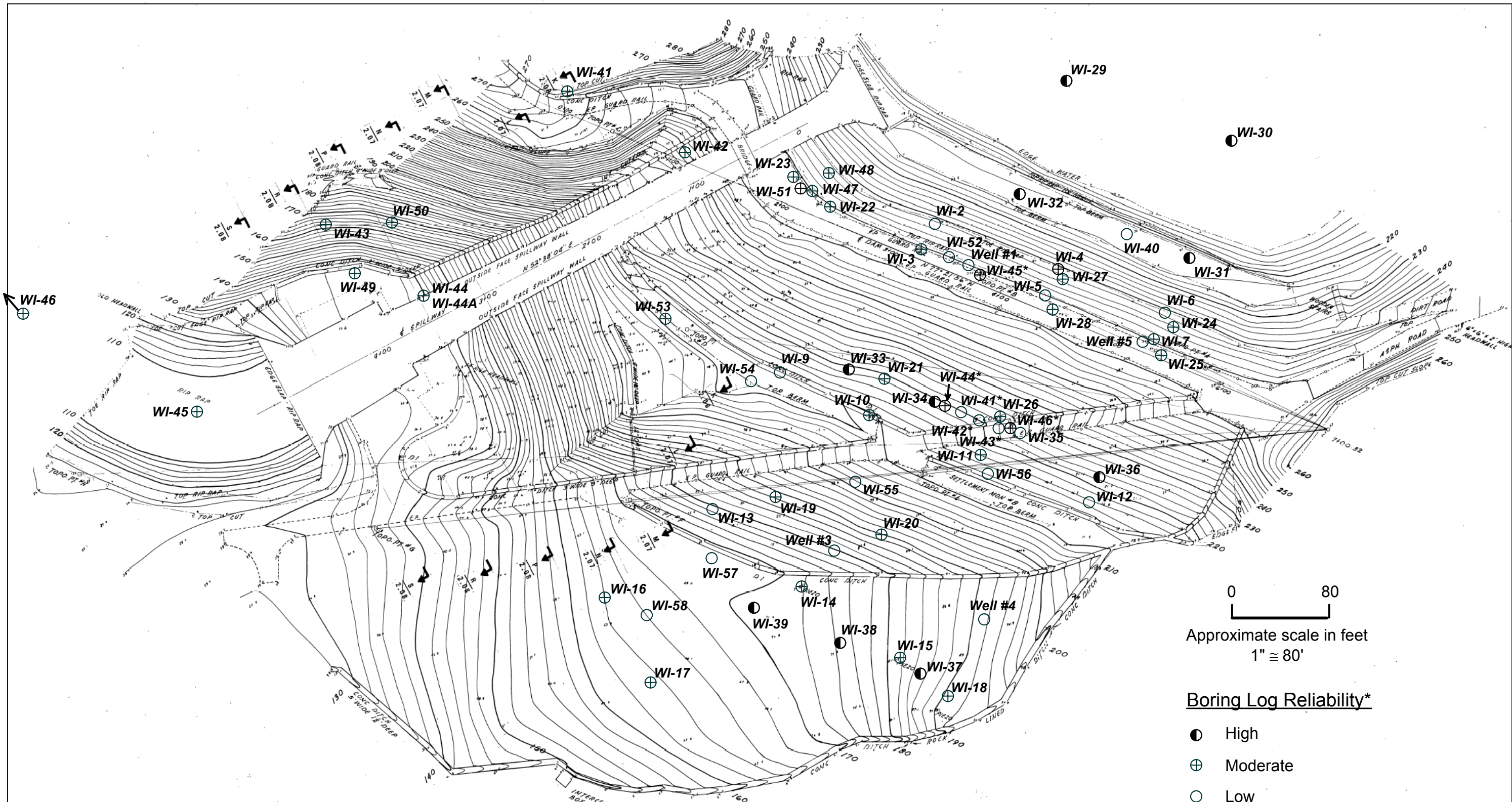
The laboratory test program was conducted at the URS Pleasant Hill laboratory. Prior to finalizing the test program, the soil and rock samples were carefully inspected in the laboratory by the URS team and representatives of the DSOD. Appropriate tests were selected to assist in subsequent evaluation of material properties for use in the dam dynamic stability analyses. The types of tests performed are listed below, along with their ASTM designations.

- In-situ moisture-density (ASTM D2216, D2937)
- Sieve analysis (ASTM D422)
- Hydrometer analysis (ASTM D422)
- Atterberg Limits (ASTM D4318)
- Isotropically consolidated undrained (ICU) triaxial compression tests with pore pressure measurements (ASTM D4267).
- Unconfined compression strength tests (ASTM D2166)

The laboratory tests were conducted in general accordance with the noted ASTM standards. Consolidation pressures for the ICU tests were selected based on the estimated overburden pressure at each sample depth. The test results are tabulated in Appendix F. Summary plots of the test results are also presented in Appendix F along with the laboratory reports for each test. Abbreviated test results for each sample are also included in the boring logs at the appropriate depths.

**Table 4-1
Summary of Borings**

Boring No.	Boring Type	Location	Surface Elev. (feet)	Depth (feet)	Materials Encountered (Approximate Depths/Remarks)
WI-59	Rotary Wash	Mid-bench, downstream face	210	99	90 feet (ft) embankment fill; rhyolite and serpentinite bedrock. (Geophysical survey).
WI-60	“	Downstream toe	179	105	55 ft embankment fill; 17 ft native soil; serpentinite, shale, and gabbro bedrock. (Geophysical survey).
WI-61	“	Crest	250	166	140 ft embankment fill; rhyolite bedrock. (Geophysical survey).
WI-62	“	Downstream mid-slope access road	224	140	92 ft embankment fill; 20 ft native soil; basalt, rhyolite, and serpentinite bedrock. (Geophysical survey).
WI-63	“	Downstream toe	172	68	50 ft embankment fill; serpentinite and gabbro bedrock.
WI-64	“	Crest	250	140	128 ft embankment fill; rhyolite bedrock.
WI-65	“	Downstream toe	168	65	54 ft embankment fill; 8 ft native soil; gabbro bedrock.
WI-66	“	Upstream toe (barge)	179	66	37 ft reservoir sediment and embankment fill; 19ft native soil; shale bedrock.
WI-67	“	Upstream toe (barge)	174	67	58 ft reservoir sediment and embankment fill; 2 ft native soil; shale/claystone/siltstone bedrock.
BPT-1	Becker Hammer	Downstream toe, near WI-60	179	80	No samples retrieved
BPT-2	“	Downstream toe, near WI-63	172	65	No samples retrieved
BPT-3	“	Downstream toe, near WI-65	170	63	No samples retrieved



0 80
 Approximate scale in feet
 1" = 80'

Boring Log Reliability*

- High
- ⊕ Moderate
- Low

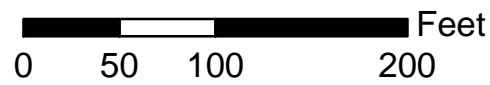
* For purposes of this study

Notes:

1. Base topo map from EBMUD drawing "As Built Topography", No. 6948-G-1.03.1, dated December 1982
2. Boring locations from :
 - Shannon & Wilson Report "Review of Stability, Chabot Dam", Figure 2, dated September 1965
 - WCC Report "Evaluation of Seismic Stability of Chabot Dam Modification", Figure 4-5, dated August 1977
 - EBMUD Drawing "Existing Topography & Location of Borings", No. 6948-G-1.05, dated December 1982
 - EBMUD Drawing "Paving, Drainage & Instrumentation Plan", No. 6948-G-4.01, dated September 1999

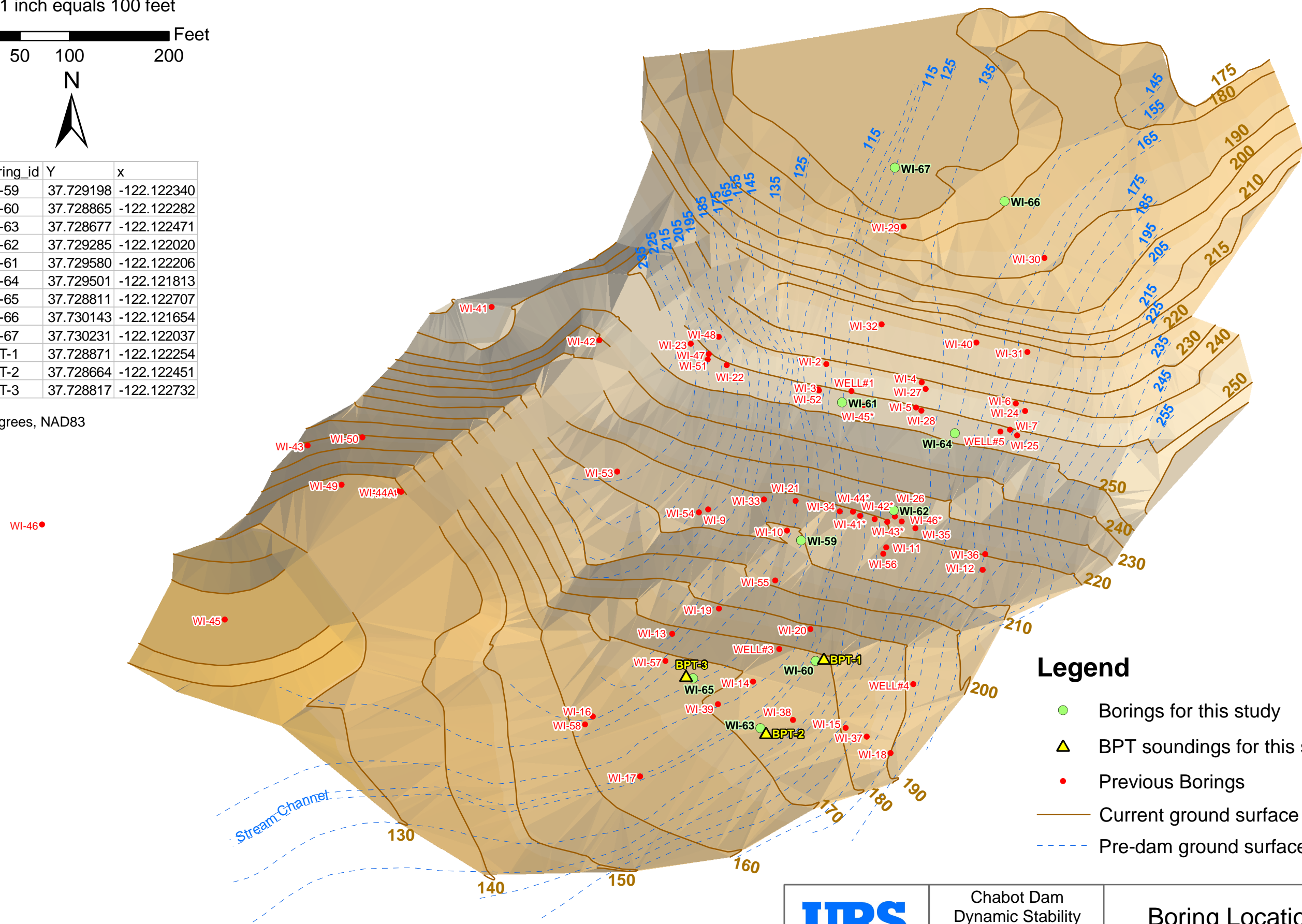
Project No. 26814536	Chabot Dam Seismic Stability	Location of Borings From Previous Studies	FIGURE 4-1
URS			

1 inch equals 100 feet



Boring_id	Y	x
WI-59	37.729198	-122.122340
WI-60	37.728865	-122.122282
WI-63	37.728677	-122.122471
WI-62	37.729285	-122.122020
WI-61	37.729580	-122.122206
WI-64	37.729501	-122.121813
WI-65	37.728811	-122.122707
WI-66	37.730143	-122.121654
WI-67	37.730231	-122.122037
BPT-1	37.728871	-122.122254
BPT-2	37.728664	-122.122451
BPT-3	37.728817	-122.122732

Degrees, NAD83



Legend

- Borings for this study
- ▲ BPT soundings for this study
- Previous Borings
- Current ground surface contours (ft)
- - - Pre-dam ground surface contours (ft)

URR Corporation L:\Projects\Chabot_Dam_26814536\MXD\Current Working Documents\Fig_1 Boring Locations for Dynamic Stability.mxd Date: 8/11/2004 10:53:40 AM Name: dhwright

This study included a review of geologic mapping from previous studies, additional reconnaissance-level geologic mapping in the vicinity of the dam site, review of the seismotectonic environment of the East Bay hills, and updated characterization of the seismic sources that could affect the dam. This work was conducted by Dr. John Wakabayashi and William Lettis & Associates under subcontract to URS. Their reports are included in Appendices G and H and are summarized below and in Section 6.

5.1 REGIONAL GEOLOGY

Chabot Dam is located within the seismically active region between the Pacific plate on the west and the Sierra Nevada-Central Valley (“Sierran”) microplate on the east. Geodetic data demonstrate that net motion between the two plates is obliquely convergent. The oblique motion of the Sierran microplate relative to the strike of the San Andreas and Hayward faults results in a small component of net convergence normal to these structures, which is accommodated by both strike-slip and thrust faulting in the eastern San Francisco Bay area.

The dam and reservoir are situated in a narrow canyon near the western edge of the East Bay hills, which limit San Francisco Bay on the east. The East Bay hills region is within the central Coast Range geomorphic province of California and is bounded by the Hayward fault on the west and the Northern Calaveras fault on the east.

5.2 SITE GEOLOGY

The site geology in the vicinity of the dam is illustrated in Figure 5-1. In approximate upstream to downstream order, the bedrock at the dam site consists of the following units:

- Upper Jurassic Knoxville Formation shale and sandstone north and east of the dam,
- Jurassic Leona Rhyolite on both abutments, beneath the axis of the dam, and south and east of the canyon downstream of the dam, and
- Jurassic basalt and gabbro west (downstream) of the dam, along with volcanic and intrusive rocks of the middle-to-upper Jurassic Coast Range ophiolite.

Quaternary units present in the site area include alluvium and colluvium. Colluvium mantles most of the slopes in the area where bedrock outcrops are not seen, but its depth is difficult to assess, so colluvial deposits are not shown on Figure 5-1. Alluvium is present in the stream bottom downstream of the dam. No bedrock exposures were seen in the streambed, so the streambed probably consists of alluvium and colluvium. Beneath the dam embankment, several borings encountered alluvium or colluvium, which ranges in composition from gravelly sandy clay to gravelly sand and clayey gravel.

The mapped bedrock contacts in the site area appear to include both depositional and tectonic features. However, faulted Quaternary deposits have not been identified along any of the contacts at the site. In approximate upstream to downstream order, the mapped geologic contacts are as follows:

- 1) The contact between the northern exposure of Leona Rhyolite and the Knoxville Formation to the north. This contact may pass beneath the upstream toe of the dam and it is not clear whether it is tectonic or depositional. However, since the contact is folded, it is unlikely to

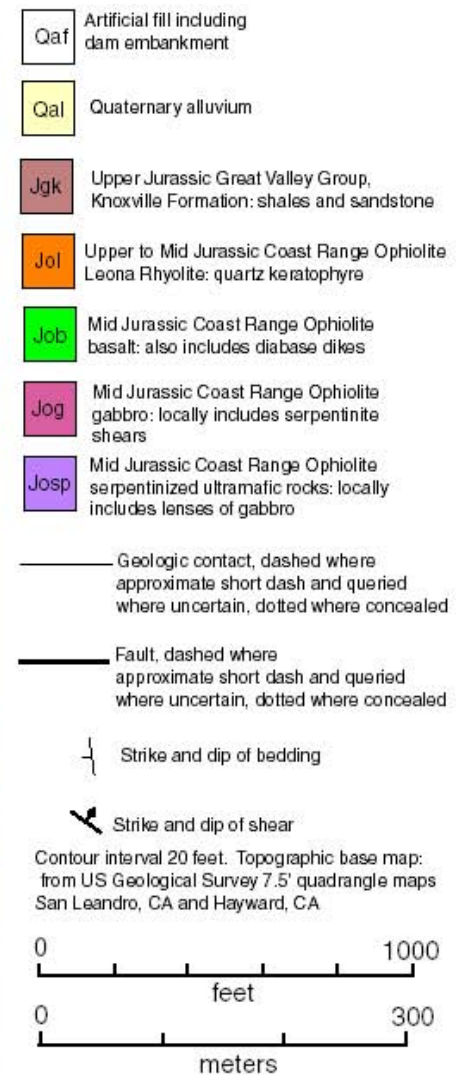
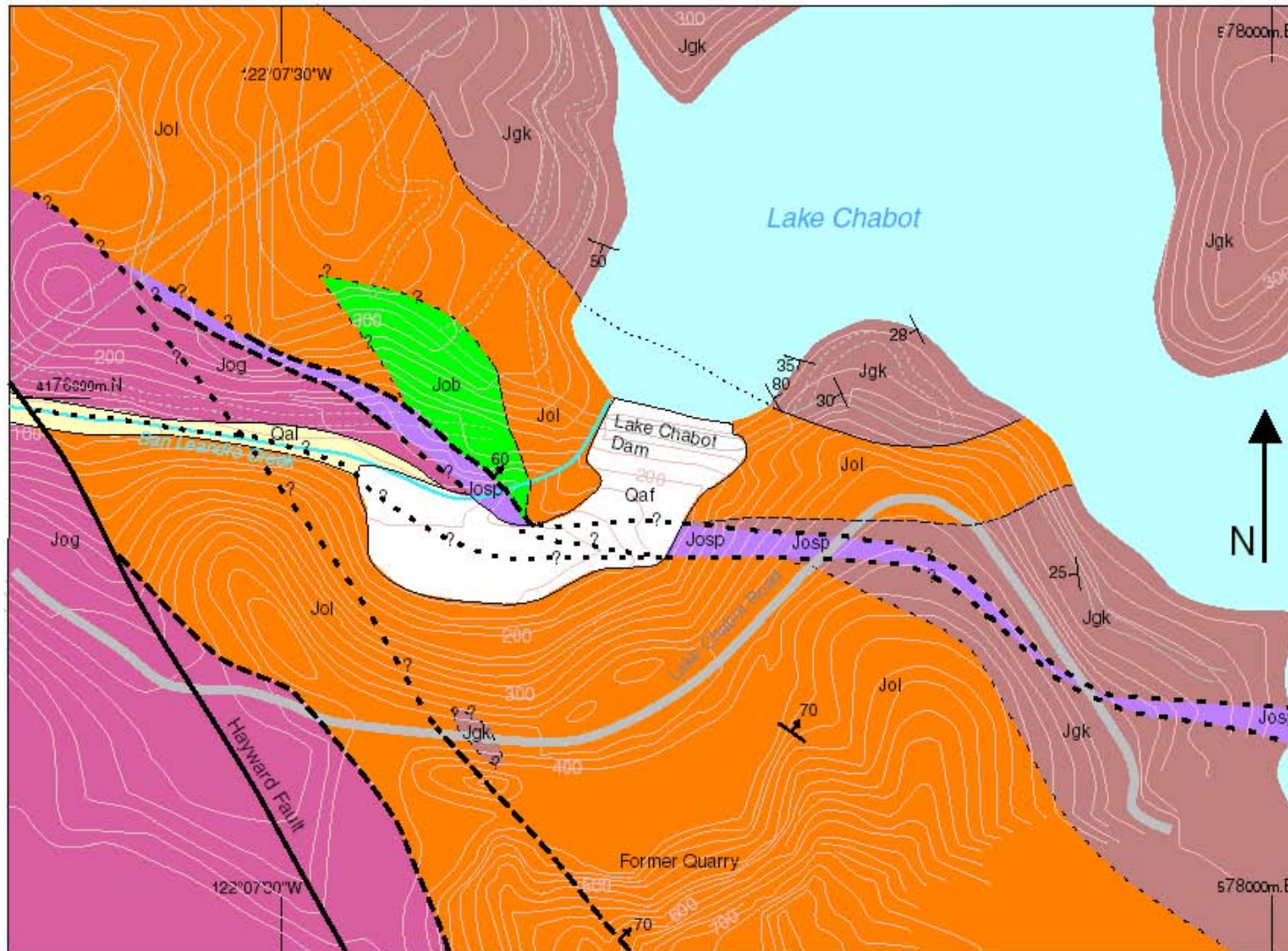
have been active in the late Quaternary time, if it is a fault. No geomorphic features suggestive of late Quaternary activity of this contact were observed.

- 2) The serpentinite shear zone that is exposed in the spillway cut passes beneath the downstream toe of the dam. This zone is folded, so it is unlikely to have been active during the late Quaternary. Also, no geomorphic features suggestive of late Quaternary activity along this contact were noted in airphotos or during the field reconnaissance.
- 3) The fault that locally follows the stream valley axis downstream of the dam separates gabbro from Leona Rhyolite. This feature may pass beneath the downstream toe of the dam. It is difficult to determine whether the serpentinite shear zone truncates this fault or whether this fault truncates and offsets the serpentinite shear zone. In any case, the fault appears to have been inactive during the late Quaternary. Part of the stream valley segment occupied by this fault is fairly linear, but no geomorphic features consistent with late Quaternary fault movement were observed in airphotos or during field reconnaissance along the hypothetical projection of this feature southeast and east of the dam.
- 4) Lienkaemper's (1992) map of recently active traces of the Hayward fault shows an eastern splay of the Hayward fault zone passing through the western wall of a now-inactive quarry south of Lake Chabot dam. The extension of that splay projects northwestward to cross San Leandro Creek about 350 m downstream (west) of the dam (Figure 5-1). Detailed geologic review of previous investigations and review of airphotos confirms that this splay fault does not pass beneath Lake Chabot Dam.

5.3 FAULT RUPTURE

As noted above, no evidence of late Quaternary activity associated with any of the faults passing near the dam was found in this investigation. Bedrock structural relationships indicate that these faults are inactive. Accordingly, the likelihood for sympathetic movement on faults passing beneath the dam in response to a large earthquake on the Hayward fault is judged to be very low.

Previous investigations have also addressed this question. Those studies concluded that if sympathetic movement were to occur on the faults at the dam site, such movement would be less than 1 foot (Marliave, 1978; WCC, 1978), and the dam would be able to safely withstand the effects of such movement (EBMUD, 1978). Those earlier conclusions are judged to be reasonable in view of the information obtained for the present investigation.



Project No. 26814536	Chabot Dam Seismic Stability	Site Geological Map	Figure
URS			5-1

6.1 GENERAL APPROACH

The approach used to develop the design acceleration response spectra for analysis of Chabot Dam consisted of the following steps:

- Identification of seismic sources that can generate significant earthquake ground motions at the dam site;
- Estimation of the maximum earthquake magnitudes and the closest distances to the dam site for the identified seismic sources;
- Identification of the controlling earthquake sources and the Maximum Credible Earthquake (MCE) on each source;
- Assessment of site conditions for purpose of estimating earthquake ground motions;
- Selection of appropriate attenuation relationships to estimate ground motions as a function of earthquake magnitude, distance, faulting style, and site condition;
- Development of design acceleration response spectra based on the results of the above steps; and
- Adjustment of the design response spectra to include near-field effects.

6.2 SEISMIC SOURCES

The Hayward-Rodgers Creek fault is located about 0.5 kilometers (km) west of the dam site. This fault was the source of an estimated M6.8 earthquake on 21 October 1868. The Northern Calaveras fault, located about 13 km east of the dam, has a historical record of small earthquakes. However, paleoseismic trenching studies indicate that the fault has produced multiple surface ruptures during late Quaternary time. Other active faults within 50 km of the dam that are considered as potential sources of future large earthquakes include the San Andreas, San Gregorio-Seal Cove, Greenville, Mt. Diablo and Concord-Green Valley faults. The locations of potential seismic sources in the region are shown in Figure 6-1.

Within the East Bay Hills region, potential seismic sources include the Moraga, Miller Creek and Palomares faults, the Contra Costa Shear Zone, which represents a complex system of strike-slip faults (Cull Canyon, Lafayette and Reliez Valley faults) and poorly integrated shear zones, and the Mt. Diablo Thrust fault, a 25-km long west-northwest trending fold north of Livermore Valley.

The maximum magnitudes for each identified seismic source were estimated based on the potential rupture length and seismogenic depth, using an empirical relationship that relates earthquake magnitude and rupture area as proposed by Wells and Coppersmith (1994). Site-to-source distances were measured from the center of the dam to the main trace of each fault. The estimated maximum earthquake magnitudes and site-to-source distances for each fault are listed in Table 6-1. A more detailed description of the seismic sources is presented in Appendix H.

Because of its magnitude and site-to-source distance, the Hayward-Rodgers Creek fault is likely to generate the strongest ground motions at the dam site. The estimated maximum magnitude for this fault is $M_w 7\frac{1}{4}$. The San Andreas fault, located about 30 km west of dam, is capable of

generating long duration shaking due to its large maximum magnitude (M_w 8.0). All other intermediate faults have estimated maximum magnitudes lower than the Hayward-Rodgers Creek fault. Therefore, the Hayward and San Andreas faults are considered as the controlling earthquake sources for analysis of the dam.

6.3 DESIGN RESPONSE SPECTRA

6.3.1 Site Conditions

Because the dam is underlain predominantly by hard rhyolitic rock, the design ground motions were developed for a rock site condition. This required characterization of the bedrock shear-wave velocity near the surface (top 30 m) and selection of appropriate ground motion attenuation models. Since measurements of the shear wave velocity (V_s) of the foundation rock at the site were not available at the time the ground motions were developed, a V_s value of 700 meters/second (m/sec) was assumed based on shear wave velocities measured in similar bedrock formations (Fumal, 1978). This velocity was judged at the time to be somewhat conservative for use in developing ground motion estimates.

The shear wave velocity of the bedrock was subsequently measured in the downhole geophysical surveys. The measured value is about 820 m/sec (or 2,700 fps), slightly higher than the assumed value. The difference is sufficiently small so that no change to the recommended design response spectra was judged necessary.

6.3.2 Attenuation Relationships

To characterize the ground motions at the dam site, empirical attenuation relationships were used to predict peak and spectral accelerations. Three independent relationships were used, to account for epistemic uncertainty. The relationships were selected on the basis of the site conditions and the tectonic environment.

Table 6-2 lists the three selected relationships along with their magnitude and distance definitions and limits of applicability. The site conditions assumed for each relationship are also listed in the table. Use of the relationship by Boore et al. (1997) for the San Andreas fault MCE required slight extrapolation beyond the limits of applicability stated by its authors. The selected attenuation relationships were weighted equally for developing the design ground motions.

6.3.3 Deterministic Ground Motion Analysis

A deterministic analysis was used to estimate the ground motions at the dam site for the MCEs on the two controlling seismic sources. This approach is consistent with current DSOD guidelines (Fraser and Howard, 2002).

Given the estimated slip rates on the Hayward and San Andreas faults (about 9 and 24 mm/year, respectively) and the consequence class weight associated with the dam, the DSOD Consequence Hazard Matrix dictates the use of 84th-percentile ground motions for deterministic analysis. Figure 6-2 shows the 84th-percentile horizontal acceleration response spectra calculated using the three selected attenuation relationships for the MCE on the Hayward-Rodgers Creek fault. A similar plot for the MCE on the San Andreas fault is shown in Figure 6-3.

Figures 6-2 and 6-3 also show the arithmetic mean spectra calculated using the three selected models. The calculated horizontal peak ground accelerations are summarized in Table 6-3.

Because of the short site-to-source distance for the Hayward Fault MCE, the vertical ground motions at the site are expected to be of similar (or possibly higher) intensity as the horizontal motions, at high frequencies. Strong vertical motions are also expected for the San Andreas fault MCE. However, vertical motions induce primarily normal stresses in the body of an embankment (as opposed to shear stresses) and so are not expected to result in development of significant excess pore water pressures or shear deformations. For that reason, vertical motions are not usually input into the dynamic analysis of embankment dams.

6.3.4 Fault Rupture Directivity Effects

Because the dam is located in close proximity to the Hayward and San Andreas faults, the effects of fault rupture directivity were considered in selecting the design ground motions. Fault rupture directivity increases the intensity of long-period motions (periods > 0.6 seconds) when the rupture propagates toward the site (forward directivity), and decreases the intensity of motions when it propagates away from the site. Two types of effects are considered: a) average amplification due to forward directivity, and b) amplification due to orientation with respect to fault strike. The latter effect produces stronger long-period motions in the direction normal to fault strike.

For this study, fault rupture directivity effects for strike-slip faults were accounted for in a manner consistent with DSOD's guidelines (Fraser and Howard, 2002) as follows:

- The directivity effects were applied to the average response spectrum (with no directivity) developed at the appropriate statistical level of design for the project;
- The Somerville et al. (1997) near-source factors, as modified by Abrahamson (2000), were used to develop spectra for average directivity effects and for the fault-normal and fault-parallel components. The portion of the fault that ruptures towards the site was assumed to be 40% of the total rupture length.
- The spectrum for the fault-parallel component was assumed to be no lower than the spectrum for the average component without directivity

The effects of directivity on the duration of strong shaking were accounted for through the selection of time histories for analysis.

6.3.5 Design Response Spectra

The design response spectra for the dam were developed from the results of the deterministic analysis, modified for fault rupture directivity effects. Figures 6-4 and 6-5 show the mean 84th-percentile horizontal acceleration response spectra for MCEs on the Hayward and San Andreas faults, respectively. These figures also show the response spectra modified for average, fault-normal, and fault-parallel directivity. Figure 6-4 illustrates that the fault-parallel response spectrum calculated for the MCE on the Hayward fault is similar to that without directivity effects. For the MCE on the San Andreas fault, however, the calculated fault-parallel response spectrum is higher than the average spectrum without directivity effects (see Figure 6-5).

Because the longitudinal axis of the dam is oriented at about 45° with respect to the strike of the Hayward and San Andreas faults, we recommend that the spectrum corresponding to the average directivity effects be used for dynamic stability analysis of the dam. The recommended spectral values are tabulated in Table 6-4. The recommended response spectra are applicable to a free-field rock condition and a damping value of 5 percent.

The response spectrum for the MCE on the San Andreas fault is lower than that for the Hayward fault. However, the MCE on the San Andreas fault has a larger magnitude (M_w 8.0) and will produce longer duration shaking.

6.4 SPECTRUM-COMPATIBLE ACCELERATION TIME HISTORIES

Acceleration time histories were developed for each recommended design response spectrum. The time histories were selected from a database of past earthquake records and then modified to match the recommended design response spectra.

To evaluate the sensitivity of the dam's dynamic analysis to the time history details, two acceleration time histories were developed for the Hayward fault MCE. The time histories were based on the 270-degree and the 0-degree components of the Lucerne Valley record of the 1992 Landers earthquake. The 360-degree component of the Carlo record from the 2002 Denali earthquake was used for the San Andreas fault MCE. The key characteristics of the recorded time histories are shown in Table 6-5. The recorded acceleration, velocity and displacement time histories and the corresponding 5%-damped acceleration response spectra are plotted in Figures 6-6 through 6-11.

The selected recorded time histories were modified so that their spectra after modification closely match the recommended spectra for each MCE. The records were modified using the procedures developed by Lilhanand and Tseng (1988), as modified by Abrahamson (1993).

In matching the time histories to the target spectra, the following criteria were used:

- For each time history, and over the period range of interest (0.2 to 1.0 seconds), the average of the ratios of the spectral accelerations for the modified time history to the corresponding target spectral accelerations should be approximately equal to 1.0.
- The spectrum for each time history should not be more than about 15 percent lower than the target spectrum at any period over the period range of interest (0.2 to 1.0 seconds).

The recommended time histories and comparisons between their response spectra and the target spectra are shown in Figures 6-12 through 6-16. Figures 6-12 and 6-13 show the two recommended time histories for the Hayward fault MCE. The spectra for those time histories are compared with the target spectrum in Figure 6-14. Figure 6-15 shows the recommended time history for the San Andreas fault MCE. Its spectrum is compared with the target spectrum in Figure 6-16. As shown in Figures 6-14 and 6-16, the spectra for the recommended time histories match the target spectra reasonably well.

**Table 6-1
Earthquake Sources Affecting Chabot Dam**

Fault	Maximum Magnitude, M_w	Site-to-source Distance, km	Activity³
Hayward-Rodgers Creek	7 ¼	0.5	Active
Miller Creek	6 ¼	4	Active
Contra Costa Shear Zone ¹	6 ½	6	Conditionally Active
Northern Calaveras	7	13	Active
Mt. Diablo Thrust	6 ¾	15	Active
Contra Costa Shear Zone ²	6 ½	17	Conditionally Active
Concord-Green Valley	6 ¾	24	Active
San Andreas	8	30	Active
Greenville	7	33	Active
San Gregorio-Seal Cove	7 ½	41	Active

Note:

- (1) Cull Canyon-Lafayette-Reliz Valley Faults.
- (2) Lineament zones, northern East Bay hills.
- (3) Defined in accordance with DSOD guidelines.

**Table 6-2
Selected Attenuation Relationships**

Attenuation Relationship	Definitions		Limits of Applicability		Site Condition
	Magnitude	Distance	Magnitude	Distance	
Abrahamson and Silva (1997)	M_w^1	R_{rup}^2	(see note 4)	(see note 4)	Rock
Sadigh et al. (1997)	M_w^1	R_{rup}^2	$4.0 \leq M_w \leq 8+$	$R_{rup} \leq 100$ km	Rock
Boore et al. (1997)	M_w^1	R_{jb}^3	$5.5 \leq M_w \leq 7.5$	$R_{jb} \leq 80$ km	$V_s=700$ m/s

Note:

- 1 = Moment magnitude.
- 2 = Closest distance to rupture surface.
- 3 = Closest horizontal distance to vertical projection of rupture surface.
- 4 = Not stated by the authors of the relationship; assumed applicable up to M_w 8+, and to the site-to-source distances, based on range of data used for its development.

**Table 6-3
Calculated Horizontal Peak Ground Acceleration**

MCE	M _w	Distance, km	Calculated 84 th -% Horizontal Peak Ground Acceleration, g			
			AS 97	SD 97	BR 97	Mean
Hayward-Rodgers Creek	7¼	0.5	1.25	1.09	0.81	1.05
San Andreas	8.0	30	0.32	0.35	0.32	0.33

Note:

AS 97 = Abrahamson and Silva (1997)

SD 97 = Sadigh et al. (1997)

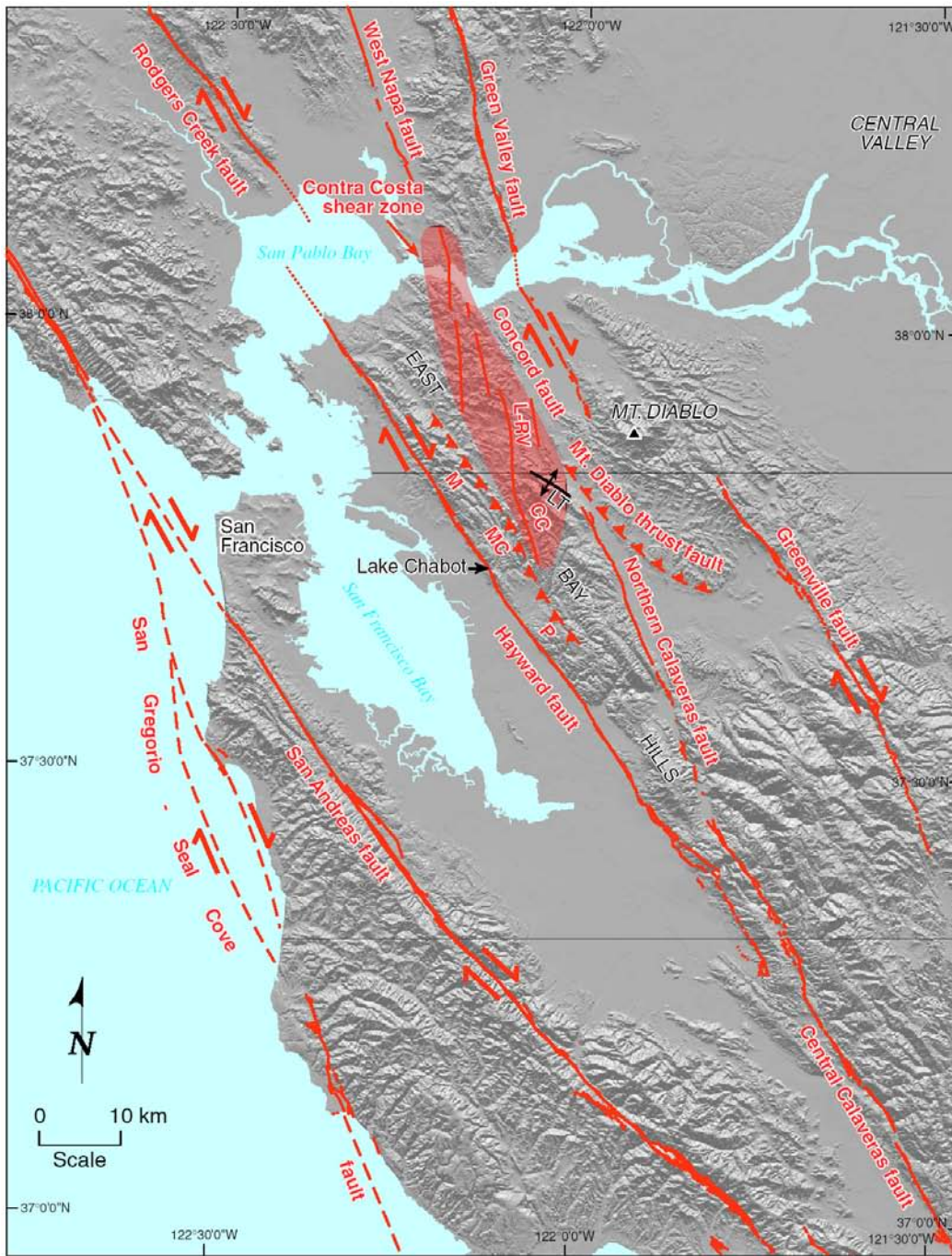
BR 97 = Boore et al. (1997)

**Table 6-4
Recommended Design Response Spectral Values**

Period, seconds	Recommended Design Response Spectral Values, g	
	Hayward-Rodgers Creek Fault	San Andreas Fault
PGA	1.046	0.331
0.02	1.046	0.331
0.05	1.493	0.390
0.075	1.779	0.444
0.10	2.050	0.518
0.15	2.411	0.644
0.20	2.545	0.718
0.30	2.442	0.751
0.40	2.257	0.727
0.50	2.037	0.680
0.75	1.672	0.588
1.0	1.404	0.528
1.5	0.954	0.418
2.0	0.696	0.344
3.0	0.428	0.227
4.0	0.295	0.164

**Table 6-5
 Earthquake Records Used to Develop Time Histories
 for Hayward-Rodgers Creek Fault and San Andreas Fault MCEs**

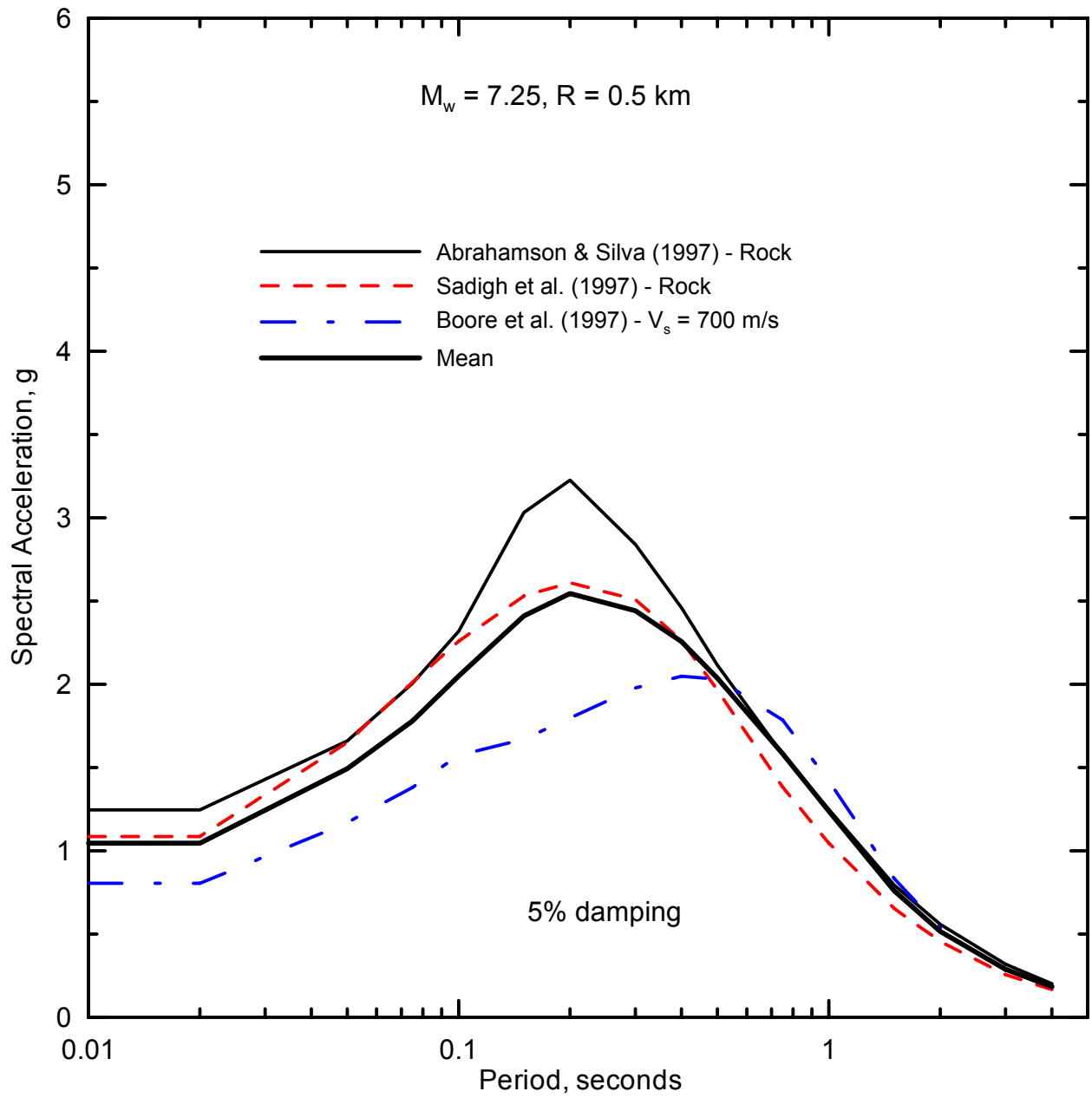
Earthquake	M _w	Recording Station			Component
		Station	Distance (km)	Site Condition	
Hayward fault MCE					
1992 Landers, California	7.3	Lucerne Valley	2	6m Decomposed Granite	270-deg
					0-deg
San Andreas fault MCE					
2002 Denali, Alaska	7.9	Carlo, Alaska Station	64	Shallow Alluvium over Rock	360-deg



Explanation		
	Strike-slip fault	
	Thrust or reverse fault (teeth on hanging wall; dashed where blind or approximately located)	
	Anticline	
	L-RV Lafayette-Reliez Valley faults	MC Miller Creek fault
	CC Cull Canyon fault	P Palomares fault
	M Moraga fault	LT Las Trampas anticline
	Faults and lineaments of the Contra Costa shear zone	

	Project No. 26814536	Seismic Sources Map	Figure 6-1
	Chabot Dam Seismic Stability		

x:\x_geo\chabot dam\Task G -- Engineering Report\Figures\Figure 6-1.grf



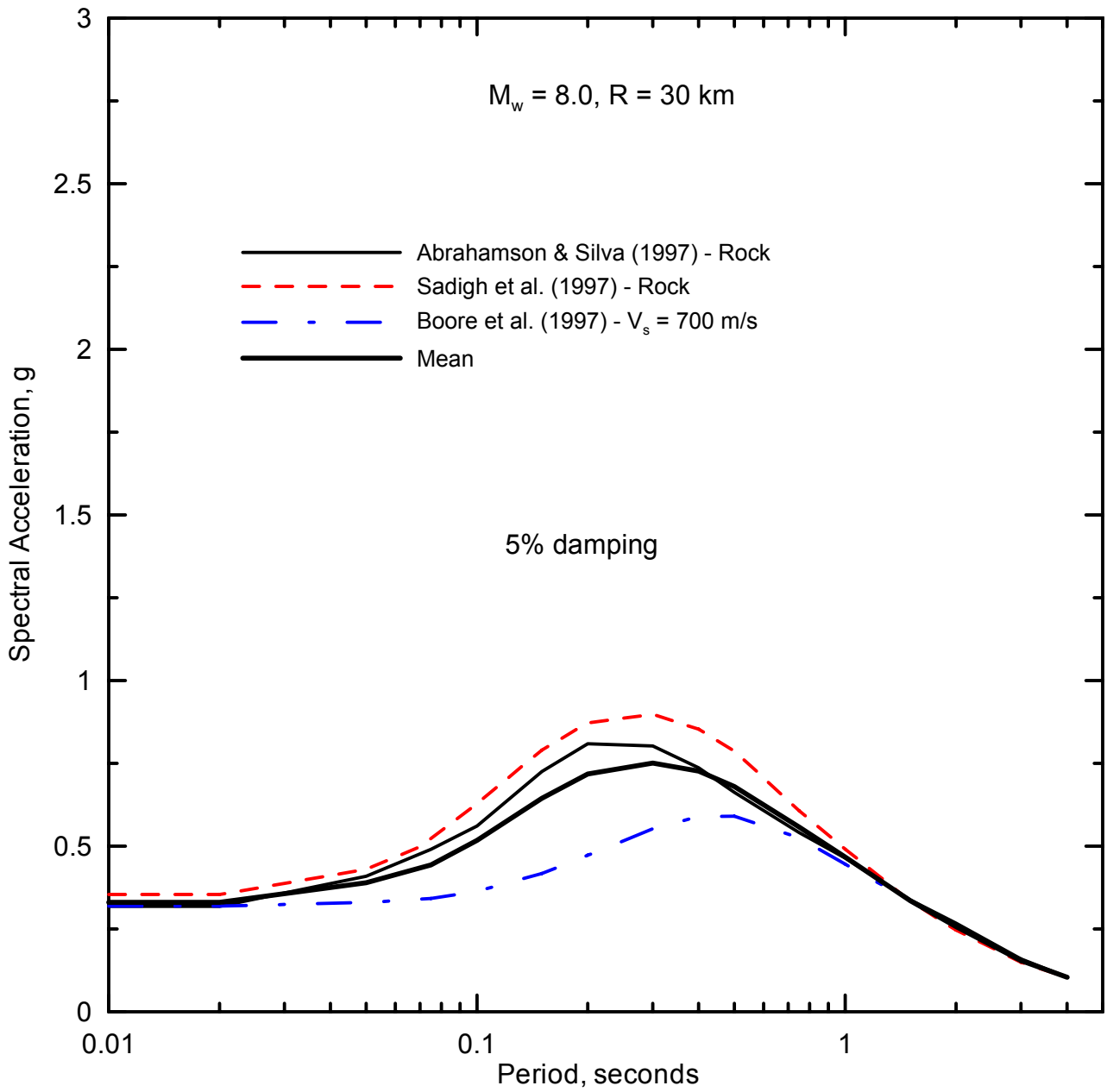
Project No. 26814536

Chabot Dam
Seismic Stability

Calculated 84th-percentile Acceleration Response
Spectra for Hayward-Rodgers Creek Fault MCE

Figure

6-2

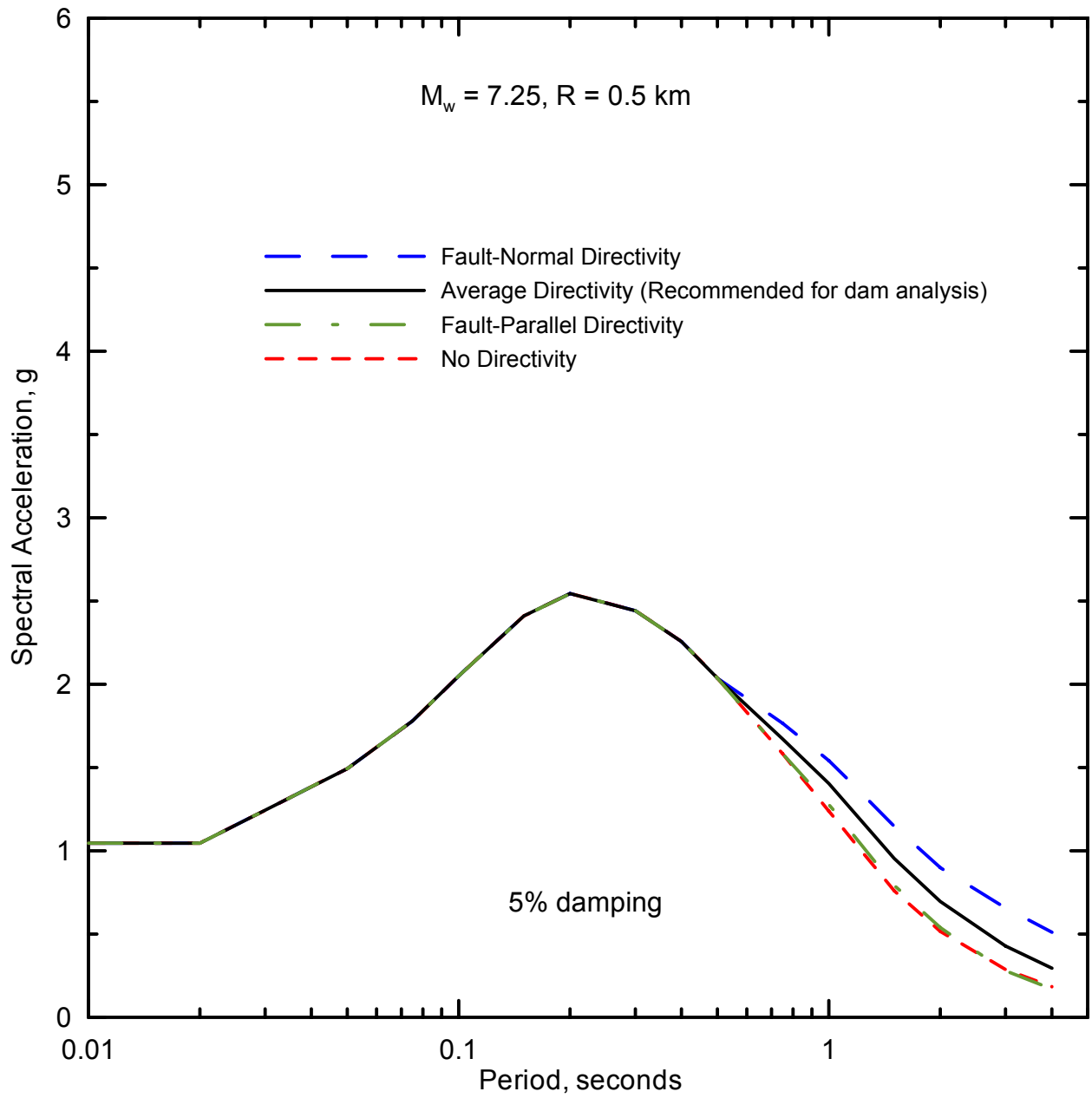


Project No. 26814536

Chabot Dam
Seismic Stability

Calculated 84th-percentile Acceleration Response
Spectra for San Andreas Fault MCE

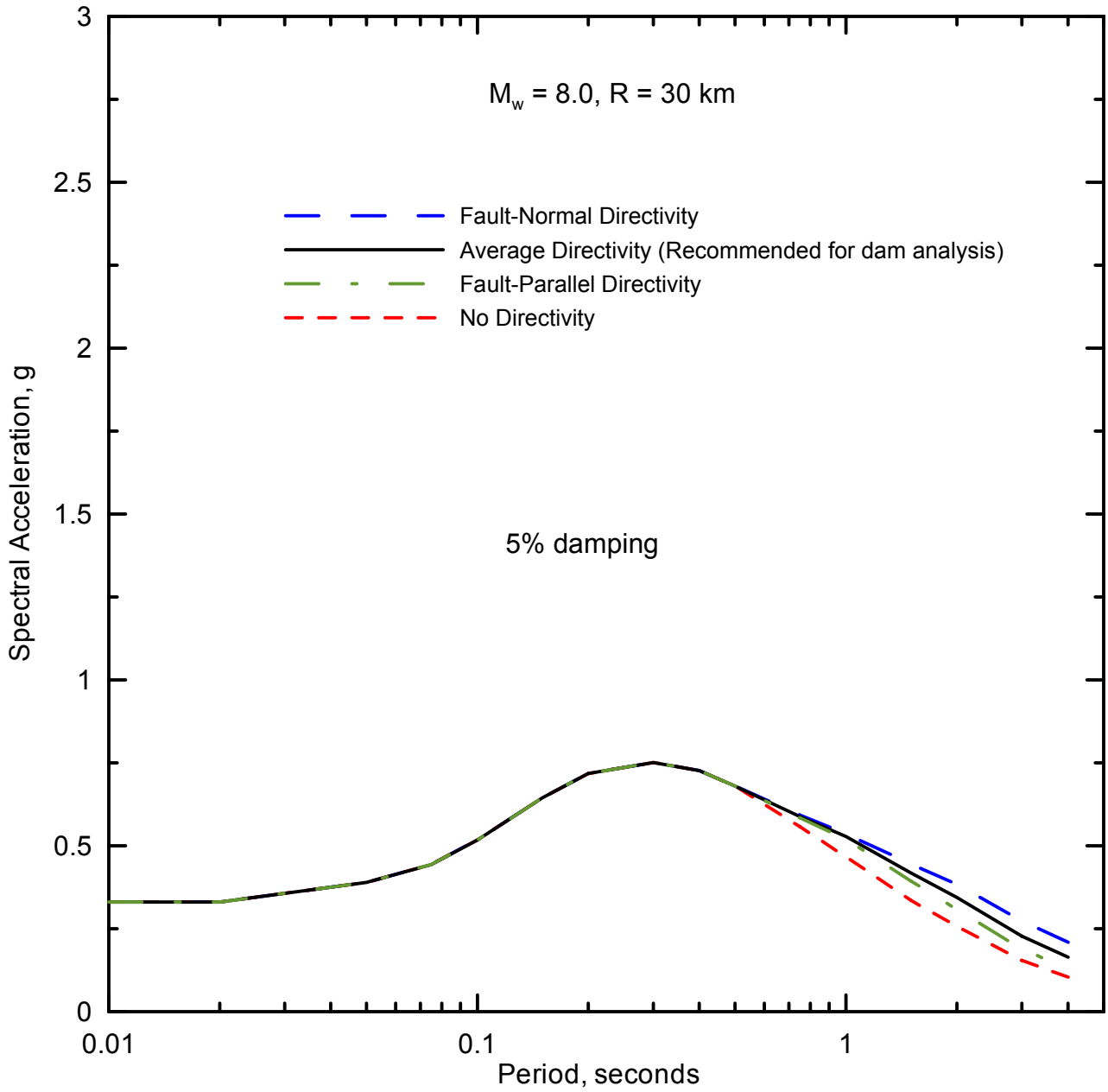
Figure
6-3



Project No. 26814536
 Chabot Dam
 Seismic Stability

**Design Acceleration Response Spectra
 for Hayward-Rodgers Creek Fault MCE**

Figure
 6-4



Project No. 26814536

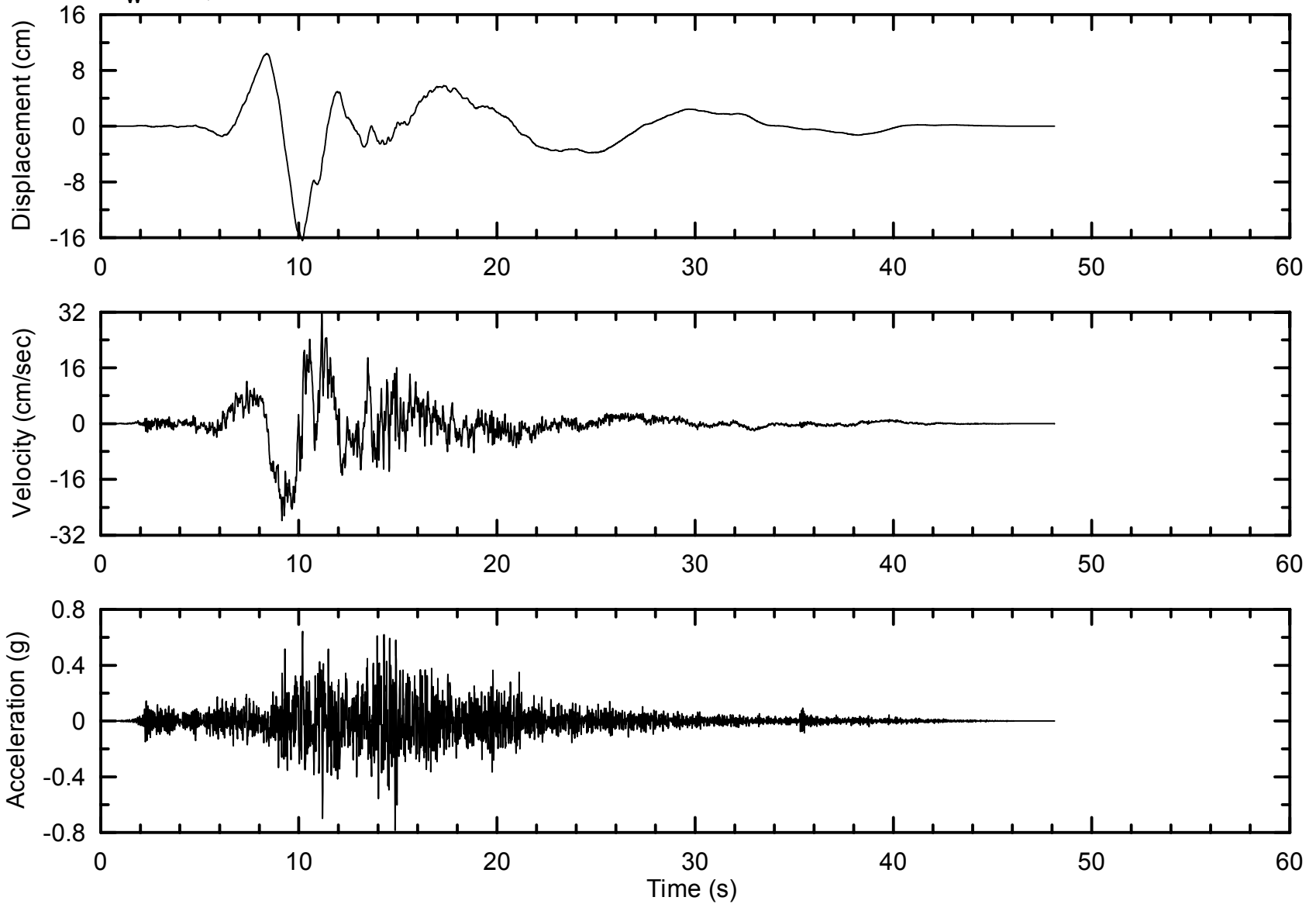
Chabot Dam
Seismic Stability

**Design Acceleration Response
Spectra for San Andreas Fault MCE**

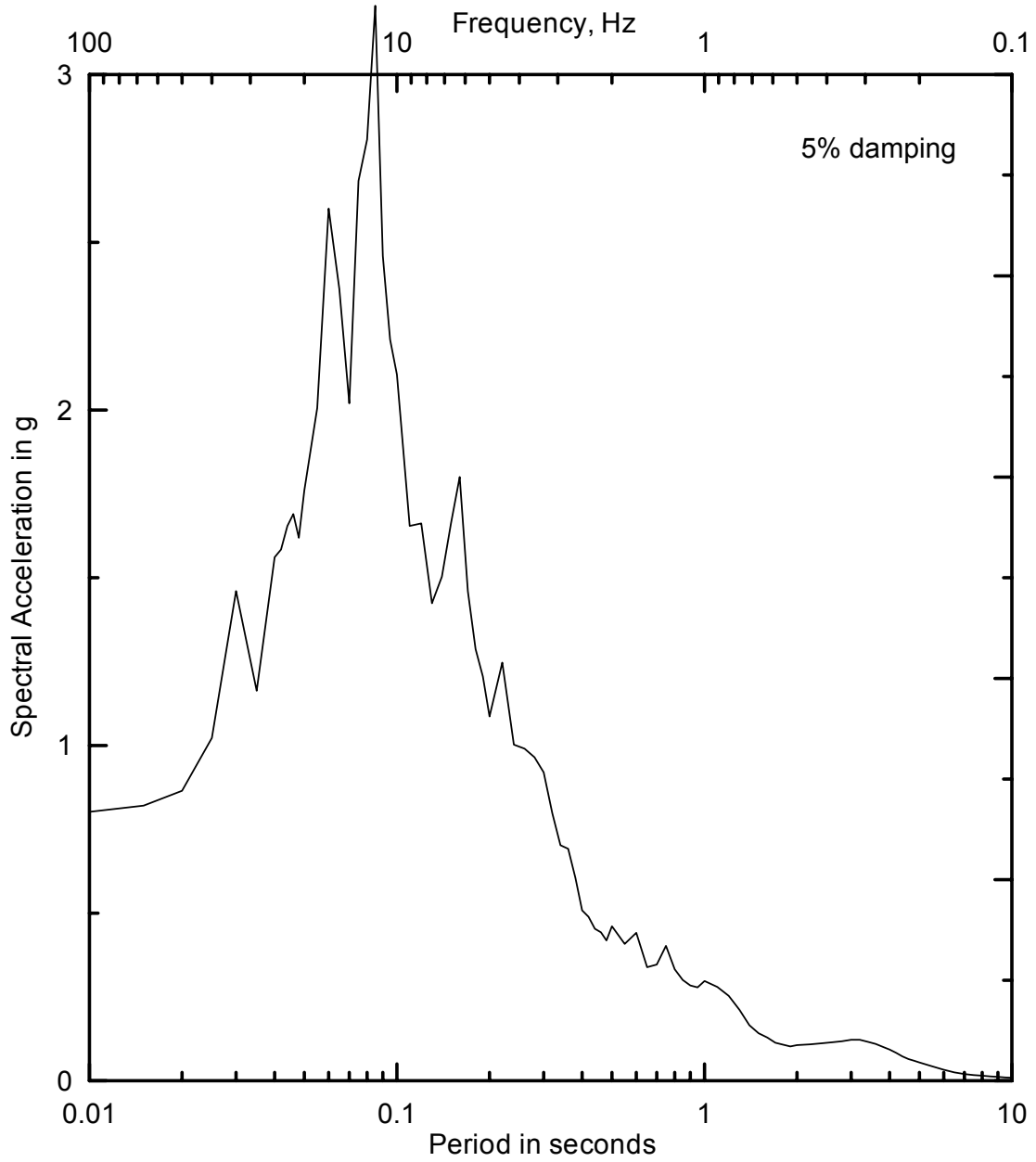
Figure

6-5

1992 Landers, CA Earthquake Time History
 at Lucerne Valley Station,
 $M_W = 7.3$, $R = 2.0$ km



Project No. 26814536	Chabot Dam Seismic Stability	Recorded Time History 1992 Landers, CA Earthquake at Lucerne Valley Station, Horizontal Component, 000 deg.	Figure 6-6
URS			



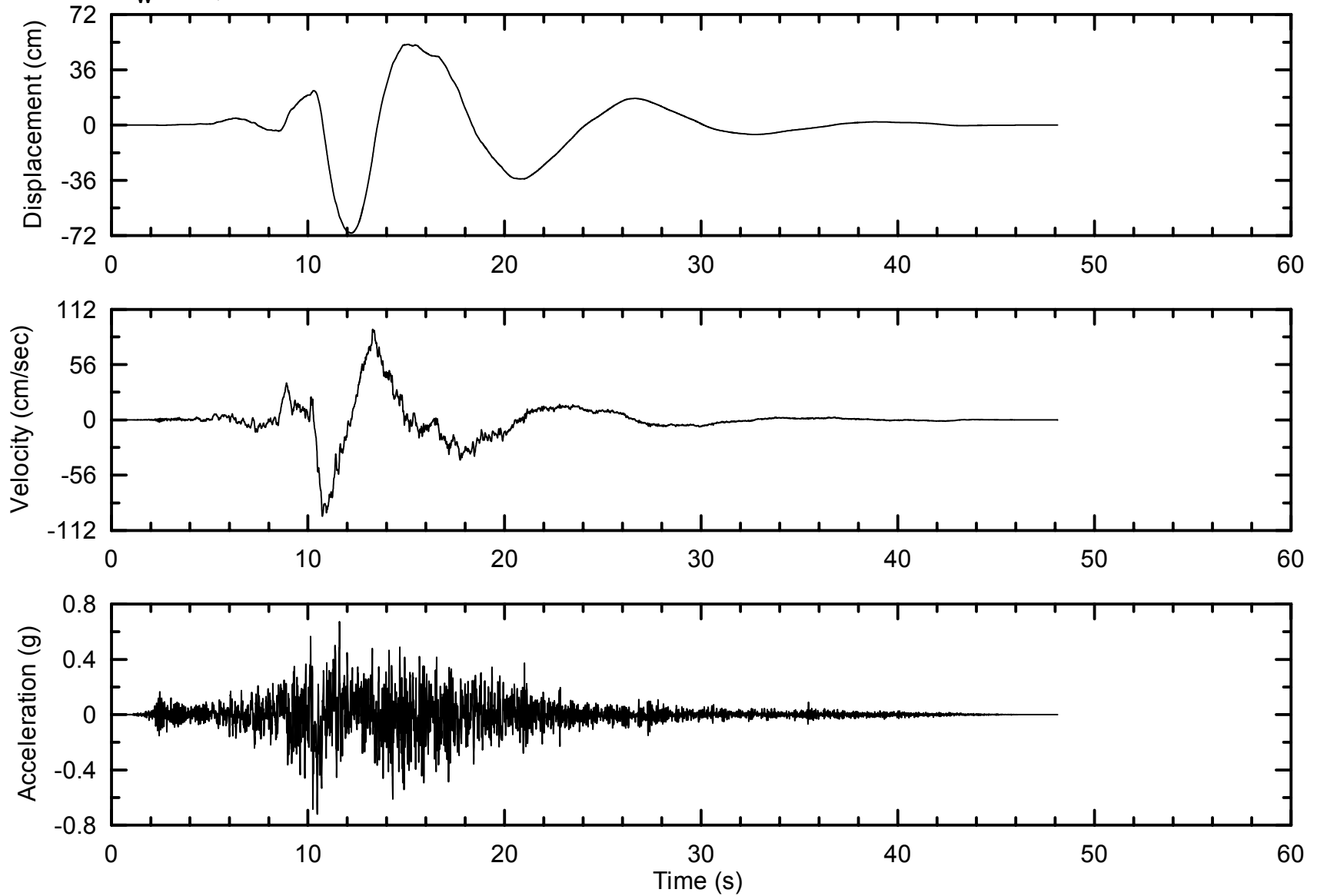
Project No. 26814536

Chabot Dam
Seismic Stability

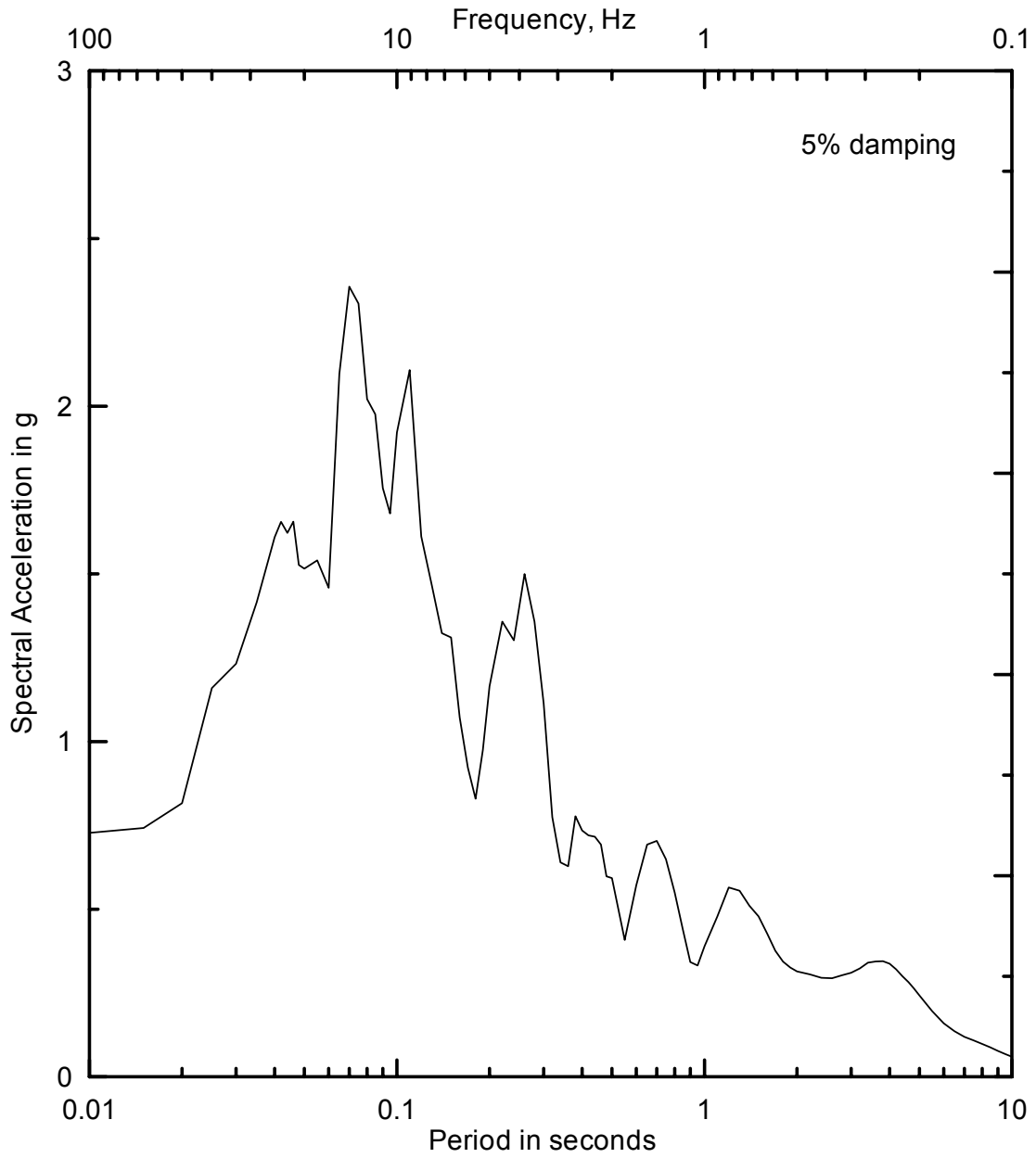
**Acceleration Response Spectra
1992 Landers, CA Earthquake at Lucerne
Valley Station, Horizontal Component 000 deg.**

Figure
6-7

1992 Landers, CA Earthquake Time History
 at Lucerne Valley Station,
 $M_w = 7.3$, $R = 2.0$ km

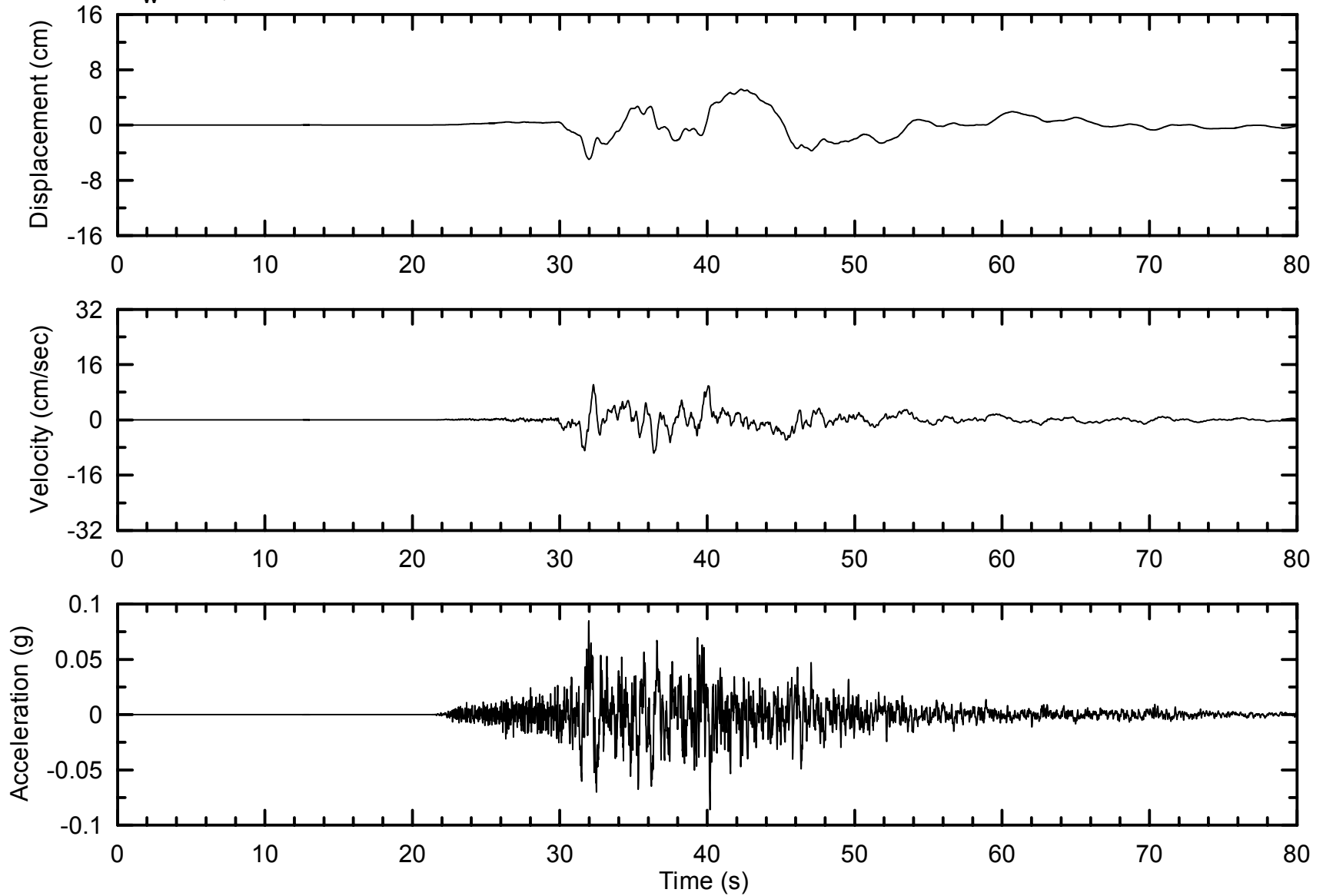


Project No. 26814536	Chabot Dam Seismic Stability	Recorded Time History 1992 Landers, CA Earthquake at Lucerne Valley Station, Horizontal Component, 270 deg.	Figure 6-8
URS			



URS	Project No. 26814536	Acceleration Response Spectra 1992 Landers, CA Earthquake at Lucerne Valley Station, Horizontal Component 270 deg.	Figure
	Chabot Dam Seismic Stability		6-9

2002 Denali, Alaska Earthquake Time History
 Recorded at Carlo, Alaska Station,
 $M_W = 7.9$, $R = 64$ km



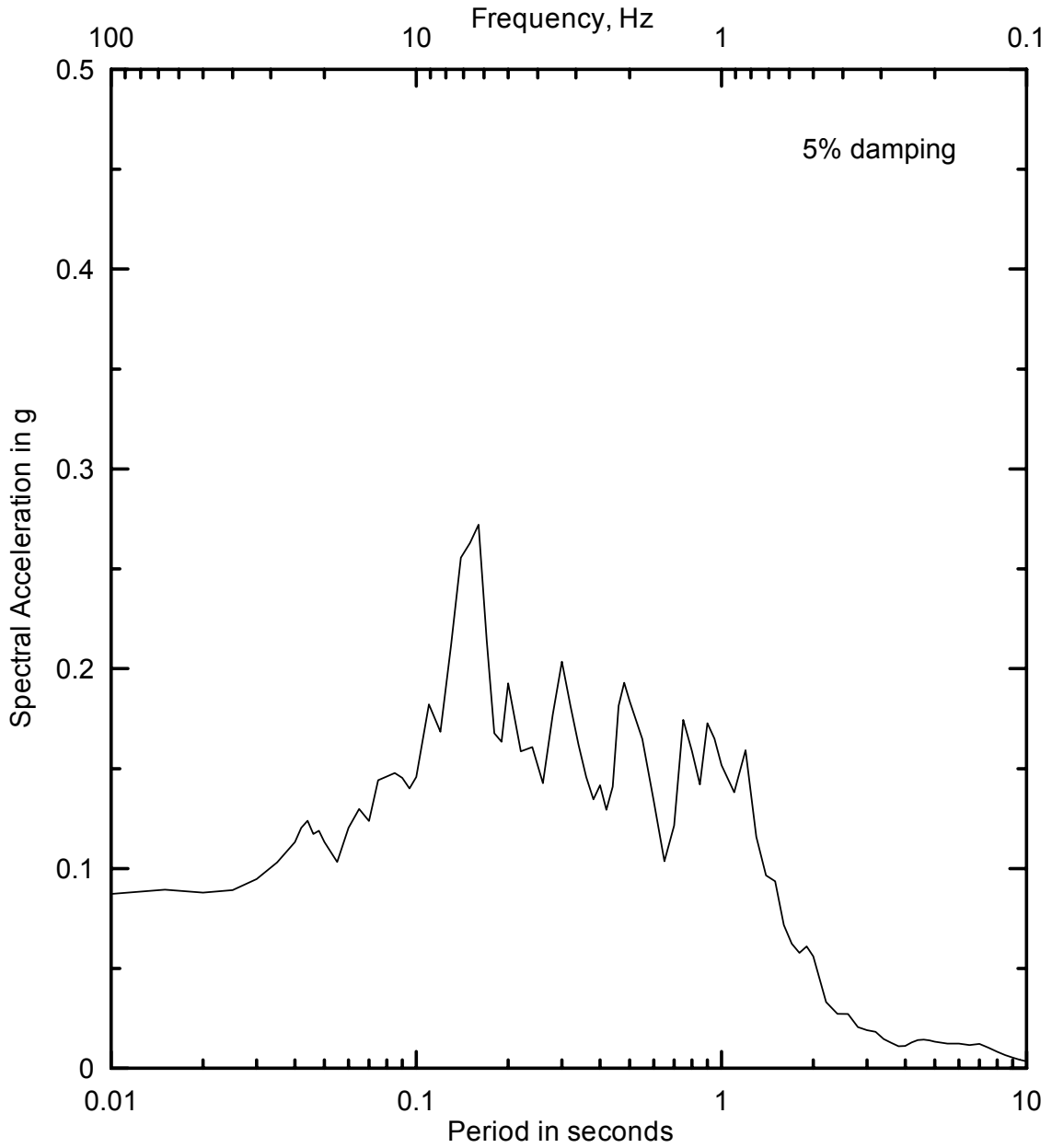
Project No.
26814536

Chabot Dam
Seismic Stability

Recorded Time History
2002 Denali, Alaska Earthquake
at Carlo, Alaska Station,
Horizontal Component, 360 deg.

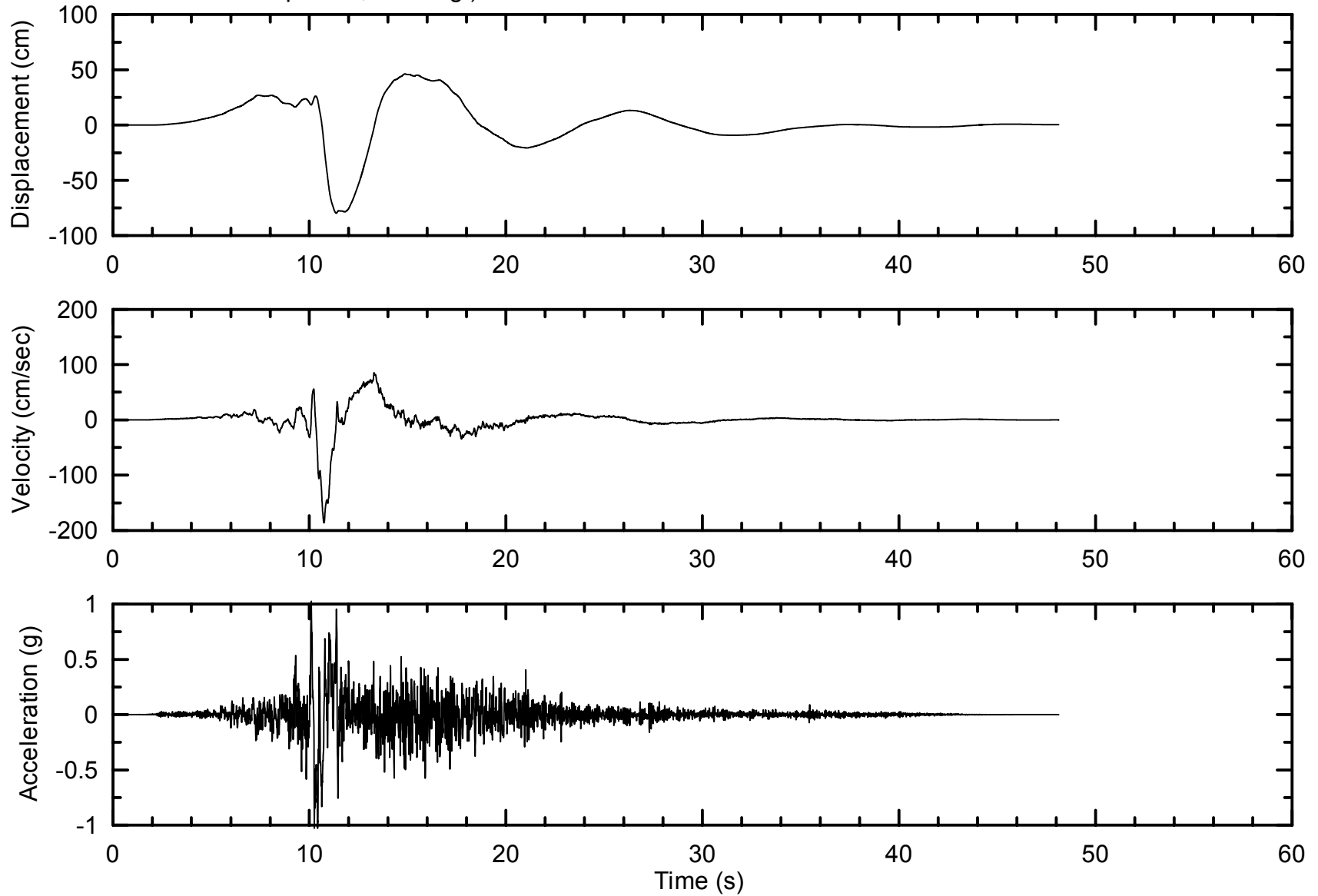
Figure
6-10

URS



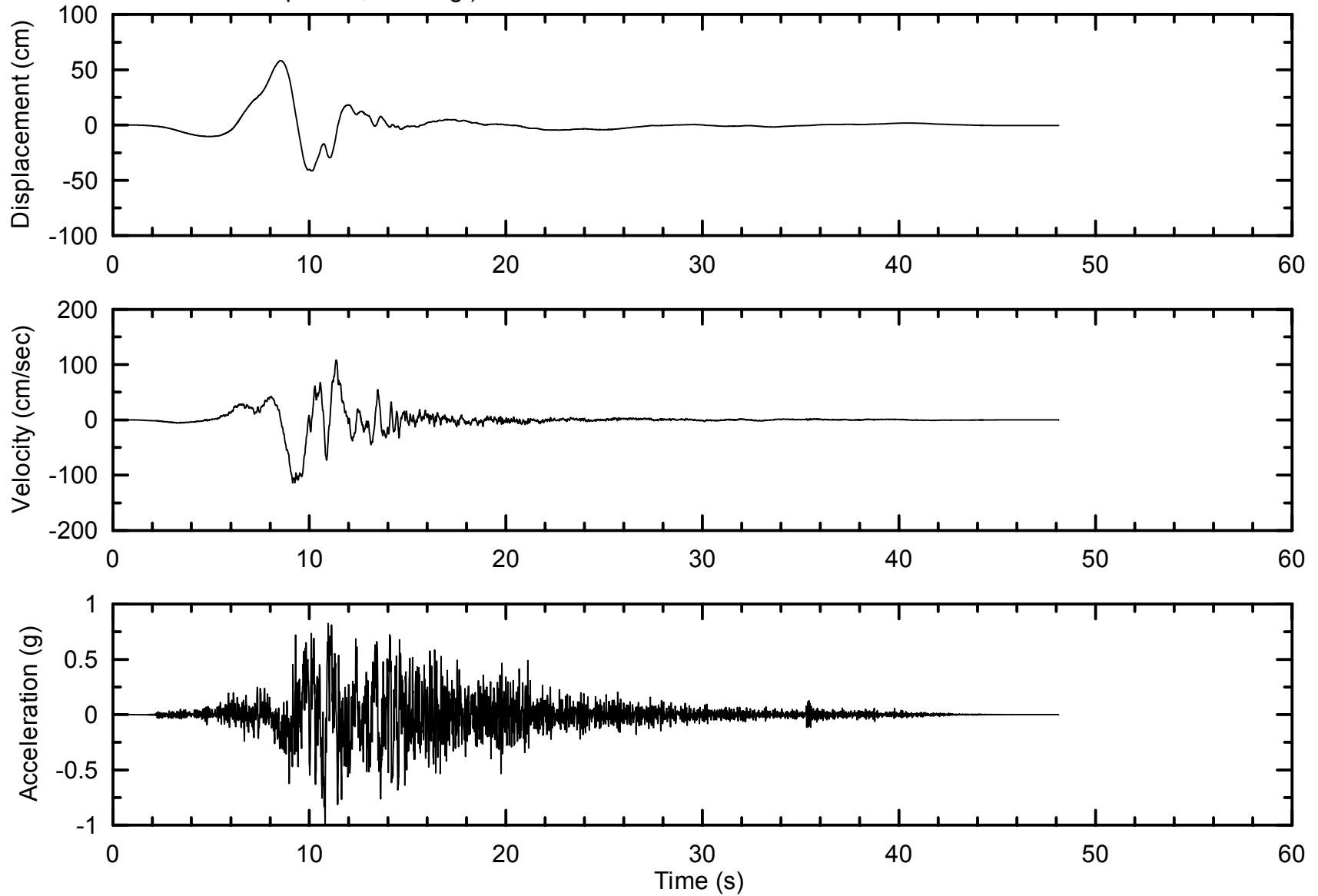
URS	Project No. 26814536	Acceleration Response Spectra 2002 Denali, Alaska Earthquake at Carlo, Alaska Station, Horizontal Component 360 deg.	Figure
	Chabot Dam Seismic Stability		6-11

Hayward - Rodgers Creek Fault Event - Recommended Time History No.1
 (Modified from 1992 Landers, CA Earthquake - Lucerne Valley Station,
 Horizontal Component, 270 deg.)

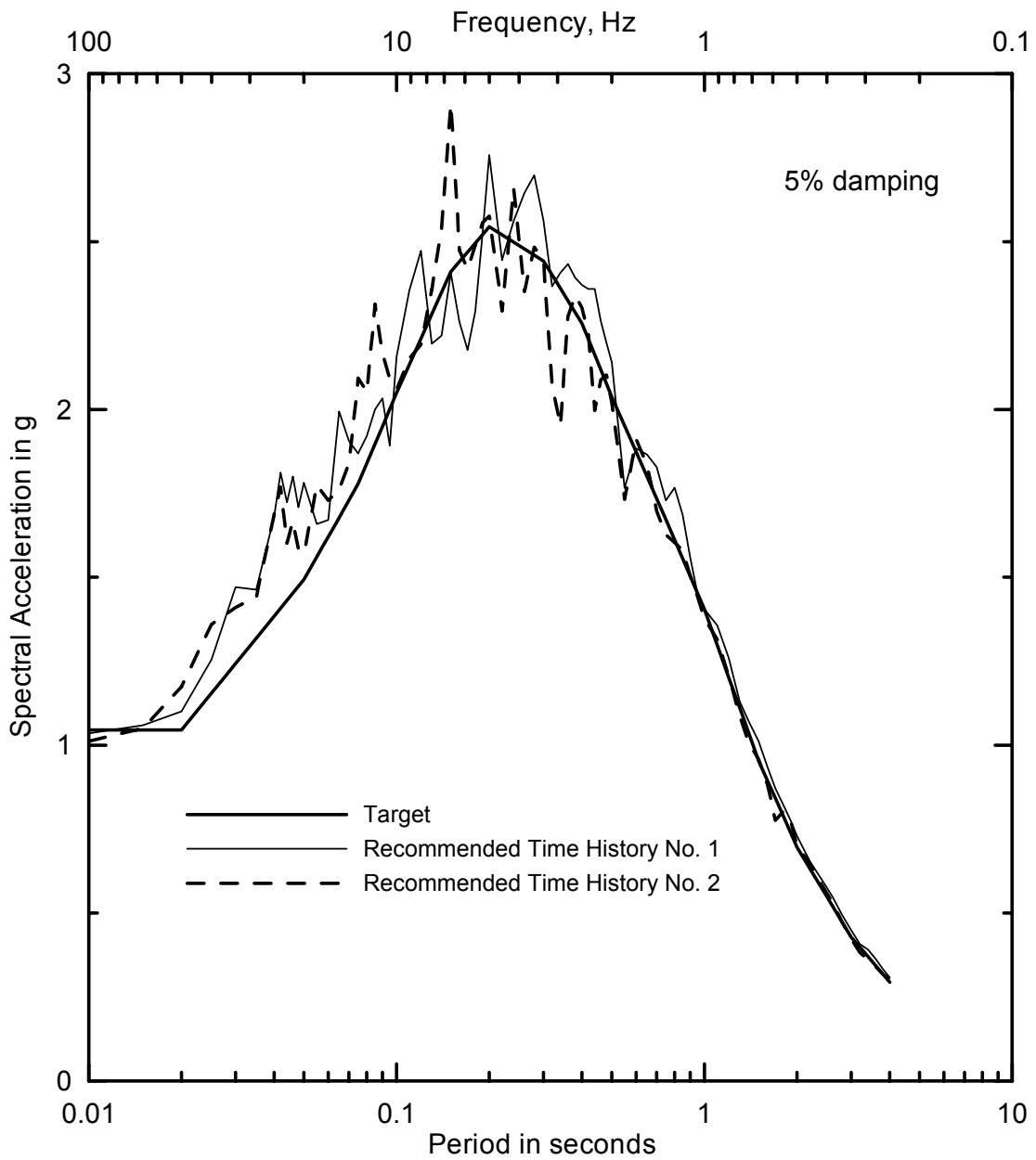


Project No. 26814536	Chabot Dam Seismic Stability	Hayward - Rodgers Creek Fault MCE Recommended Time History No.1	Figure 6-12
URS			

Hayward - Rodgers Creek Fault Event - Recommended Time History No.2
 (Modified from 1992 Landers, CA Earthquake - Lucerne Valley Station,
 Horizontal Component, 000 deg.)



Project No. 26814536	Chabot Dam Seismic Stability	Hayward - Rodgers Creek Fault MCE Recommended Time History No.2	Figure 6-13
URS			



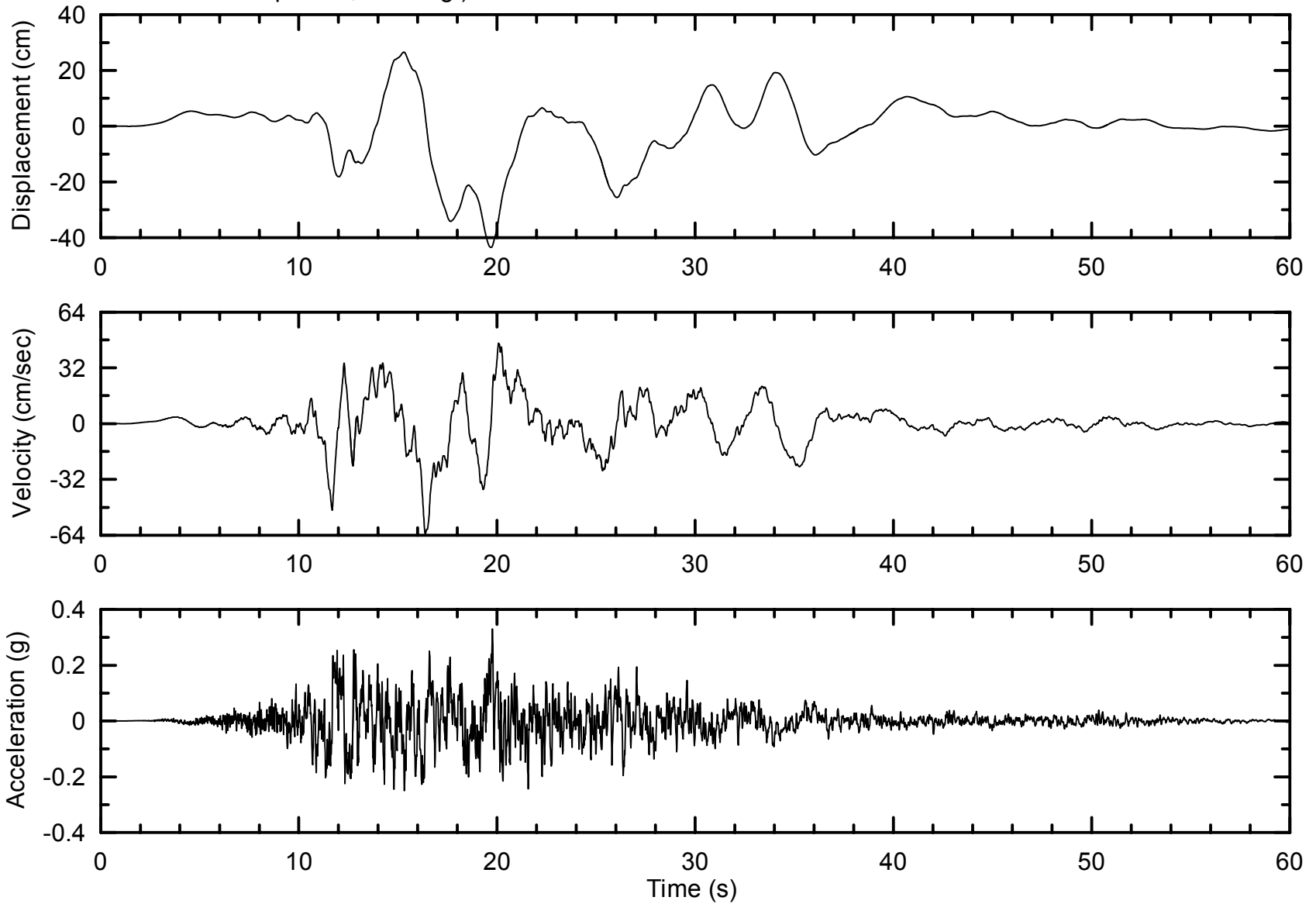
Project No. 26814536

Chabot Dam
Seismic Stability

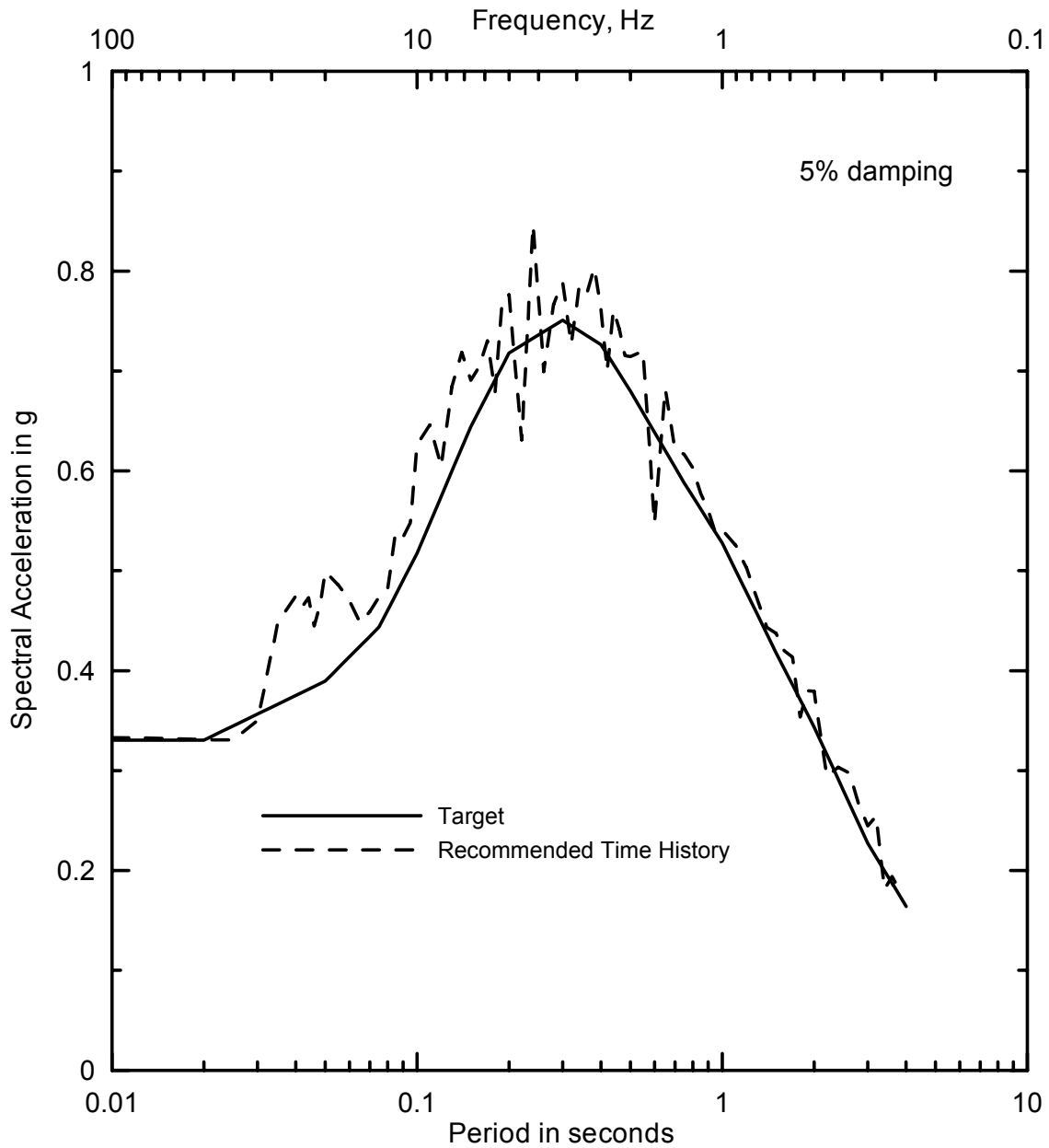
**Comparison of Acceleration Response
Spectra for Hayward-Rodgers Creek Fault MCE**

Figure
6-14

San Andreas Fault Event - Recommended Time History
 (Modified from 2002 Denali, Alaska Earthquake - Carlo, Alaska Station,
 Horizontal Component, 360 deg.)



Project No. 26814536	Chabot Dam Seismic Stability	San Andreas Fault MCE Recommended Time History	Figure 6-15
URS			



Project No. 26814536

Chabot Dam
Seismic Stability

**Comparison of Acceleration Response
Spectra for San Andreas Fault MCE**

Figure
6-16

This section presents the geotechnical characterization of the embankment and foundation conditions. The characterization consisted of three main elements: 1) identifying the material zones that make up the embankment and foundation, 2) characterizing their engineering properties, and 3) defining the groundwater conditions and location of the phreatic surface for analysis. This work was based on the field and laboratory investigations conducted as part of this study, and on the data from previous investigations of the dam. Piezometric data provided by EBMUD were used in characterizing the groundwater conditions within the dam. The locations of the borings and piezometers used to characterize the site conditions are shown in Figure 7-1, along with the locations of three cross-sections used to illustrate the dam conditions .

As part of the geotechnical characterization work, the subsurface data were incorporated into a 3-D GIS model. The GIS model helped visualize the 3-D geometry of the dam, as well as the spatial distribution of the borings and SPT sampling, soil classifications, and foundation soil thickness. A graphical view of the model is presented in Figure 7-2. The electronic data for the model were previously submitted to EBMUD in the form of shape files. Additional details on the GIS model are presented in Appendix I.

7.1 DAM MATERIALS AND ZONATION

The dam consists mainly of the following materials: the wagon fill placed between 1874 and 1875, the sluiced fill placed between 1875 and 1888, additional fill placed between 1890 and 1892, and modern fill and random fill placed in 1980.

In order to develop a model of the material zonation in the dam and foundation, three interpretive cross-sections were prepared based on data from selected borings in the GIS model and on topographic data obtained at various times in the dam's history. These sections are shown in Figures 7-3, 7-4 and 7-5. Some zone boundaries cannot be located with certainty, for example the contact between the wagon fill and the sluiced fill in the downstream shell. As shown in Figure 7-3, boring WI-20 contains a significant portion of sandy and gravelly material that could potentially be sluiced fill. The interpretive sections shown in these figures present a best estimate of the zonation within the dam embankment and foundation. The uncertainty regarding the boundary between the sluiced fill and wagon fill is further discussed in Section 9.

A small amount of reservoir silt was encountered in the upstream toe area of the embankment in the reservoir borings. However, since this material is light in weight and has very low shear strength, it was modeled as part of the reservoir. There is some uncertainty about the upstream boundary between the wagon fill and the reservoir silt, and the interpretive cross sections show the best estimate based on the available data. The dam foundation can be zoned into foundation soil and bedrock. The geotechnical characteristics and engineering properties of the embankment and foundation materials are described in the following sections and summarized in Tables 7-1 through 7-4.

7.2 EMBANKMENT CONDITIONS

7.2.1 Wagon Fill

General Characteristics

The wagon fill materials were reportedly selected from nearby sources so as to have sufficient clay to “bind and pack” and were placed in one-foot layers, sprinkled with water, and compacted by horse and wagon traffic. The records suggest that the materials were placed selectively to form a clay core, and that a core trench 10 to 30 feet deep and 40 to 90 feet wide was excavated to bedrock along the dam axis. The wagon fill was placed in at last two separate phases, in the 1870s and 1890s.

As shown in Figures 7-3 and 7-4, the boring data suggest that clayey soils are in fact more predominant in the central portion of the wagon fill, at least in the upper part of the embankment above about Elevation 200. Thus, the wagon fill can be separated into three subzones, consisting of the upstream wagon fill, downstream wagon fill, and central wagon fill. However, the available data indicate that the overall material characteristics and engineering properties of the wagon fill are relatively similar from upstream to downstream.

Gradation and Plasticity

The wagon fill consists primarily of clayey sands and sandy clays, with gravel. The gradations of wagon fill samples obtained in the downstream shell, upstream shell and crest borings are shown in Figures 7-6 through 7-8, respectively. These figures show that the wagon fill materials have a broad range of gradations, with similar ranges for all locations.

Pockets of gravels and sands and silty sands were also occasionally found in the wagon fill. The log of boring WI-20 suggests that there is a zone of gravelly sands present near the downstream limit of the wagon fill (Figure 7-3). However, no laboratory gradations were obtained on the materials to confirm the field logs. Based on the material descriptions in the field logs, it is possible that this boring encountered the sluiced fill. It is also possible that the boring encountered a granular pocket within the wagon fill, given the high densities measured in the soil samples.

The gravel contents of the wagon fill materials are plotted against elevation in Figures 7-9 and 7-10. Figure 7-9 shows the data from this investigation, whereas Figure 7-10 shows data from previous investigations. The wagon fill materials have gravel contents up to about 40%, and there is good agreement between the data from this and previous investigations. Although the observed gravel contents are not high enough to control the behavior of the materials under shear, they are sufficiently high to impact SPT blow counts.

The fines contents of the wagon fill materials from current and previous investigations are plotted in Figures 7-11 and 7-12, respectively. The fines contents generally range from about 15 to 70% and average about 40%. Because of the broadly graded nature of the materials, the fines contents are expected to control the overall material behavior under shear and cyclic loading. The results of Atterberg limits tests from this and previous investigations, shown in Figures 7-13 and 7-14, indicate that the fines typically are of medium plasticity. Figure 7-15 indicates that the plasticity of the fines is about the same for the clayey sands and sandy clays.

Figures 7-16 and 7-17 show the plasticity index and liquid limit of the materials plotted against elevation. The plasticity index for the wagon fill generally ranges from about 10 to 25 and the liquid limit ranges from about 25 to 45. These ranges are roughly constant with elevation, and are consistent with the data from previous investigations.

Density and Moisture Content

Figures 7-18 and 7-19 present dry unit weight data for the wagon fill materials from this and previous investigations, respectively. The data from the current investigation show a relatively uniform range of dry densities with elevation whereas the data from previous investigations show a wider range, a lower average, and a trend of decreasing dry density above Elevation 200. These differences are probably associated with the following factors: 1) the data from previous investigations includes a larger number of samples taken at higher elevations near the spillway where predominantly clayey materials were placed at higher water contents, and 2) the data from previous investigations were mainly from 2-inch diameter samples while the data from the current investigation came from 2.8-inch and 2.5-inch diameter samples, which have less disturbance. Similar trends are illustrated in Figures 7-20 and 21, which present moisture content data. An apparent higher average moisture content above Elevation 200 is visible by comparing the data from previous investigations with the current investigation data. Figure 7-22 shows that the total unit weight of the wagon fill materials ranges between about 120 and 145 pounds per cubic foot (pcf) and is relatively uniform with elevation.

Shear Strength

As part of this investigation, 12 isotropically consolidated-undrained (ICU) triaxial strength tests with pore pressure measurements were performed on 2.8-inch-diameter Pitcher barrel samples of the wagon fill. These data were combined with data from the previous investigations and were used to evaluate the shear strength of the wagon fill materials.

Figure 7-23 shows the results of the tests from this investigation, plotted in terms of effective stress-path parameters at 10% axial strain. In the figure, the data are identified by sample location (C=crest, DS=downstream shell, US=upstream shell) and type of material. The data for clayey sands (SC) and sandy clays (CL) fall within a narrow range regardless of location. The data supports using the same effective shear strength parameters for the central, upstream, and downstream portions of the wagon fill. The test results are best represented by an effective stress friction angle of 30°.

The results of the tests in terms of total stress-path parameters are shown in Figure 7-24. Again, the data supports using the same total strength parameters for the central, upstream, and downstream portions of the wagon fill. The test results can be represented by a total friction angle of 21.5° and a cohesion intercept of 200 pounds per square foot (psf).

The results of the previous ICU and anisotropically consolidated-undrained (ACU) triaxial tests conducted on the wagon fill during the 1965 Shannon & Wilson study are compared with the results from the current ICU tests in Figures 7-25 and 7-26. The results of the previous tests are in good agreement with the data from this investigation. During the Shannon & Wilson study, a large number of ICU tests without pore pressure measurements were also conducted, using samples retrieved with a 2-inch modified California sampler driven by hammer blows. These tests are judged to be unreliable because of sample disturbance. Furthermore, the results can

only be interpreted in terms of total stresses because of the lack of pore pressure measurements. Nonetheless, the results of these tests are compared in Figure 7-27 with the representative total strength parameters selected based on the current tests. As shown, the selected total strength parameters fit reasonably well with the data for most of the CL samples tested, especially at lower confining pressures.

Liquefaction Susceptibility

The fines contents of the wagon fill are sufficiently high such that the behavior of the materials under monotonic shear and cyclic loading is expected to be controlled by the fines fraction. Because of the clayey nature of the fines along with moderate water contents and medium plasticity, the wagon-fill soils are judged not susceptible to liquefaction. This conclusion was reached by applying the modified Chinese criteria proposed by Seed and Idriss (1982) and the criteria recently proposed by Seed et al. (2003). The conclusion is also supported by the criteria recently proposed by Boulanger and Idriss (2004). The criteria proposed by Andrews and Martin (2000) were also considered, but given less weight since recent research (Bray et al., 2001) has shown the content of clay size particles to be an unreliable indicator of liquefaction susceptibility.

As shown in Figure 7-28, the bulk of the sandy clays and clayey sands in the wagon fill are not susceptible to liquefaction, based on comparison of the water content and the liquid limit. On average, the water content of the materials (15 to 25%) is significantly lower than the liquid limit (25 to 45%). Although some pockets of sands and silty sands are present, they are of limited extent and thus, will not affect the overall strength of the wagon fill zone significantly.

Although liquefaction is not expected, the wagon fill materials can develop excess pore pressures during strong earthquake shaking. Such excess pore pressures will result in a reduced undrained strength. The strength loss potential of the material as a result of cyclic loading is discussed in Section 11. The dynamic properties are discussed in Sections 10 and 12.

7.2.2 Sluiced Fill

General

Relatively little information is available regarding the construction of the downstream sluiced fill zone. Reportedly, the sluiced materials were transported by water along a ditch and flume. The sluicing operation reportedly occurred only during the rainy seasons for a number of years. An EBMUD drawing dated 1937 indicates that a retaining dike was built in the stream channel a few hundred feet downstream from the dam to retain the sluicing water and fines.

Gradation and Plasticity

The sluiced fill consists primarily of silty and clayey sands with gravel. Pockets of cleaner sands and gravels and lenses of clays are also present. The gradations of the samples obtained from this investigation in the downstream toe area are shown in Figure 7-29. With exception of a few clay samples, the gradations fall within a relatively narrow band, consistent with placement by sluicing. Figures 7-30 and 7-31 show the fines contents measured in this and previous investigations, respectively. Figures 7-32 and 7-33 show the corresponding gravel contents, and

Figures 7-34 and 7-35 summarize the measured Atterberg limits of the fines fraction. In general, the data on the sluiced fill from this and previous investigations are consistent.

The measured gravel content of the sluiced fill materials generally ranged from about 15 to 35%, based on the samples obtained. The actual gravel contents in-situ may be somewhat higher, since the samplers used cannot representatively sample larger gravels approaching the sampler diameter in size. In contrast with the wagon fill, the fines contents of the granular sluiced fill generally range between about 10 and 25%. Such fines contents are not high enough to control the behavior of the material under shear or cyclic loading. Thus, the sluiced fill is expected to behave predominantly as a granular cohesionless material.

Density and Moisture Content

Few measurements of the sliced fill density and moisture content were performed for this investigation because of sample disturbance. Figures 7-36 and 7-37 summarize the dry unit weights and moisture contents measured in previous investigations. The corresponding total unit weights are shown in Figure 7-38. The dry unit weight of the sluiced fill generally ranges from about 100 to 125 pcf while the moisture content ranges from about 10 to 40% and the total unit weight ranges from about 110 to 145 pcf.

Shear Strength

Because it is difficult to obtain undisturbed samples of the sluiced fill materials, little or no reliable laboratory test data are available on the shear strength of the sluiced fill. A significant number of ICU tests without pore pressure measurements were performed on driven 2-inch modified California samples for the 1965 S&W study. As noted, those tests are of questionable reliability because of sample disturbance. Also, the tests lacked pore pressure measurements and thus do not provide effective strength data.

The insitu test data indicate that the sluiced fill materials are generally loose to medium dense, which is consistent with their method of placement. Based on an average standard penetration test (SPT) blow count N_{60} of about 8, and considering the fines contents, an effective friction angle of about 33° was estimated for the sluiced fill materials. For monotonic loading, total strength parameters corresponding to a cohesion of 350 psf and a friction angle of 32° were estimated based on the S&W tests.

Liquefaction Susceptibility

In view of their granular nature and relatively low fines contents, the sluiced fill materials are considered susceptible to liquefaction when saturated. The liquefaction resistance of the materials and their residual strength after liquefaction are best assessed based on available empirical correlations with SPT resistance (e.g. Seed et al., 2003; Seed and Harder, 1990). The liquefaction potential and residual strength of the sluiced fill are discussed in Section 11. The dynamic properties of the sluiced fill are discussed in Sections 10 and 12.

7.2.3 Modern Fill

Compacted fill was placed on the downstream slope of the embankment to raise the crest during the 1980 dam modifications. The material was obtained primarily from the excavation for the new spillway, and was specified to be free of organics and rocks larger than 6 inches. The specifications also called for at least 89% relative compaction as determined by ASTM D 698 modified to a compaction energy of 20,000 ft-lb/ft³. The results of field control tests indicate that the material was placed at an average dry unit weight of about 122 pcf and a moisture content of 10 percent. The fill consists mainly of medium dense to dense gravelly clayey sand. Laboratory tests on selected samples from this investigation indicate that the fines content is between about 30 and 40% and the gravel content is between about 10 and 20%. The effective stress friction angle of the material is estimated to be about 35° based on the compaction effort and the SPT resistance of the materials. This value agrees reasonably well with published data for similar materials.

The fill placed on the upstream portion of the crest during the 1980 modifications was specified to be relatively impervious material, e.g. clayey silt or sandy clay, and was specified to be compacted to at least 94% relative compaction. For the purposes of this study, this material was assumed to have the same properties as the fill placed on the downstream slope.

The fillet fill placed on the downstream slope after the 1965 S&W study was also compacted. Because of its small volume, this fill does not play a key role in the stability of the dam. For analysis, it was assumed to have the same engineering properties as the fill placed in 1980.

7.2.4 Random Fill

Random fill was placed in a designated disposal area near the downstream toe during the 1980 dam modifications. The bulk of the random fill reportedly consists of materials similar to those placed in the modern fill. The random fill was specified to be placed in 10-inch maximum lifts and compacted to at least 85% relative compaction as determined by ASTM D 698. The fill reportedly also includes broken concrete, masonry rubble, and other materials removed for the dam modifications. Voids were reportedly filled with sluiced or jetted soil, and the disposal area was covered with a minimum 3-foot-thick cover of soil. Because of its location and thickness, this zone is not expected to play a key role in the stability of the dam. Its properties were assumed to be the same as those of the sluiced fill. The random fill is located entirely above the measured phreatic surface and, therefore, is not considered susceptible to liquefaction.

7.3 FOUNDATION CONDITIONS

7.3.1 Foundation Soils

The dam site was reportedly stripped about 2 to 3 feet deep to remove vegetation and loose soil during original construction. However, except for the core trench, it appears that the existing foundation soils were mostly left in place. The field investigations conducted for this and previous studies encountered significant depths of foundation soils consisting primarily of alluvium and colluvium deposits.

As shown in Figure 7-3, the thickness of foundation soils along the main section of the dam, near the former stream channel, is estimated to be generally less than about 10 feet. In some areas of

the channel there appears to be little or no foundation soil. At the location of cross-section B-B' (Figure 7-4) the foundation soils are estimated to be up to about 20 to 25 feet thick. This estimate is based on the thickness of colluvium/alluvium logged in borings WI-62 and 66, the approximate contours of the pre-dam ground surface, and the average estimated top of bedrock elevations. The pre-dam contours in Figure 7-1 appear to show a terrace in this area, which could correspond with the greater foundation soil thickness. A similar terrace appears to be present on the west side of the stream channel in the area of boring WI-65.

The depths of foundation soil logged in the borings drilled for this investigation agree relatively well (to within ± 10 feet) with the values inferred from the difference in elevation between the pre-dam ground surface contours and the estimated top of bedrock. That comparison indicates that the greatest thickness of foundation soil is present in the area of boring WI-13 and that the foundation soils thin down considerably on the steep slopes of the abutments.

The boring data from this and previous investigations indicate that the foundation soils consist primarily of medium dense clayey sands and stiff sandy clays with gravel, similar to the wagon fill materials. Pockets of relatively clean alluvial sands and gravels were encountered in some of the borings. However, the extent of these materials appears to be primarily confined to locations near the original stream channel. Because of their limited extent, the presence of these materials, which are potentially liquefiable, is judged unlikely to significantly affect the stability of the dam.

Figure 7-39 shows the gradations of samples of the foundation soils obtained during the current investigation. Comparison of this figure with Figures 7-6, 7-7, and 7-8 shows that the range of gradations of the foundation soils is very similar to that of the wagon fill materials. The laboratory test data from this and previous investigations indicate that other engineering characteristics of the foundation soils are also very similar to those of the wagon fill. This is shown in the plots of index and strength properties of the wagon fill, which also show results for the foundation soils (Figures 7-9 through 7-37). On this basis, the material properties of the foundation soils for analysis are assumed to be the same as those of the wagon fill.

7.3.2 Bedrock

Shales and siltstones of the Knoxville formation, were encountered in borings WI-66 and 67, beneath the upstream shell of the dam. The central portion of the dam is underlain by Leona Rhyolite, which was encountered in borings WI-59, 61, 62, and 64. Rock types beneath the downstream shell include basalt (encountered in boring WI-62), serpentinite (encountered in borings WI-60 and 63), and gabbro (encountered in boring WI-65). Based on the available information and mapping, the foundation bedrock appears to be free of major weaknesses or discontinuities that could affect the stability of the dam. For the purposes of analysis, the rock mass is judged to be much stronger than the embankment and foundation soils.

Data from previous investigations indicate that the total density of the rock ranges between about 130 and 150 pcf, with a representative average of about 140 pcf. The downhole seismic surveys conducted for this investigation indicate that the shear wave velocity of the rock immediately beneath the dam ranges between about 1,500 and 5,000 feet per second (fps), with a representative average of about 2,700 fps.

7.4 GROUNDWATER CONDITIONS

The piezometric data obtained by EBMUD were reviewed to assess the groundwater conditions within the dam and to estimate the location of the phreatic line for analysis. These data are recorded in piezometers located as shown in Figure 7-1. Some of the piezometer locations include multiple installations with up to three piezometers in one boring. The installations in borings WI-51 to 58 consist of up to two piezometers, an upper and a lower piezometer (A and B), in each boring.

The interpreted phreatic surface through the dam was developed based on piezometric data corresponding to a full reservoir level at spillway Elevation 227. The result is shown in the cross-sections in Figures 7-3 through 7-5. The piezometric data indicate a moderate gradient in the upstream shell with water levels decreasing gradually from the reservoir level to about Elevation 190 beneath the dam crest. With exception of the upper piezometer (A) in WI-55 (Figure 7-3), all other piezometers indicate a gentle gradient downstream, with water levels at about Elevation 155 in the toe area decreasing to about Elevation 135 in the valley downstream.

The cause for the high reading in upper piezometer WI-55A within the embankment has not been determined. This piezometer was recently tested by the District (along with piezometer WI-15A) and found to be in working order. Because the piezometer tip appears to be located within the embankment fill materials, it is unlikely that the elevated level reflects water levels in the foundation. It is possible, however, that the piezometer intercepts a permeable layer within the embankment that is affected by high natural groundwater levels. The piezometric level reported in WI-55A is at approximately the same elevation as in the crest piezometers and is higher than WI-56, located further upstream. If accurate, this would indicate a flat or slightly upward gradient from WI-56 to WI-55A, which does not make sense. Thus, the high piezometric level observed in WI-55A appears likely to represent only a localized condition rather than a large zone of the embankment. On this basis, a level intermediate between piezometers WI-55A and B was used to define the phreatic surface through the embankment, as shown in Figures 7-3 through 7-5. This phreatic surface was used in the stability analysis of the dam.

Table 7-1
Representative Index Properties of Embankment and Foundation Materials⁽¹⁾

Material	Dry Unit Weight (pcf)	Total Unit Weight (pcf)	Liquid Limit (%)	Plasticity Index (%)	Fines Content (%)	Gravel Content (%)
Modern Fill	122	134	-	-	(35 - 40)	(15 - 20)
Random Fill ⁽²⁾	109	130	-	-	-	-
Wagon Fill	115 (90 - 120)	133 (120 - 145)	38 (27 - 45)	18 (10 - 25)	40 (20 - 60)	15 (0 - 30)
Sluiced Fill	109 (80 - 125)	130 (110 - 140)	36 ⁽³⁾	18 ⁽³⁾	15 (10 - 95)	25 (0 - 45)
Foundation Soils	115 (90 - 120)	133 (120 - 145)	33 (25 - 45)	13 (10 - 20)	40 (25 - 60)	10 (0 - 30)
Bedrock	-	140	-	-	-	-

Notes:

- (1). Typical range shown in parentheses.
(2). Random fill placed at the downstream toe as a part of the 1980's modification.
(3). Values represent only the fines fraction of the sluiced fill.

Table 7-2
Strength Parameters for Embankment and Foundation Soils

Material (Zone)	Total Unit Weight	Total Strength Parameters		Effective Strength Parameters		Residual Strength
	γ_t	c	ϕ	c'	ϕ'	S _r
	(pcf)	(psf)	(°)	(psf)	(°)	(psf)
Modern Fill	134	-	-	0	35	-
Random Fill	130	-	-	0	33	-
Wagon Fill (D/S and U/S)	133	200	21.5	0	30	-
Wagon Fill (Core)	133	200	21.5	0	30	-
Sluiced Fill	130	350	32	0	33	150
Foundation Soils	133	200	21.5	0	30	-

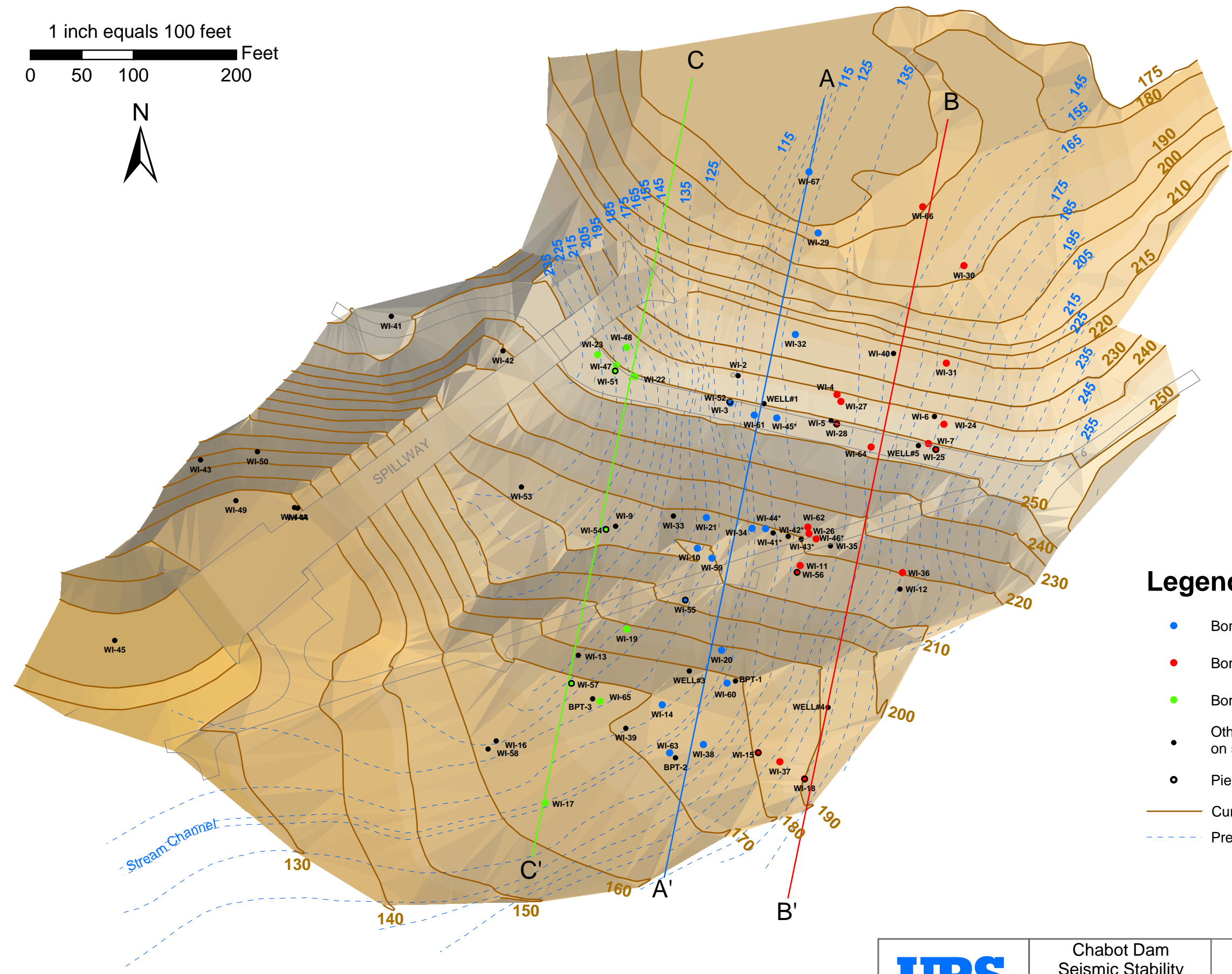
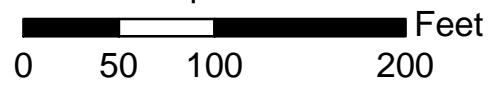
Table 7-3
Comparison of Effective Stress Strength Parameters Between This and Previous Studies

Material (Zone)	This Study		S&W, 1965		DSOD, 2003		
	c'	ϕ'	c'	ϕ'	c'	ϕ'	DSOD Zone Designation
	(psf)	(°)	(psf)	(°)	(psf)	(°)	
Modern Fill	0	35	-	-	-	-	Embankment Fill 2
Wagon Fill	0	30	0	35	-	-	Embankment Fill Wagon Fill Upper Wagon Fill Lower
Sluiced Fill	0	33	0	35	-	-	Hydraulic Fill Lower
Random Fill	0	33	-	-	-	-	Hydraulic Fill Upper
Foundation Soils	0	30	0	35	-	-	Foundation

Table 7-4
Comparison of Total Stress Strength Parameters Between This and Previous Studies

Material (Zone)	This Study		S&W, 1965		DSOD, 2003		
	c	ϕ	c	ϕ	c	ϕ	DSOD Zone Designation
	(psf)	(°)	(psf)	(°)	(psf)	(°)	
Modern Fill	-	-	-	-	0	37	Embankment Fill 2
Wagon Fill	200	21.5	800	16.5	0 550 375	37 20 30	Embankment Fill Wagon Fill Upper Wagon Fill Lower
Sluiced Fill	350	32	800	16.5	450	34	Hydraulic Fill Lower
Random Fill	-	-	-	-	450	34	Hydraulic Fill Upper
Foundation Soils	200	21.5	800	16.5	375	30	Foundation

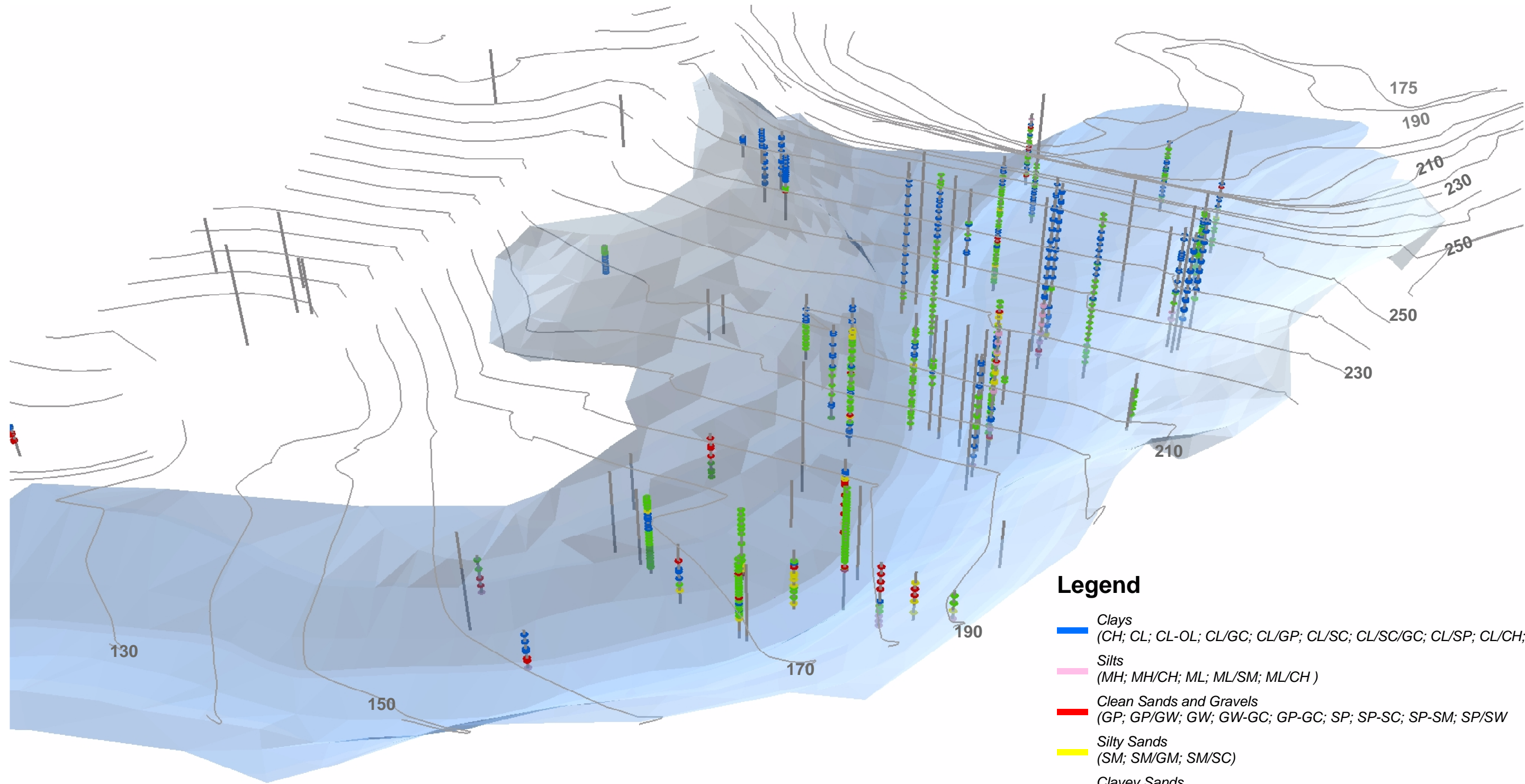
1 inch equals 100 feet



Legend

- Borings shown on Section A-A'
- Borings shown on Section B-B'
- Borings shown on Section C-C'
- Other borings, not shown on sections
- Piezometer
- Current ground surface contours (ft)
- - - Pre-dam ground surface contours (ft)

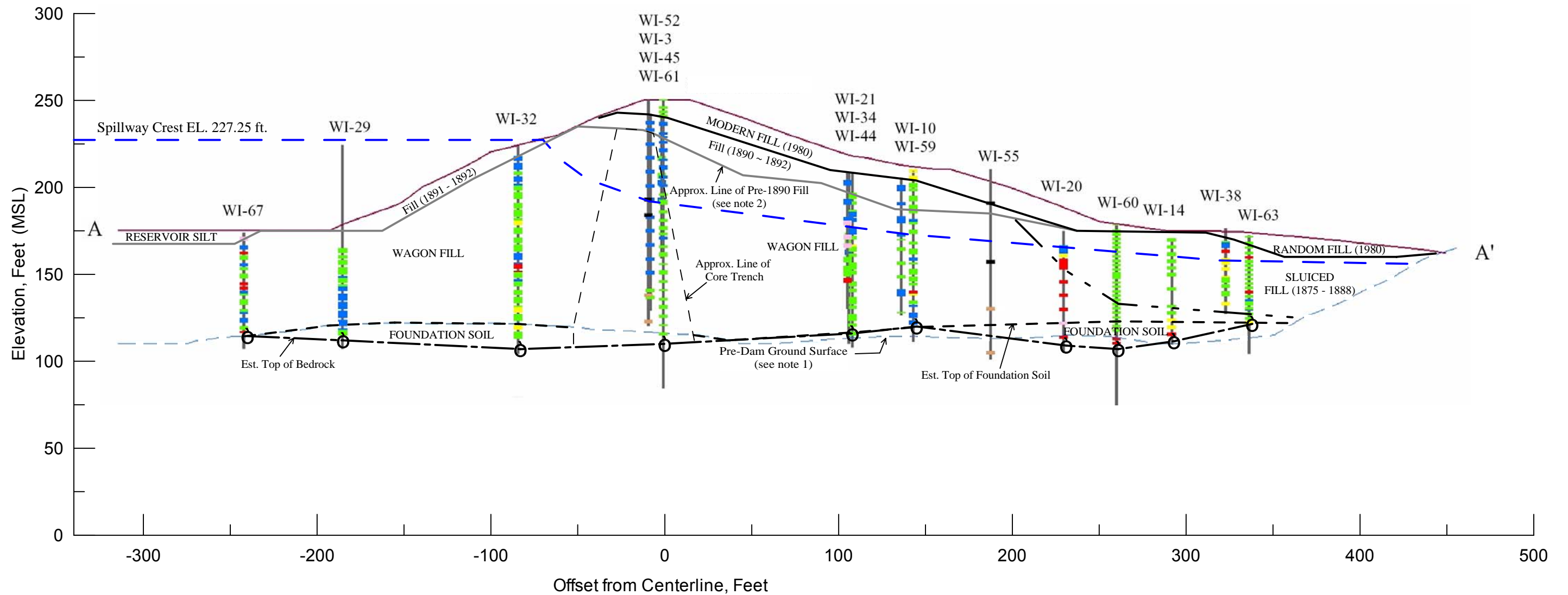
	Chabot Dam Seismic Stability	Plan View of Dam and Cross-sections	Figure 7-1
	26814536		



Legend

- █ Clays
(CH; CL; CL-OL; CL/GC; CL/GP; CL/SC; CL/SC/GC; CL/SP; CL/CH; CL-ML)
 - █ Silts
(MH; MH/CH; ML; ML/SM; ML/CH)
 - █ Clean Sands and Gravels
(GP; GP/GW; GW; GW-GC; GP-GC; SP; SP-SC; SP-SM; SP/SW)
 - █ Silty Sands
(SM; SM/GM; SM/SC)
 - █ Clayey Sands
(GC; SC/GC; SC/CL; SC; SC/Fm; SC-SM)
- ← Boring extent

URS	Chabot Dam Seismic Stability	GIS Model - Distribution of Soil Types in Embankment and Foundation	Figure 7-2
	26814536		



Legend

- Clays
(CH; CL; CL-OL; CL/GC; CL/GP; CL/SC; CL/SC/GC; CL/SP; CL/CH; CL-ML)
- Silts
(MH; MH/CH; ML; ML/SM; ML/CH)
- Sands and Gravels
(GP; GP/GW; GW; GW-GC; GP-GC; SP; SP-SC; SP-SM; SP/SW)
- Silty Sands
(SM; SM/GM; SM/SC)
- Clayey Sands
(GC; SC/GC; SC/CL; SC; SC/Fm; SC-SM)
- ← Piezometer reading (grey if dry)
- ← Piezometer tip
- ← Top of bedrock

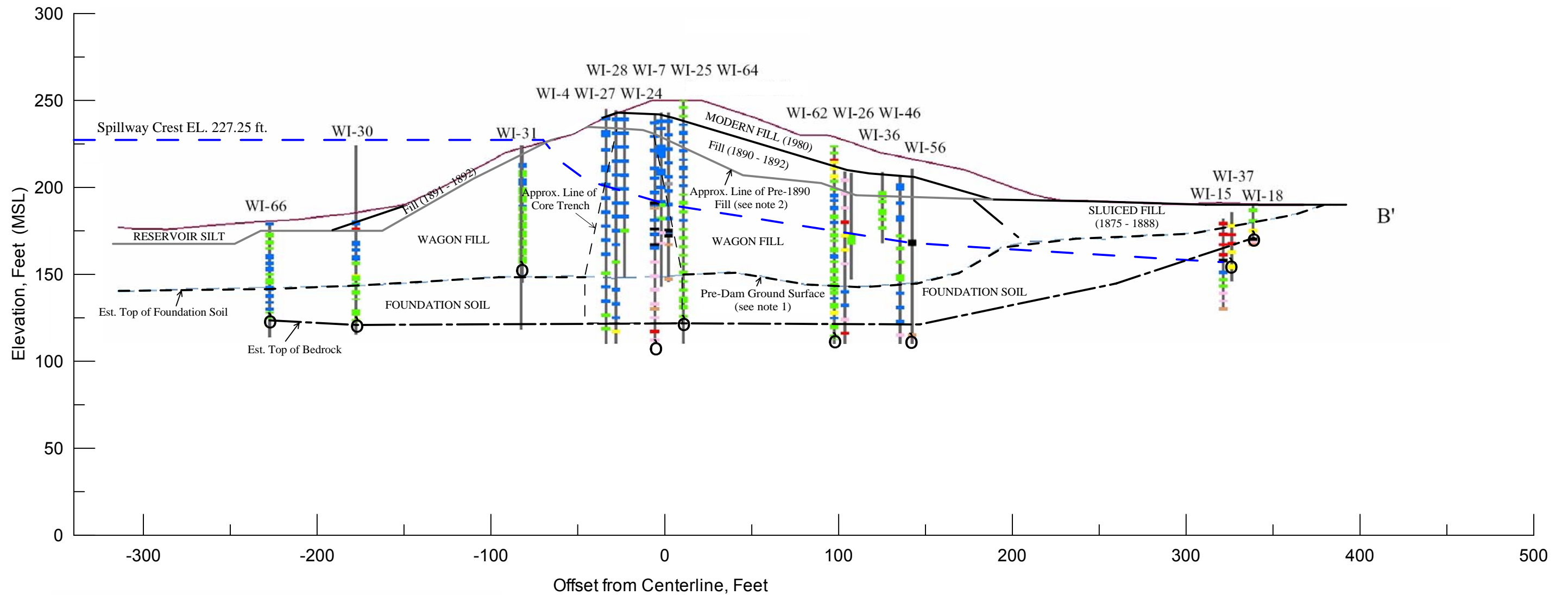
Notes:

1. Pre-Dam Ground Surface is taken from Reference Drawing (1) and is considered approximate. Surface is used as a guide in estimating the top of foundation soil and is shown for reference purposes only.
2. Approx. Line of Pre-1890 Fill is taken from Reference Drawing (3) and is considered approximate.
3. Contact between Fill (1890-1892) and Modern Fill/Random Fill is taken from Reference Drawings (4) and (5).
4. Current Ground Surface is taken from Reference Drawings (2) and (6).

Reference Drawings:

- (1) EBMUD Drawing No. 1497-R-1, Topography - 1934 Survey, dated 1934;
- (2) EBMUD Drawing No. 1487-R-1, Topography, dated March 10, 1967;
- (3) EBMUD Drawing No. 41D, Cross Section of Dam Showing Various Stages of Construction, dated April 26, 1937;
- (4) EBMUD Drawing No. 6948-G-2.04, Earthwork Sections, dated December 7, 1982;
- (5) EBMUD Drawing No. 6948-G-1.05, Existing Topography & Location of Borings, dated December 7, 1982;
- (6) EBMUD Drawing No. 6948-G-1.03.1, As Built Topography, dated December 7, 1982.

Project No. 26814536	Chabot Dam Seismic Stability	Cross Section A - A'	FIGURE 7-3
URS			



Legend

- Clays
(CH; CL; CL-OL; CL/GC; CL/GP; CL/SC; CL/SC/GC; CL/SP; CL/CH; CL-ML)
- Silts
(MH; MH/CH; ML; ML/SM; ML/CH)
- Sands and Gravels
(GP; GP/GW; GW; GW-GC; GP-GC; SP; SP-SC; SP-SM; SP/SW)
- Silty Sands
(SM; SM/GM; SM/SC)
- Clayey Sands
(GC; SC/GC; SC/CL; SC; SC/Fm; SC-SM)
- ← Piezometer reading (grey if dry)
- ← Piezometer tip
- ← Top of bedrock

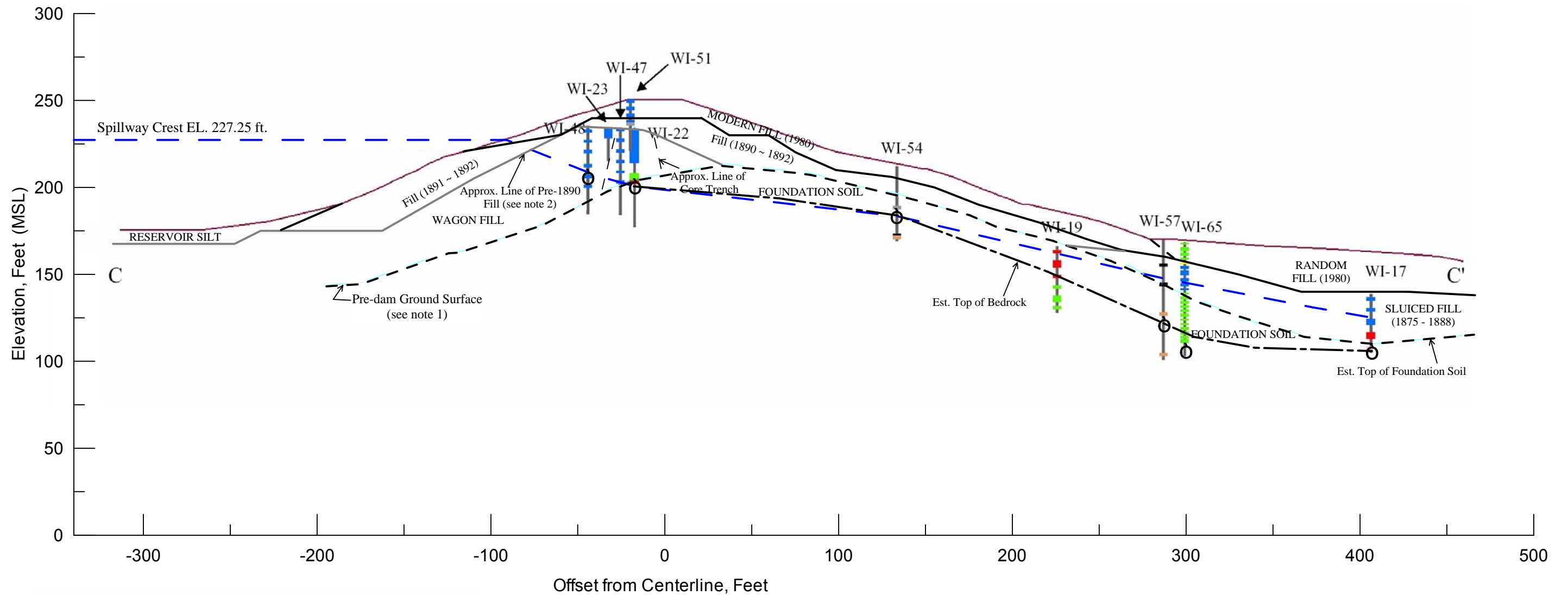
Notes:

1. Pre-Dam Ground Surface is taken from Reference Drawing (1) and is considered approximate. Surface is used as a guide in estimating the top of foundation soil and is shown for reference purposes only.
2. Approx. Line of Pre-1890 Fill is taken from Reference Drawing (3) and is considered approximate.
3. Contact between Fill (1890-1892) and Modern Fill/Random Fill is taken from Reference Drawings (4) and (5).
4. Current Ground Surface is taken from Reference Drawings (2) and (6).

Reference Drawings:

- (1) EBMUD Drawing No. 1497-R-1, Topography - 1934 Survey, dated 1934;
- (2) EBMUD Drawing No. 1487-R-1, Topography, dated March 10, 1967;
- (3) EBMUD Drawing No. 41D, Cross Section of Dam Showing Various Stages of Construction, dated April 26, 1937;
- (4) EBMUD Drawing No. 6948-G-2.04, Earthwork Sections, dated December 7, 1982;
- (5) EBMUD Drawing No. 6948-G-1.05, Existing Topography & Location of Borings, dated December 7, 1982;
- (6) EBMUD Drawing No. 6948-G-1.03.1, As Built Topography, dated December 7, 1982.

Project No. 26814536	Chabot Dam Seismic Stability	Cross Section B - B'	FIGURE 7-4
URS			



Legend

- Clays
(CH; CL; CL-OL; CL/GC; CL/GP; CL/SC; CL/SC/GC; CL/SP; CL/CH; CL-ML)
- Silts
(MH; MH/CH; ML; ML/SM; ML/CH)
- Sands and Gravels
(GP; GP/GW; GW; GW-GC; GP-GC; SP; SP-SC; SP-SM; SP/SW)
- Silty Sands
(SM; SM/GM; SM/SC)
- Clayey Sands
(GC; SC/GC; SC/CL; SC; SC/Fm; SC-SM)
- ← Piezometer reading (grey if dry)
- ← Piezometer tip
- ← Top of bedrock

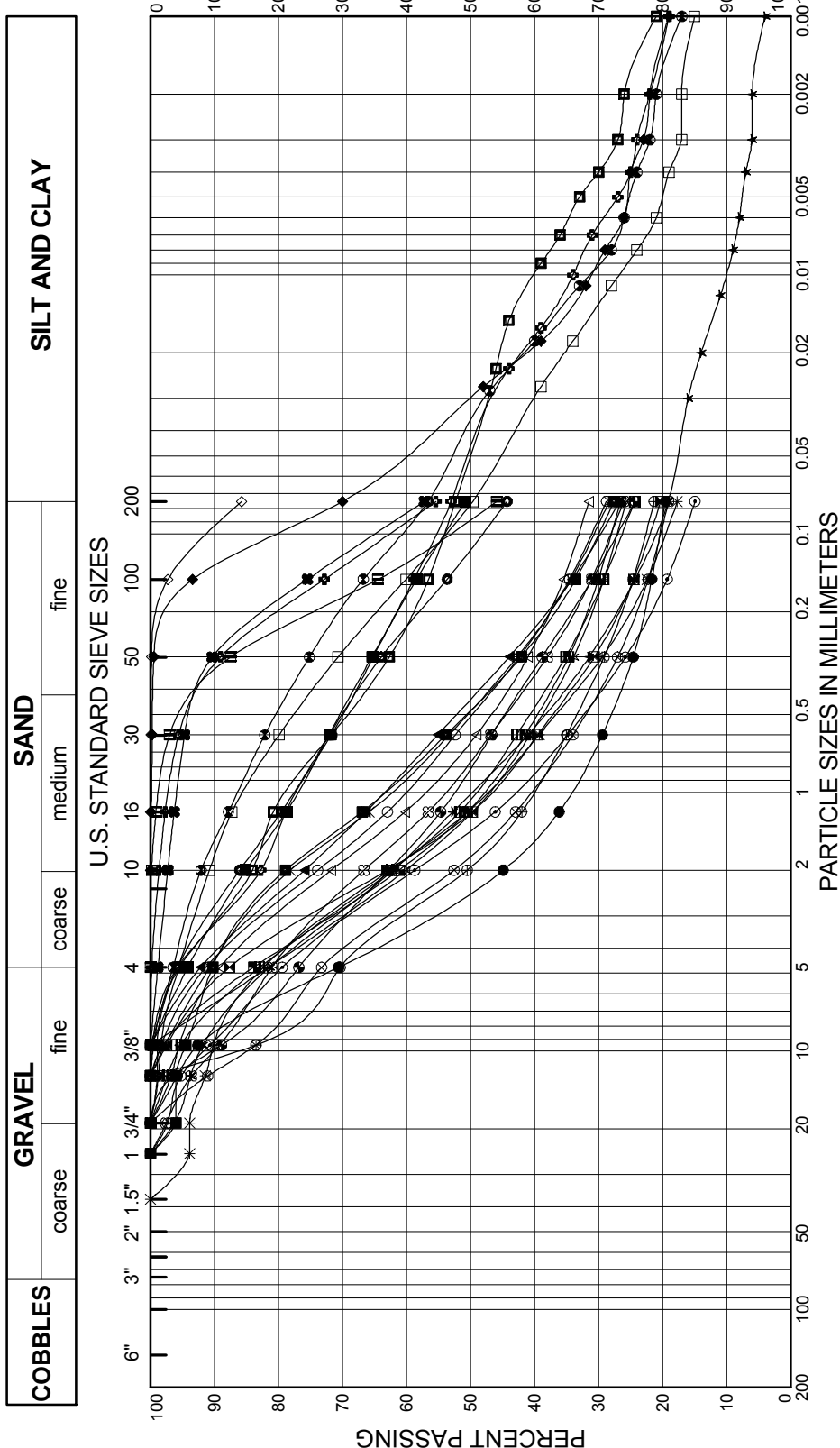
Notes:

1. Pre-Dam Ground Surface is taken from Reference Drawing (1) and is considered approximate. Surface is used as a guide in estimating the top of foundation soil and is shown for reference purposes only.
2. Approx. Line of Pre-1890 Fill is taken from Reference Drawing (3) and is considered approximate.
3. Contact between Fill (1890-1892) and Modern Fill/Random Fill is taken from Reference Drawings (4) and (5).
4. Current Ground Surface is taken from Reference Drawings (2) and (6).

Reference Drawings:

- (1) EBMUD Drawing No. 1497-R-1, Topography - 1934 Survey, dated 1934;
- (2) EBMUD Drawing No. 1487-R-1, Topography, dated March 10, 1967;
- (3) EBMUD Drawing No. 41D, Cross Section of Dam Showing Various Stages of Construction, dated April 26, 1937;
- (4) EBMUD Drawing No. 6948-G-2.04, Earthwork Sections, dated December 7, 1982;
- (5) EBMUD Drawing No. 6948-G-1.05, Existing Topography & Location of Borings, dated December 7, 1982;
- (6) EBMUD Drawing No. 6948-G-1.03.1, As Built Topography, dated December 7, 1982.

Project No. 26814536	Chabot Dam Seismic Stability	Cross Section C - C'	FIGURE 7-5
URS			



SILT AND CLAY

SAND

GRAVEL

COBBLES

fine medium coarse fine coarse

BORING NUMBER	DEPTH (FT)	SAMPLE NUMBER	SYMBOL	DESCRIPTION
WI-62	33-33.5	10B	◆	Sandy Clay (CL)
WI-62	37-37.5	11B	◇	Sandy Clay (CL)
WI-62	37.5-38	12A	×	Clay (CL)
WI-62	38.5-39	12C	◆	Clayey Sand (SC)
WI-62	45-46.5	14	◆	Sandy Clay (CL)
WI-62	49-50.5	15	◆	Clayey Sand (SC)
WI-62	61-61.5	18B	◆	Clayey Sand with Gravel (SC)
WI-62	65-66	20T	◆	Sandy Clay (CL)
WI-62	66.5-67.5	20B	◆	Clayey Sand with Gravel (SC)
WI-62	73-73.5	22B	◆	Clayey Sand with Gravel (SC)
WI-62	81.5-82	25C	◆	Clayey Sand (SC)
WI-62	83-84.5	26	◆	Clayey Sand (SC)
WI-62	88.5-90	28	◆	Sandy Clay (CL)

BORING NUMBER	DEPTH (FT)	SAMPLE NUMBER	SYMBOL	DESCRIPTION
WI-59	17.5-18	8B	●	Clayey Sand with Gravel (SC)
WI-59	22.5-25	10	⊠	Clayey Sand (SC)
WI-59	31.5-33	13	▲	Clayey Sand (SC)
WI-59	43-44.5	15	★	Silty Clayey Sand with Gravel (SC-SM)
WI-59	48-48.5	16B	◆	Silty Clayey Sand with Gravel (SC-SM)
WI-59	52.5-53.5	18T	◆	Sandy Clay (CL)
WI-59	53.5-54.5	18B	○	Clayey Sand (SC)
WI-59	60-61.5	21	△	Clayey Sand (SC)
WI-59	67-68	23B	⊗	Clayey Sand with Gravel (SC)
WI-59	72.5-74	25	⊕	Silty Sand with Gravel (SM)
WI-59	78-79	26B	□	Sandy Clay (CL/CH)
WI-59	86-86.5	29B	◆	Sandy Clay (CL)
WI-62	10-10.5	3C	◆	Silty Sand with Gravel (SM)
WI-62	21.5-23	7	★	Clayey Sand with Gravel (SC)
WI-62	26-27.5	8	⊗	Clayey Sand with Gravel (SC)

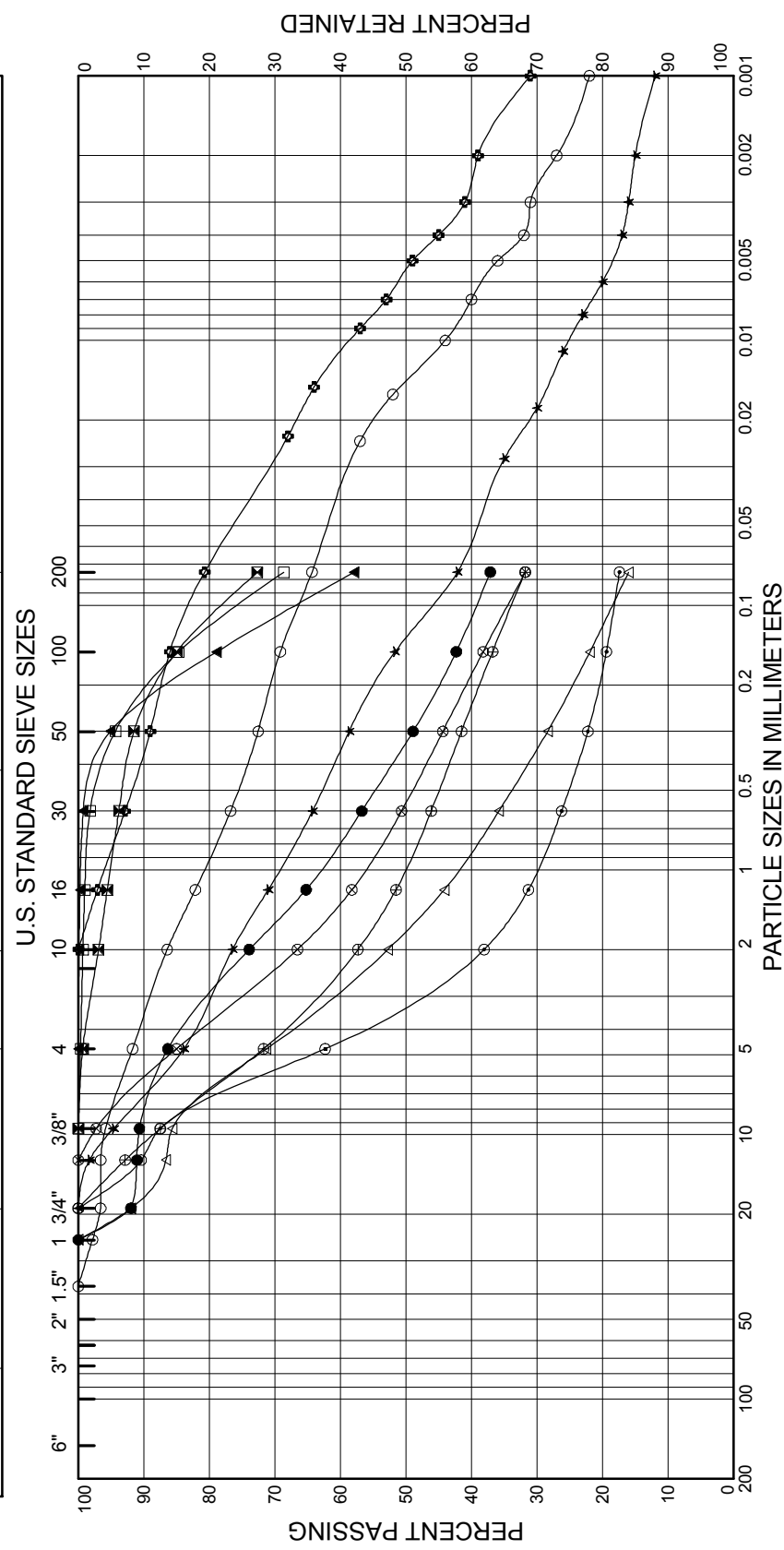
Dynamic Stability of Chabot Dam
Lake Chabot Dam, San Leandro, California
26814536.C0000

GRADATION OF WAGON FILL
IN DOWNSTREAM SHELL BORINGS
FIGURE 7-6



GRAVEL **SAND** **SILT AND CLAY**

coarse fine coarse medium fine



BORING NUMBER	DEPTH (FT)	SAMPLE NUMBER	SYMBOL	DESCRIPTION

BORING NUMBER	DEPTH (FT)	SAMPLE NUMBER	SYMBOL	DESCRIPTION
WI-66	7-7.5	2B	●	Clayey Sand (SC)
WI-66	15.5-16.5	5B	⊠	Clay with Sand (CL)
WI-66	24-25	8T	▲	Sandy Clay (CL)
WI-66	25-26	8B	★	Clayey Sand with Gravel (SC)
WI-66	33-34.5	13	⊕	Clayey Sand with Gravel (SC)
WI-67	10-12.5	2	○	Clay with Sand (CL)
WI-67	19.5-21	6A	△	Sandy Clay (CL)
WI-67	21.5-23	7	⊙	Clayey Sand with Gravel (SC)
WI-67	26.5-27.5	9A	⊗	Clayey Sand with Gravel (SC)
WI-67	41-41.5	14B	⊕	Clayey Sand with Gravel (SC)
WI-67	50.5-51	18A	□	Sandy Clay (CL)

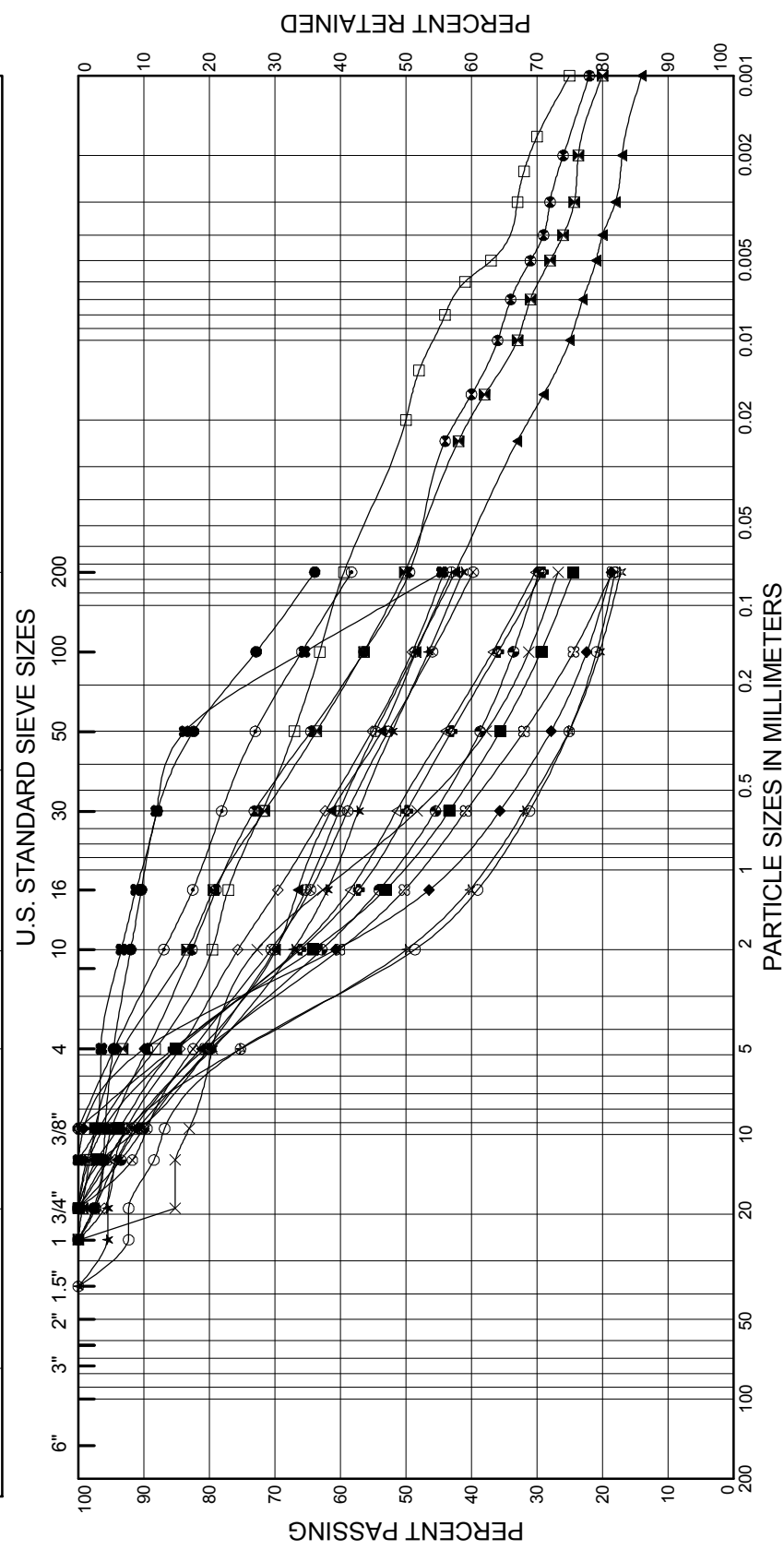
Dynamic Stability of Chabot Dam
 Lake Chabot Dam, San Leandro, California
 26814536.C0000

**GRADATION OF WAGON FILL
 IN UPSTREAM SHELL BORINGS
 FIGURE 7-7**



COBBLES **GRAVEL** **SAND** **SILT AND CLAY**

coarse 1.5" 2" 3" 6" coarse 3/8" 1 1 3/4" 2" 3" 4" coarse medium fine fine



BORING NUMBER	DEPTH (FT)	SAMPLE NUMBER	SYMBOL	DESCRIPTION
WI-64	90.5-91	19B	■	Clayey Sand with Gravel (SC)
WI-64	95-96.5	20	◆	Clayey Sand (SC)
WI-64	111-111.5	23C	◇	Clayey Sand with Gravel (SC)
WI-64	115.5-116	24B	×	Clayey Sand with Gravel (SC)
WI-64	125-126.5	27	●	Silty Clayey Sand (SC-SM)

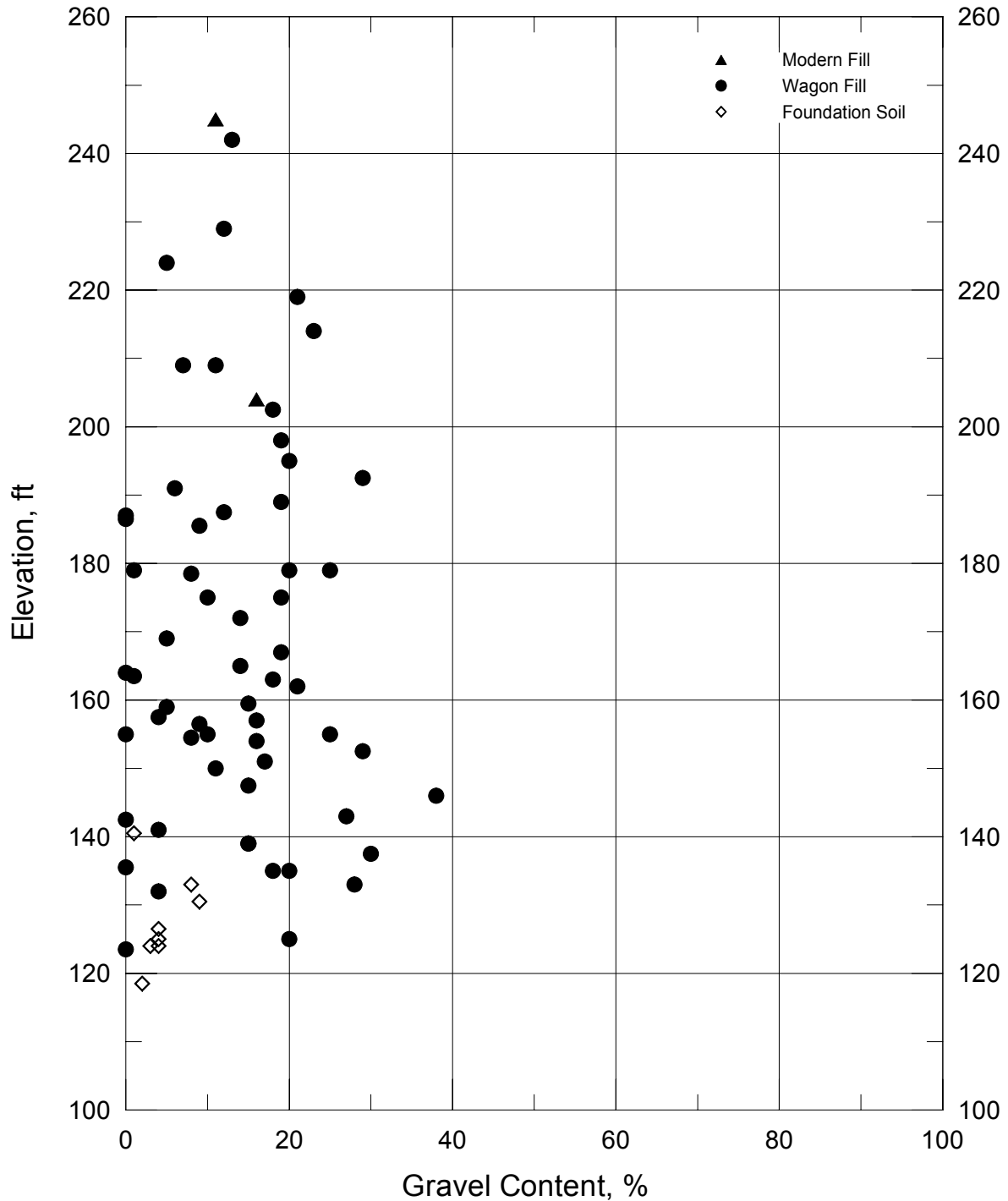
BORING NUMBER	DEPTH (FT)	SAMPLE NUMBER	SYMBOL	DESCRIPTION
WI-61	26-56.5	8B	●	Sandy Clay (CL)
WI-61	41-42.5	11B	⊠	Sandy Clay (CL)
WI-61	61-62.5	15B	▲	Clayey Sand with Gravel (SC)
WI-61	71-71.5	17B	★	Clayey Sand with Gravel (SC)
WI-61	81-81.5	20B	⊙	Sandy Clay (CL)
WI-61	85-86.5	21	⊕	Clayey Sand (SC)
WI-61	95-96.5	23	○	Clayey Sand with Gravel (SC)
WI-61	111-111.5	26C	△	Clayey Sand with Gravel (SC)
WI-61	115-116.5	27	⊗	Clayey Sand with Gravel (SC)
WI-61	125-126.5	29	⊕	Clayey Sand with Gravel (SC)
WI-64	20-22.5	5B	□	Sandy Clay (CL)
WI-64	40-42.5	9B	⊕	Clayey Sand (SC)
WI-64	55-56.5	12	◆	Clayey Sand with Gravel (SC)
WI-64	71-71.5	15C	★	Clayey Sand with Gravel (SC)
WI-64	75-76.5	16	⊗	Clayey Sand with Gravel (SC)

Dynamic Stability of Chabot Dam
Lake Chabot Dam, San Leandro, California
26814536.C0000

GRADATION OF WAGON FILL
IN CREST BORINGS
FIGURE 7-8



Chabot Dam - Gravel Content of Different Soil Types



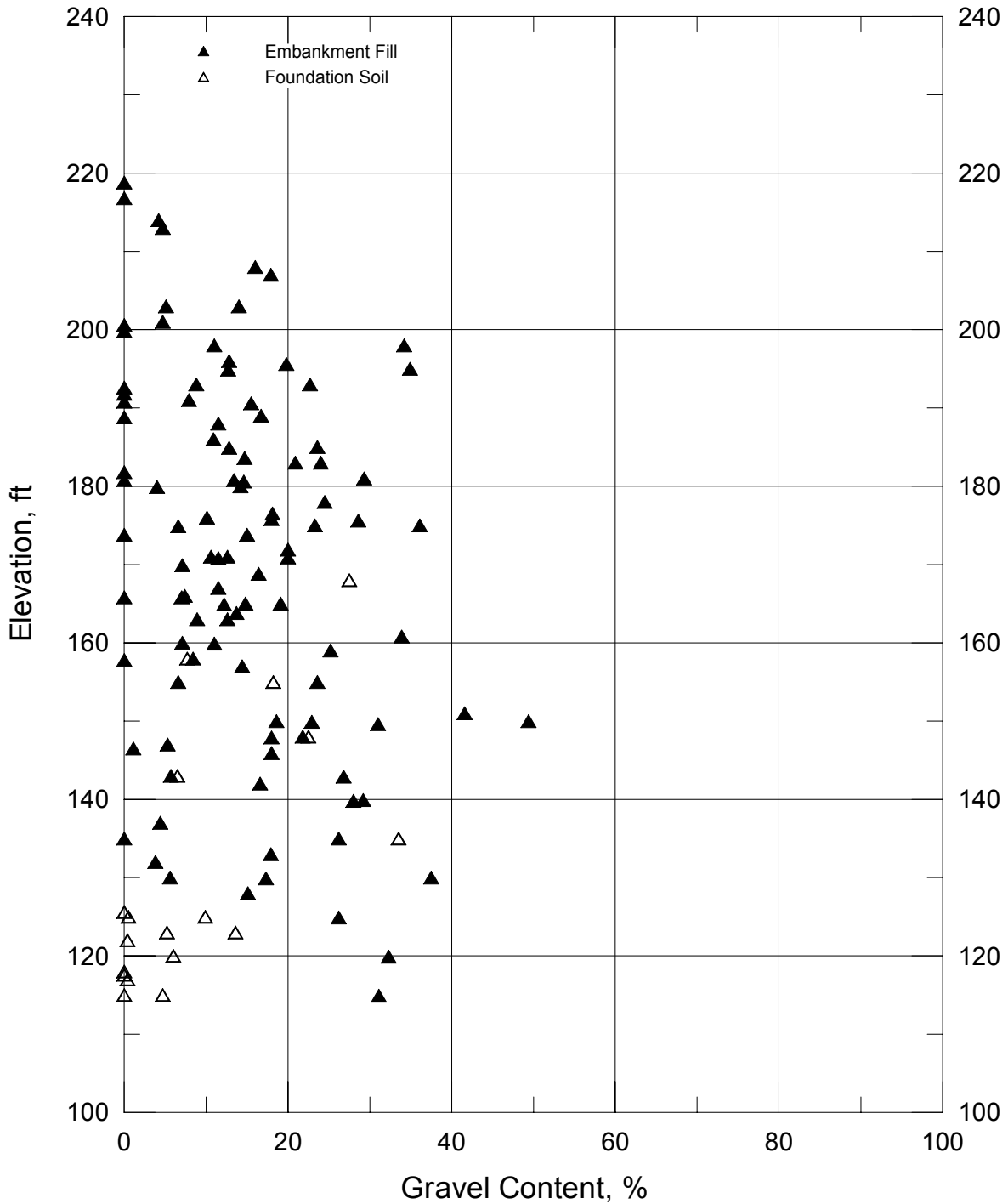
Project No. 26814536

Chabot Dam
Seismic Stability

Gravel Content
From Borings WI-59, 61, 62, 64, 66 and 67
Wagon Fill Zone

Figure
7-9

Chabot Dam - Gravel Content of Different Soil Types



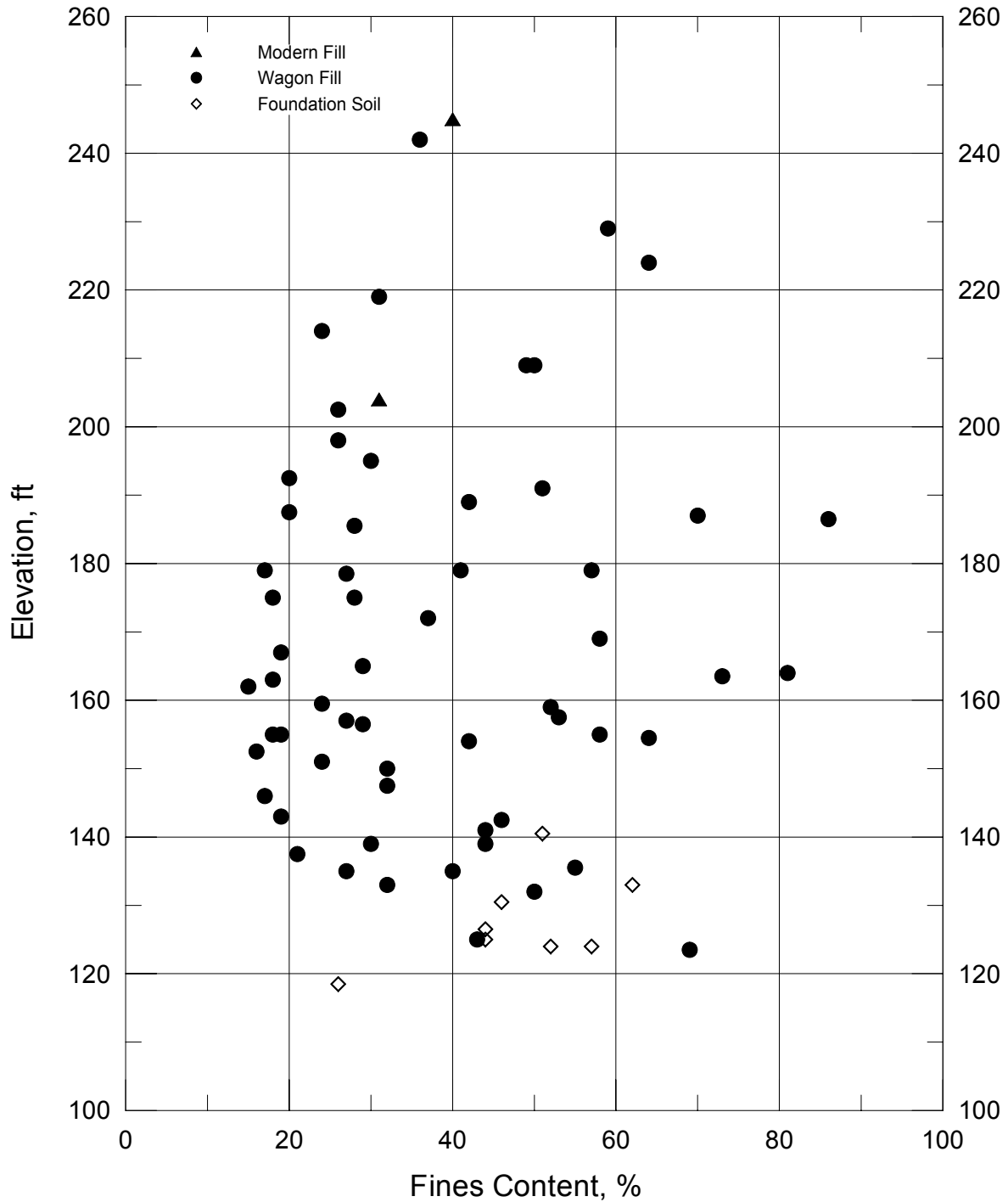
Project No. 26814536

Chabot Dam
Seismic Stability

**Gravel Content
From Previous Borings in Wagon Fill Zone**

Figure
7-10

Chabot Dam - Fines Content of Different Soil Types



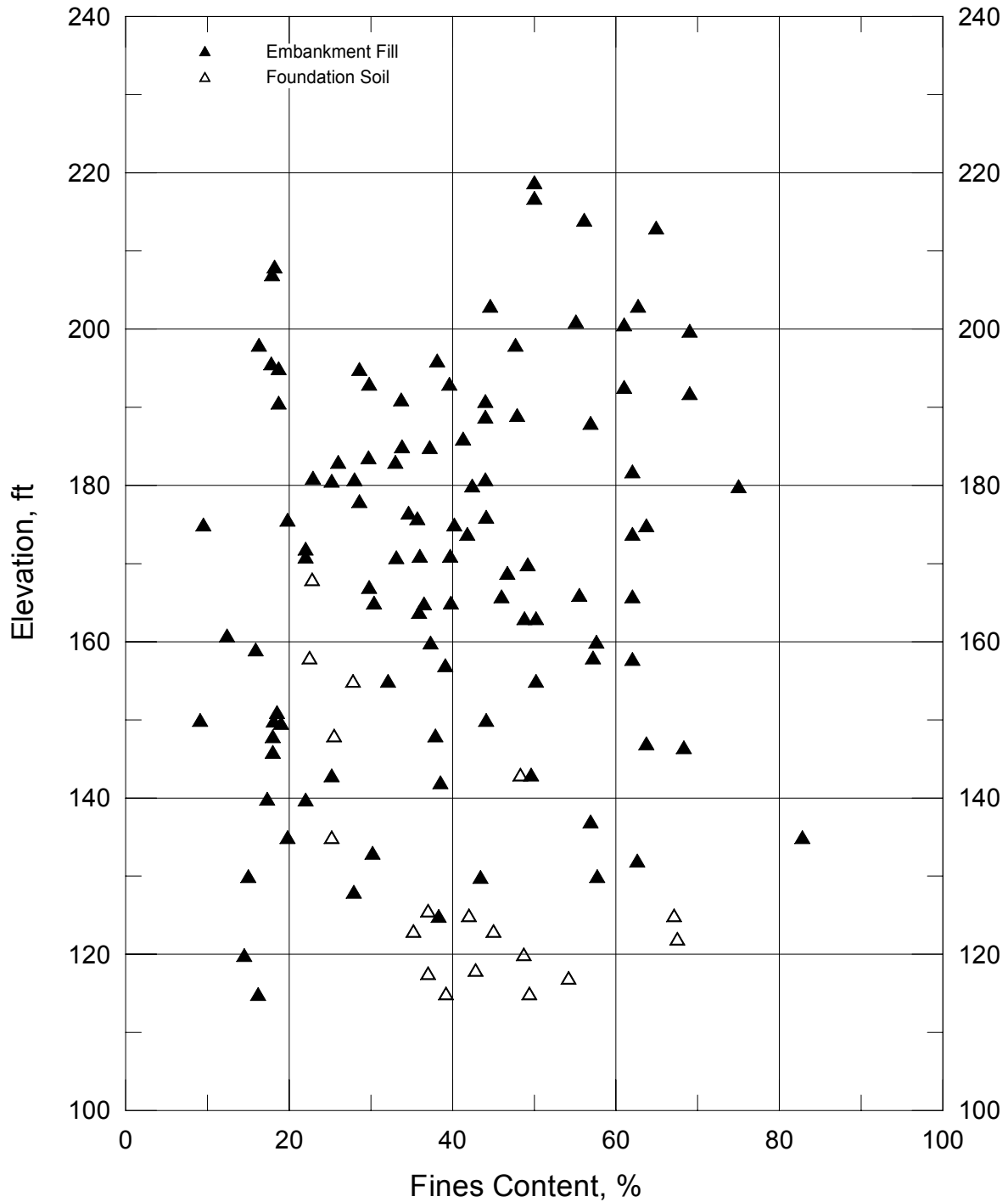
Project No. 26814536

Chabot Dam
Seismic Stability

**Fines Content
From Borings WI-59, 61, 62, 64, 66 and 67
Wagon Fill Zone**

Figure
7-11

Chabot Dam - Fines Content of Different Soil Types

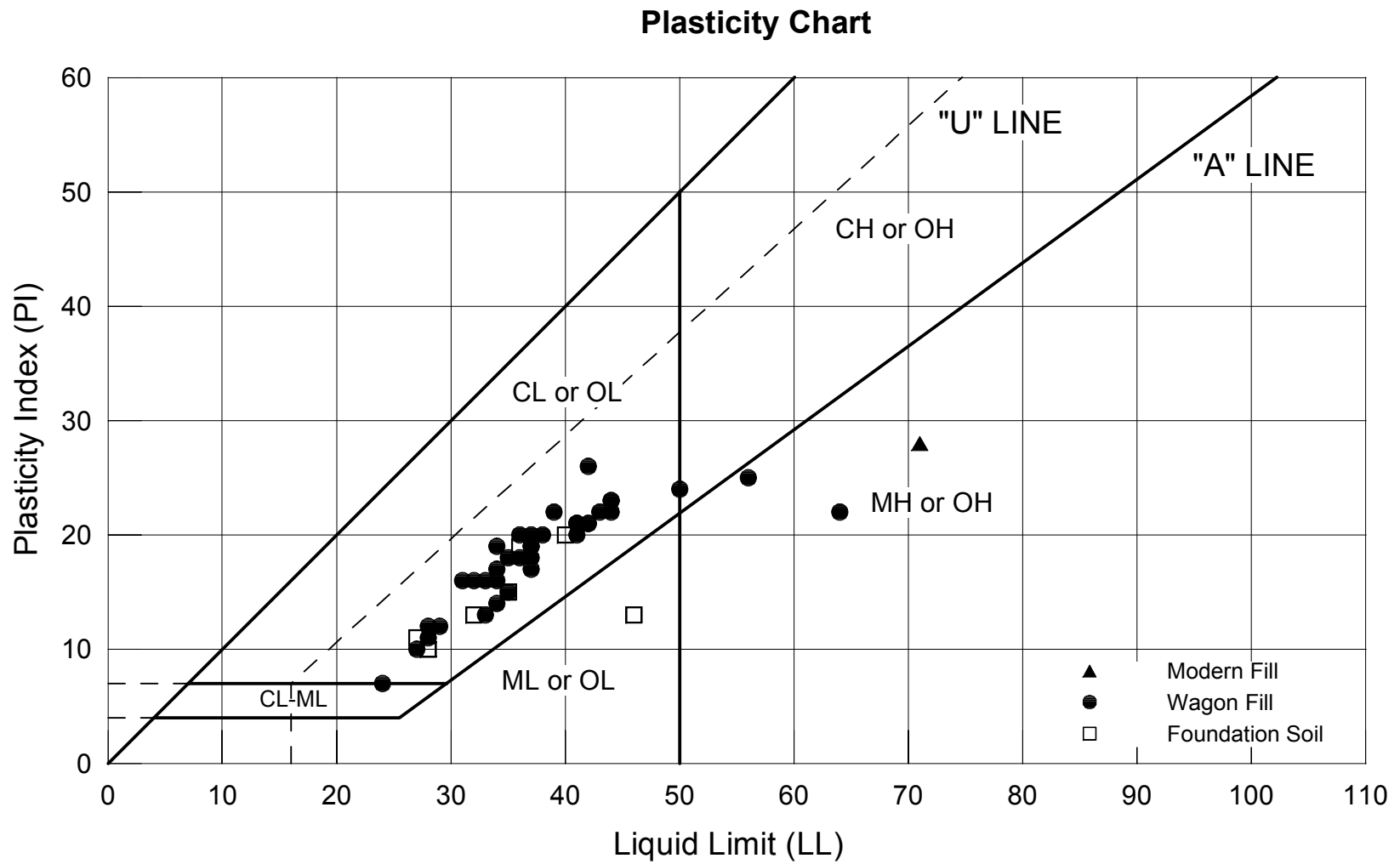


Project No. 26814536

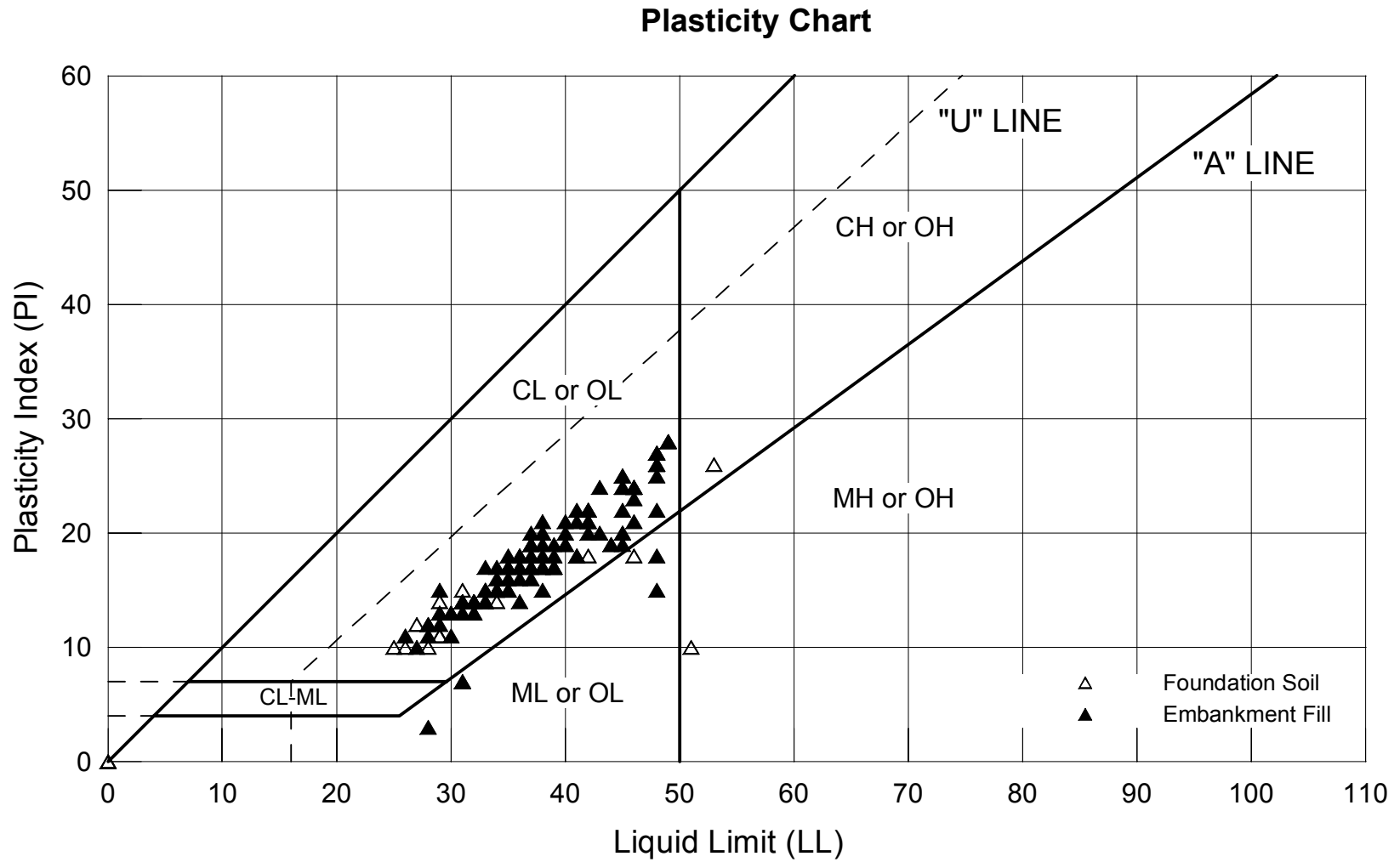
Chabot Dam
Seismic Stability

**Fines Content
From Previous Borings in Wagon Fill Zone**

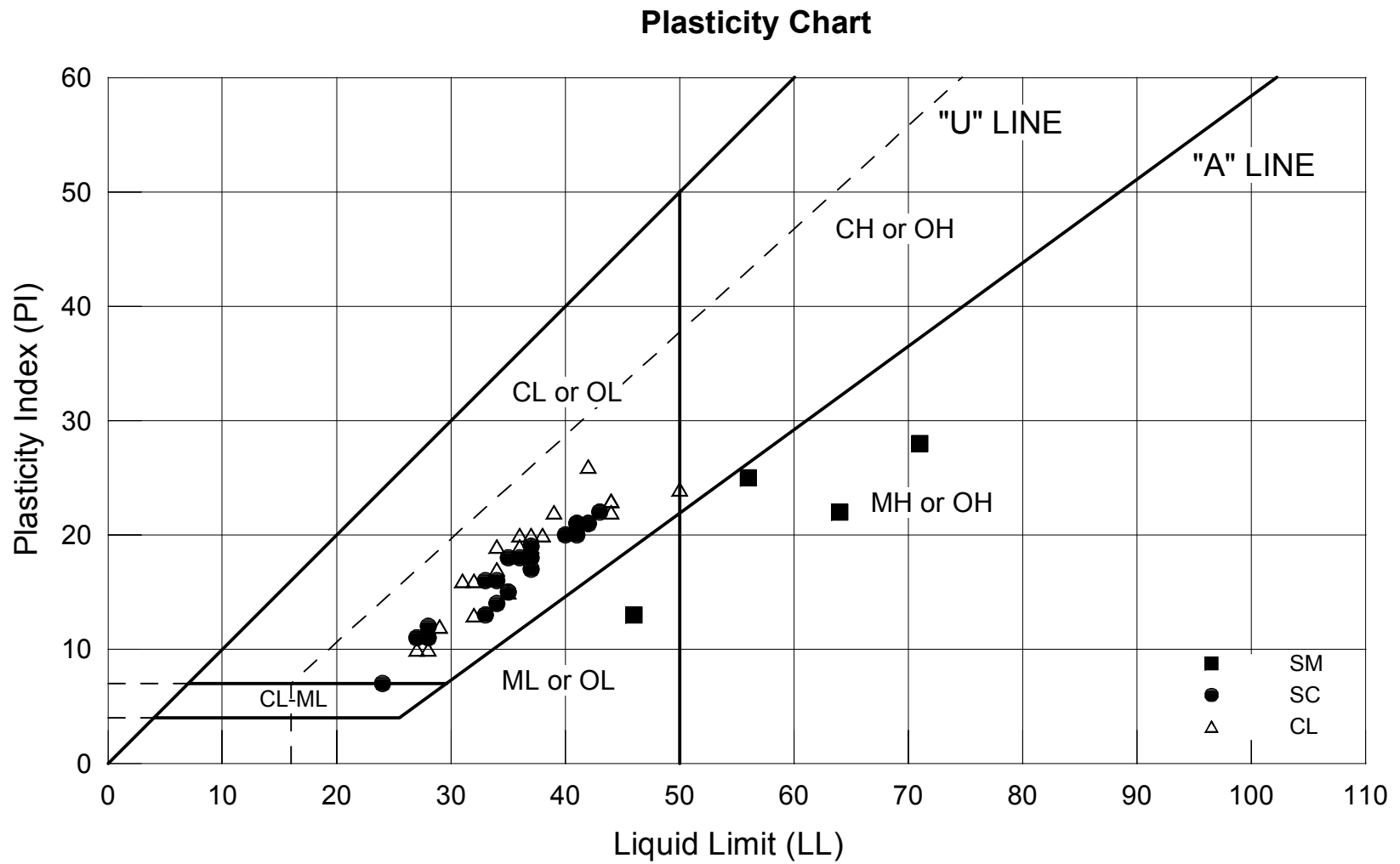
Figure
7-12



Project No. 26814536	Chabot Dam Seismic Stability	Plasticity from Borings WI-59, 61, 62, 64, 66 and 67 Wagon Fill Zone (by Material Zone)	Figure
URS			7-13

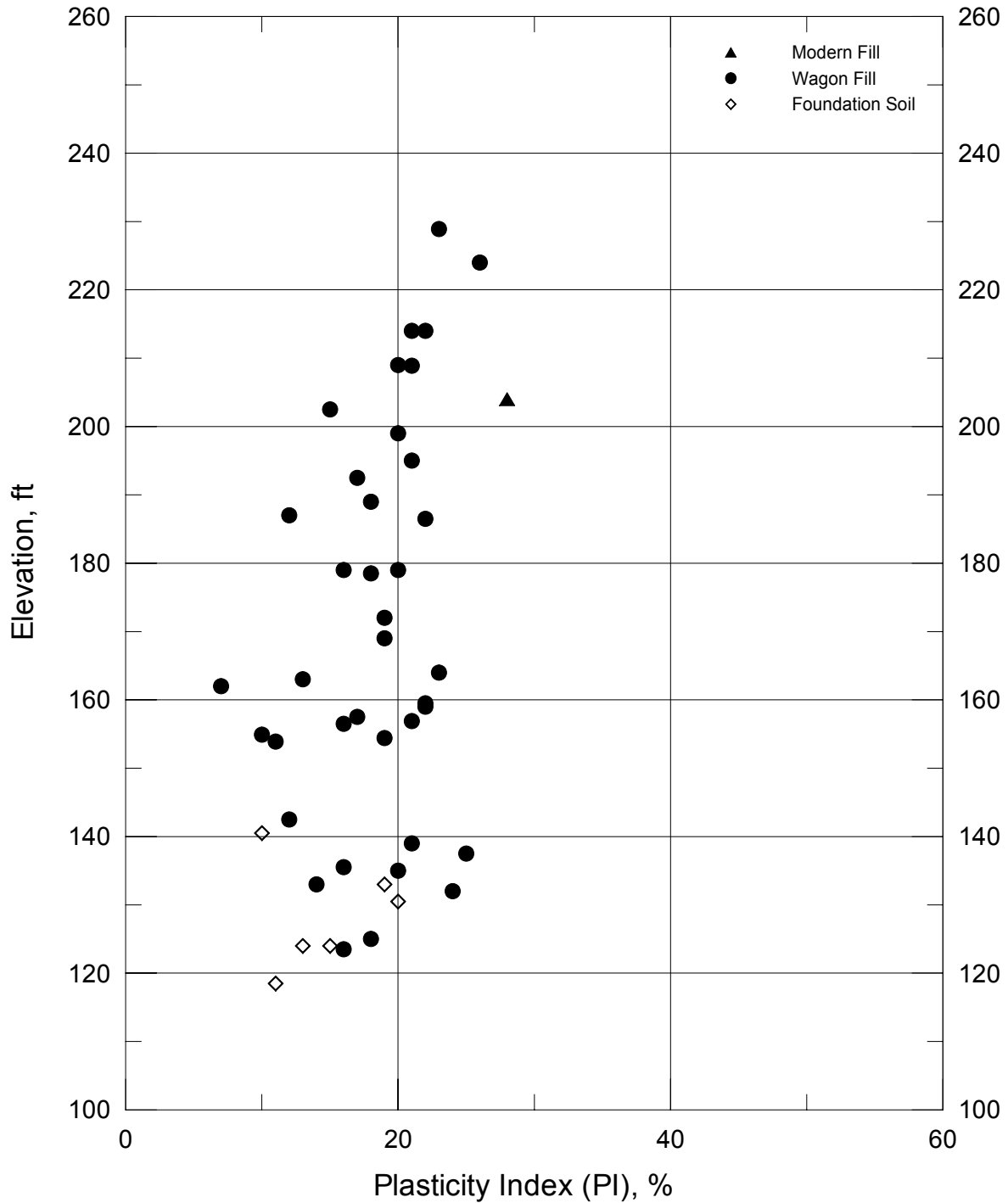


Project No. 26814536	Chabot Dam Seismic Stability	Plasticity from Previous Borings in Wagon Fill Zone	Figure
URS			7-14



Project No. 26814536	Chabot Dam Seismic Stability	Plasticity from Borings WI-59, 61, 62, 64, 66 and 67 Wagon Fill Zone (by Soil Classification)	Figure 7-15
URS			

Chabot Dam - Plasticity Index of Different Soil Types



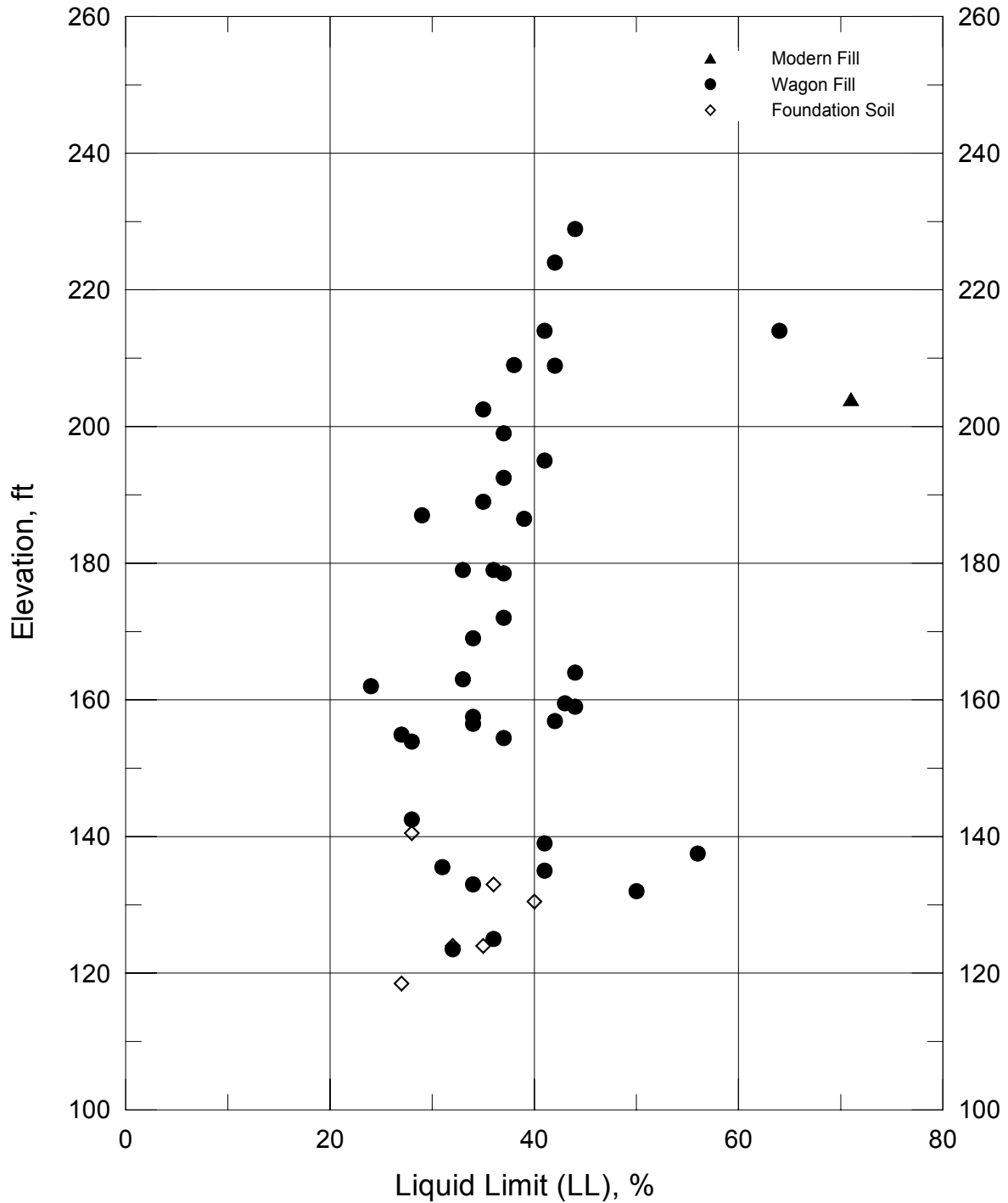
Project No. 26814536

Chabot Dam
Seismic Stability

**Plasticity Index
From Borings WI-59, 61, 62, 64, 66 and 67
Wagon Fill Zone**

Figure
7-16

Chabot Dam - Liquid Limit of Different Soil Types



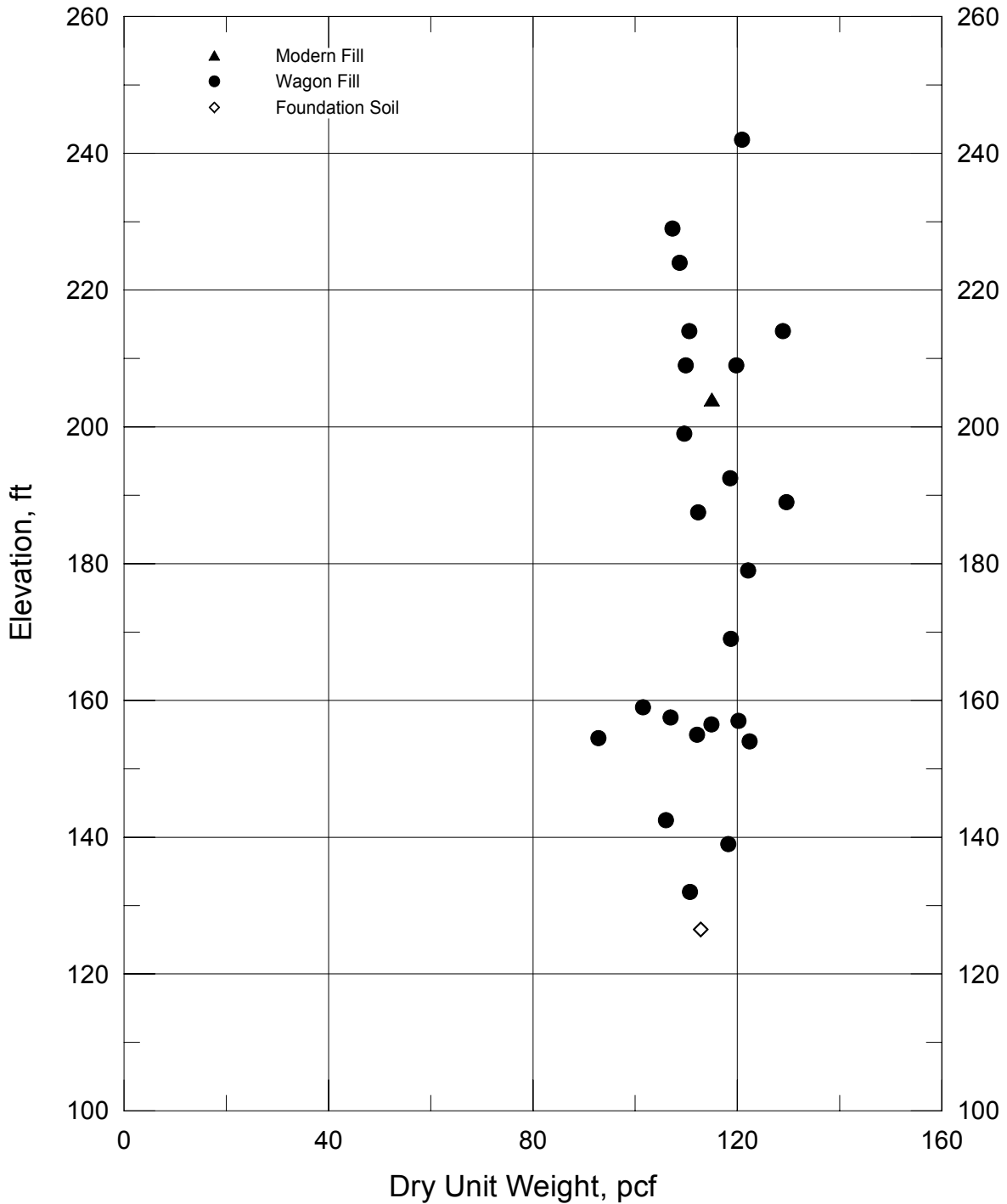
Project No. 26814536

Chabot Dam
Seismic Stability

Liquid Limit
From Borings WI-59, 61, 62, 64, 66 and 67
Wagon Fill Zone

Figure
7-17

Chabot Dam - Dry Unit Weight of Different Soil Types



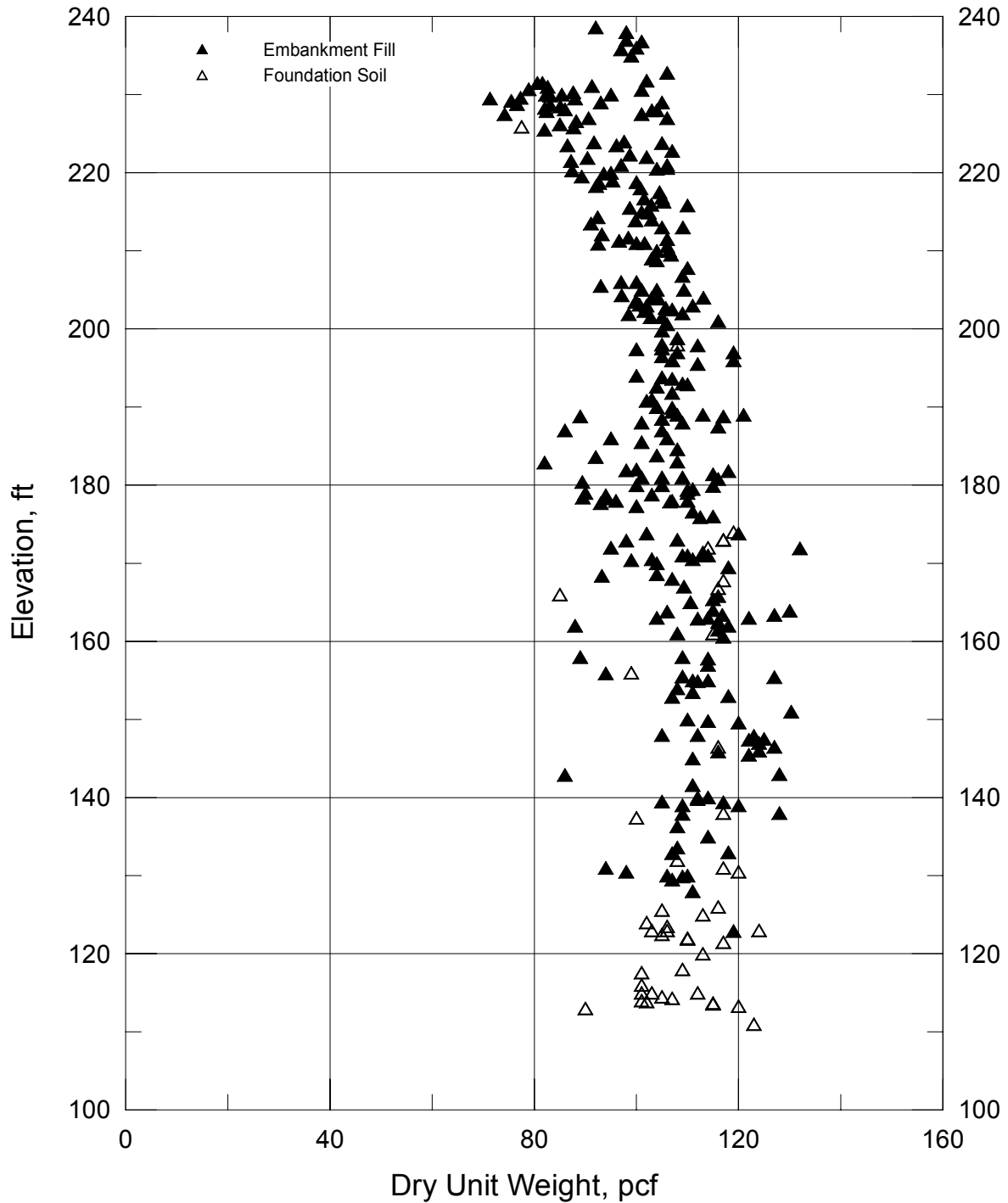
Project No. 26814536

Chabot Dam
Seismic Stability

**Dry Unit Weight
From Borings WI-59, 61, 62, 64, 66 and 67
Wagon Fill Zone**

Figure
7-18

Chabot Dam - Dry Unit Weight of Different Soil Types



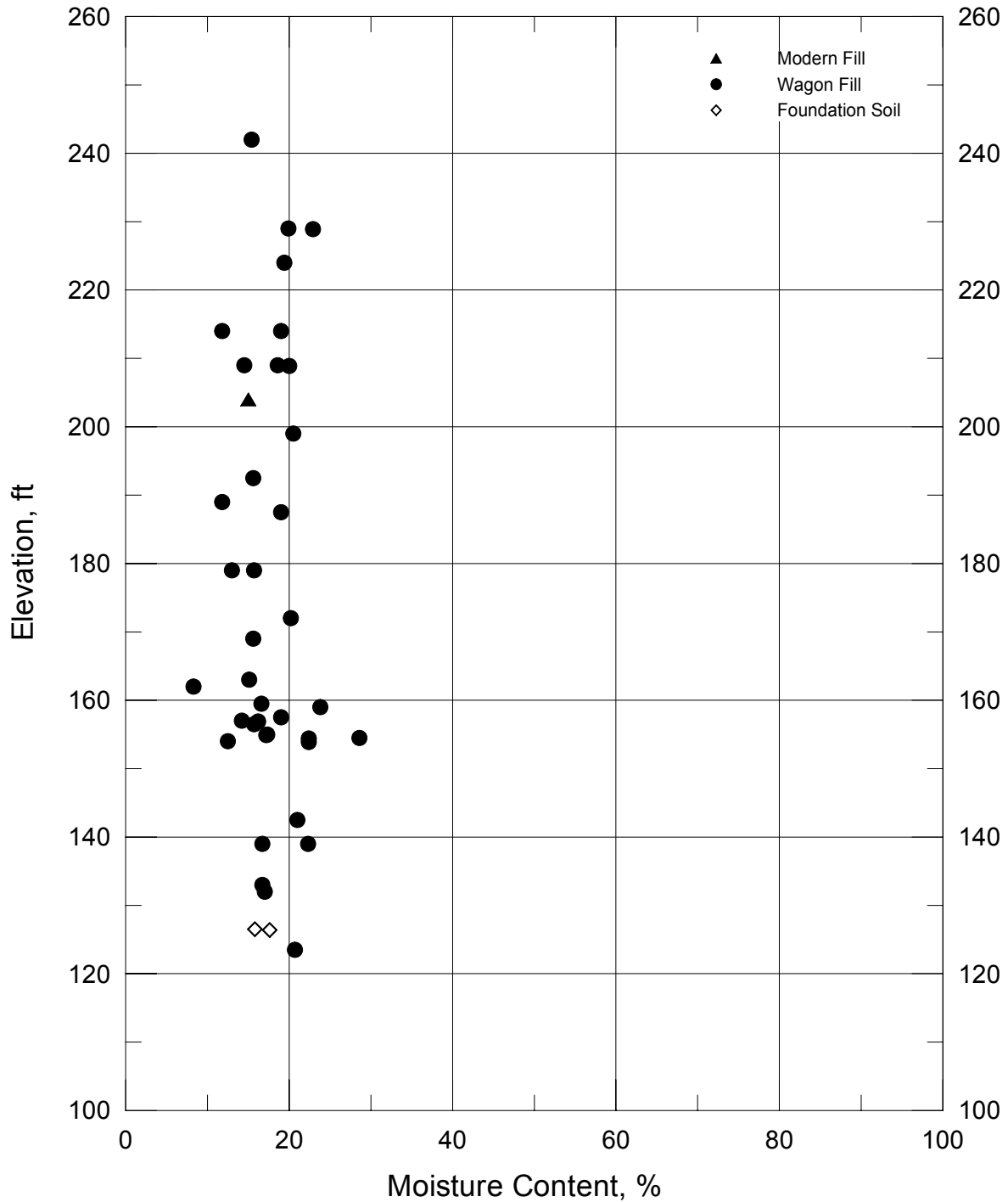
Project No. 26814536

Chabot Dam
Seismic Stability

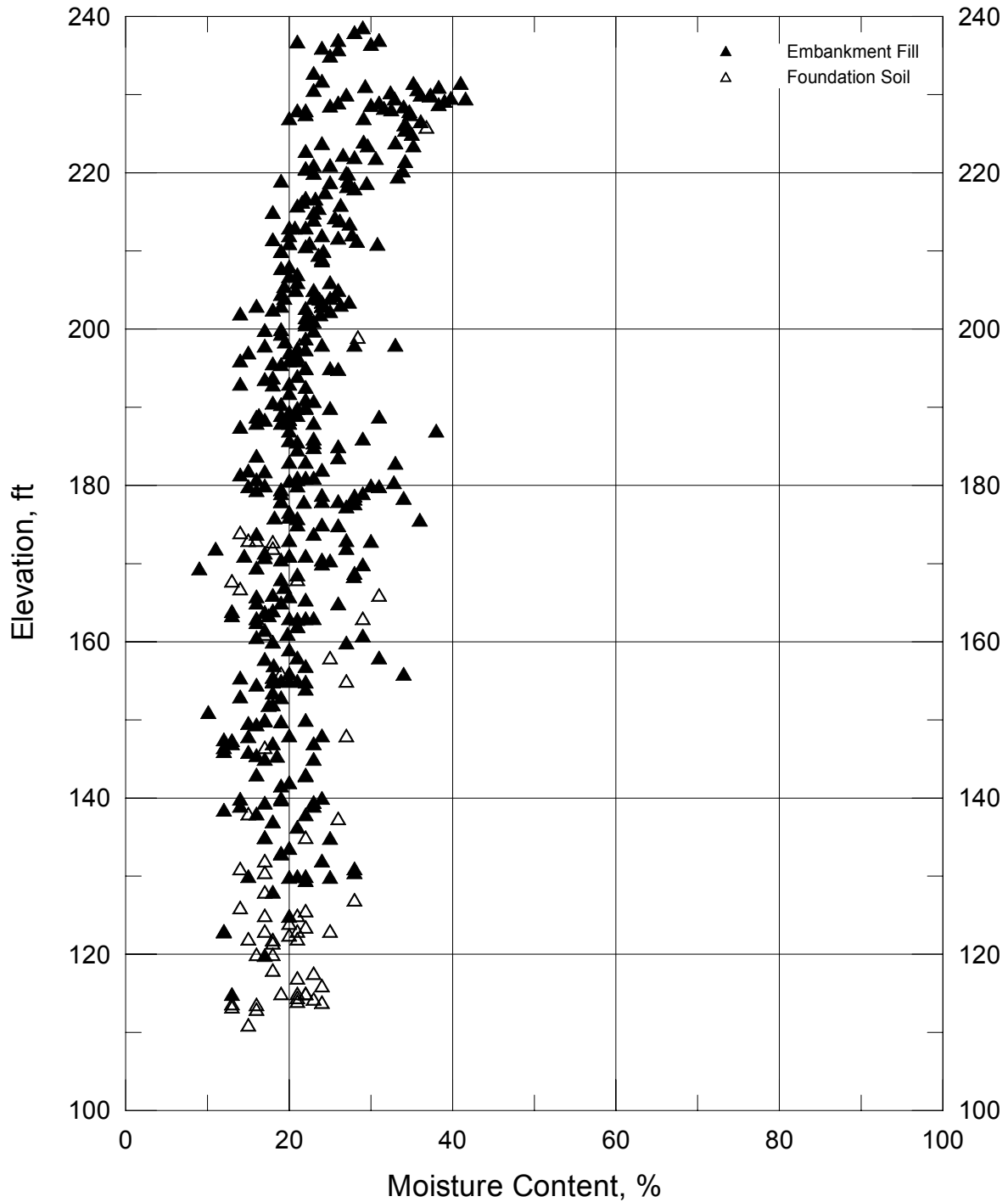
**Dry Unit Weight
From Previous Borings in Wagon Fill Zone**

Figure
7-19

Chabot Dam - Moisture Content of Different Soil Types



Chabot Dam - Moisture Content of Different Soil Types

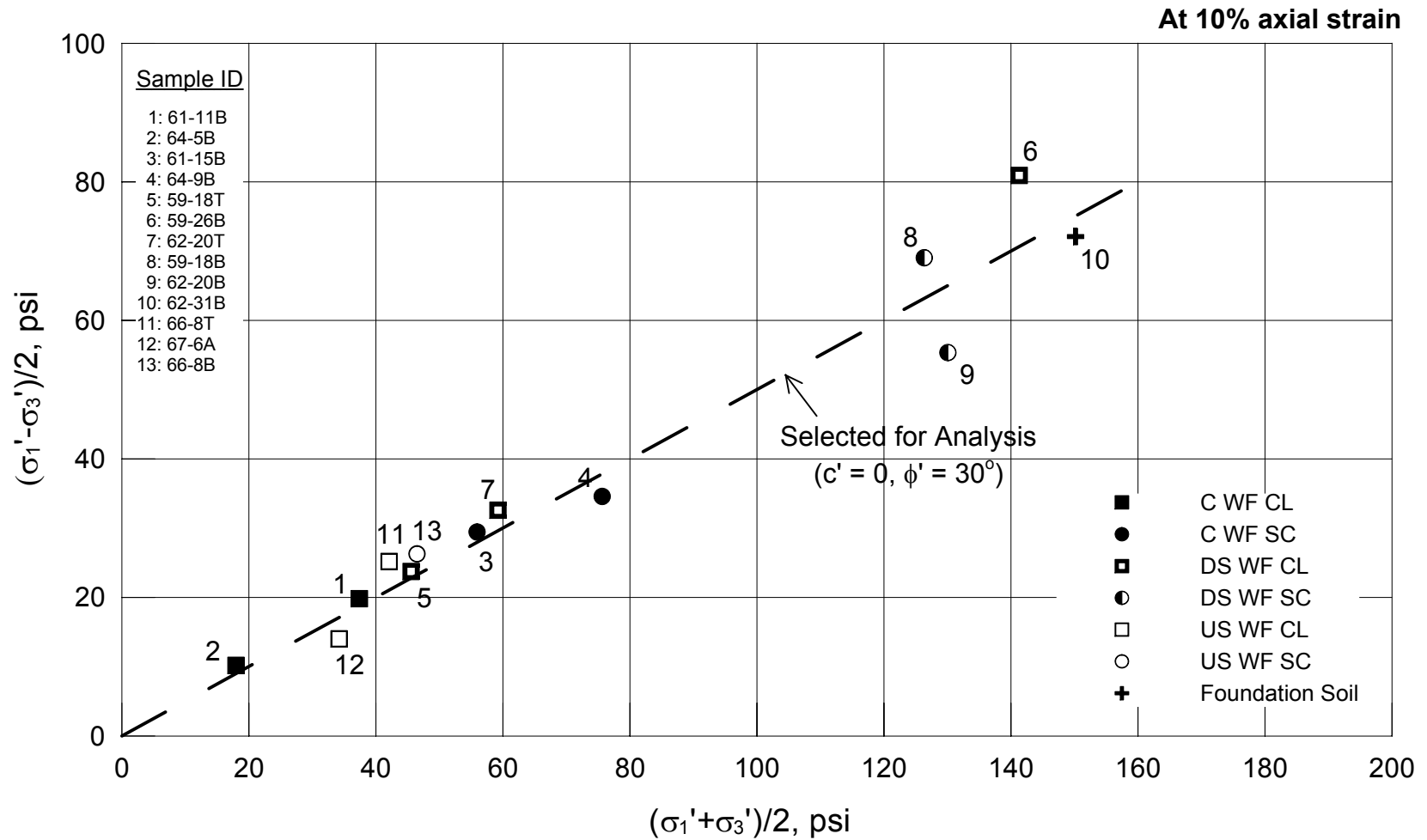


Project No. 26814536

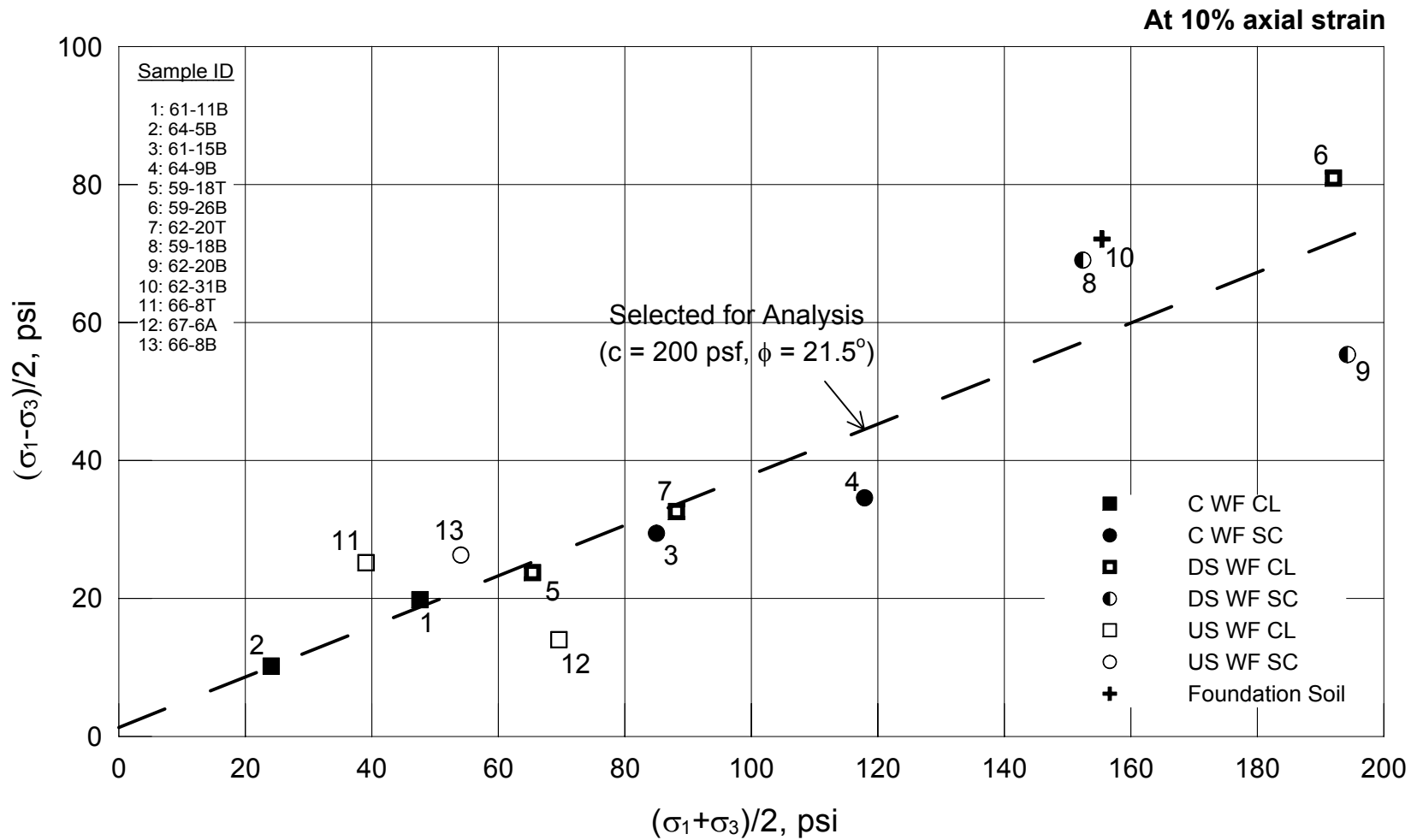
Chabot Dam
Seismic Stability

**Moisture Content
From Previous Borings in Wagon Fill Zone**

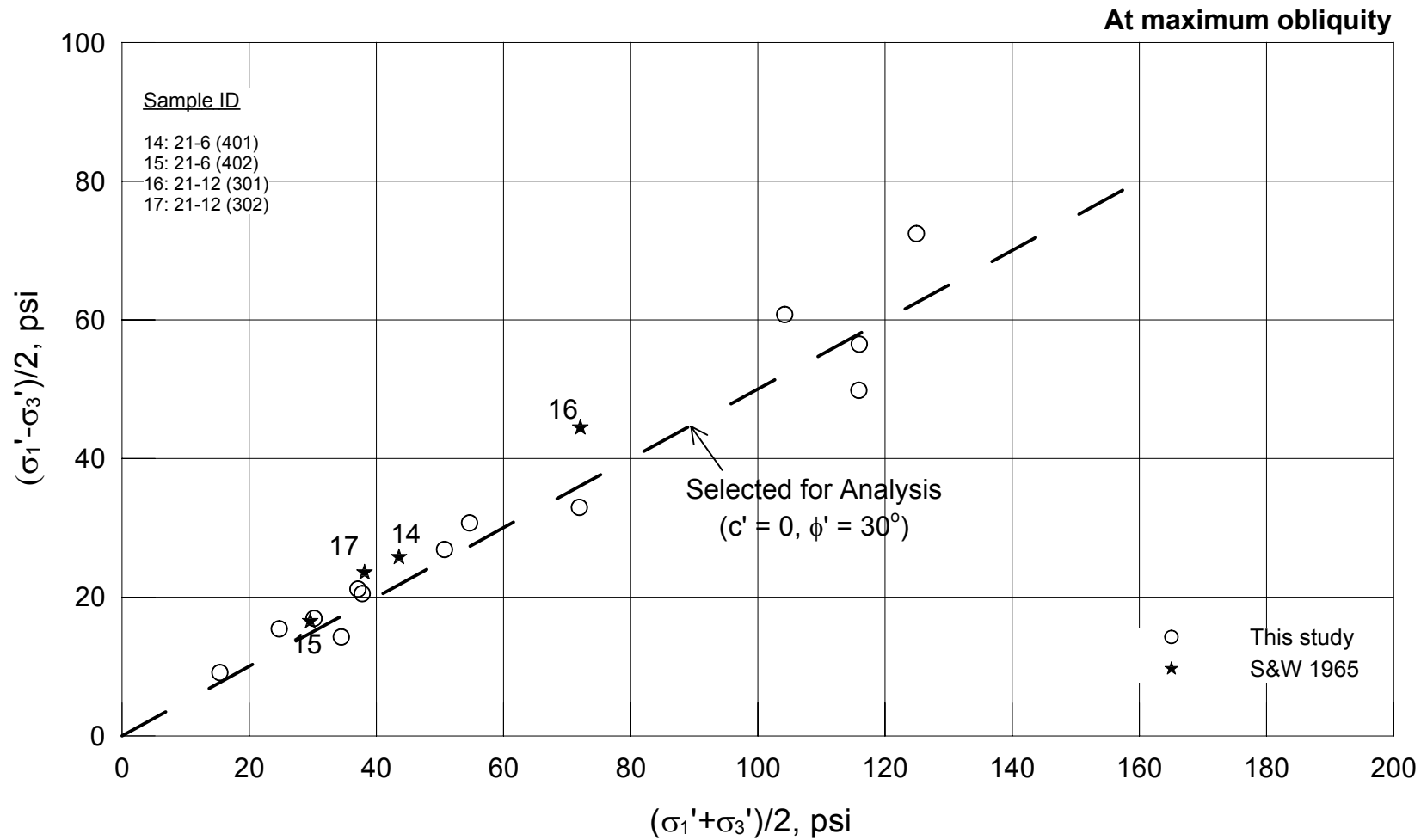
Figure
7-21



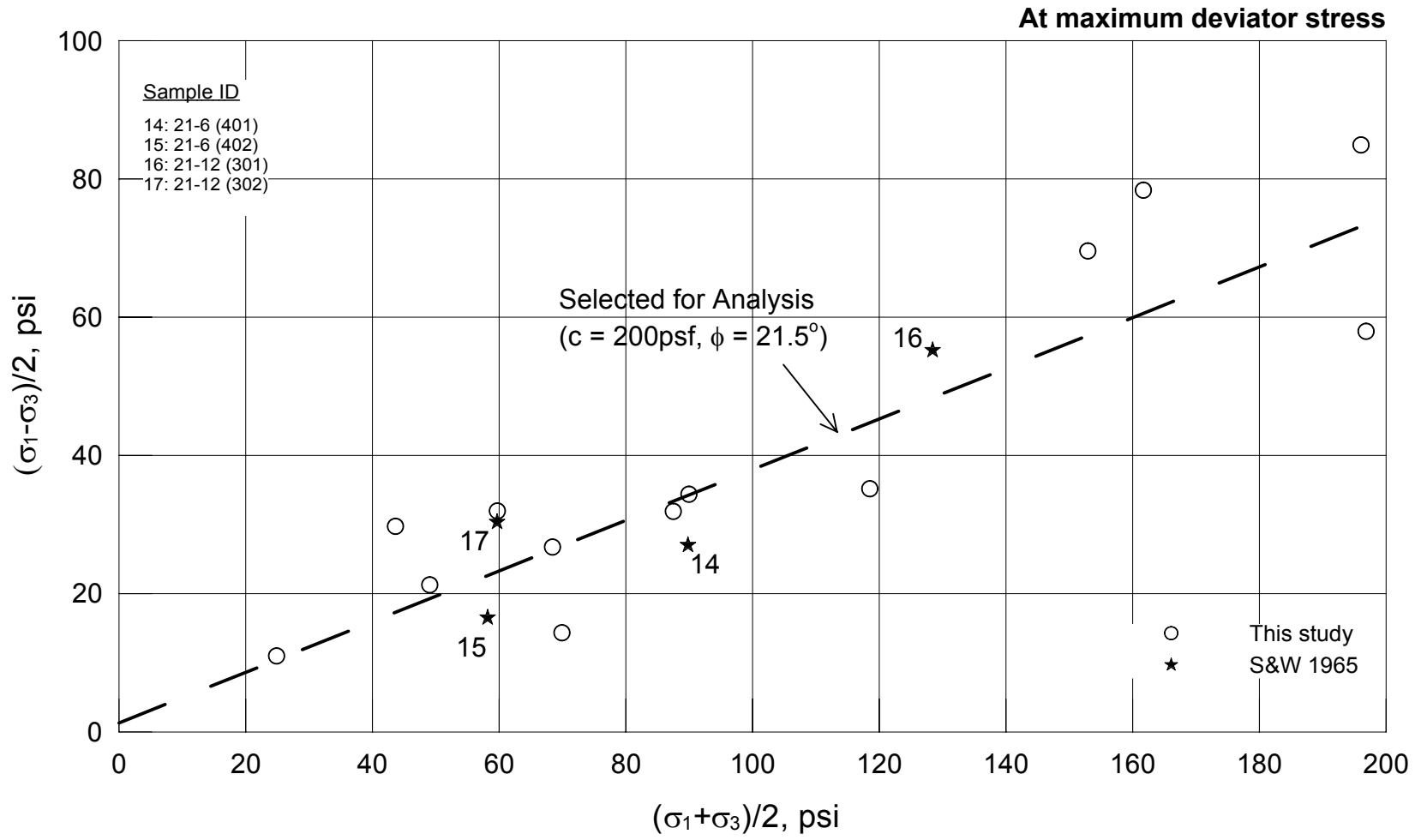
Project No. 26814536	Chabot Dam Seismic Stability	Wagon Fill Effective Shear Strength from ICU Triaxial Compression Tests	Figure
URS			7-23



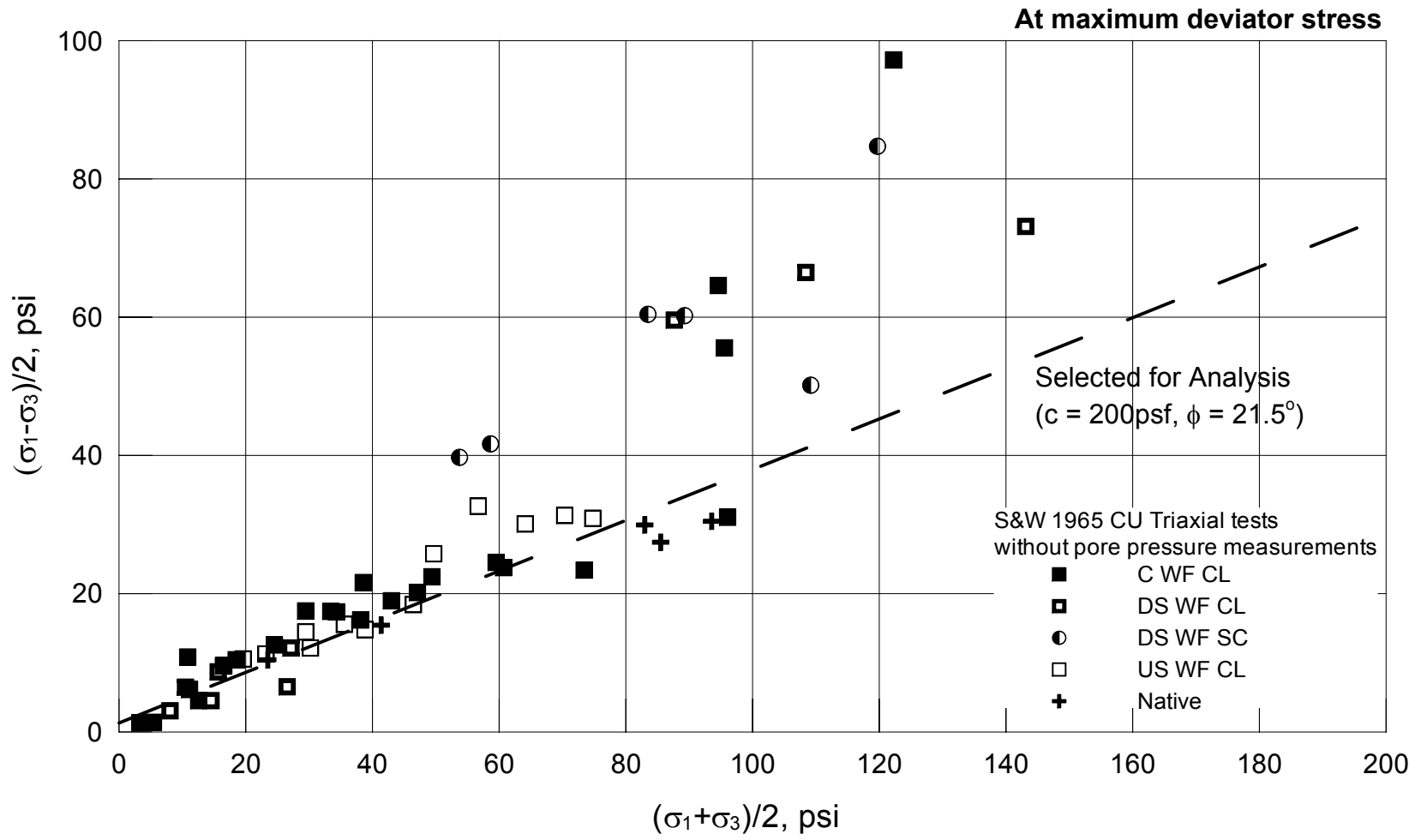
Project No. 26814536	Chabot Dam Seismic Stability	Wagon Fill Total Shear Strength from ICU Triaxial Compression Tests	Figure 7-24
URS			



Project No. 26814536	Chabot Dam Seismic Stability	Wagon Fill Effective Shear Strength from ICU Triaxial Compression Tests Comparison with Prior Data	Figure
URS			7-25

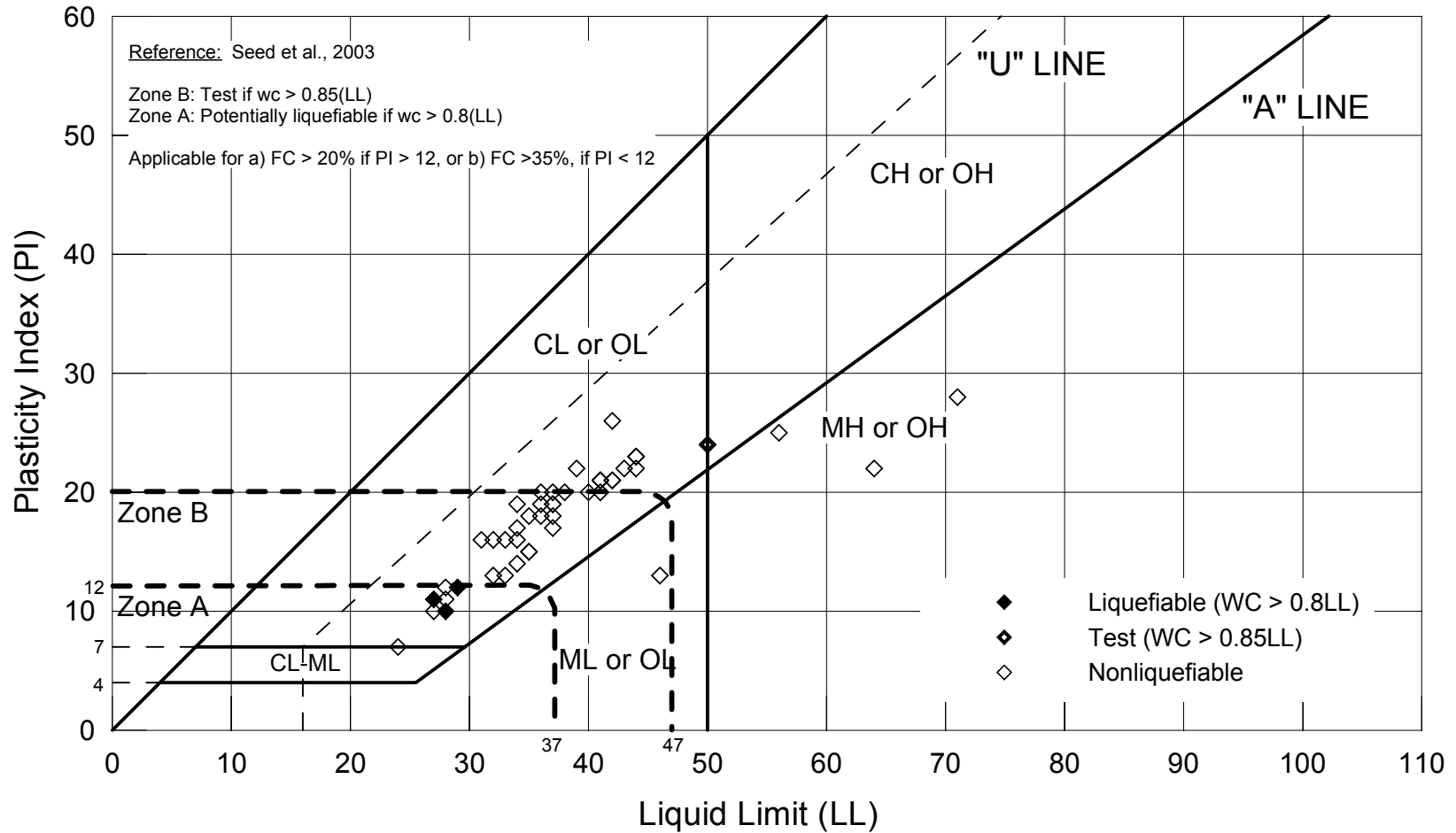


Project No. 26814536	Chabot Dam Seismic Stability	Wagon Fill Total Shear Strength from ICU Triaxial Compression Tests Comparison with Prior Data	Figure
URS			7-26



Project No. 26814536	Chabot Dam Seismic Stability	Wagon Fill Total Shear Strength from S&W CU Triaxial Compression Tests on Modified California Samples	Figure 7-27
URS			

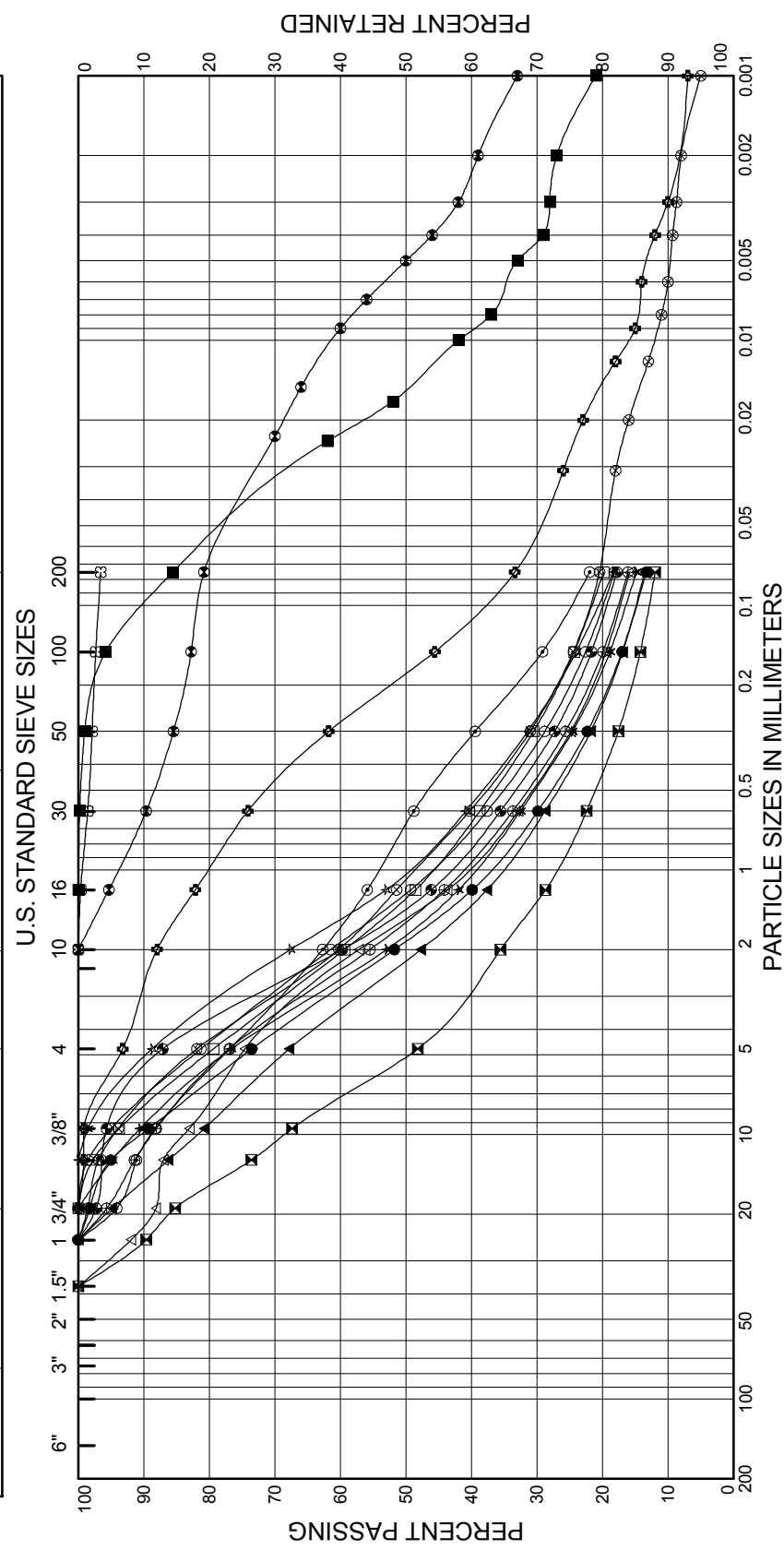
Plasticity Chart



Project No. 26814536	Chabot Dam Seismic Stability	Liquefaction Susceptibility Chart WI-59, 61, 62, 64, 66 and 67 Wagon Fill Zone	Figure 7-28
URS			

GRAVEL **SAND** **SILT AND CLAY**

coarse fine medium fine



BORING NUMBER	DEPTH (FT)	SAMPLE NUMBER	SYMBOL	DESCRIPTION
WI-65	22.5-24.5	10	■	Clay (CL)

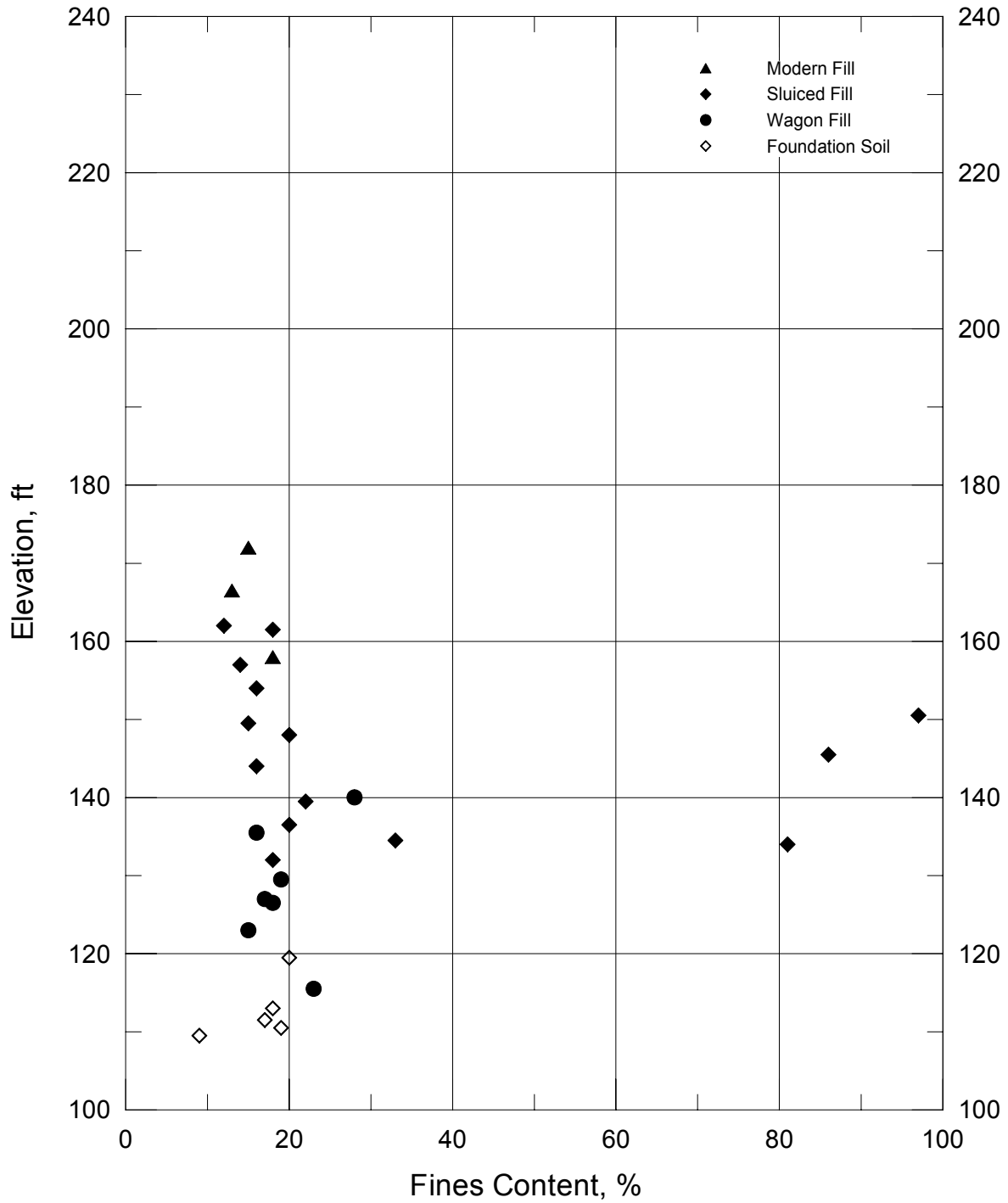
BORING NUMBER	DEPTH (FT)	SAMPLE NUMBER	SYMBOL	DESCRIPTION
WI-60	12.5-13	5B	●	Silty Clayey Sand with Gravel (SC-SM)
WI-60	17-18.5	7	⊠	Clayey Gravel with Sand (GC)
WI-60	22-23.5	9	▲	Clayey Sand with Gravel (SC)
WI-60	29.5-31	12	★	Clayey Sand with Gravel (SC)
WI-60	39.5-41	16	⊙	Clayey Sand with Gravel (SC)
WI-60	44.5-46	18	⊕	Clayey Sand (SC)
WI-63	10.5-12	4	○	Clayey Sand with Gravel (SC)
WI-63	18-19.5	7	△	Clayey Sand with Gravel (SC)
WI-63	24-24.5	9B	⊗	Clayey Sand with Gravel (SC)
WI-63	28-29.5	11	⊕	Clayey Sand with Gravel (SC)
WI-63	35.5-37	14	□	Clayey Sand with Gravel (SC)
WI-63	38-39.5	15	⊕	Clay with Sand (CH)
WI-63	40-42.5	16	★	Clayey Sand (SC)
WI-65	10-11.5	5	☆	Clayey Sand (SC)
WI-65	17.5-19	8	⊘	Clay (CH)

Dynamic Stability of Chabot Dam
Lake Chabot Dam, San Leandro, California
26814536.C0000

GRADATION OF SLUCED FILL
IN DOWNSTREAM TOE BORINGS
FIGURE 7-29



Chabot Dam - Fines Content of Different Soil Types



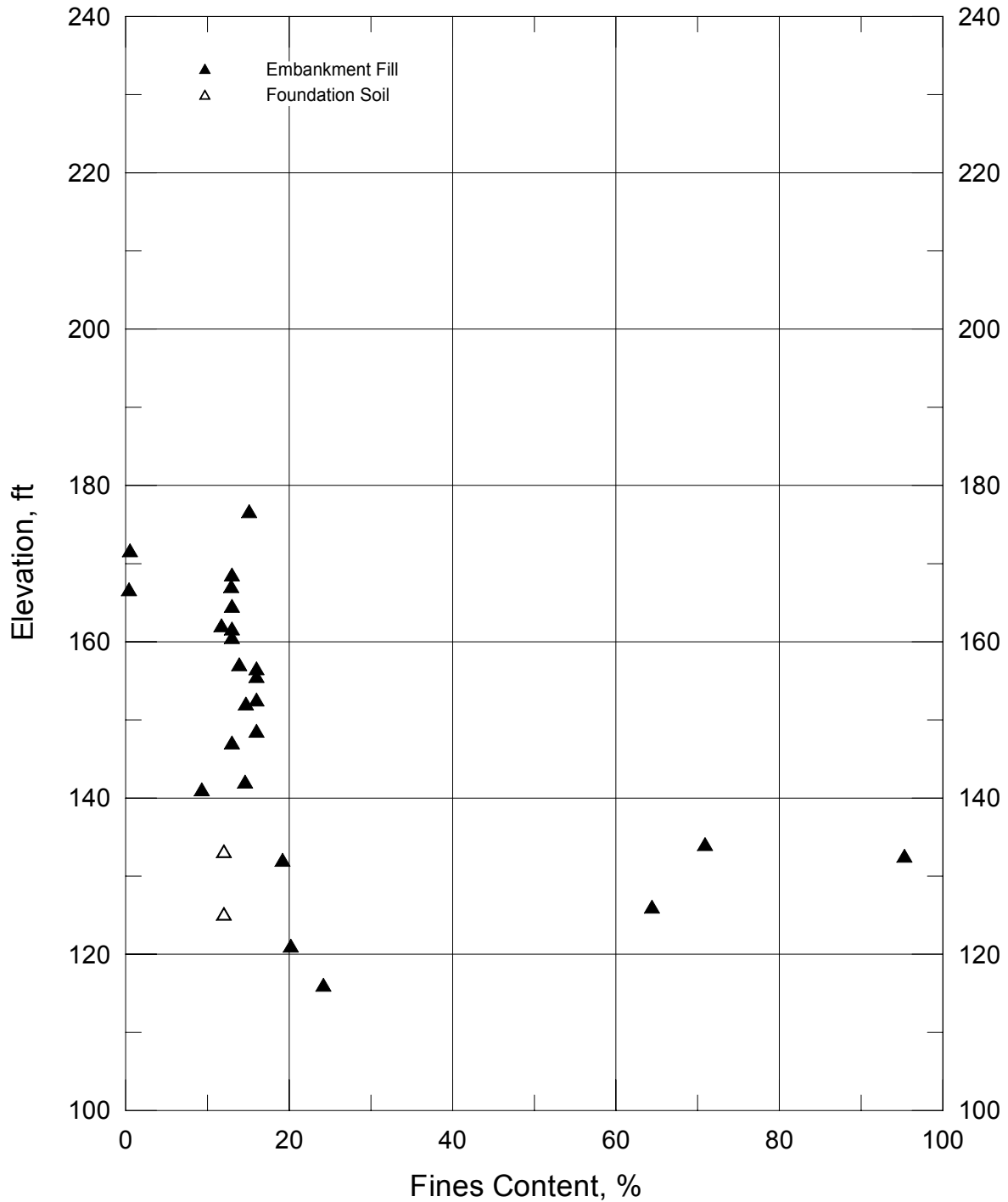
Project No. 26814536

Chabot Dam
Seismic Stability

**Fines Content
From Borings WI-60, 63 and 65
Sluiced Fill Zone**

Figure
7-30

Chabot Dam - Fines Content of Different Soil Types



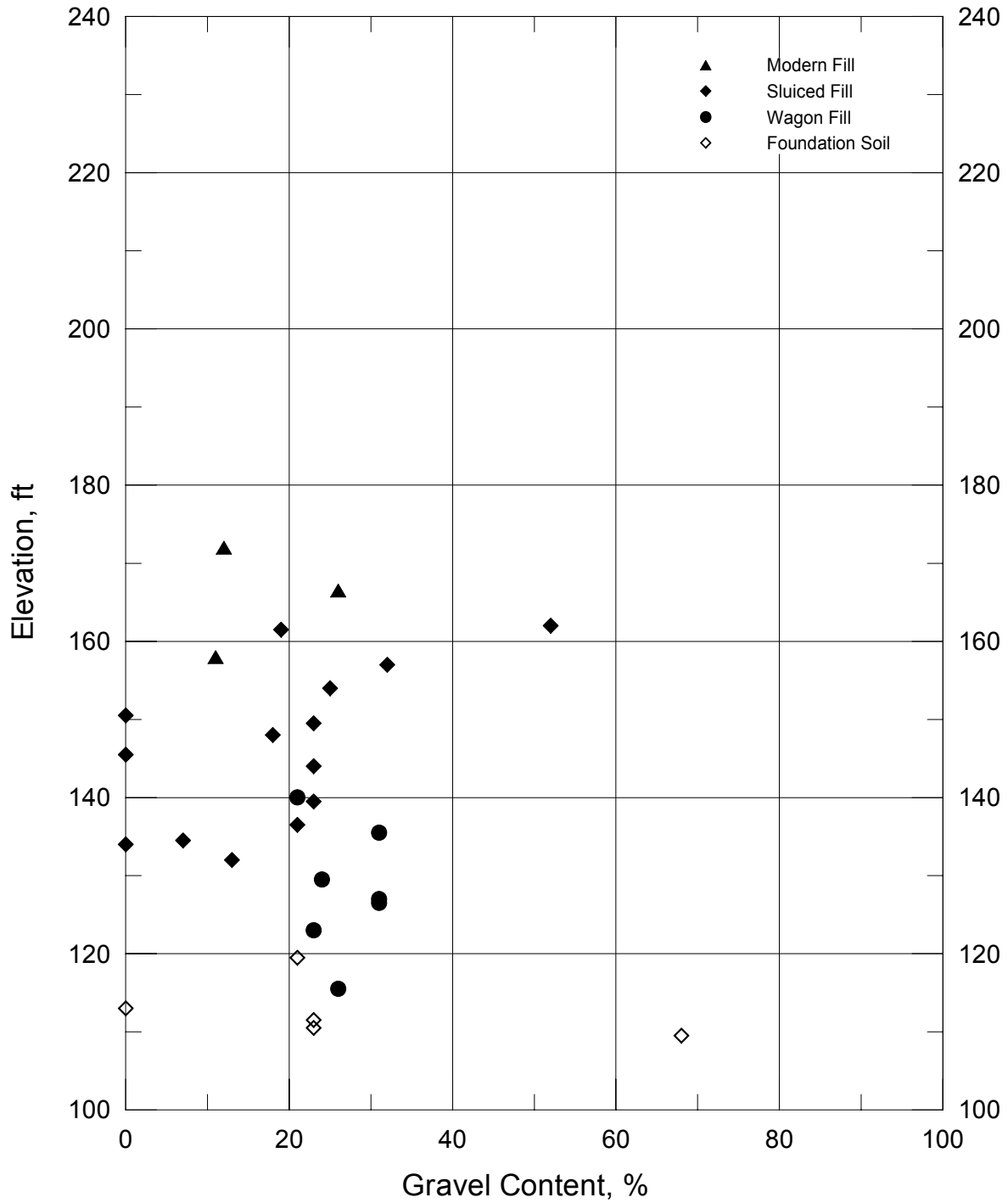
Project No. 26814536

Chabot Dam
Seismic Stability

**Fines Content
From Previous Borings in Sluiced Fill Zone**

Figure
7-31

Chabot Dam - Gravel Content of Different Soil Types



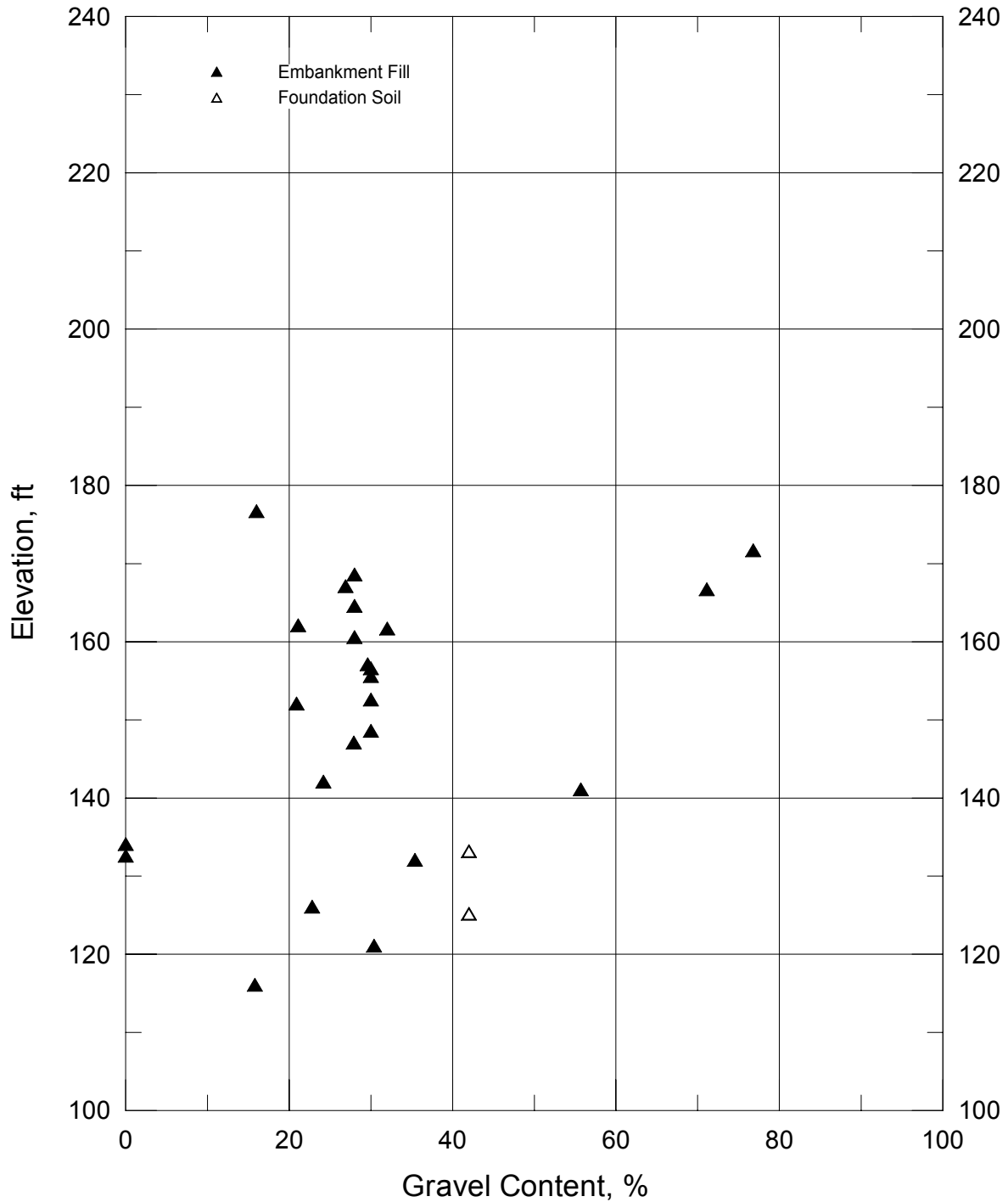
Project No. 26814536

Chabot Dam
Seismic Stability

**Gravel Content
From Borings WI-60, 63 and 65
Sluiced Fill Zone**

Figure
7-32

Chabot Dam - Gravel Content of Different Soil Types



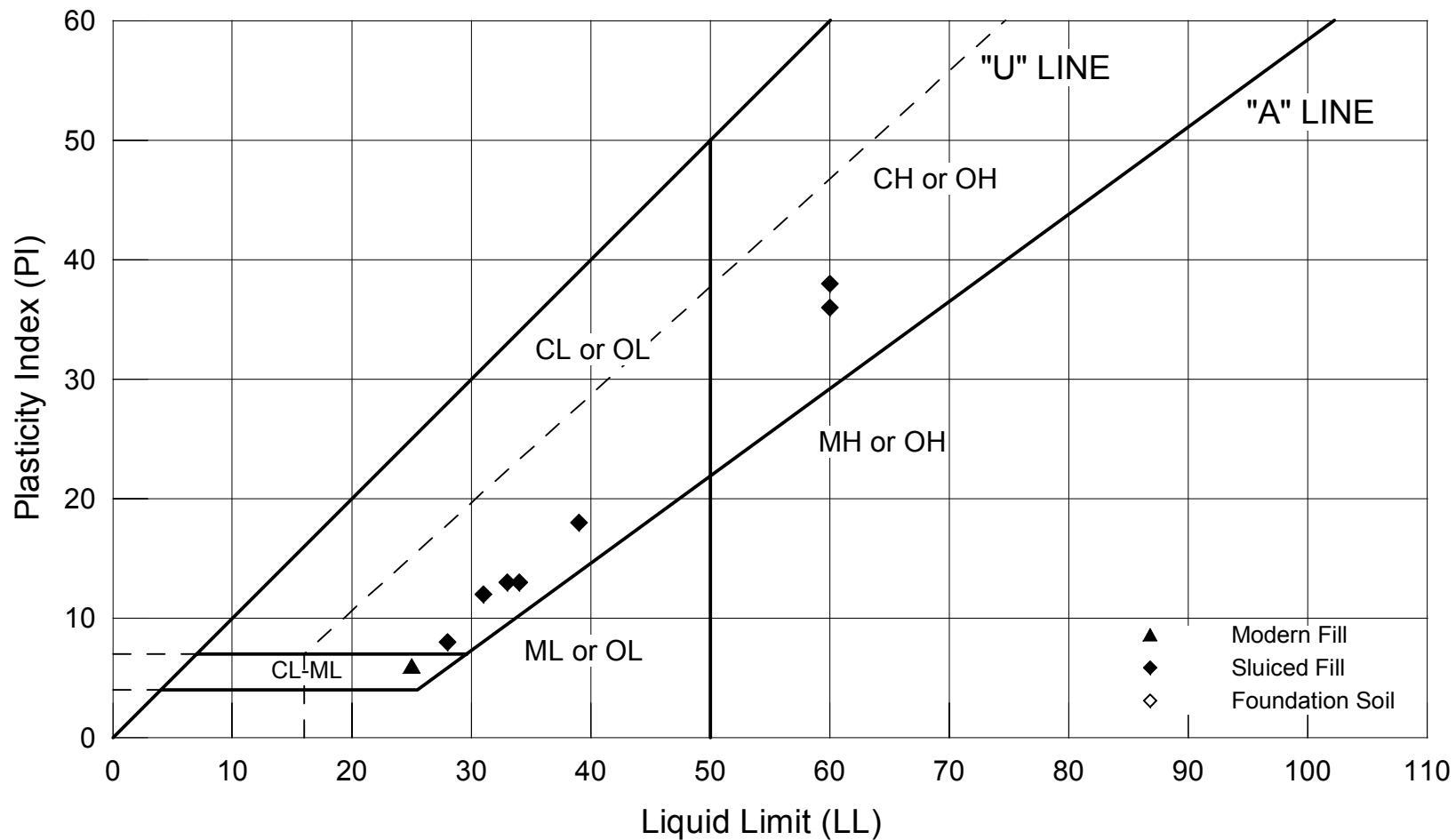
Project No. 26814536

Chabot Dam
Seismic Stability

**Gravel Content
From Previous Borings in Sluiced Fill Zone**

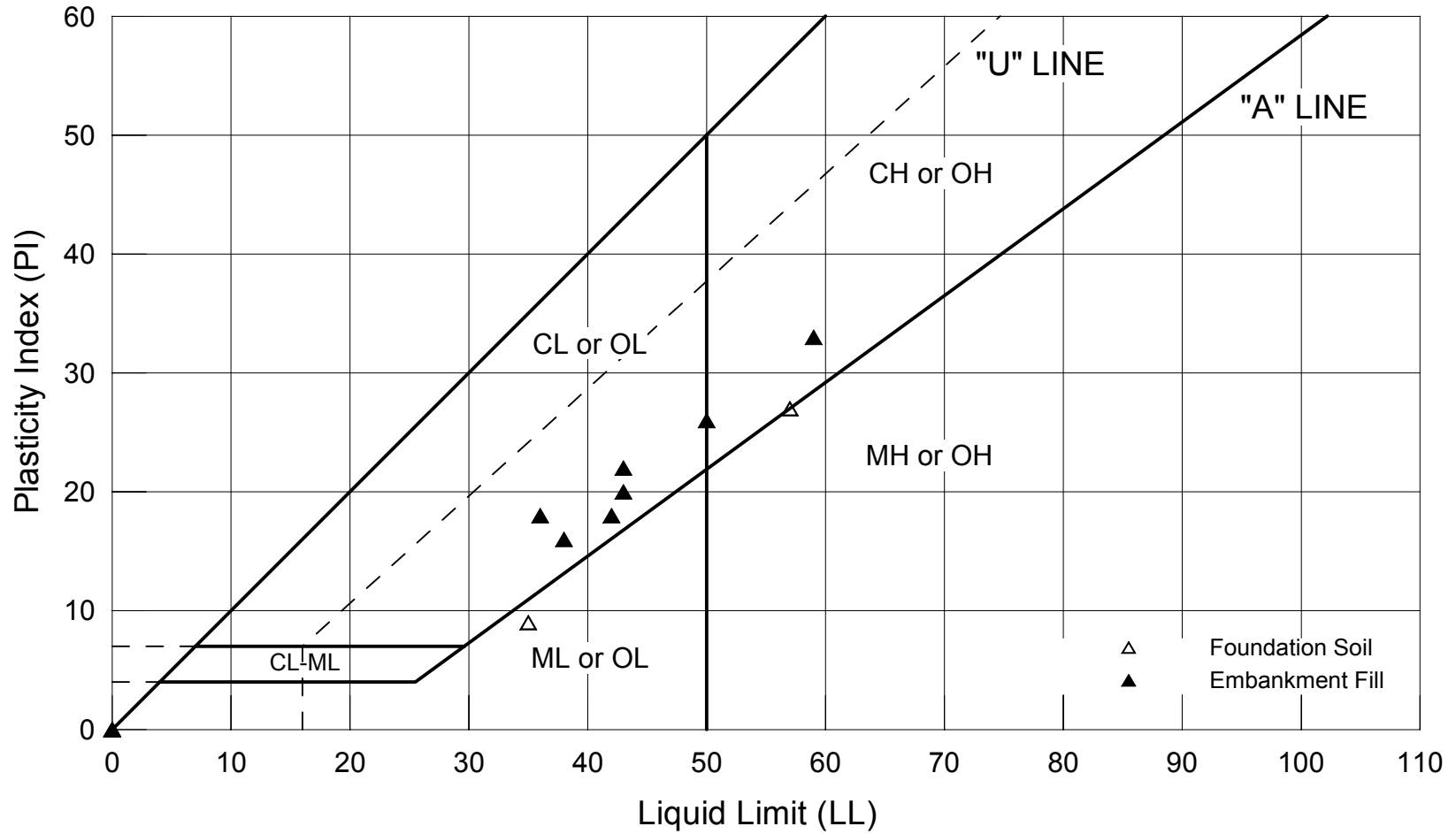
Figure
7-33

Plasticity Chart



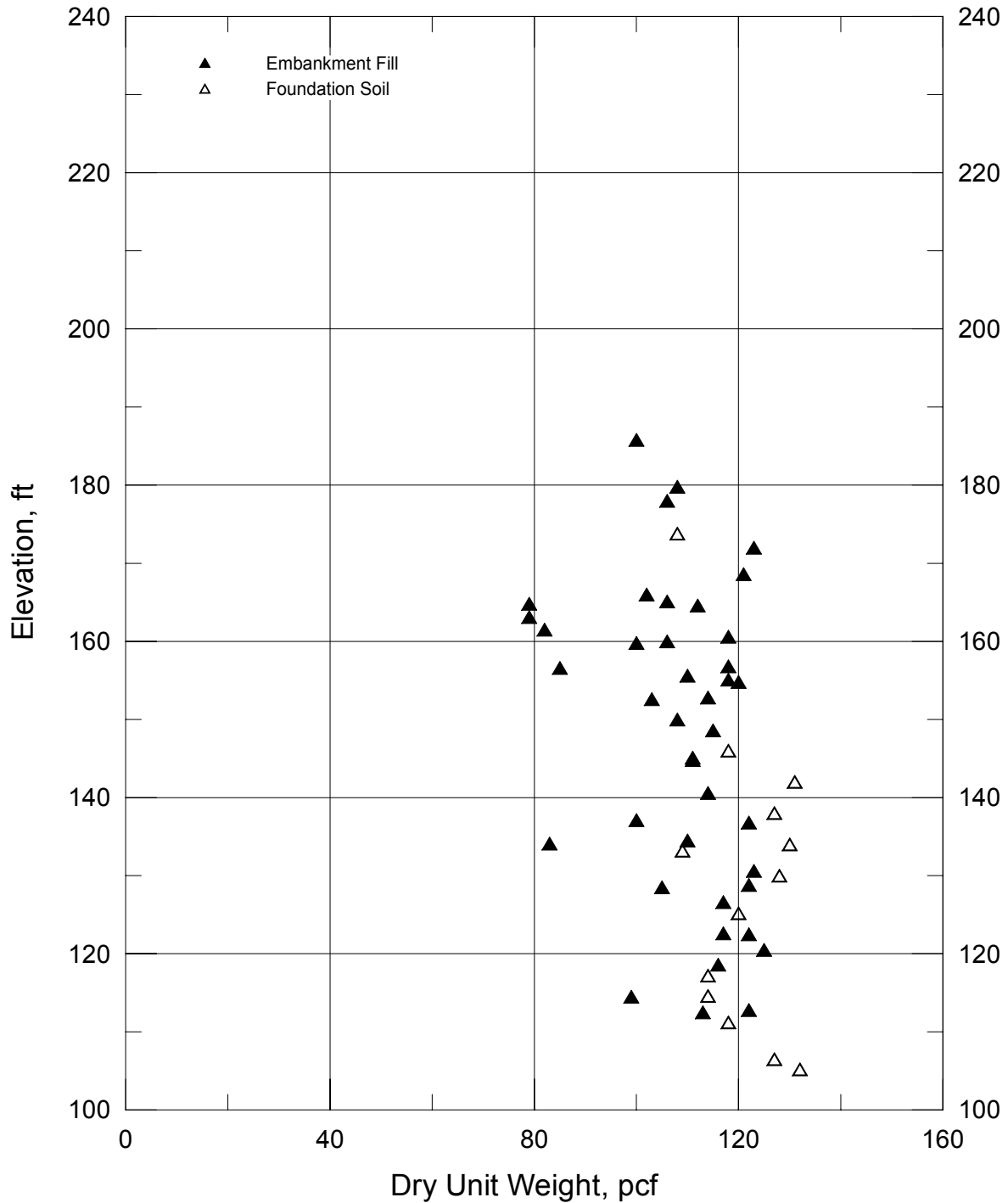
Project No. 26814536	Chabot Dam Seismic Stability	Plasticity from Borings WI-60, 63 and 65 Sluiced Fill Zone	Figure 7-34
URS			

Plasticity Chart



Project No. 26814536	Chabot Dam Seismic Stability	Plasticity from Previous Borings in Sluiced Fill Zone	Figure
URS			7-35

Chabot Dam - Dry Unit Weight of Different Soil Types



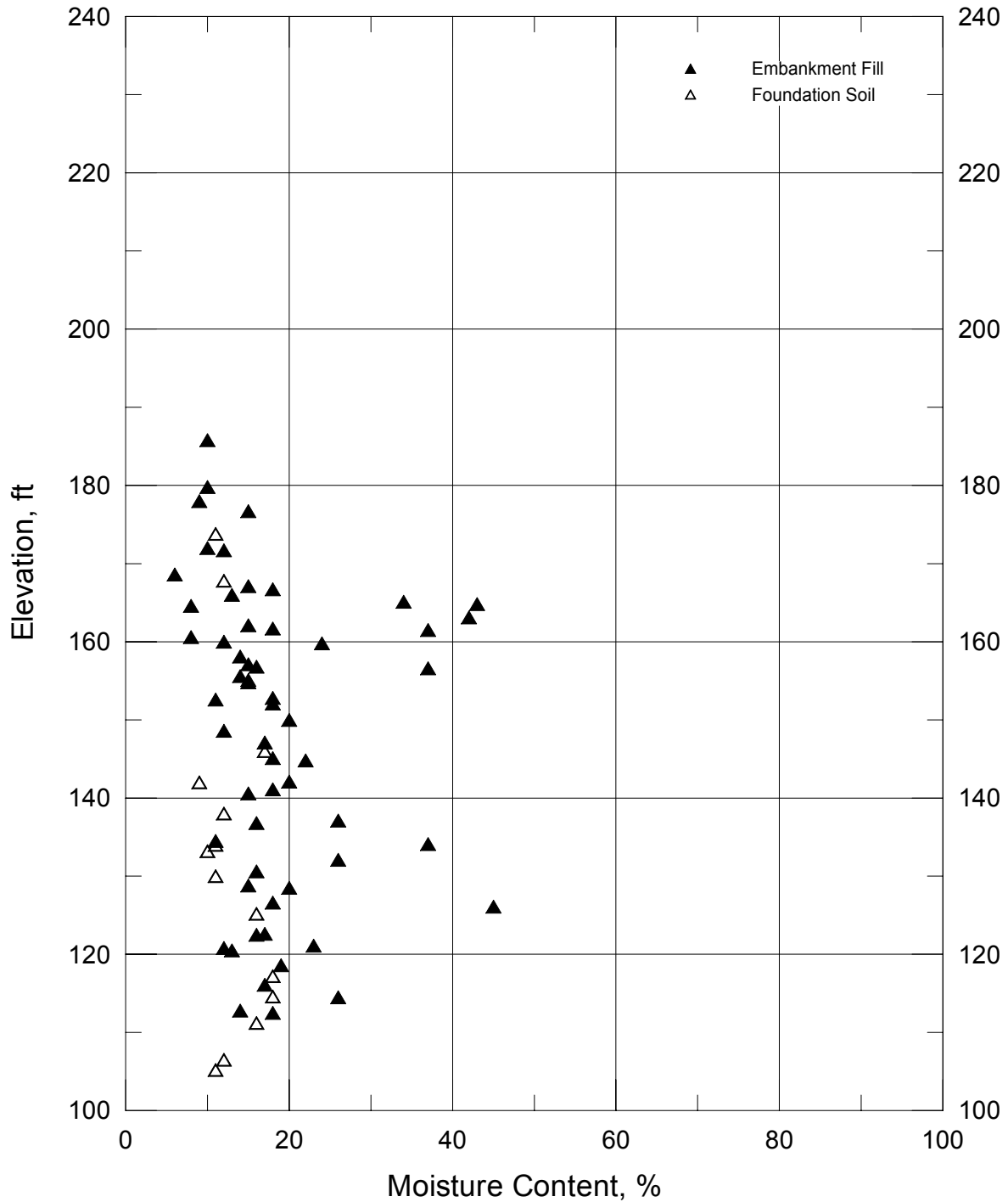
Project No. 26814536

Chabot Dam
Seismic Stability

**Dry Unit Weight
From Previous Borings in Sluiced Fill Zone**

Figure
7-36

Chabot Dam - Moisture Content of Different Soil Types



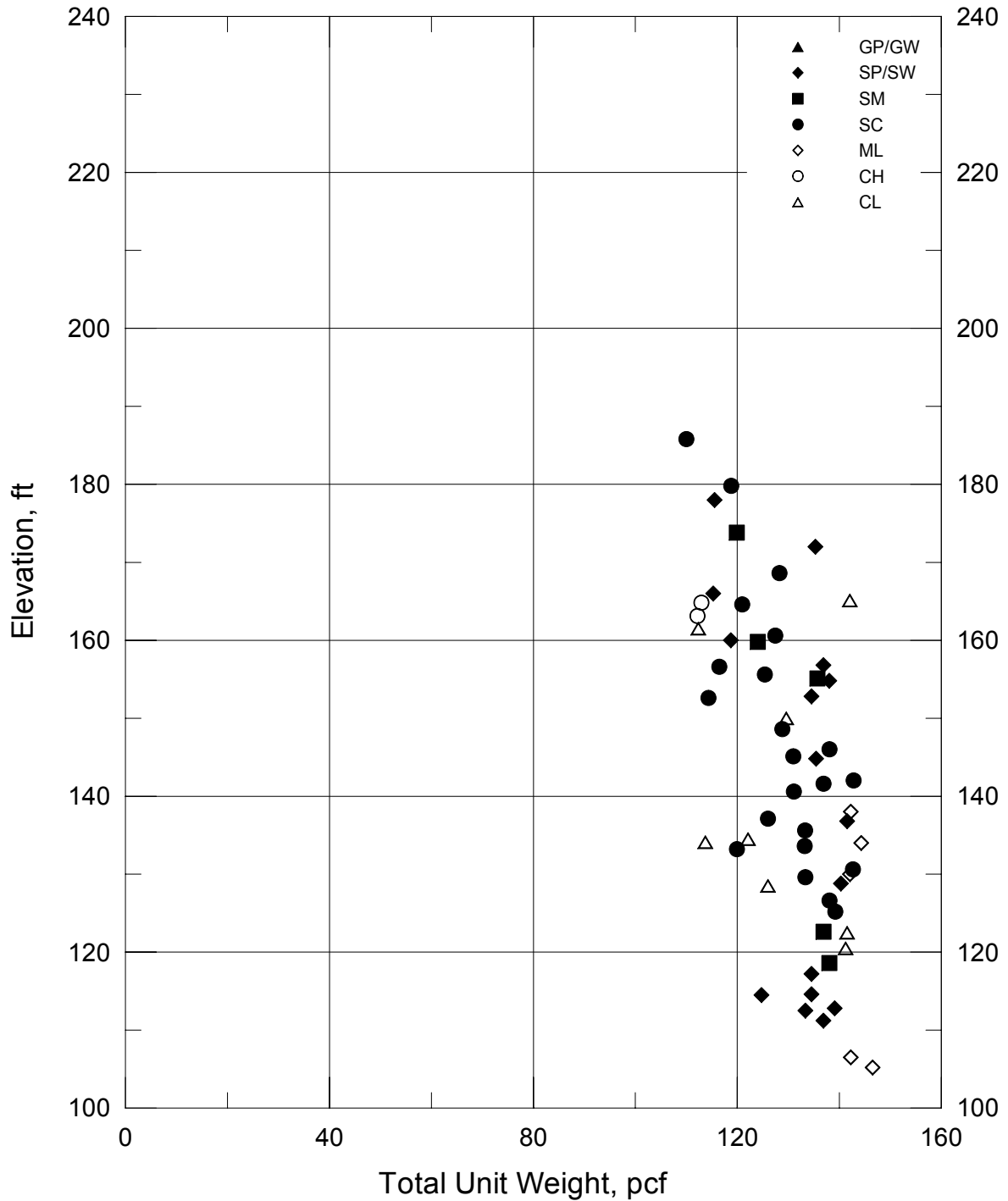
Project No. 26814536

Chabot Dam
Seismic Stability

**Moisture Content
From Previous Borings in Sluiced Fill Zone**

Figure
7-37

Chabot Dam - Total Unit Weight of Different Soil Types



Project No. 26814536

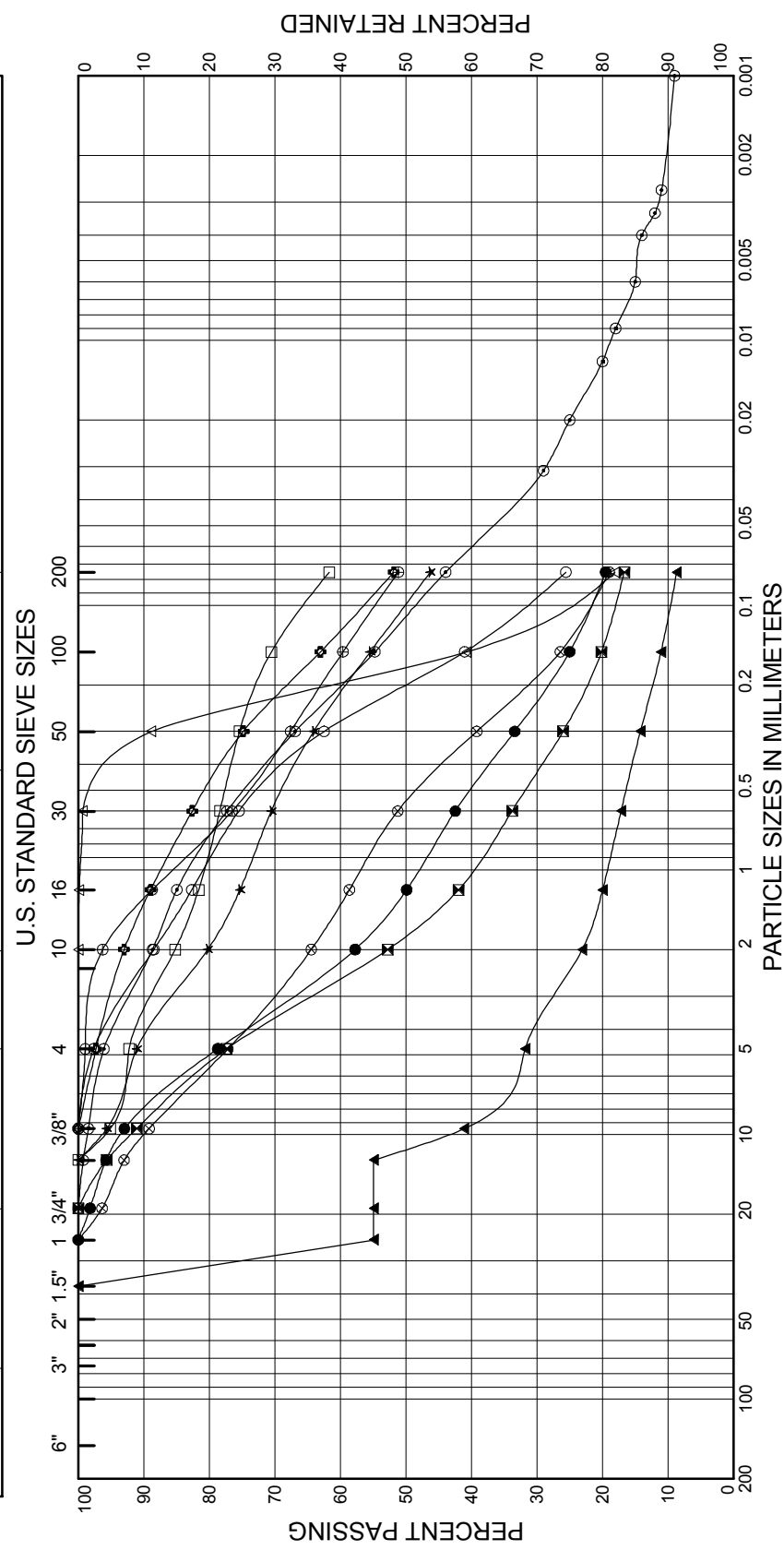
Chabot Dam
Seismic Stability

**Total Unit Weight
From Previous Borings in Sluiced Fill Zone**

Figure
7-38

GRAVEL **SAND** **SILT AND CLAY**

coarse fine coarse medium fine



BORING NUMBER	DEPTH (FT)	SAMPLE NUMBER	SYMBOL	DESCRIPTION
WI-60	59.5-61	24	●	Clayey Sand with Gravel (SC)
WI-60	67.5-68.5	27B	⊠	Clayey Sand with Gravel (SC)
WI-60	69.5-71	28	▲	Poorly Graded Gravel with Clay (GP-GC)
WI-62	93.5-95	30	★	Clayey Sand (SC)
WI-62	97.5-100	31B	⊕	Silty Sand (SM)
WI-62	100-101.5	32	⊙	Sandy Clay (CL)
WI-62	105.5-107	34	○	Clayey Sand (SC)
WI-65	55-56.5	23	△	Clayey Sand (SC)
WI-65	57.5-59	25	⊗	Clayey Sand with Gravel (SC)
WI-66	39-40	16B	⊕	Sandy Clay (CL)
WI-66	46-47.5	18	□	Sandy Clay (CL)

BORING NUMBER	DEPTH (FT)	SAMPLE NUMBER	SYMBOL	DESCRIPTION
WI-60	59.5-61	24	●	Clayey Sand with Gravel (SC)
WI-60	67.5-68.5	27B	⊠	Clayey Sand with Gravel (SC)
WI-60	69.5-71	28	▲	Poorly Graded Gravel with Clay (GP-GC)
WI-62	93.5-95	30	★	Clayey Sand (SC)
WI-62	97.5-100	31B	⊕	Silty Sand (SM)
WI-62	100-101.5	32	⊙	Sandy Clay (CL)
WI-62	105.5-107	34	○	Clayey Sand (SC)
WI-65	55-56.5	23	△	Clayey Sand (SC)
WI-65	57.5-59	25	⊗	Clayey Sand with Gravel (SC)
WI-66	39-40	16B	⊕	Sandy Clay (CL)
WI-66	46-47.5	18	□	Sandy Clay (CL)

Dynamic Stability of Chabot Dam
 Lake Chabot Dam, San Leandro, California
 26814536.C0000

GRADATION OF FOUNDATION SOIL

FIGURE 7-39



The general approach to assessing the seismic stability of the dam consisted of evaluating its dynamic response to the design earthquake motions, evaluating the potential for strength loss of the embankment and foundation materials under the earthquake shaking, estimating the deformations likely to be induced by the earthquake, and assessing the post-earthquake stability of the dam and its overall condition after the earthquake. This general approach is known as the Seed-Lee-Idriss approach (Seed, 1979).

The design earthquake was defined as the MCE on the Hayward-Rodgers Creek Fault since this earthquake is likely to generate the strongest ground motions at the site. Because the MCE on the San Andreas fault could result in strong shaking of long duration, the seismic stability of the dam was also evaluated for that earthquake. As a check of the analysis procedures, the dynamic response and deformations of the dam were also analyzed for motions representative of the 1989 Loma Prieta earthquake, for which the general performance of the dam is known.

Prior to the dynamic analyses, the dam's static stability was analyzed for comparison with the known long-term stability of the dam. The static stability was analyzed for several idealized cross-sections using limit-equilibrium procedures. The results of the limit-equilibrium analyses were used to select the dam cross-section for dynamic analysis. The limit-equilibrium analyses are described in Section 9.

The dynamic response, potential for strength loss, and seismic deformations of the dam were evaluated using the following two approaches:

- In the first approach, the dynamic response of the dam to the earthquake motions is analyzed initially. The earthquake-induced shear stresses calculated from that analysis are then compared with the cyclic strength of the embankment and foundation materials. From this comparison, the excess pore pressures, liquefaction potential, and strength loss in the materials are evaluated. The estimated strength loss in the materials is used in limit equilibrium analyses to calculate yield accelerations of potential sliding blocks within the dam. Together with the earthquake-induced accelerations calculated from the dynamic response analyses, the yield accelerations are used to calculate deformations of the blocks. Because the dam's dynamic response, potential for strength loss, and deformations are evaluated in separate analyses, this is referred to as a decoupled approach.
- In the second approach, referred to as a coupled approach, the dam's dynamic response, excess pore pressures and strength loss, and earthquake-induced deformations are calculated in a single analysis. The analytical procedure is based on nonlinear models capable of tracking the accumulation of deformations and development of excess pore pressures in the dam with time during the earthquake.

The analyses of the dam's dynamic response in the decoupled approach are discussed in Section 10. Those analyses were performed using two-dimensional finite element procedures with the computer program QUAD4M (Hudson et al. 1994). The evaluation of liquefaction potential, excess pore pressures, and strength loss, and the seismic stability and deformation analyses are presented in Section 11. The timing of liquefaction of the sluiced fill and of the development of excess pore pressures and strength degradation in the wagon fill and foundation soils were evaluated first. The residual strength of the liquefied sluiced fill and the degraded undrained strength of the wagon fill and foundation soils were then used in slope stability analyses to calculate yield accelerations and post-earthquake stability. Seismically induced

deformations of the dam were evaluated with Newmark-type procedures using the calculated yield accelerations and the results of the dynamic response analyses.

The non-linear dynamic analyses of the coupled approach were carried out with the two-dimensional finite difference computer code FLAC (Itasca, 2000). The analyses are presented in Section 12.

9.1 ANALYTICAL PROCEDURES

The static stability of the dam was analyzed using the limit-equilibrium method of slices. The computer program UTEXAS3 was used for the limit-equilibrium stability analyses. Spencer's method, which satisfies static equilibrium for each slice and overall equilibrium of the slide mass, was used in the UTEXAS analysis.

9.2 CROSS SECTIONS

We performed analyses on two basic idealized cross-sections, labeled A-A' and B-B' in Figure 9-1. These sections are shown in Figures 9-2 and 9-3. They were developed based on the subsurface information shown in Figures 7-3 and 7-4. Modified versions of these sections were also analyzed to consider uncertainty in the geometry of some of the dam zones. A modified section A-A' is shown in Figure 9-4. This modification reflects uncertainty in the location of the boundary between the wagon fill and the sluiced fill (WF/SF boundary).

Composite section A-A", shown in Figure 9-5, was developed to evaluate the effects on dam stability of the curved stream channel downstream of the dam. In composite section A-A", the top of the sluiced fill is obtained from District drawing No. 6948-G-1.05, which shows the topography prior to the 1980 dam modification, and the surface of the random fill is obtained from District drawing No. 6948-G-1.03.1, which shows the as-built topography after the dam modification. In addition, we assumed that the bedrock elevation remains constant and that the phreatic surface is essentially parallel to the top surface of the sluiced fill in the downstream direction. The WF/SF boundary was adopted from modified section A-A', which is more conservative than the preferred section A-A'.

9.3 MATERIAL PROPERTIES

The analyses were performed for long-term static and pseudo-static loading conditions (with both pre-earthquake and post-earthquake strengths). For the long-term condition, drained strengths obtained from the effective-stress strength parameters were used for all materials. For pseudo-static loading, undrained strengths were used for all saturated soils while drained strengths were used for soils above the phreatic surface.

Pseudo-static analyses were performed to evaluate the yield accelerations of potential sliding blocks within the dam for various assumed levels of undrained strength degradation induced by the earthquake shaking. Those analyses are discussed in Section 11.0. The analyses assuming no strength degradation correspond to the pre-earthquake condition and are presented in this section.

The undrained strengths of the saturated wagon fill and foundation soils for the pre-earthquake condition were obtained by direct fitting of the strength envelope to the values of shear stress on the failure plane at the time of failure versus normal stress on the failure plane after consolidation (τ_{ff} versus σ'_{fc} envelope). Thus, it is assumed that the undrained strength is a function of the effective normal stresses and the effective principal stress ratio (K_c) acting on the failure surface prior to seismic loading. This strength formulation was proposed by Duncan et al. (1990) and is incorporated in the UTEXAS3 program. The pre-earthquake undrained strength of the sluiced

fill was assumed equal to the drained strength. After liquefaction, its undrained strength was assumed equal to the residual strength.

The strength parameters used in the limit-equilibrium analyses are summarized in Tables 9-1 and 9-2. The slope stability analyses for the post-earthquake condition and pseudo-static loading with post-earthquake strength parameters are discussed in Section 11.

9.4 ANALYSIS RESULTS

The analysis results for sections A-A' and modified A-A' are presented in Figures 9-6 through 9-11. Under long-term static loading, the results for sections A-A' and modified A-A' are very similar. This is expected since the drained strengths of the sluiced fill and wagon fill materials are similar. As shown in Figures 9-6 and 9-7, the computed factors of safety (FS) against slope instability for deep-seated sliding surfaces are greater than 2.5 for the upstream and downstream slopes. For sliding surfaces passing through the crest and the upstream toe, the computed FS values are between 1.5 and 1.7. A relatively low FS of 1.2 is computed for a shallow sliding surface through the upstream toe. For sliding surfaces within the downstream shell, the computed FS values range between 2.2 and 2.4.

For the pre-earthquake loading condition, the computed FS values for deep-seated sliding surfaces are between 2.5 and 3.0 for the upstream and downstream slopes (Figures 9-8 and 9-9). For sliding surfaces passing through the crest and the upstream toe, the computed FS values are about 2.2 (Figure 9-8). For Section A-A' under pseudo-static loading, the computed yield acceleration coefficients (K_y) are equal to or greater than 0.35 for the downstream slope when pre-earthquake strengths are used (Figure 9-10). For the upstream slope, the computed values of K_y for a deep-seated sliding surface and a sliding surface through the crest and the upstream toe are 0.37 and 0.28, respectively. For modified section A-A', the computed values of FS and K_y are similar to those for Section A-A' under pre-earthquake loading (Figure 9-11).

The analysis results for Section B-B' are presented in Figures 9-12 and 9-13. Since the static analyses showed that Section B-B' is less critical than sections A-A' or modified A-A', pseudo-static analyses were not performed for Section B-B'.

The analysis results for composite section A-A'' are presented in Figure 9-14. As expected, the computed FS for the downstream slope under pre-earthquake conditions are generally similar to those computed for modified section A-A'. Pseudo-static analyses were not performed for Section A-A'' because the yield acceleration coefficients should be similar to those computed for modified section A-A'.

The analysis results indicate adequate factors of safety (1.5 or greater) in both upstream and downstream directions under long-term static conditions. This conclusion agrees well with the known long-term stability of the dam. The results also indicate that the dam should perform satisfactorily during minor earthquakes that do not trigger liquefaction of the sluiced fill or generate high pore pressures within the wagon fill. Furthermore, the analyses results indicate that Section B-B' is less critical than Section A-A'. Accordingly, the latter was used in the dynamic analysis of the dam.

Table 9-1
UTEXAS3 Input Parameters for Static Stability Analysis - Long Term Condition

Material	Total Unit Weight	Effective Strength Parameters	
	γ_t	c'	ϕ'
	(pcf)	(psf)	(°)
Modern Fill	134	0	35
Random Fill	130	0	33
Wagon Fill	133	0	30
Sluiced Fill	130	0	33
Foundation Soils	133	0	30
Reservoir Silt	90	200	0

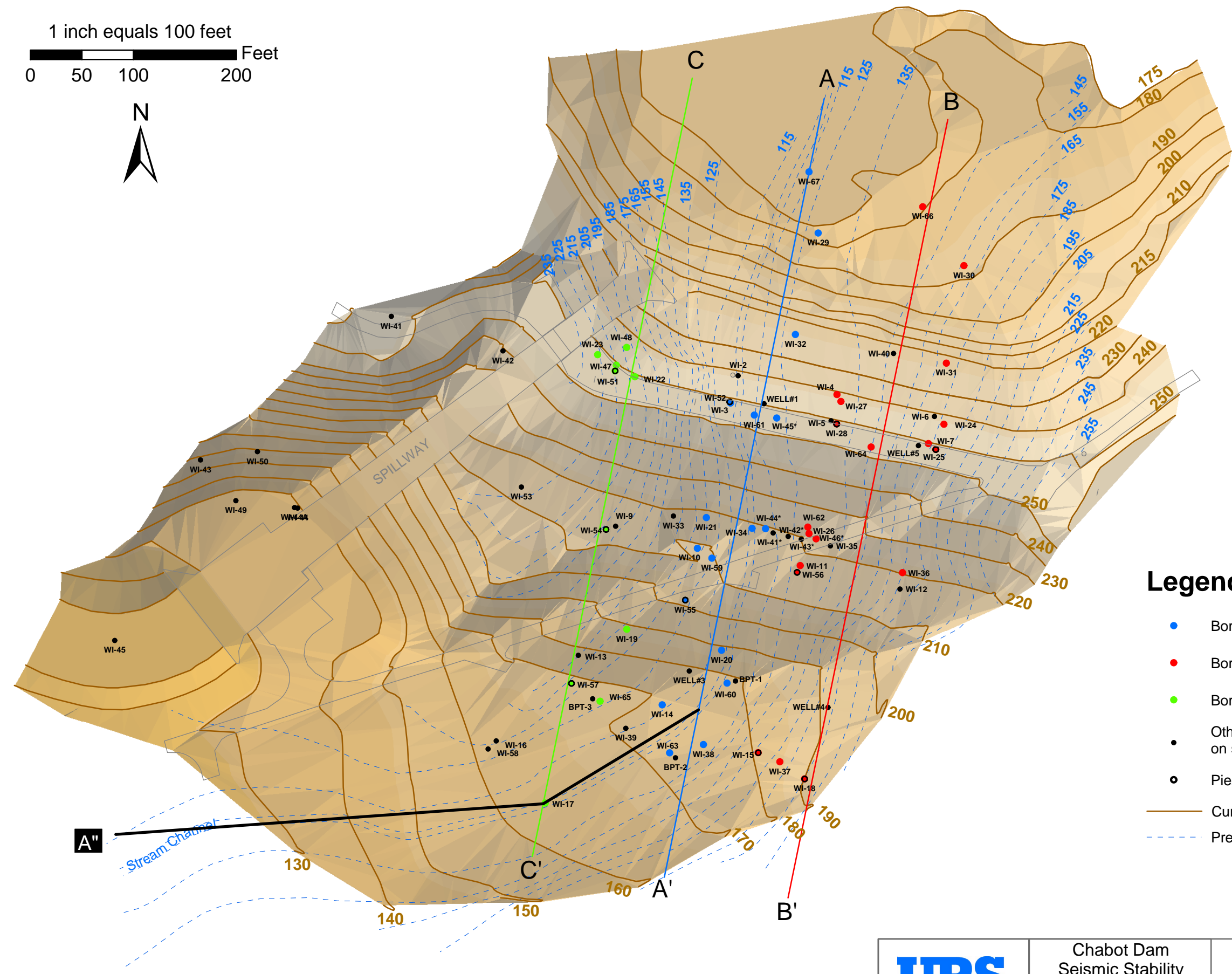
Table 9-2
UTEXAS3 Input Parameters for Seismic Stability Analysis - Pre-Earthquake Condition

Material	Total Unit Weight	Undrained Strength Envelope ($K_c = 1$) ⁽¹⁾		Effective Strength Parameters	
	γ_t	d_R	Ψ_R	c'	ϕ'
	(pcf)	(psf)	(°)	(psf)	(°)
Modern Fill	134	-	-	0	35
Random Fill	130	-	-	0	33
Wagon Fill	133	1075	22.6	0	30
Sluiced Fill	130	-	-	0	33
Foundation Soils	133	1075	22.6	0	30
Reservoir Silt	90	-	-	200	0

Note:(1) K_c = Consolidation principal stress ratio

1 inch equals 100 feet

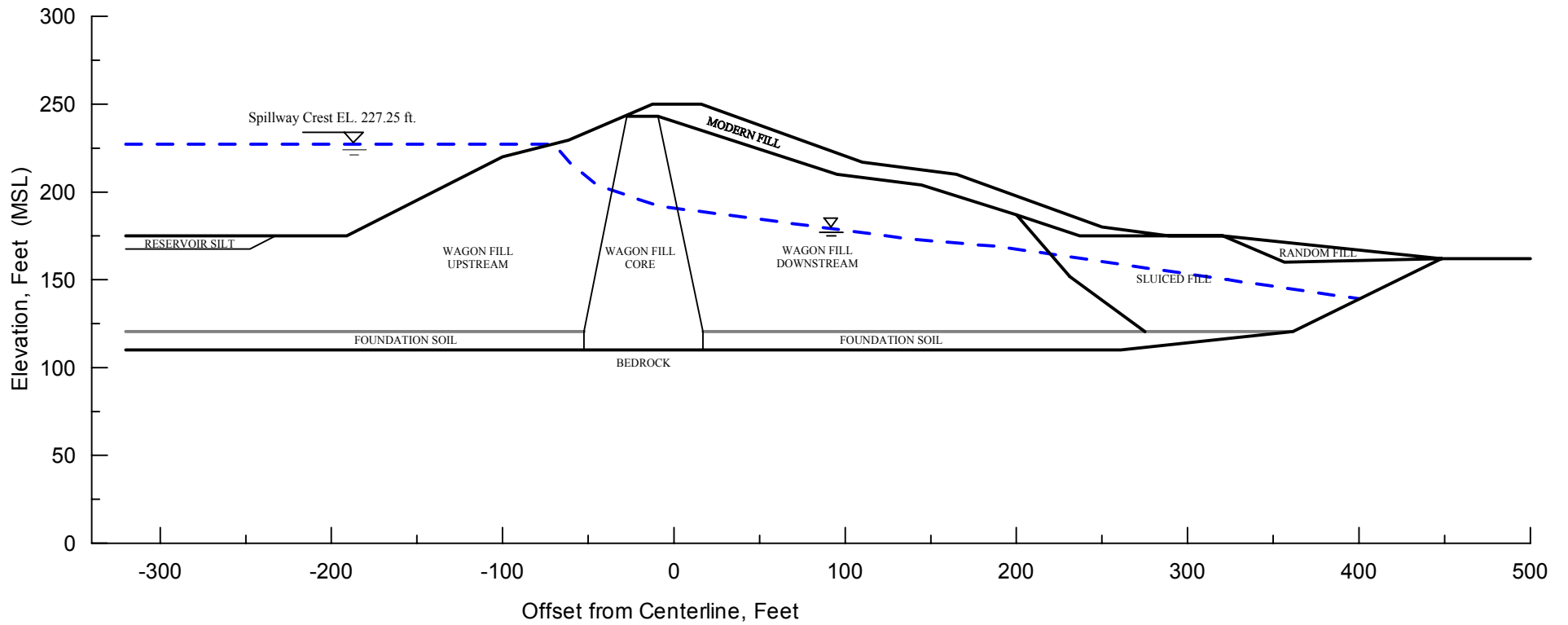
0 50 100 200 Feet



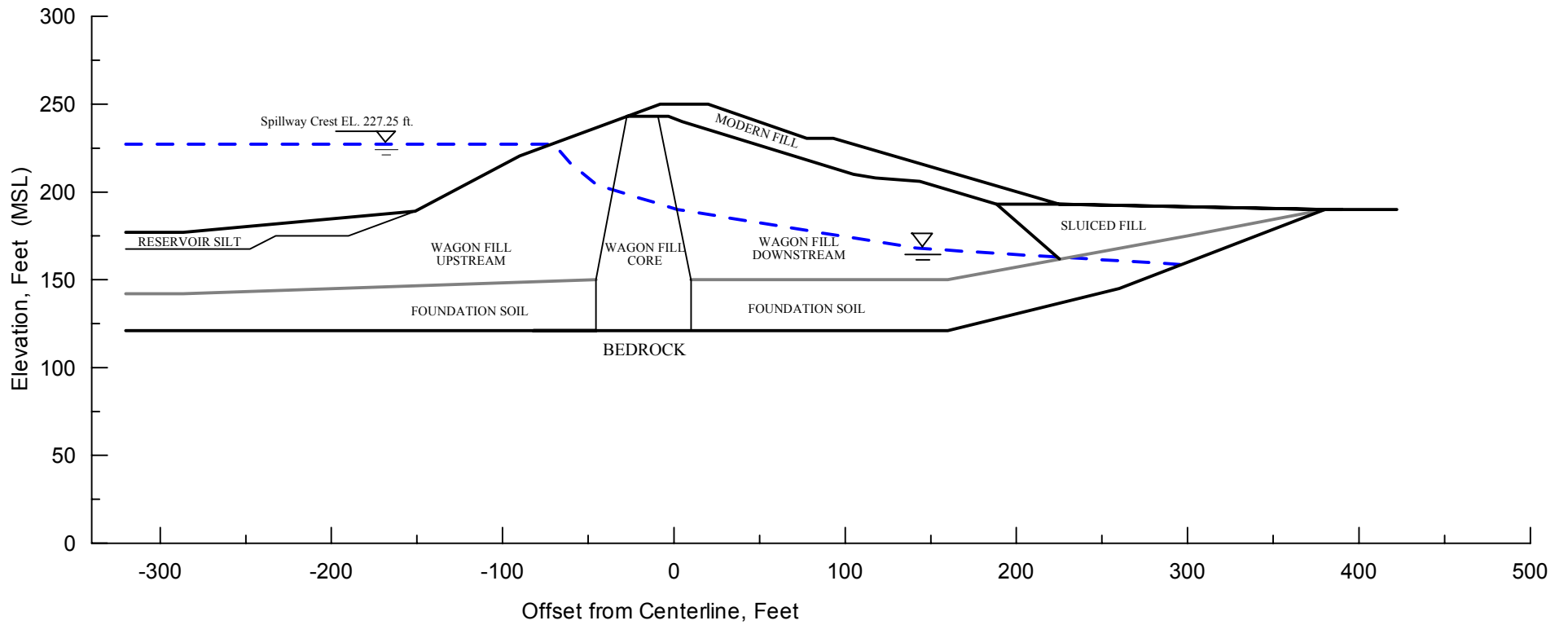
Legend

- Borings shown on Section A-A'
- Borings shown on Section B-B'
- Borings shown on Section C-C'
- Other borings, not shown on sections
- Piezometer
- Current ground surface contours (ft)
- - - Pre-dam ground surface contours (ft)

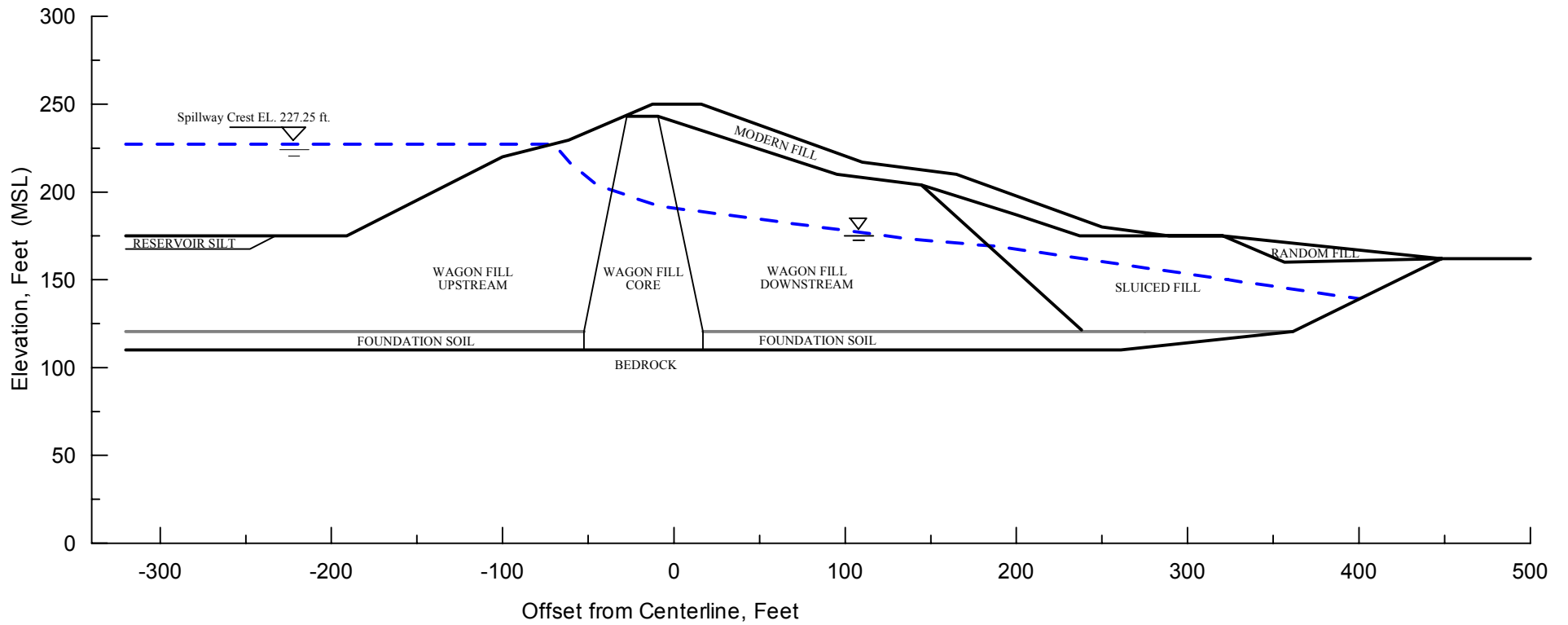
	Chabot Dam Seismic Stability	Plan View of Dam and Analysis Cross-sections	Figure 9-1
	26814536		



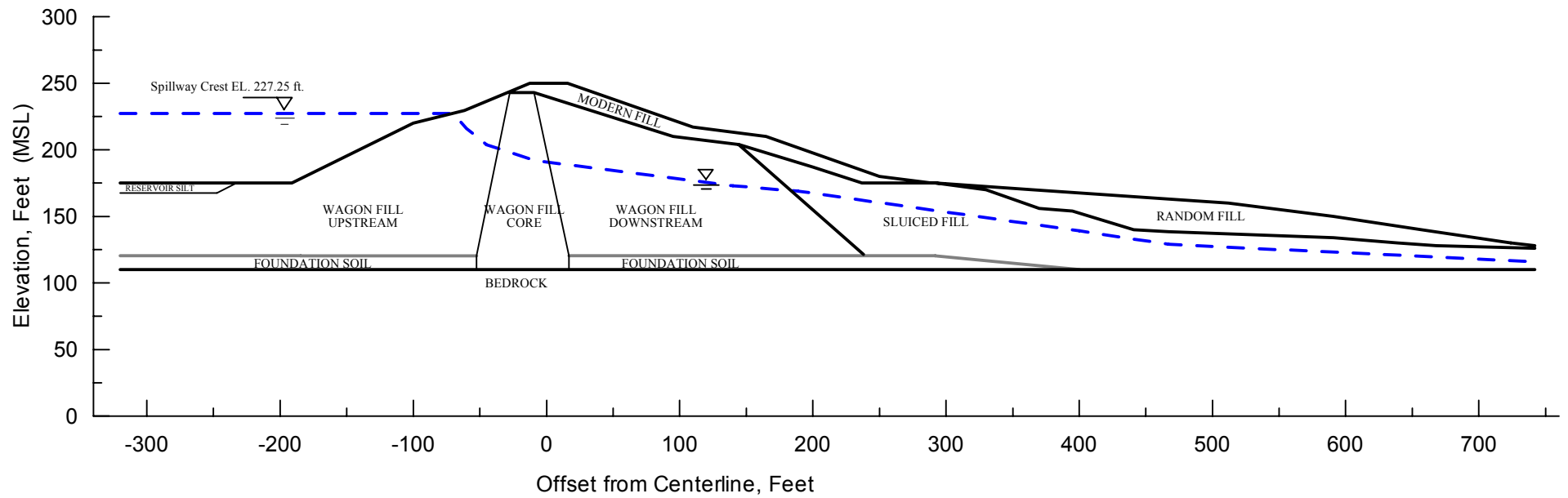
Project No. 26814536	Chabot Dam Seismic Stability Analysis	Idealized Cross Section A-A' for Stability Analysis	Figure 9-2
URS			



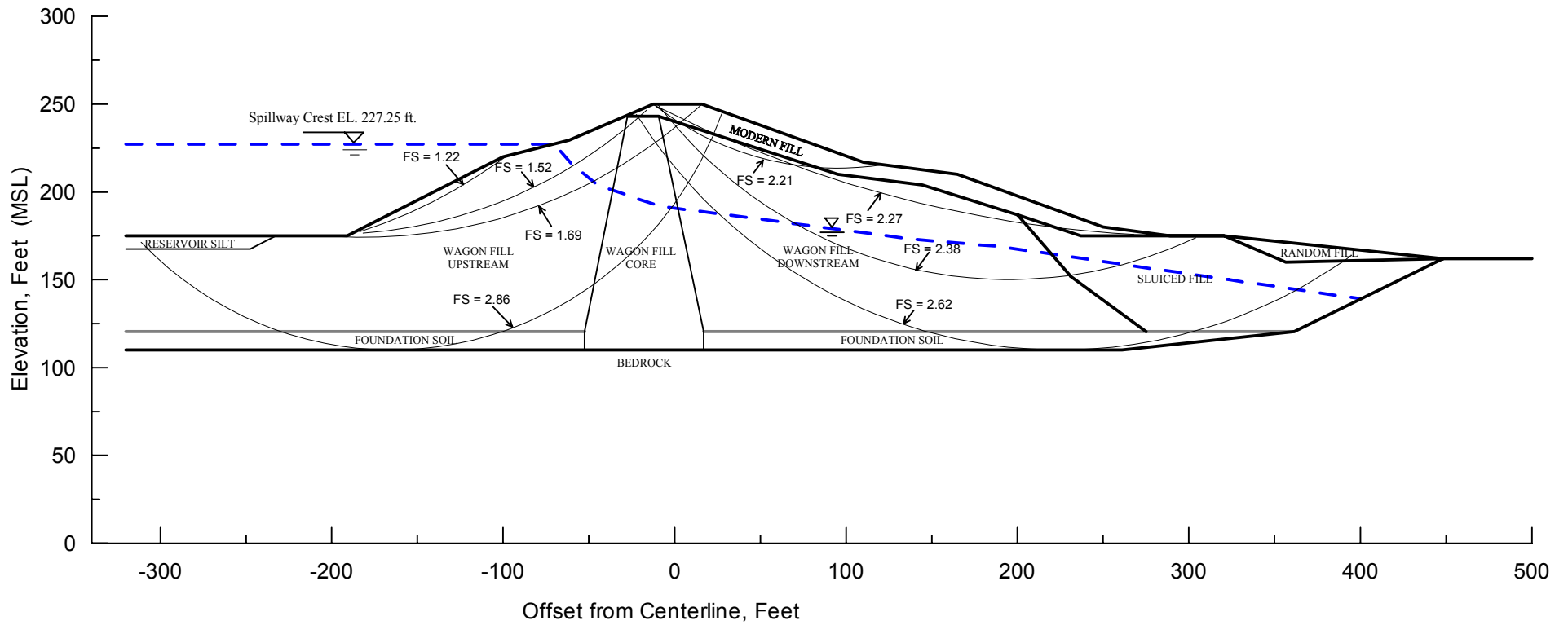
Project No. 26814536	Chabot Dam Seismic Stability Analysis	Idealized Cross Section B-B' for Stability Analysis	Figure 9-3
URS			



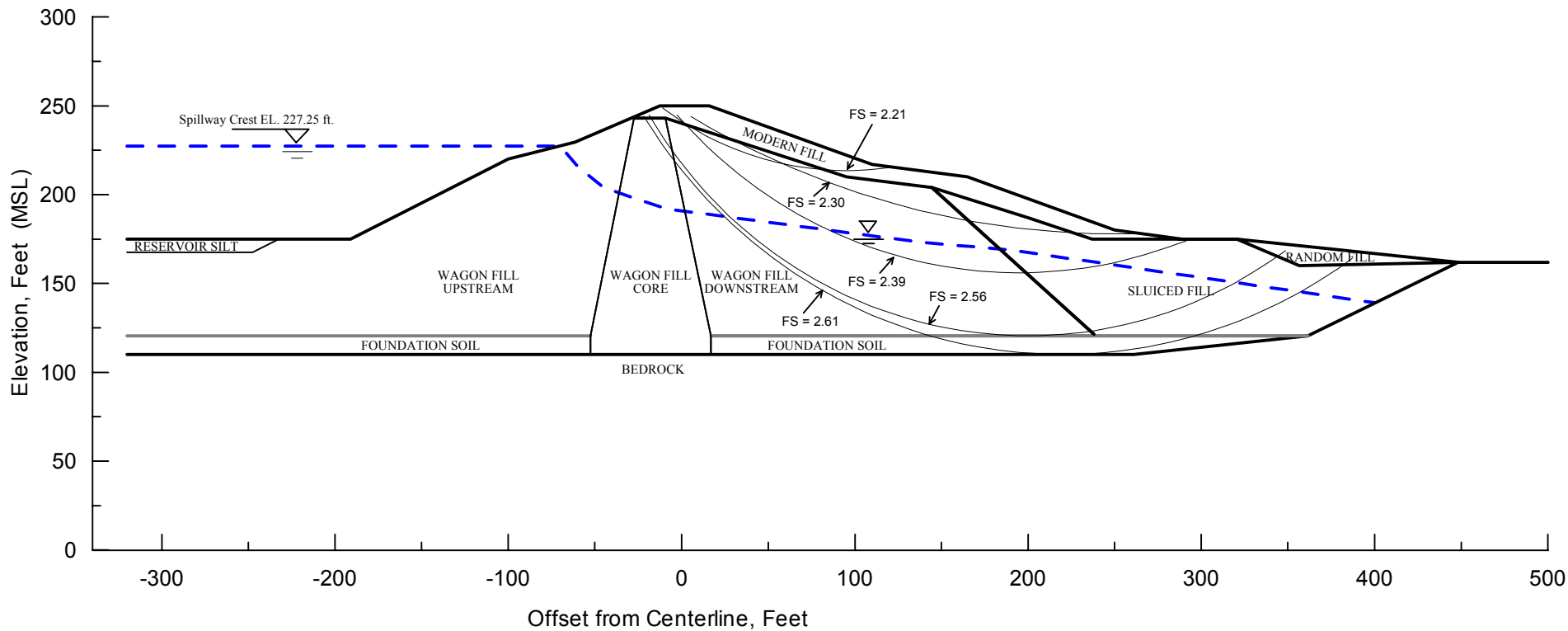
Project No. 26814536	Chabot Dam Seismic Stability Analysis	Modified Cross Section A - A' for Stability Analysis	Figure 9-4
URS			



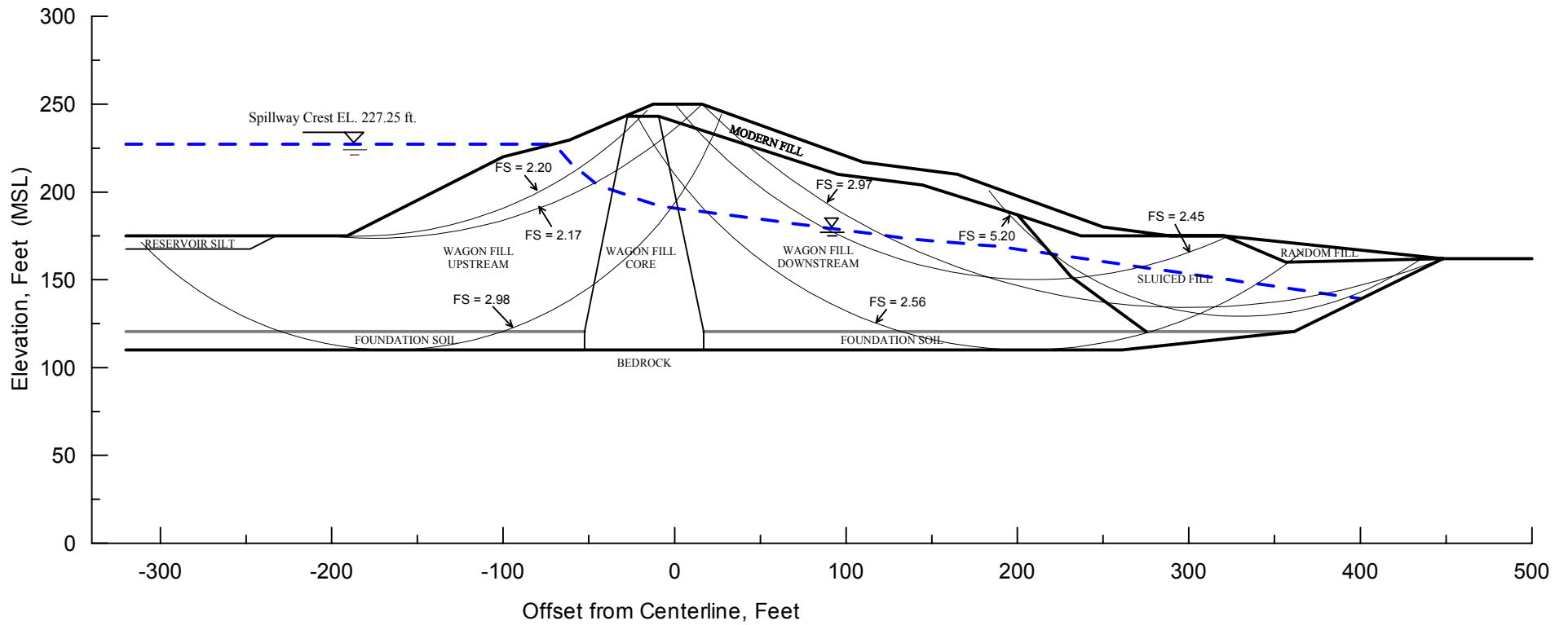
Project No. 26814536	Chabot Dam Seismic Stability Analysis	Composite Downstream Section A - A" for Stability Analysis	Figure 9-5
URS			



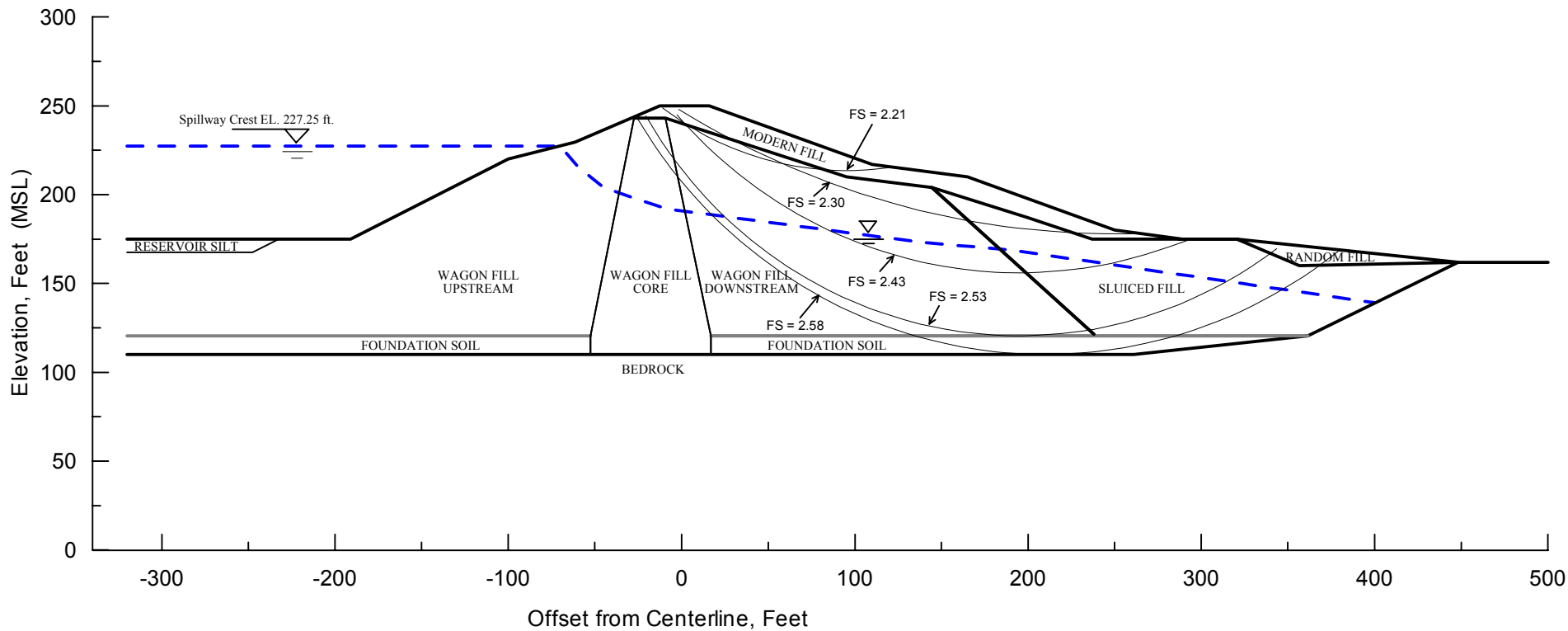
Project No. 26814536	Chabot Dam Seismic Stability Analysis	Static Stability Analysis Long-Term Condition Cross Section A-A'	Figure
URS			9-6



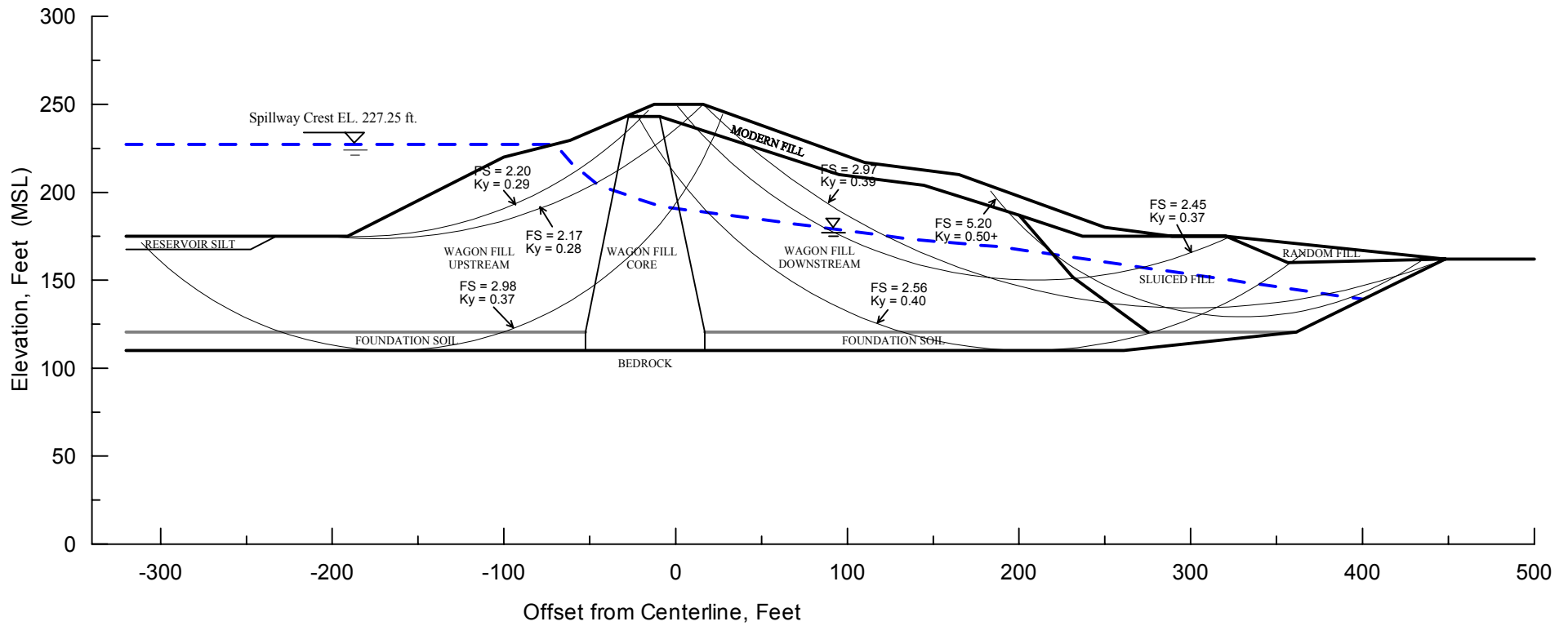
Project No. 26814536	Chabot Dam Seismic Stability Analysis	Static Stability Analysis Long-Term Condition Modified Cross Section A - A'	Figure 9-7
URS			



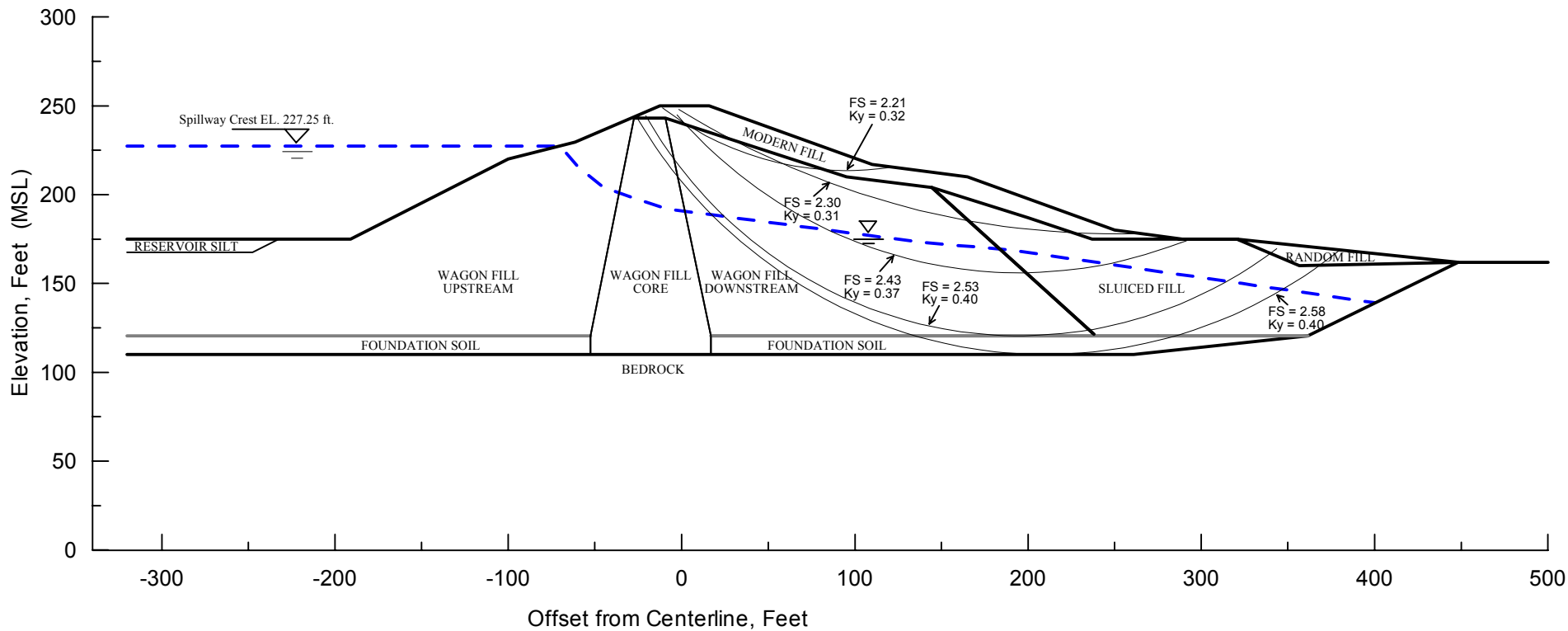
Project No. 26814536	Chabot Dam Seismic Stability Analysis	Seismic Stability Analysis Pre-Earthquake Condition Cross Section A-A'	Figure 9-8
URS			



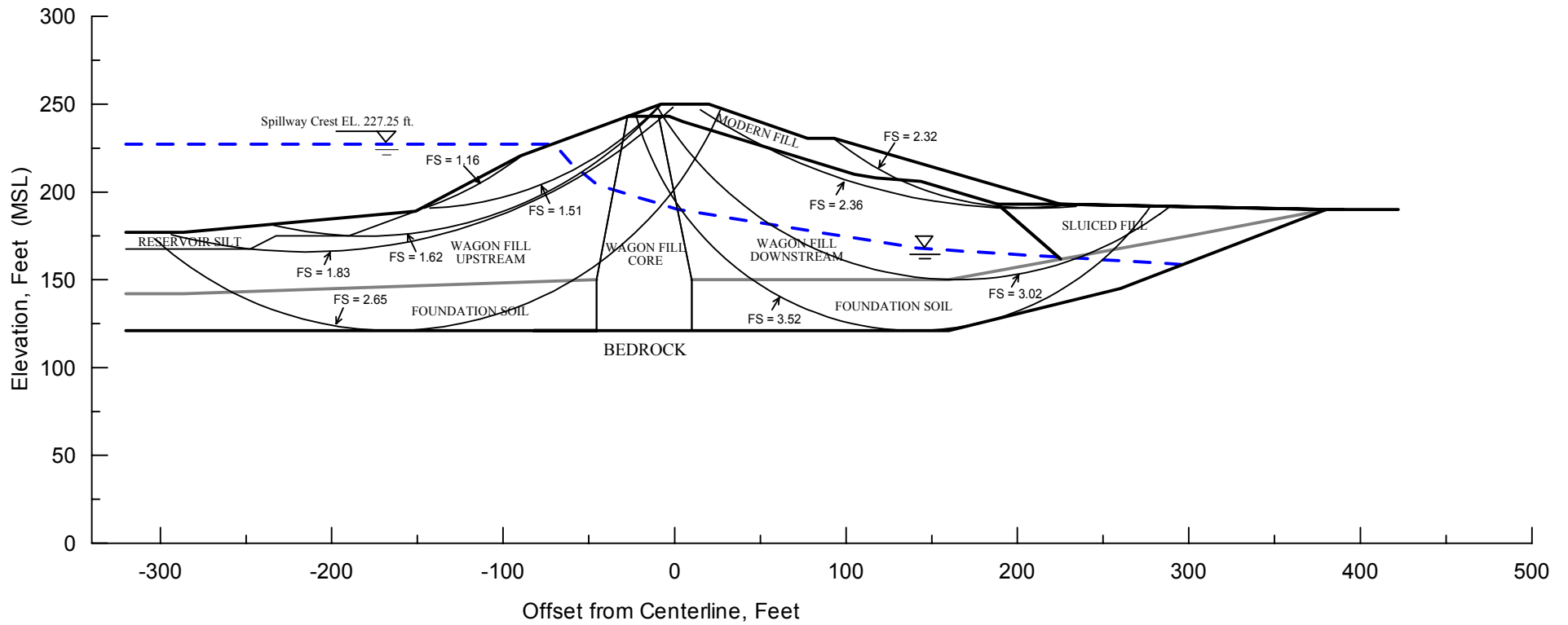
Project No. 26814536	Chabot Dam Seismic Stability Analysis	Seismic Stability Analysis Pre-Earthquake Condition Modified Cross Section A - A'	Figure
URS			9-9



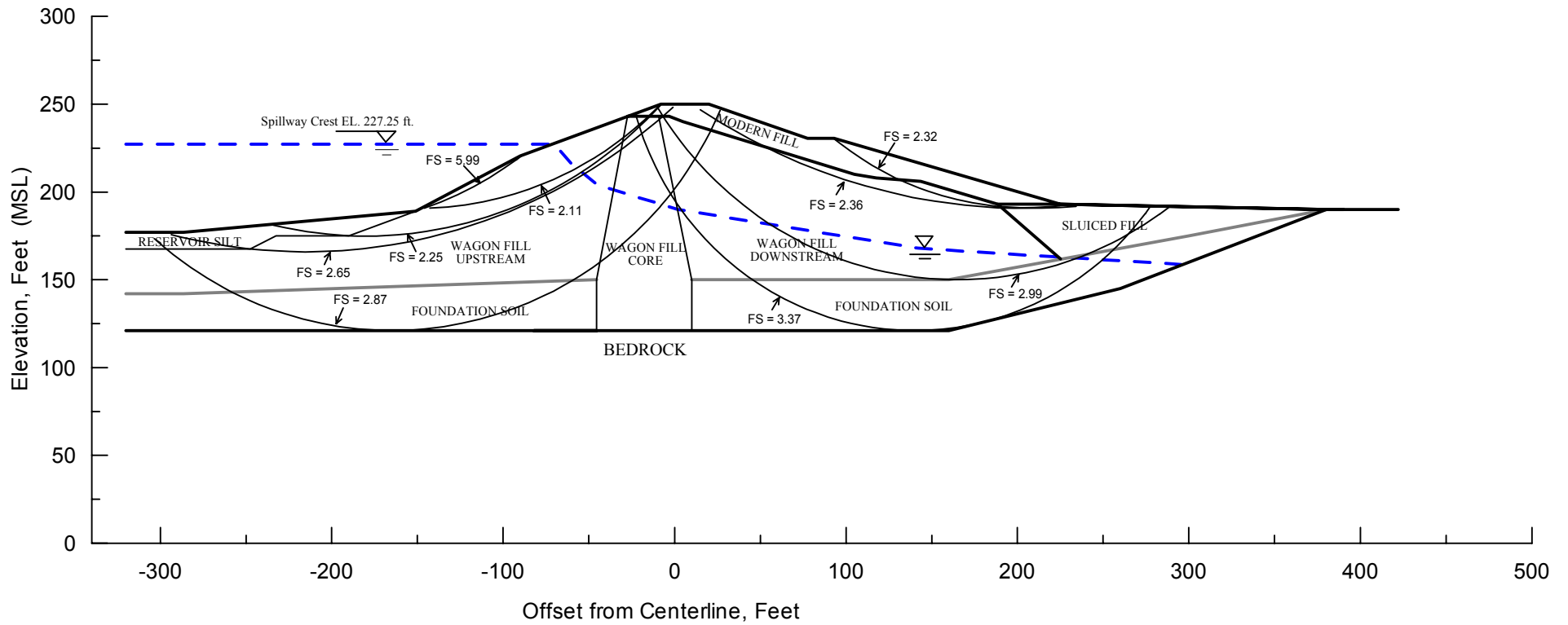
Project No. 26814536	Chabot Dam Seismic Stability Analysis	Seismic Stability Analysis Pseudo-Static Loading (Pre-Earthquake Strengths) Cross Section A-A'	Figure
URS			9-10



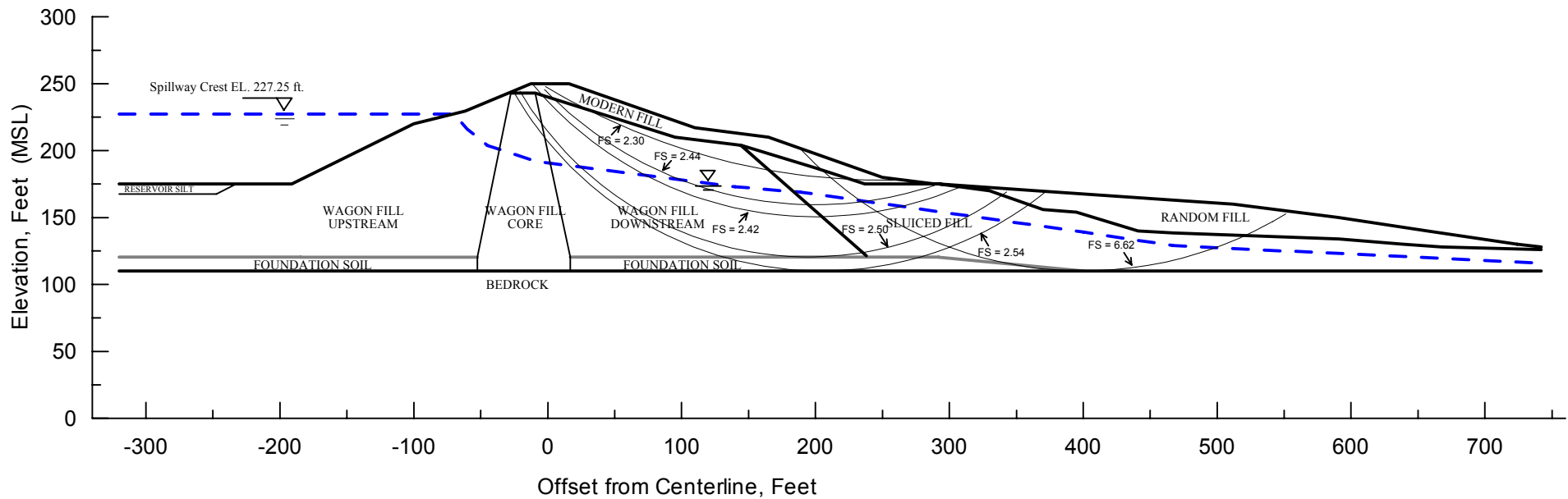
Project No. 26814536	Chabot Dam Seismic Stability Analysis	Seismic Stability Analysis Pseudo-Static Loading (Pre-Earthquake Strengths) Modified Cross Section A - A'	Figure
URS			9-11



Project No. 26814536	Chabot Dam Seismic Stability Analysis	Static Stability Analysis Long-Term Condition Cross Section B-B'	Figure 9-12
URS			



Project No. 26814536	Chabot Dam Seismic Stability Analysis	Seismic Stability Analysis Pre-Earthquake Condition Cross Section B-B'	Figure 9-13
URS			



Project No. 26814536	Chabot Dam Seismic Stability Analysis	Seismic Stability Analysis Pre-Earthquake Condition Downstream Section A - A"	Figure
URS			9-14

10.1 METHODOLOGY

Two-dimensional dynamic response analyses were performed to estimate the stresses and accelerations induced by the design earthquake within the dam. The results of the analyses were used to evaluate the liquefaction potential in the sluiced fill and the potential for strength loss in the wagon fill and foundation soils. The results were also used to evaluate the earthquake-induced average mass accelerations of selected potential sliding blocks within the dam. Together with the yield accelerations obtained from the limit equilibrium analyses, the average mass accelerations were used to calculate seismic displacements of the sliding blocks using a Newmark-type deformation analysis.

The computer program QUAD4M was used for the dynamic response analyses. QUAD4M (Hudson et al. 1994) is a dynamic, time-domain, equivalent-linear, two-dimensional, finite element program. The dynamic stress-strain behavior of the materials is assumed to be viscoelastic. The elastic modulus and viscous damping of the materials are calculated iteratively until they are compatible with the computed shear strains.

The dynamic response analyses were performed on idealized Section A-A', which corresponds to the maximum section of the dam. This section was shown to be the most critical section of the planar sections studied in the static and pseudo-static analyses. This section was also judged to be the most representative for assessing the seismic deformations of the dam. The section was discretized using the finite element mesh shown in Figure 10-1. A transmitting boundary was specified along the base of the model to simulate the unbounded extent of the foundation bedrock beneath the dam. The mesh was extended in the upstream and downstream directions to minimize the effects of side boundary reflections on the dam response, and "horizontal roller" supports were specified for the side boundaries to allow free movement in the horizontal direction. The calculated site response near the boundaries was compared with the free-field response computed with computer program SHAKE (Schnabel et al, 1972), to confirm that the boundary effects are small.

The analyses were performed for the Hayward-Rodgers Creek and San Andreas fault MCEs using the time histories developed to represent those earthquakes. The acceleration, velocity, and displacement time histories for those earthquakes are presented in Figures 6-12, 6-13 and 6-15. The acceleration time histories were input so that they would represent bedrock outcrop motions in the upstream-downstream direction.

The response of the dam was also analyzed for the estimated motions during the 1989 Loma Prieta earthquake. Based on the ground motion records obtained during that earthquake, the motions recorded at the California State University at Hayward Stadium were assumed to be reasonably representative of the motions that occurred at the dam site during the earthquake. The time history used in the analyses to represent the earthquake motions is shown in Figure 10-2. The calculated performance was compared against the known performance of the dam during that earthquake as a check of the analysis procedures and models.

A rough check on the analysis models was also made by analyzing the response of the dam to the ground motions expected to have occurred at the site during the 1906 San Francisco earthquake. This check confirmed that the analysis model is reasonable. However, it does not constitute a robust check because there is major uncertainty regarding the ground motions at the site during

that earthquake, and because of changes in the dam configuration after the earthquake. Therefore, those results are not presented herein.

10.2 DYNAMIC MATERIAL PROPERTIES

Table 1 summarizes the material properties used in the QUAD4M analyses. These parameters include total unit weight (γ), maximum shear modulus (G_{\max}), Poisson's ratio (ν), and the modulus reduction (G/G_{\max}) and damping ratio (λ) relationships with shear strain. The maximum shear modulus of the materials was obtained from their shear wave velocity. The shear wave velocities throughout the dam were expressed as a function of the mean effective stress as shown in Table 10-1. These expressions were derived from measured shear wave velocities at the dam. The mean effective stresses were obtained from a static stress analysis of the dam performed using the computer program FLAC. The FLAC analyses are discussed in Section 12.

10.2.1 Shear Wave Velocities

Down-hole geophysical surveys were performed in several borings drilled for this investigation. The measured seismic wave velocities are shown in Figures 10-3 through 10-6. The figures also show the values of Poisson's ratio calculated from the measured shear and compression velocities (V_s and V_p) using the following equation:

$$\nu = (3 \cdot K - 2 \cdot G) / (6 \cdot K + 2 \cdot G),$$

where: G = shear modulus, and K = bulk modulus. The shear and bulk moduli are obtained from:

$$G = \gamma \cdot V_s^2 / g$$

$$K = \gamma \cdot V_p^2 / g - 2 \cdot G$$

Figure 10-3 shows that, on the average, the shear wave velocity in the central wagon fill increases gradually with depth from about 900 fps at Elevation 230 to about 1500 fps at the bottom of the fill. Similar trends are observed in the measurements made in the downstream wagon fill and were used to develop a model of the seismic shear wave velocities of those materials.

Figure 10-6 shows the seismic velocities measured in boring WI-60 through the sluiced fill. The figure shows that the shear wave velocity of the materials increases gradually with depth from about 500 fps near the surface to 1000 fps at the bottom of the fill.

The seismic surveys also indicate that the shear wave velocity of the rock immediately below the dam ranges between about 1,500 and 5,000 fps. A representative average value of 2,700 fps was assigned to the bedrock. Similarly, average shear wave velocities of 1,200 and 1,300 fps were assigned to the modern fill and the foundation soils, respectively.

10.2.2 Modulus Reduction and Damping Relationships

The average modulus reduction relationship for sands proposed by Seed and Idriss (1970) was used to represent the variation in normalized shear modulus (G/G_{\max}) with effective shear strain. This relationship was selected based on the characteristics of the materials, the results of cyclic

triaxial and resonant column tests performed by Woodward-Clyde (1977), and on past experience with similar materials. It is also the same relationship used by Woodward-Clyde for their dynamic response analyses of the dam.

The lower bound damping curve for sands (Seed and Idriss, 1970) was selected for the embankment and foundation soils. In our experience, this relationship is suitable for many compacted, silty and clayey sand materials. The rock was assigned a constant shear modulus ($G/G_{\max} = 1$) and a constant damping ratio of 0.5 percent.

10.3 ANALYSIS RESULTS

The results of the QUAD4M analyses are presented in terms of: a) time histories of shear stress at the elements shown in Figure 10-7, b) acceleration outputs for the nodal points shown in Figure 10-8, and c) time histories of average mass acceleration for the sliding blocks shown in Figure 10-9. In addition, peak horizontal shear stresses were output throughout the model. Those shear stresses were used to calculate the earthquake-induced cyclic stress ratio (CSR) in the embankment and foundation materials. CSR is defined as the ratio of the average cyclic shear stress to the initial effective overburden stress.

$$\text{CSR} = \tau_{\text{ave}} / \sigma_{\text{vo}}' = 0.65 \cdot \tau_{\text{peak}} / \sigma_{\text{vo}}'$$

where: τ_{ave} = average cyclic shear stress

τ_{peak} = peak shear stress

σ_{vo}' = effective overburden stress.

These stress ratios were compared with the cyclic strength of the wagon fill and sluiced fill to evaluate the potential for liquefaction and strength loss of those materials, as will be discussed in Section 11.

The dynamic response analysis results are presented in Figures 10-10 through 10-24. The results of the analyses for the Loma Prieta earthquake are presented first, followed by the results for the Hayward and San Andreas events.

10.3.1 1989 Loma Prieta Earthquake

The analysis results for the 1989 Loma Prieta Earthquake are presented in Figures 10-10 through 10-14. Figure 10-10 shows the calculated peak accelerations at the selected points within the dam during the earthquake. The calculated peak acceleration at the crest of the dam is approximately 0.22g. The calculated cyclic stress ratios (CSR) are shown in Figure 10-11. Figures 10-12 through 10-14 show the time histories of average mass acceleration for the sliding blocks shown in Figure 10-9.

10.3.2 Hayward-Rogers Creek Fault MCE

Two time histories were developed to represent the design ground motions for the Hayward-Rogers Creek fault MCE (Section 6.0) and were used in the dynamic response analyses. The analyses results indicated that time history No. 1 induced a slightly stronger dam response than time history No. 2. Accordingly, only the results for time history No. 1 are presented herein. The analysis results for the Hayward event are presented in Figures 10-15 through 10-21.

As shown in Figure 10-15, the calculated peak acceleration at the crest is 1.15g. Figures 10-16 and 10-17 show acceleration time histories at nodal points below the crest (see Figure 10-8 for locations), and illustrate how the ground motions propagate upward through the structure.

Figure 10-18 shows contours of peak shear stress induced within the dam. Figures 10-19 and 10-20 show shear stress time histories within elements below the crest (see Figure 10-7 for locations). The calculated shear stresses generally correspond to a few cycles of high amplitude shear stress. As shown in Figure 10-18, near the center and base of the dam, the amplitude of the stresses exceeds the static undrained strength of the materials, which is a limitation of equivalent-linear methods of dynamic response analysis.

Figure 10-21 shows contours of cyclic stress ratio calculated from the peak shear stresses shown in Figure 10-18. The time histories of average mass acceleration for the selected sliding blocks used in the Newmark-type deformation analyses are shown in Section 11.

10.3.3 San Andreas Fault MCE

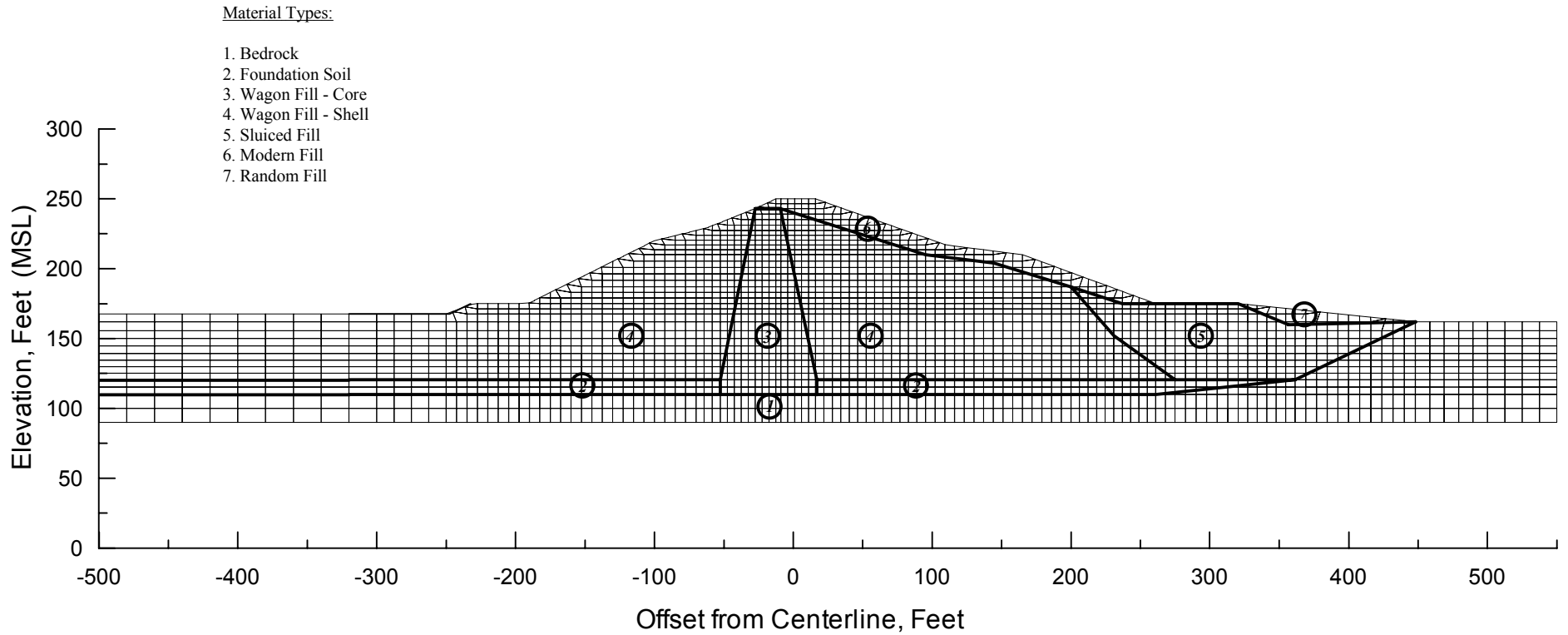
The analysis results for the San Andreas Fault MCE are illustrated in Figures 10-22 through 24. As shown in these figures, this earthquake induces a dynamic response of the dam lower than that calculated for the Hayward Fault MCE. The calculated dam accelerations, shear stresses, and cyclic stress ratios for the San Andreas event are significantly lower than those calculated for the Hayward event. Thus, the analyses indicate that the San Andreas Fault MCE is a less critical event than the Hayward Fault MCE regarding the seismic stability of the dam. The time histories of average mass acceleration for the selected sliding blocks are shown in Section 11.

Table 10-1
Material Parameters for Dynamic Response Analysis

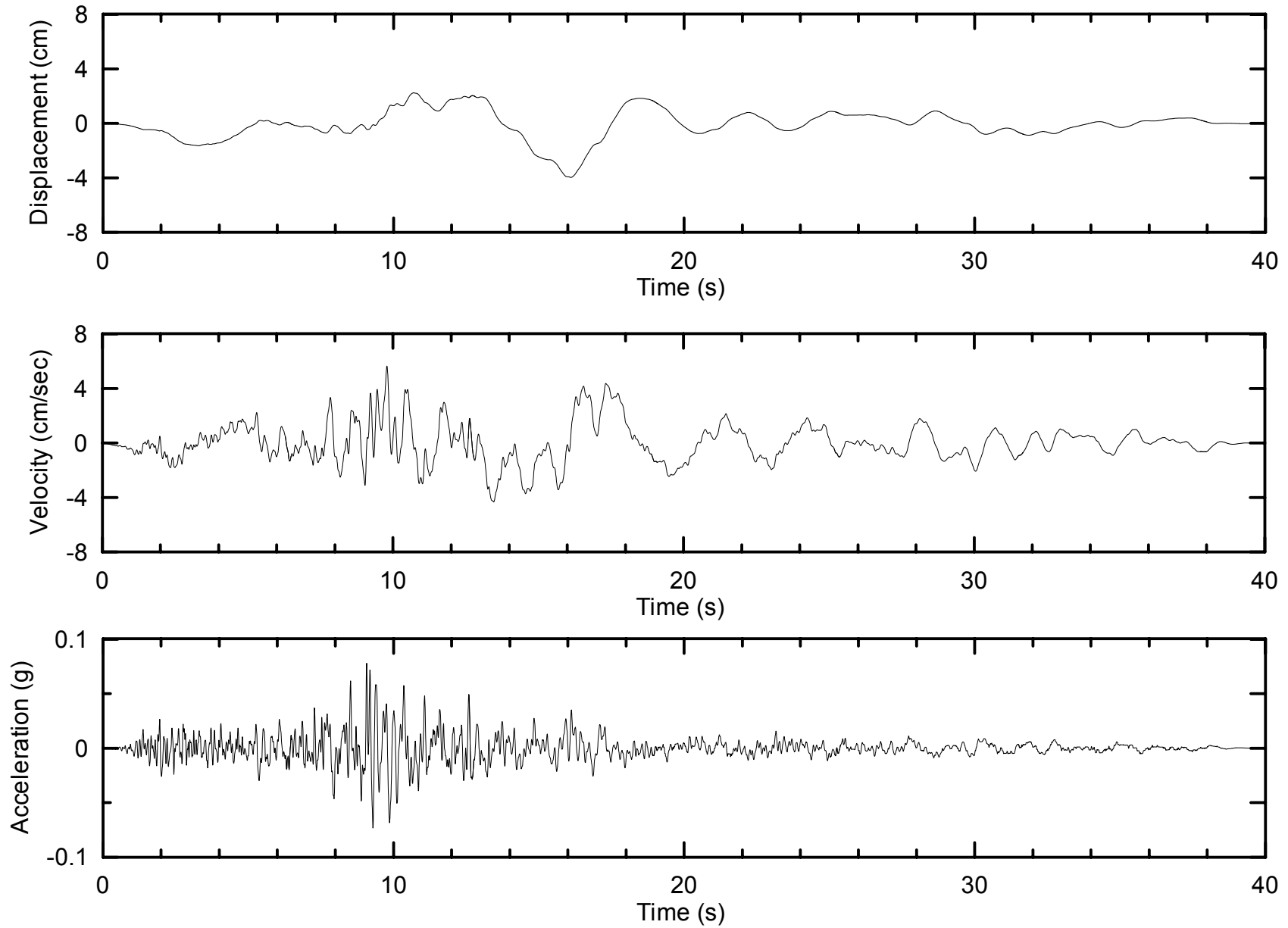
Material	γ_t (pcf)	V_s (fps)	Poisson's Ratio ⁽¹⁾	Modulus Reduction	Damping
Modern Fill	134	1,200	0.36	Sands, Ave ⁽³⁾	Sands, L/B ⁽³⁾
Random Fill	130	$695 \cdot (\sigma_m')^{0.38}$ and > 500 ⁽²⁾	0.36	Sands, Ave	Sands, L/B
Wagon Fill (D/S and U/S)	133	$650 \cdot (\sigma_m')^{0.43}$ and $> 1,000$	0.37, 0.45	Sands, Ave	Sands, L/B
Wagon Fill (Core)	133	$600 \cdot (\sigma_m')^{0.43}$ and > 900	0.4, 0.45	Sands, Ave	Sands, L/B
Sluiced Fill	130	$695 \cdot (\sigma_m')^{0.38}$ and > 500	0.36, 0.48	Sands, Ave	Sands, L/B
Foundation Soils	133	1,300	0.46	Sands, Ave	Sands, L/B
Bedrock	140	2,700	0.42	-	-

Note:

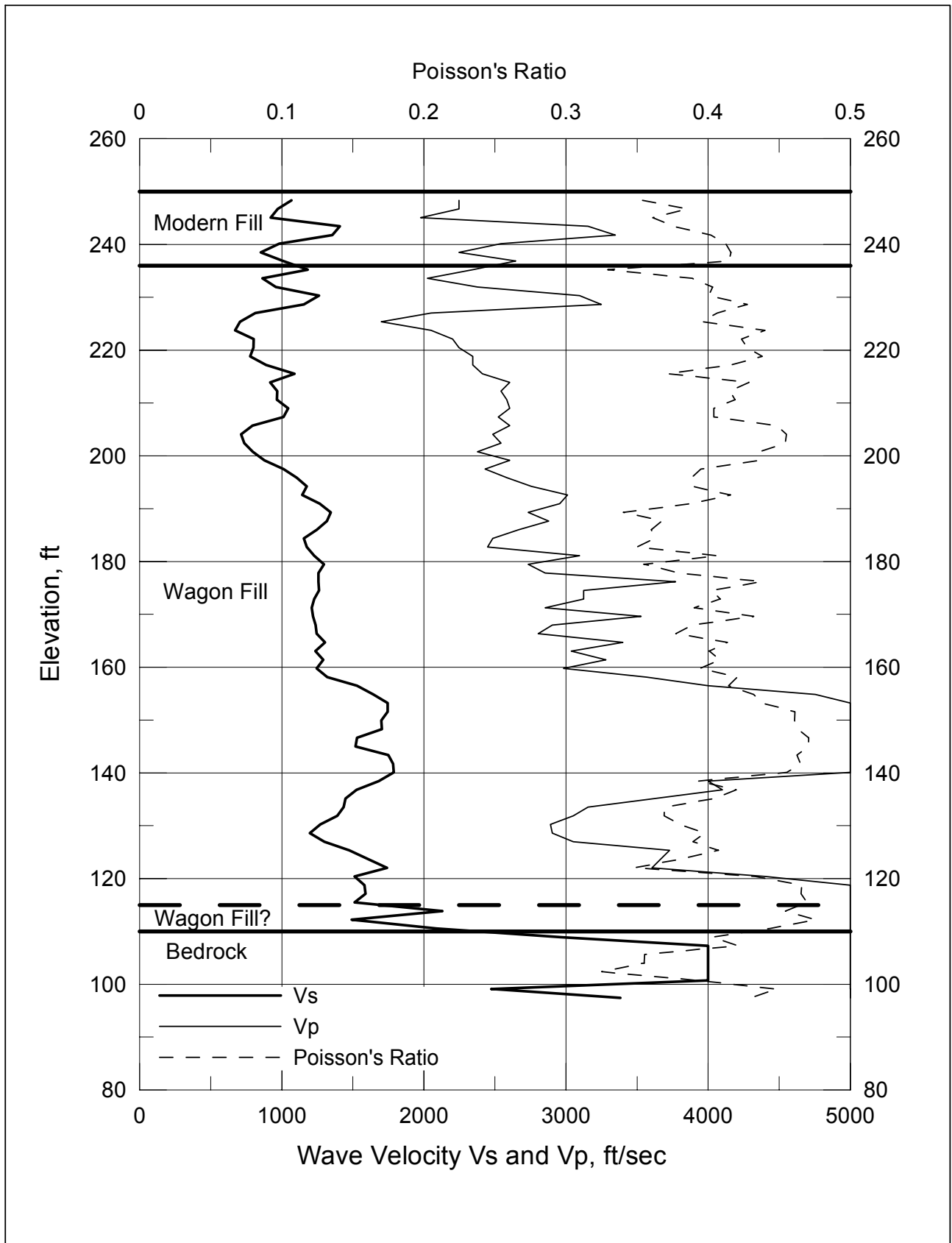
1. Dual values correspond to materials above and below the phreatic line, where applicable.
2. Mean effective stress, σ_m' , in ksf.
3. Seed and Idriss, 1970



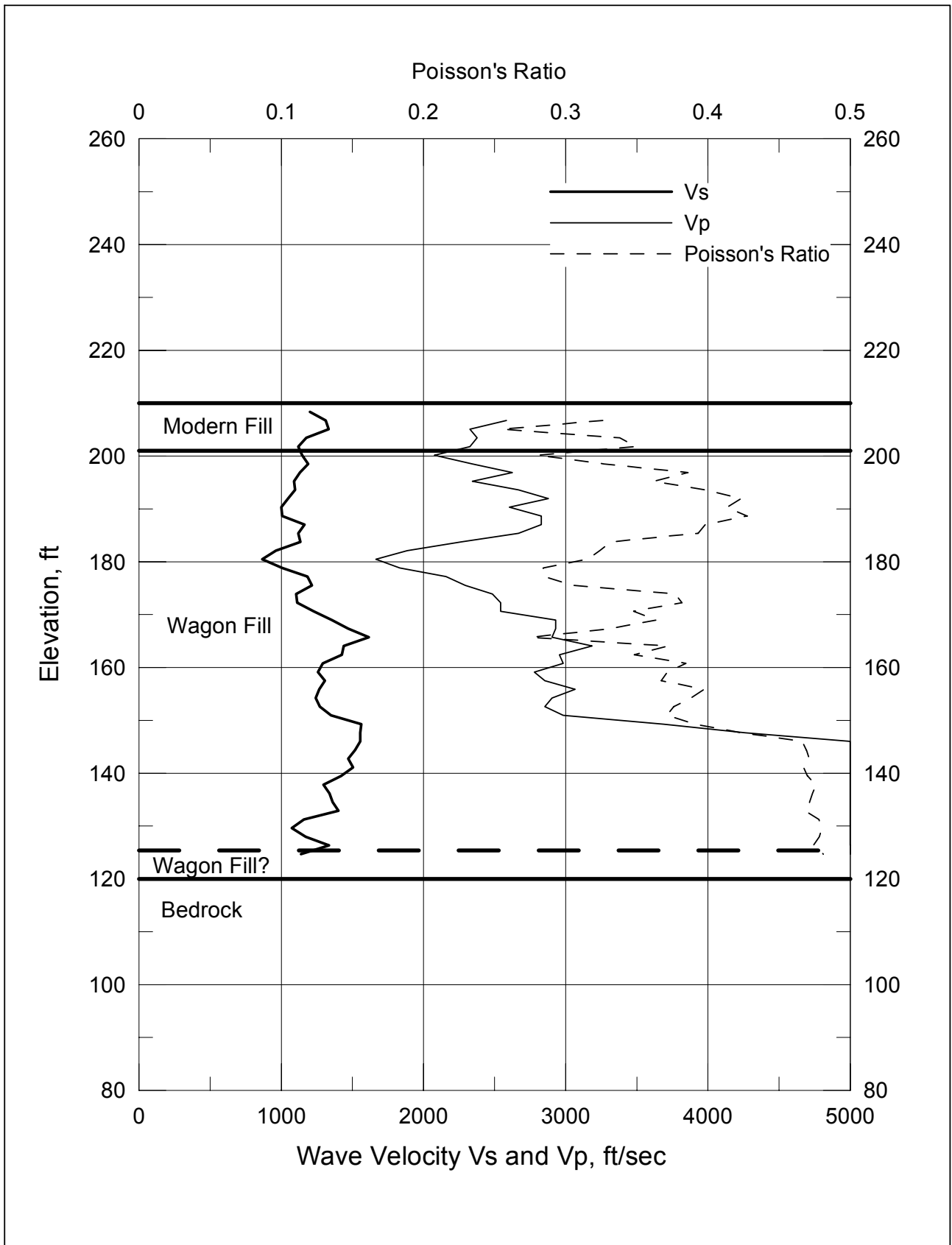
Project No. 26814536	Chabot Dam Seismic Stability Analysis	Finite Element/Difference Mesh Cross Section A - A'	Figure
URS			10-1



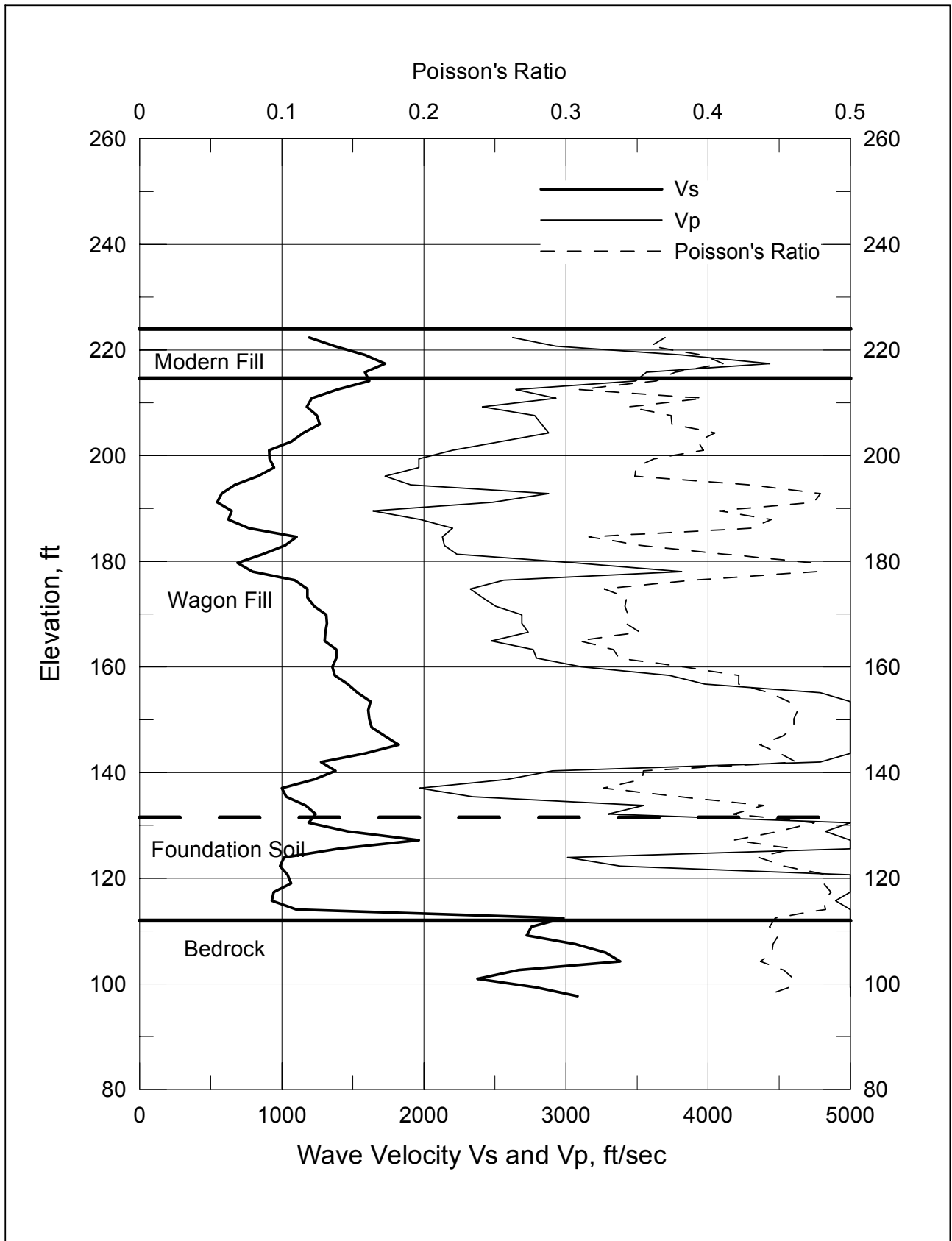
Project No. 26814536	Chabot Dam Seismic Stability Analysis	1989 Loma Prieta Earthquake Acceleration Time History (CSUH Stadium A3E000)	Figure 10-2
URS			



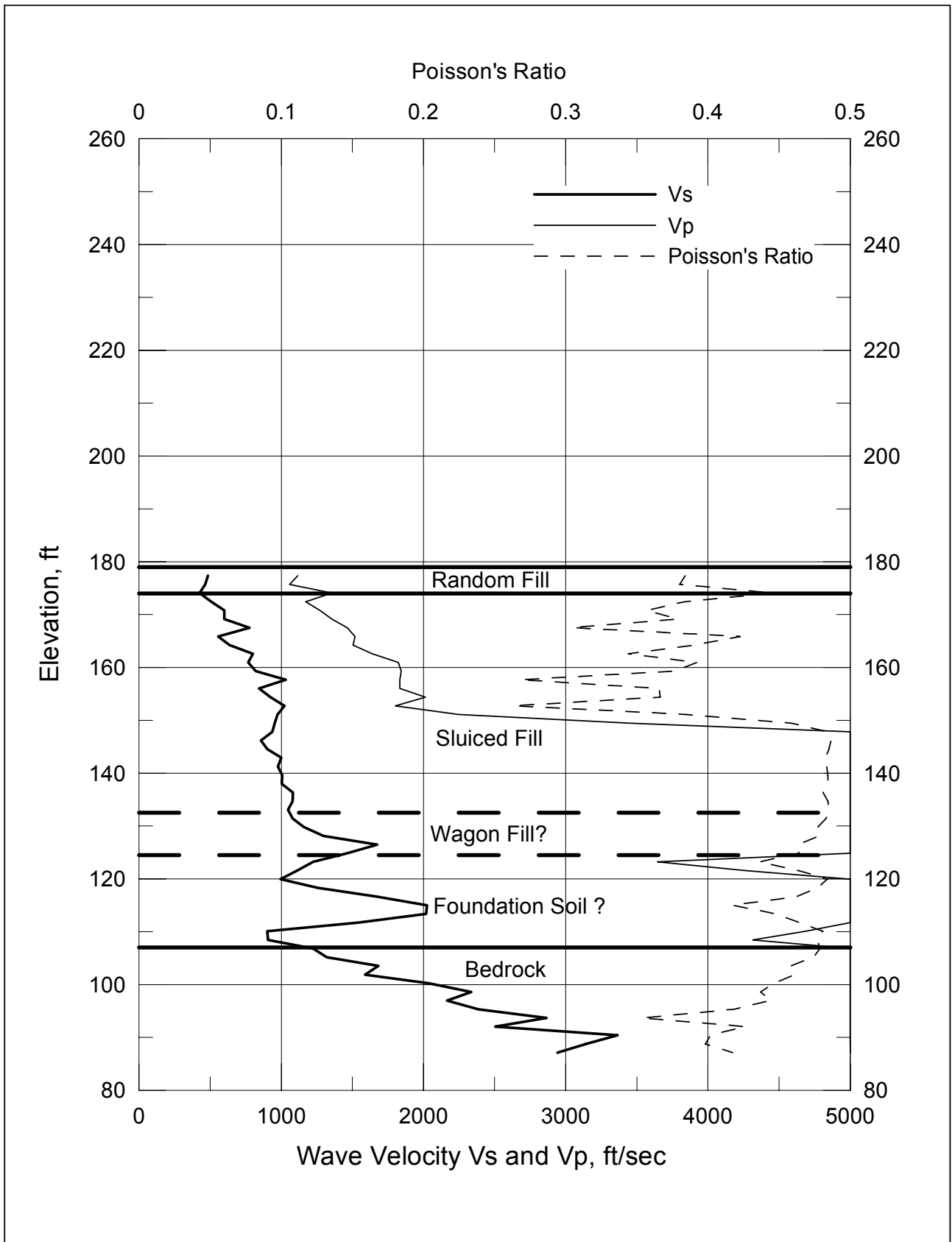
URS	Project No. 26814536	Seismic Wave Velocity Profiles and Stratigraphy of Boring WI-61	Figure
	Chabot Dam Seismic Stability		10-3



URS	Project No. 26814536	Seismic Wave Velocity Profiles and Stratigraphy of Boring WI-59	Figure
	Chabot Dam Seismic Stability		10-4

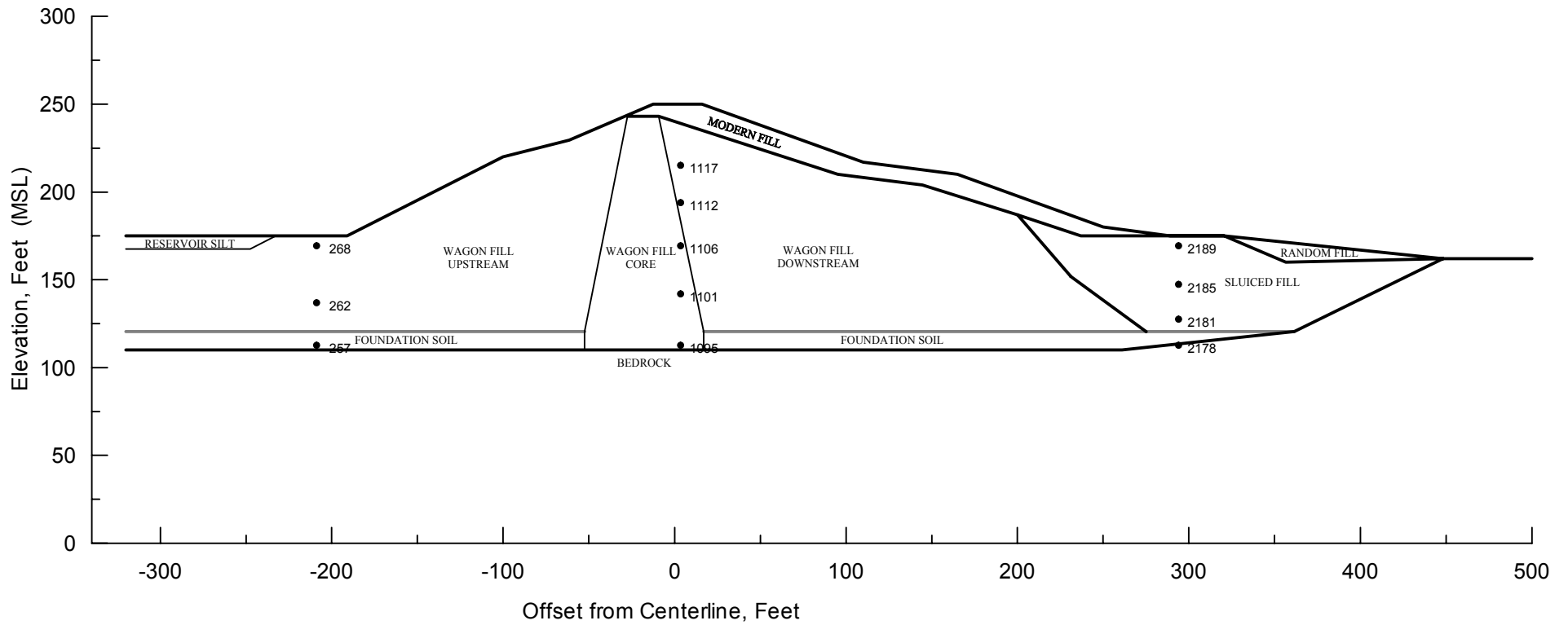


URS	Project No. 26814536	Seismic Wave Velocity Profiles and Stratigraphy of Boring WI-62	Figure
	Chabot Dam Seismic Stability		10-5



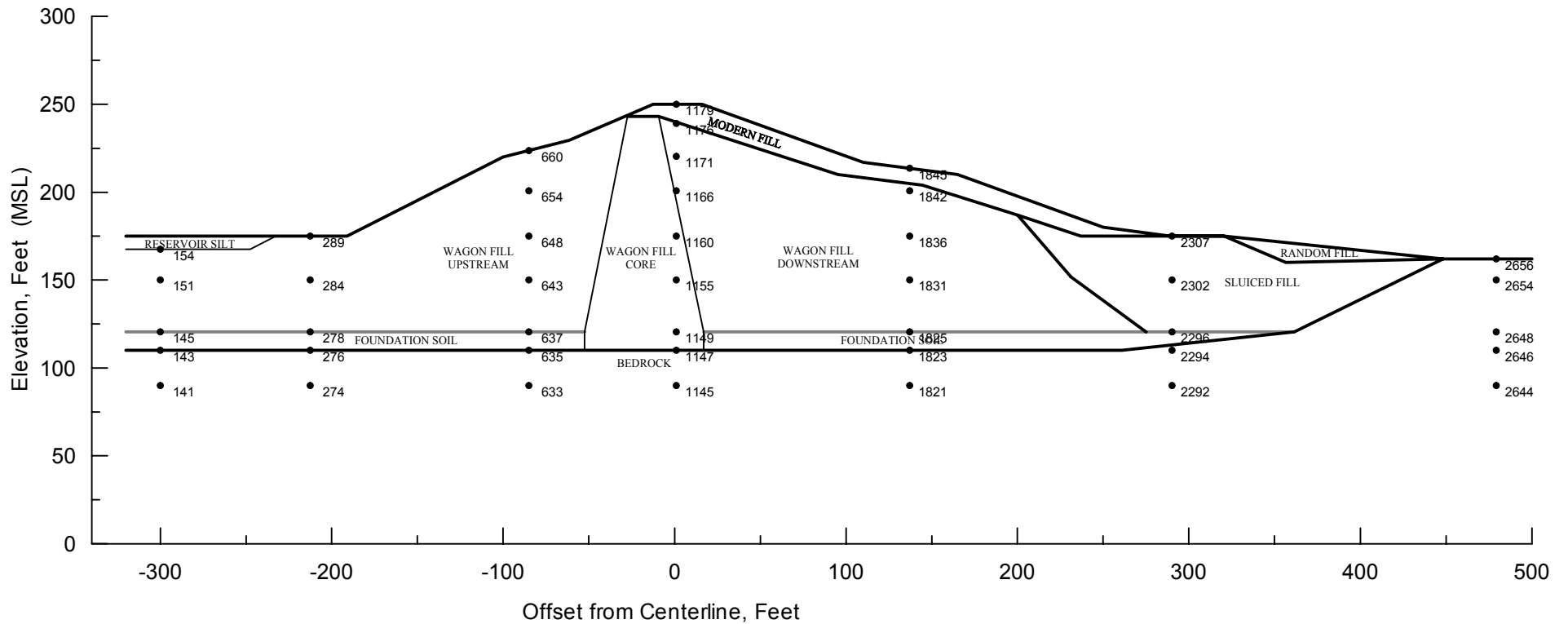
URS	Project No. 26814536	Seismic Wave Velocity Profiles and Stratigraphy of Boring WI-60	Figure
	Chabot Dam Seismic Stability		10-6

x:\x_geol\chabot dam\Task G - Engineering Report\Figures\Figure 10-6.grf

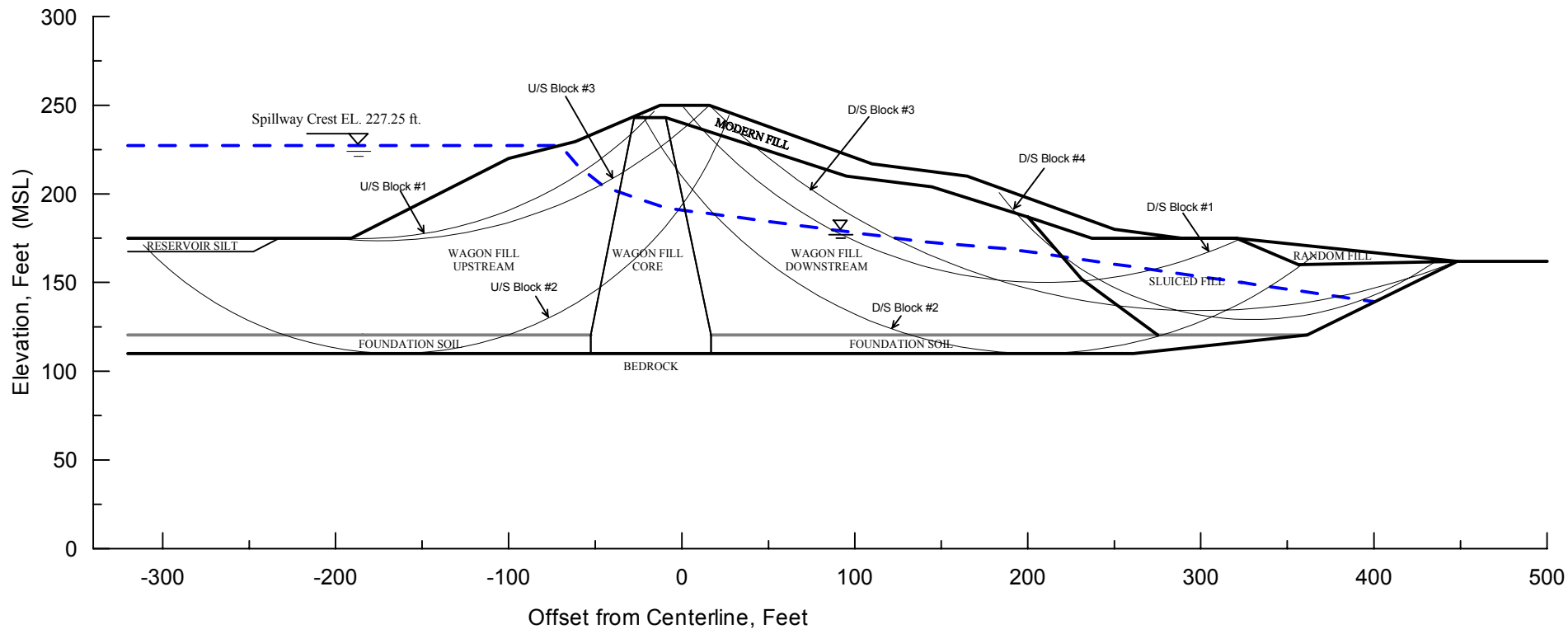


• 257 – Element number

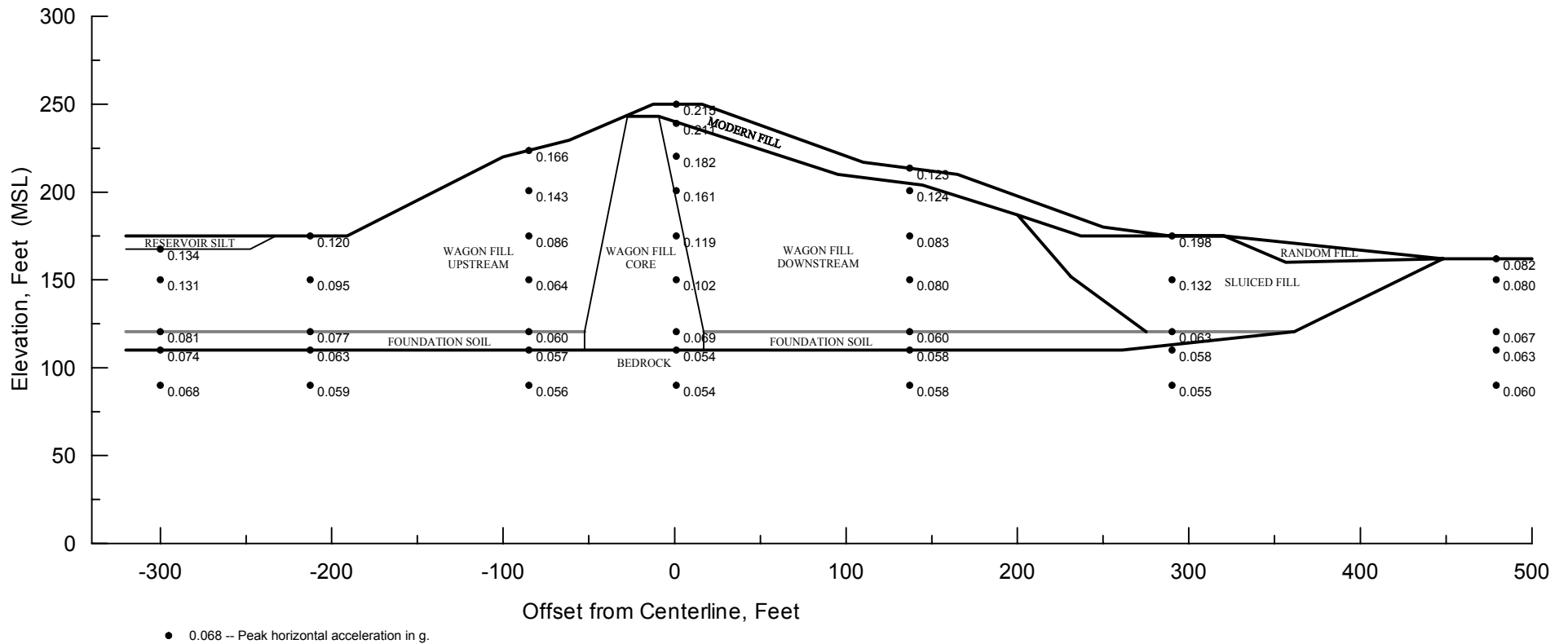
Project No. 26814536	Chabot Dam Seismic Stability Analysis	Selected Element Locations For Stress Time-history Plots QUAD4M Analysis	Figure 10-7
URS			



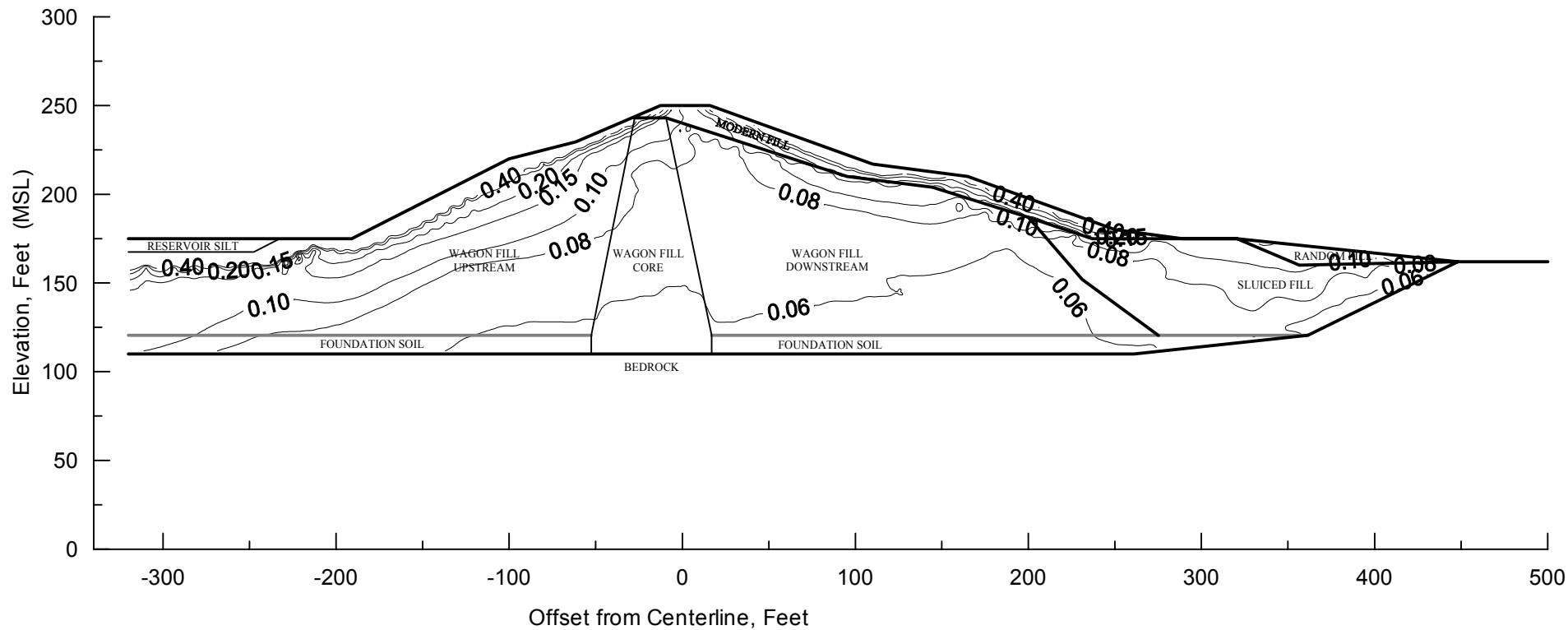
Project No. 26814536	Chabot Dam Seismic Stability Analysis	Selected Nodal Points For Acceleration Outputs QUAD4M Analysis	Figure 10-8
URS			



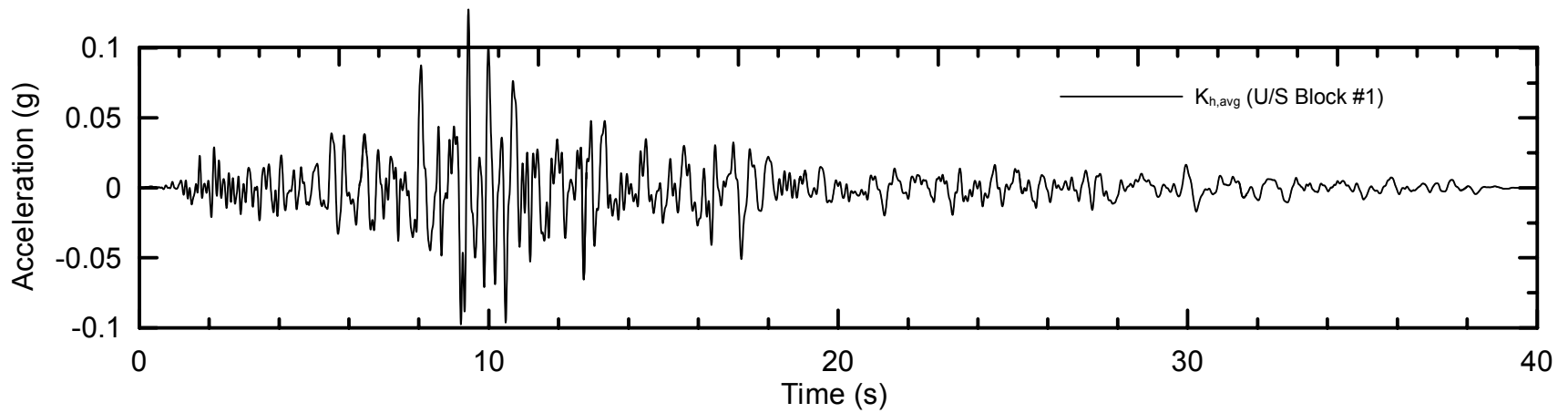
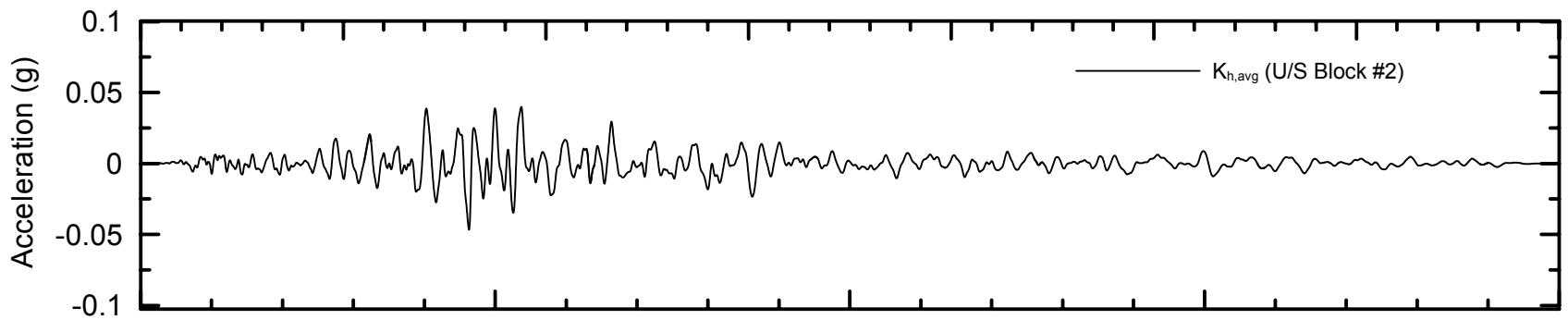
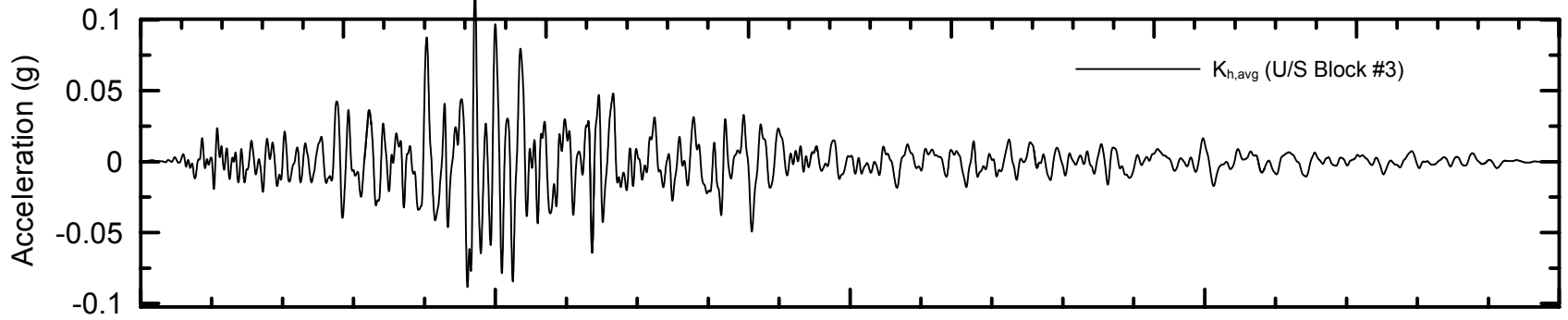
Project No. 26814536	Chabot Dam Seismic Stability Analysis	Sliding Blocks for Newmark Deformation Analyses Cross Section A-A'	Figure
URS			10-9



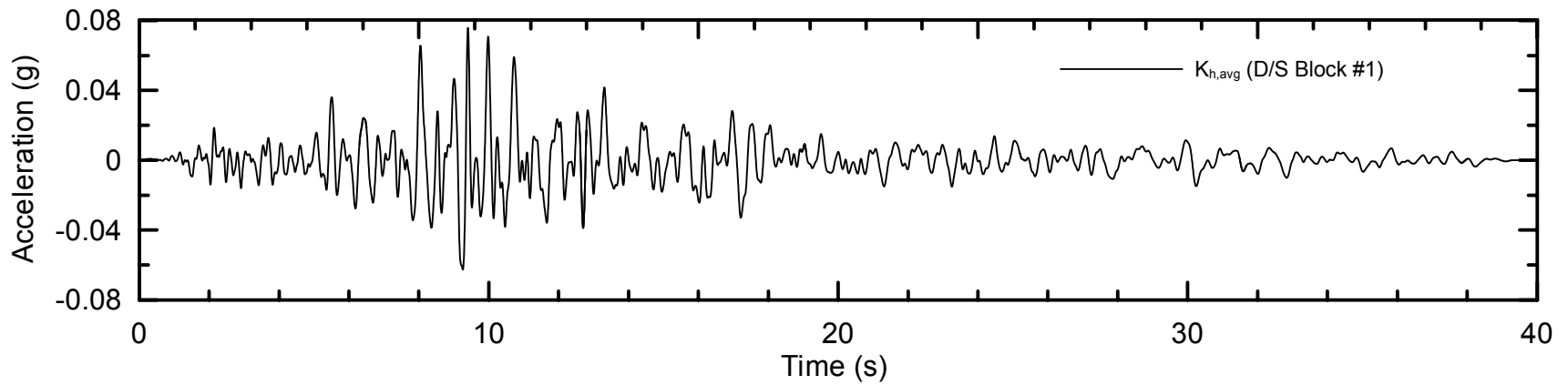
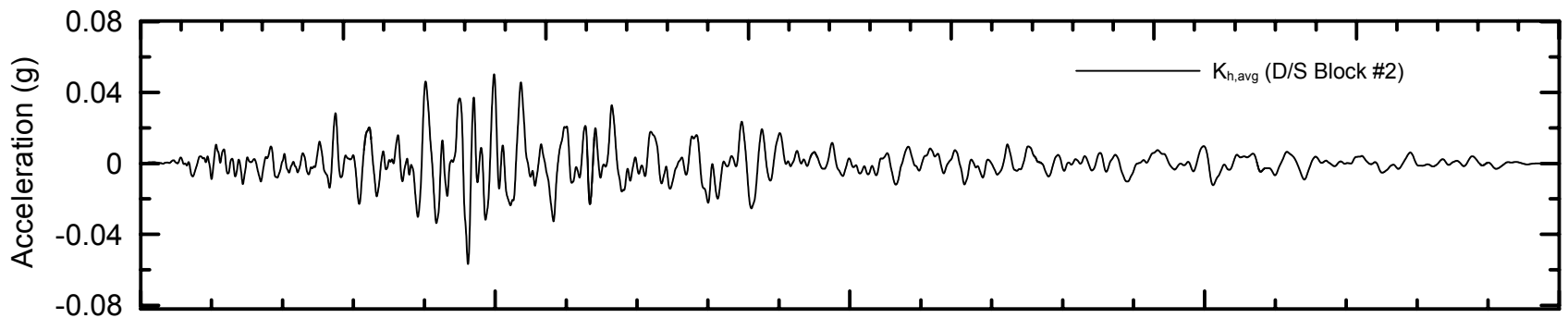
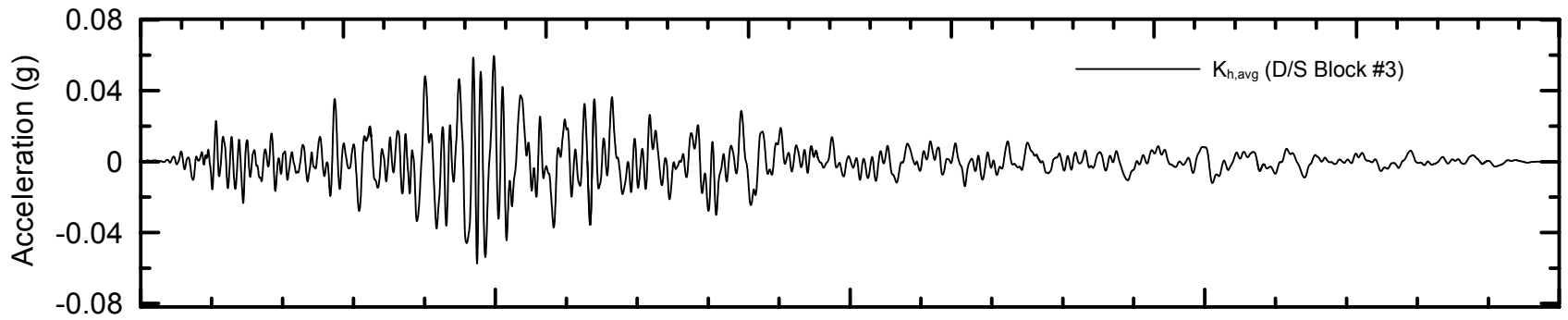
Project No. 26814536	Chabot Dam Seismic Stability Analysis	Peak Horizontal Acceleration QUAD4M Analysis 1989 Loma Prieta Earthquake	Figure 10-10
URS			



Project No. 26814536	Chabot Dam Seismic Stability Analysis	Cyclic Stress Ratio QUAD4M Analysis	Figure
URS		1989 Loma Prieta Earthquake	10-11



Project No. 26814536	Chabot Dam Seismic Stability Analysis	Average Mass Acceleration Upstream Sliding Blocks QUAD4M Analysis 1989 Loma Prieta Earthquake	Figure 10-12
URS			



Project No.
26814536

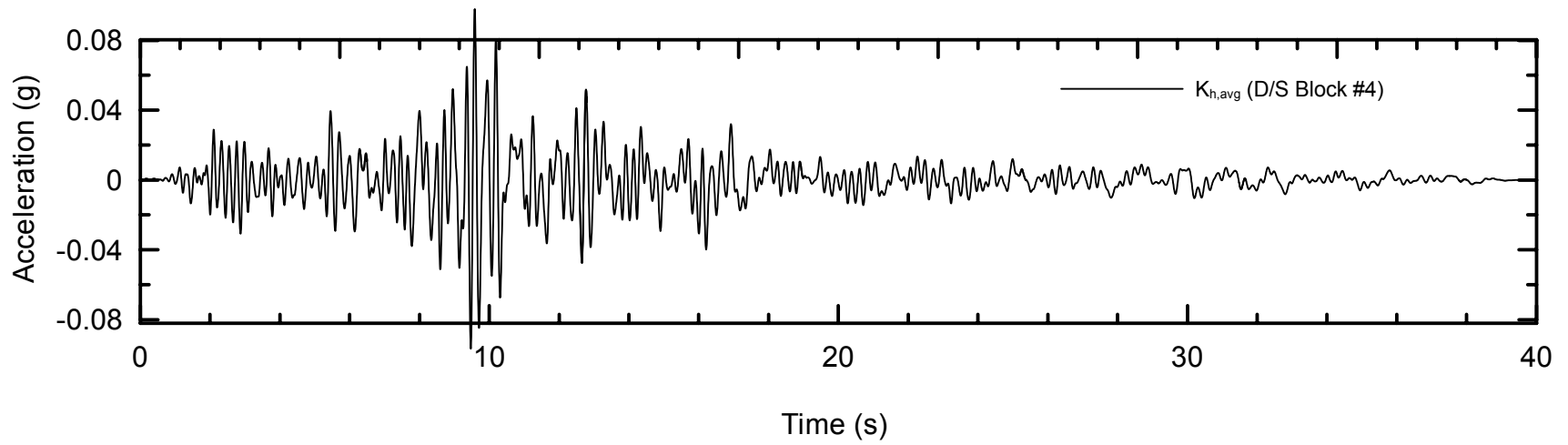
Chabot Dam
Seismic Stability Analysis

Average Mass Acceleration
Downstream Sliding Blocks
QUAD4M Analysis
1989 Loma Prieta Earthquake

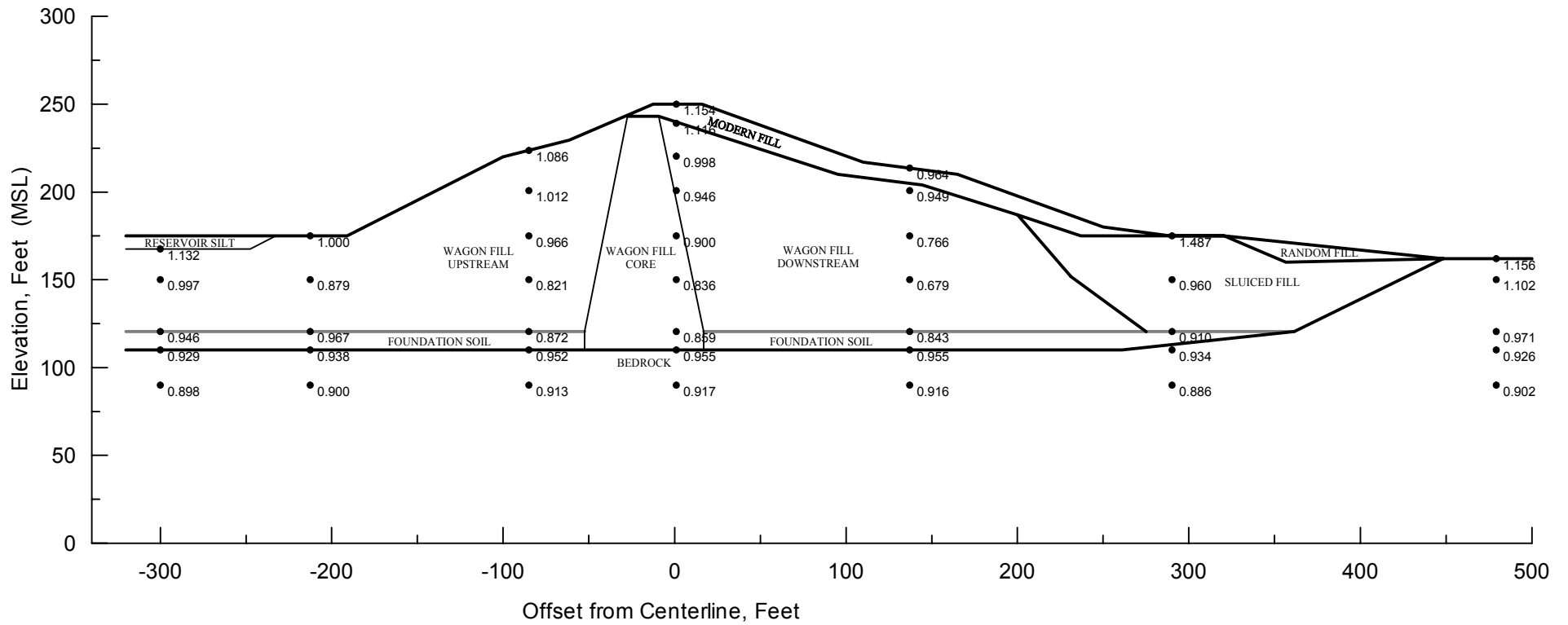
Figure

10-13

URS

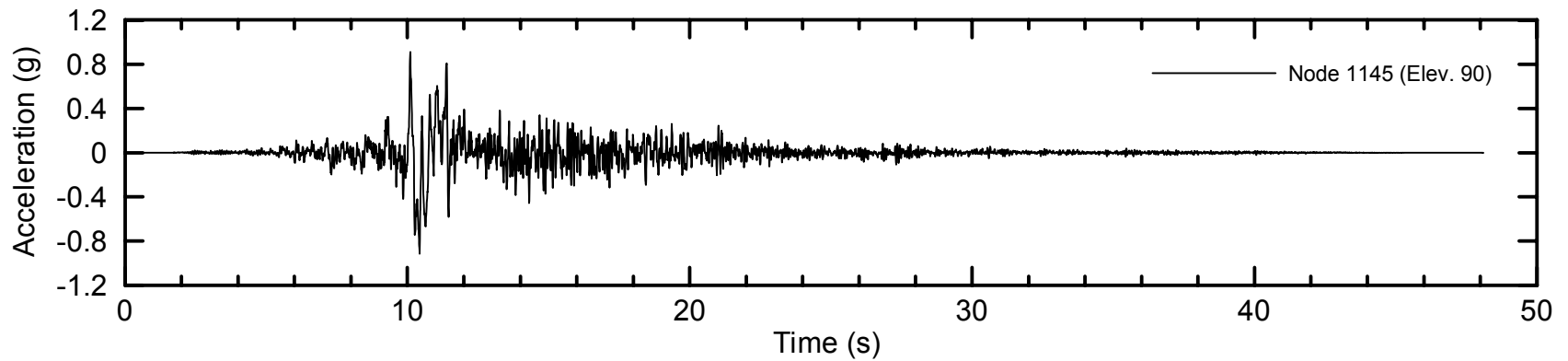
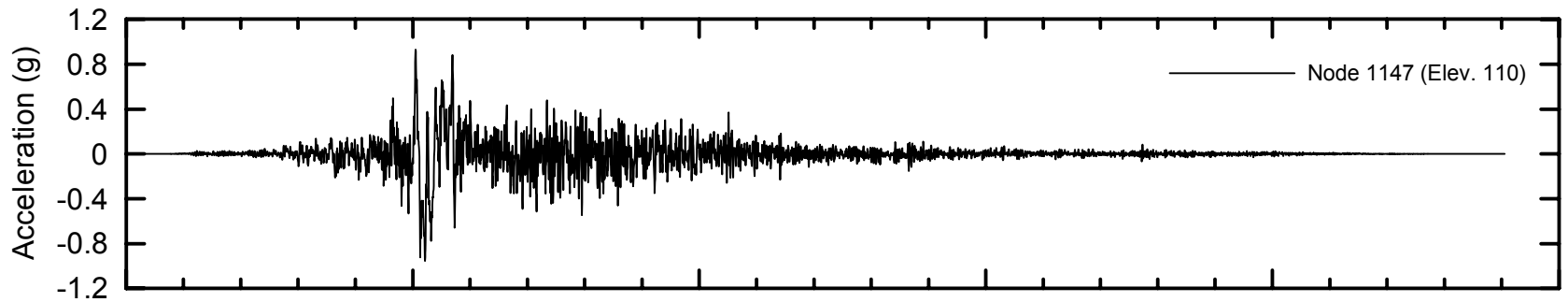
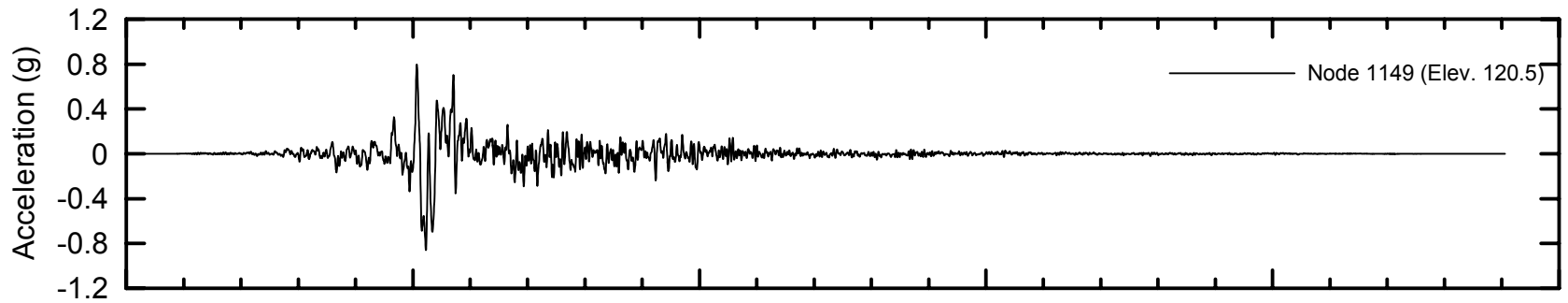


Project No. 26814536	Chabot Dam Seismic Stability Analysis	Average Mass Acceleration Downstream Sliding Block #4 QUAD4M Analysis	Figure
URS		1989 Loma Prieta Earthquake	10-14

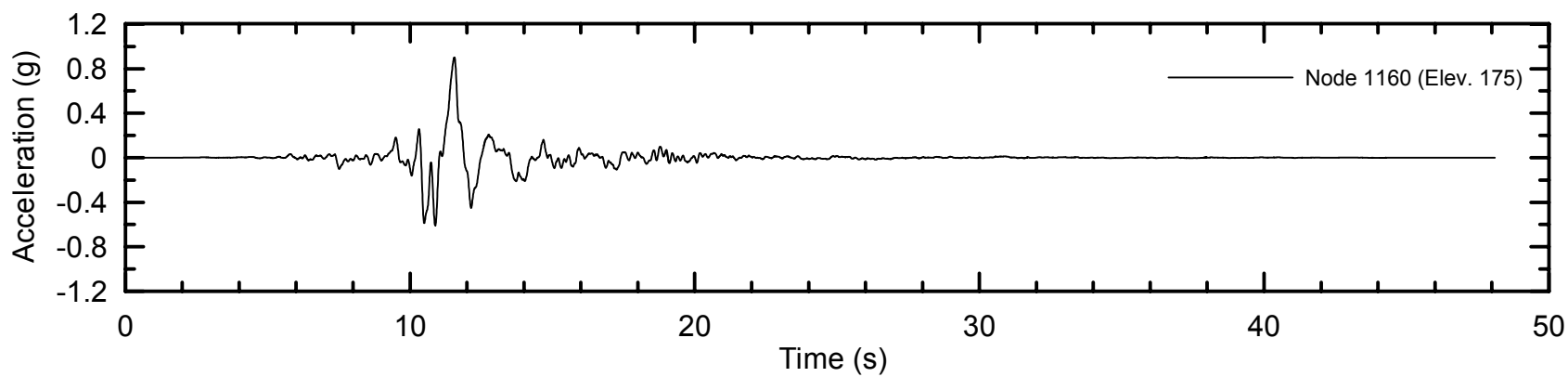
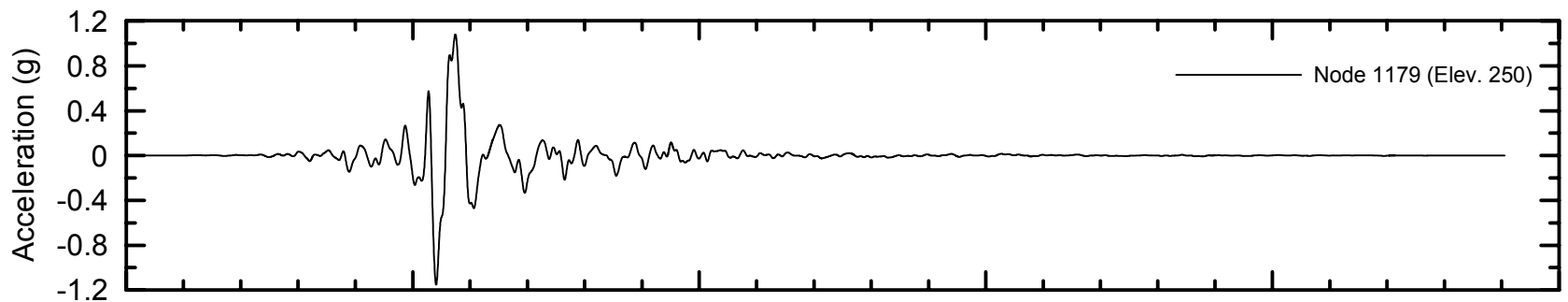


● 0.898 -- Peak horizontal acceleration in g.

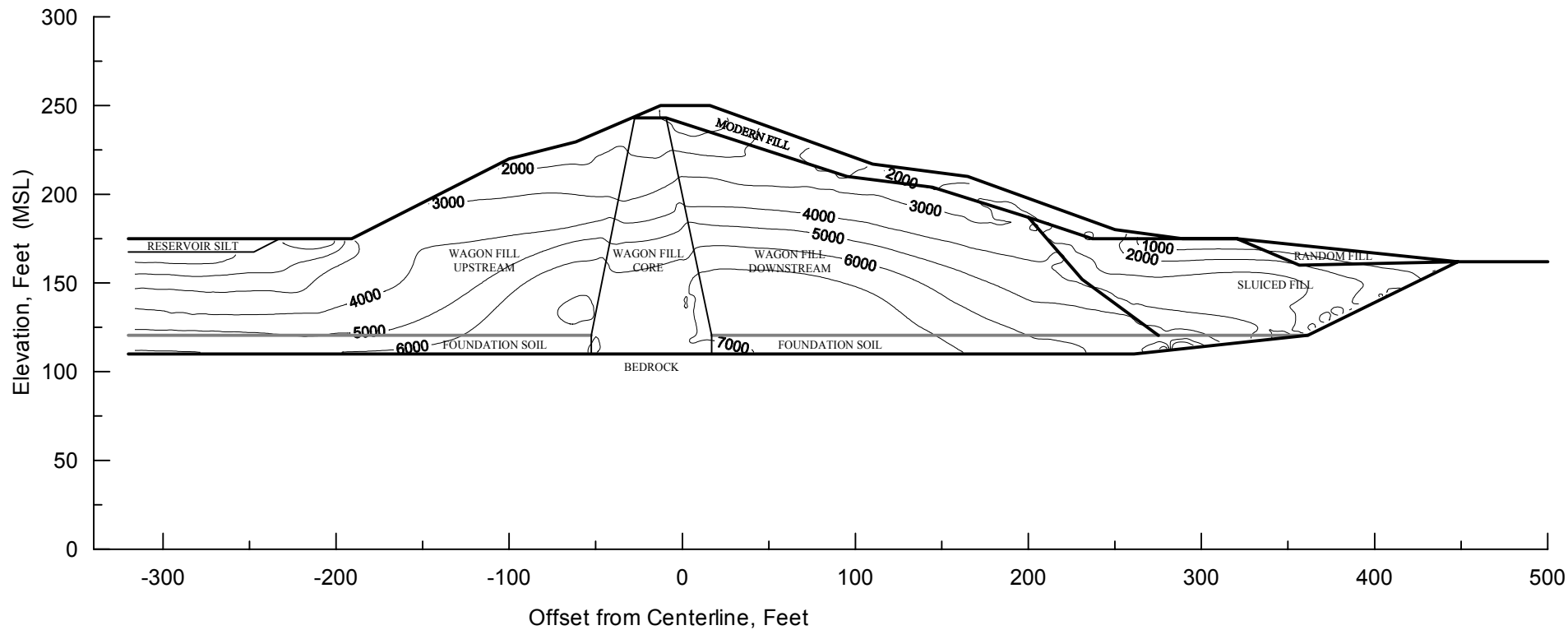
Project No. 26814536	Chabot Dam Seismic Stability Analysis	Peak Horizontal Acceleration QUAD4M Analysis Hayward Fault MCE TH #1	Figure 10-15
URS			



Project No. 26814536	Chabot Dam Seismic Stability Analysis	Acceleration Time History Beneath Crest Nodes 1145, 1147 and 1149 Hayward Fault MCE TH #1	Figure
URS			10-16

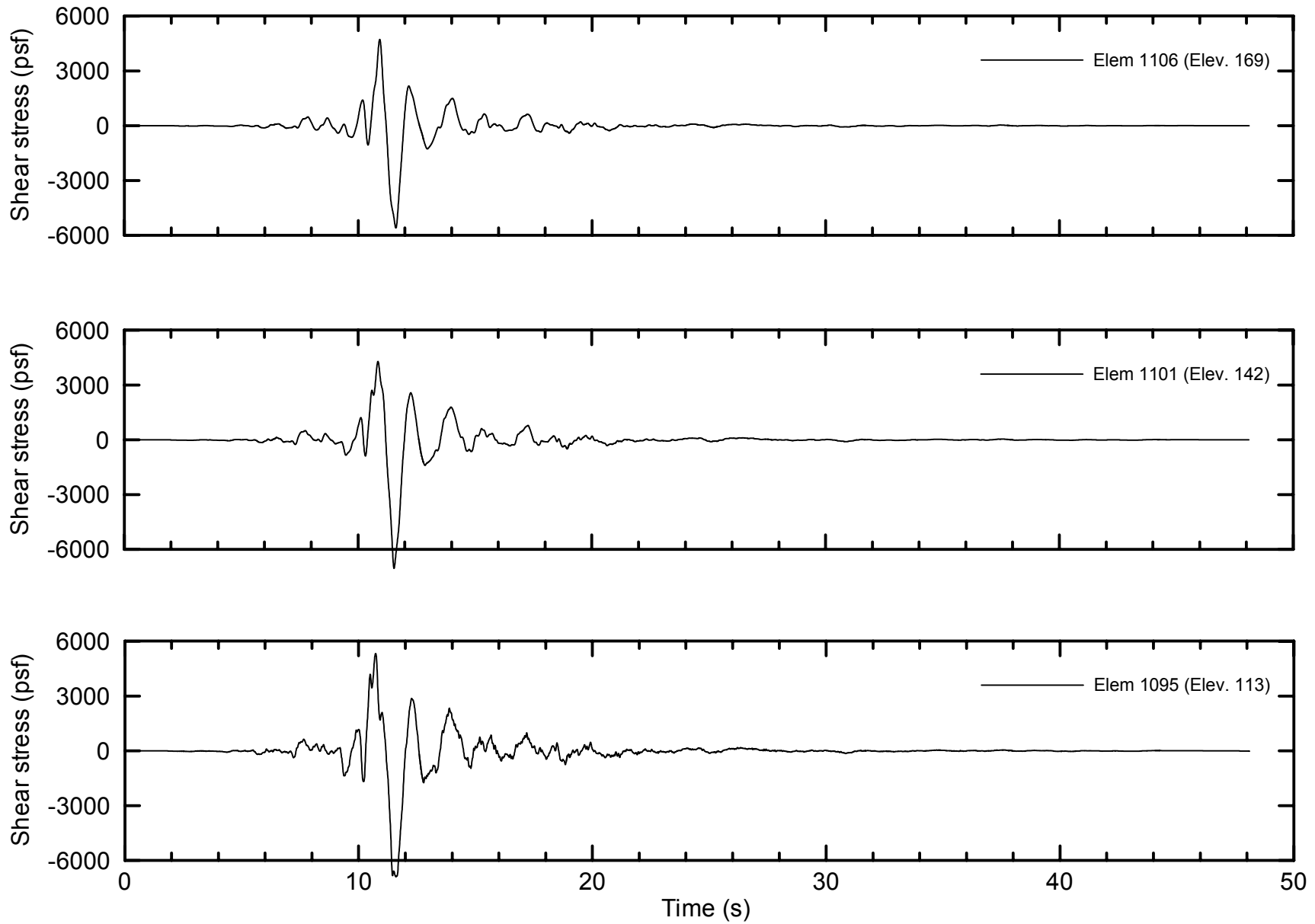


Project No. 26814536	Chabot Dam Seismic Stability Analysis	Acceleration Time History Beneath Crest Nodes 1160 and 1179	Figure 10-17
URS		Hayward Fault MCE TH #1	

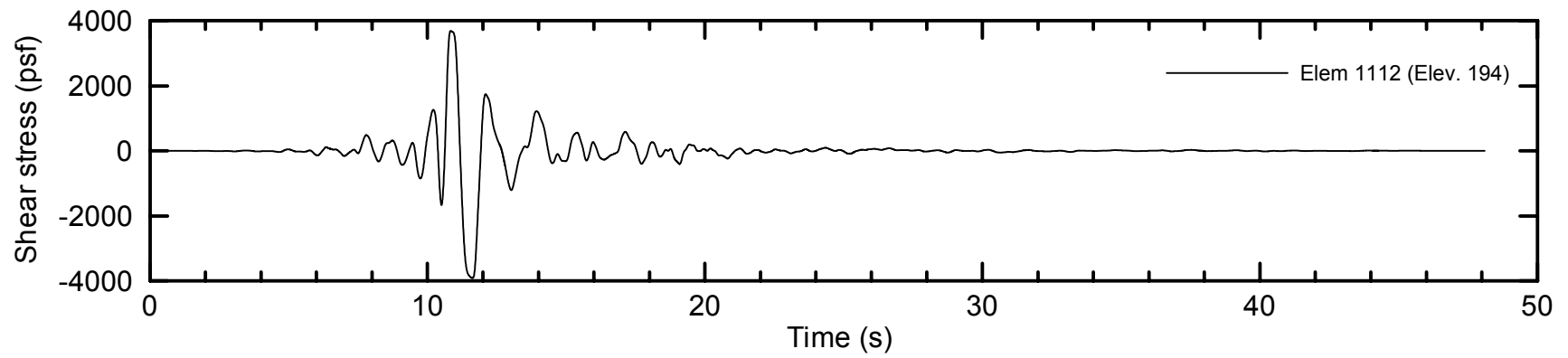
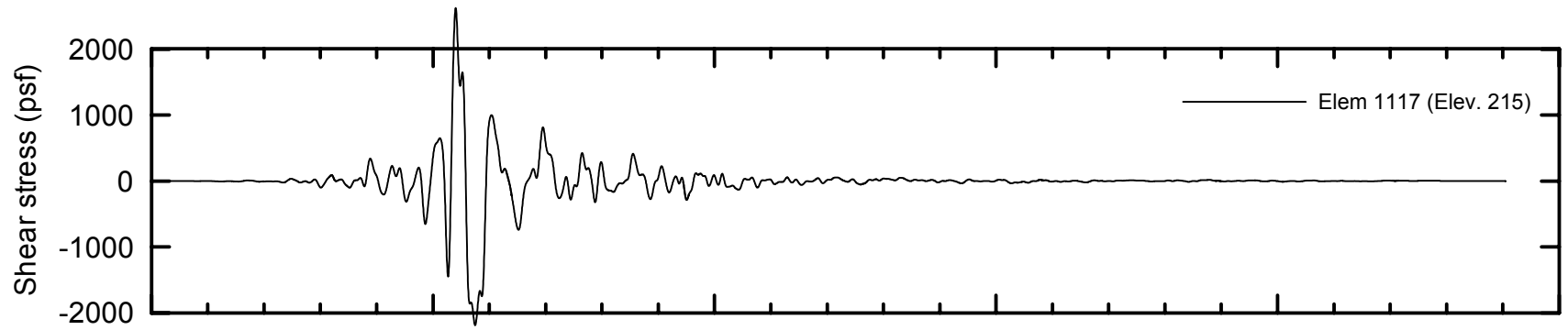


Notes: Peak shear stress contour values in pounds per square foot (psf)

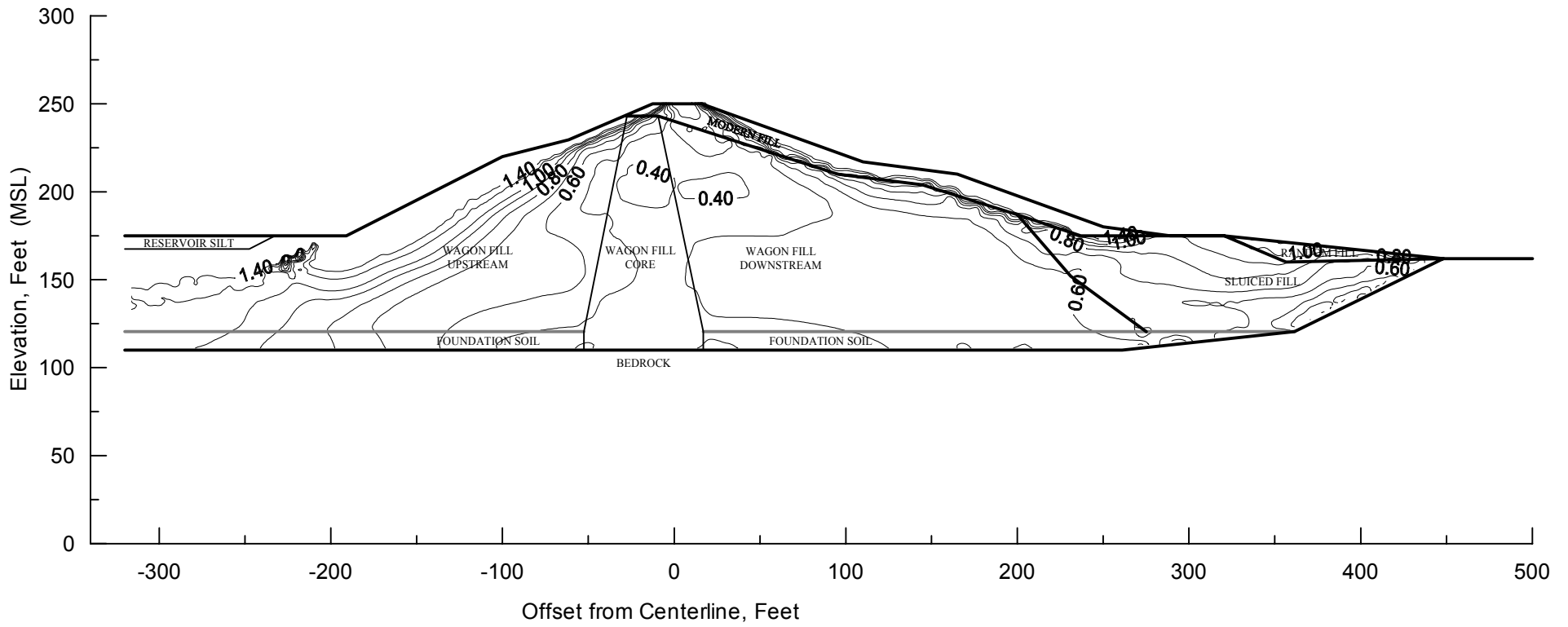
Project No. 26814536	Chabot Dam Seismic Stability Analysis	Peak Shear Stress QUAD4M Analysis Hayward Fault MCE TH #1	Figure 10-18
URS			



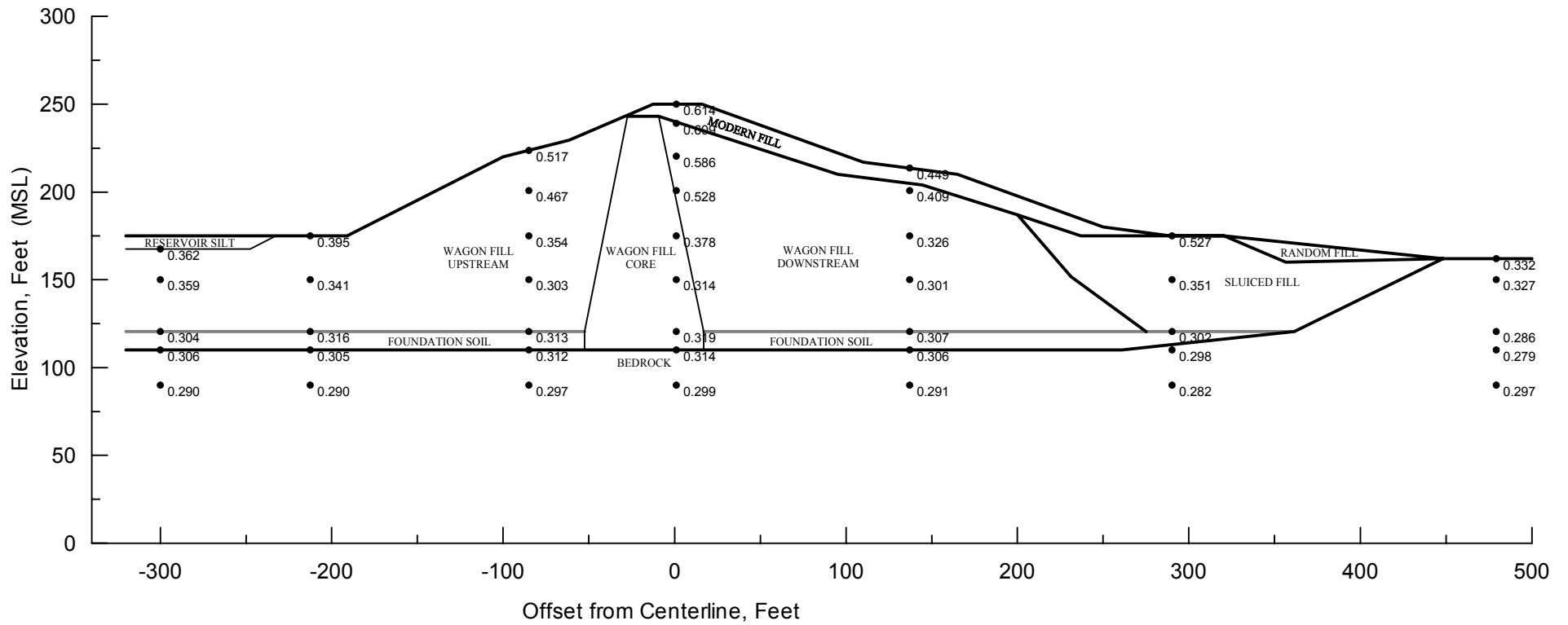
Project No. 26814536	Chabot Dam Seismic Stability Analysis	Shear Stress Time History Beneath Crest Elements 1095, 1101, and 1106 Hayward Fault MCE TH #1	Figure
URS			10-19



Project No. 26814536	Chabot Dam Seismic Stability Analysis	Shear Stress Time History Beneath Crest Elements 1112 and 1117 Hayward Fault MCE TH #1	Figure
URS			10-20

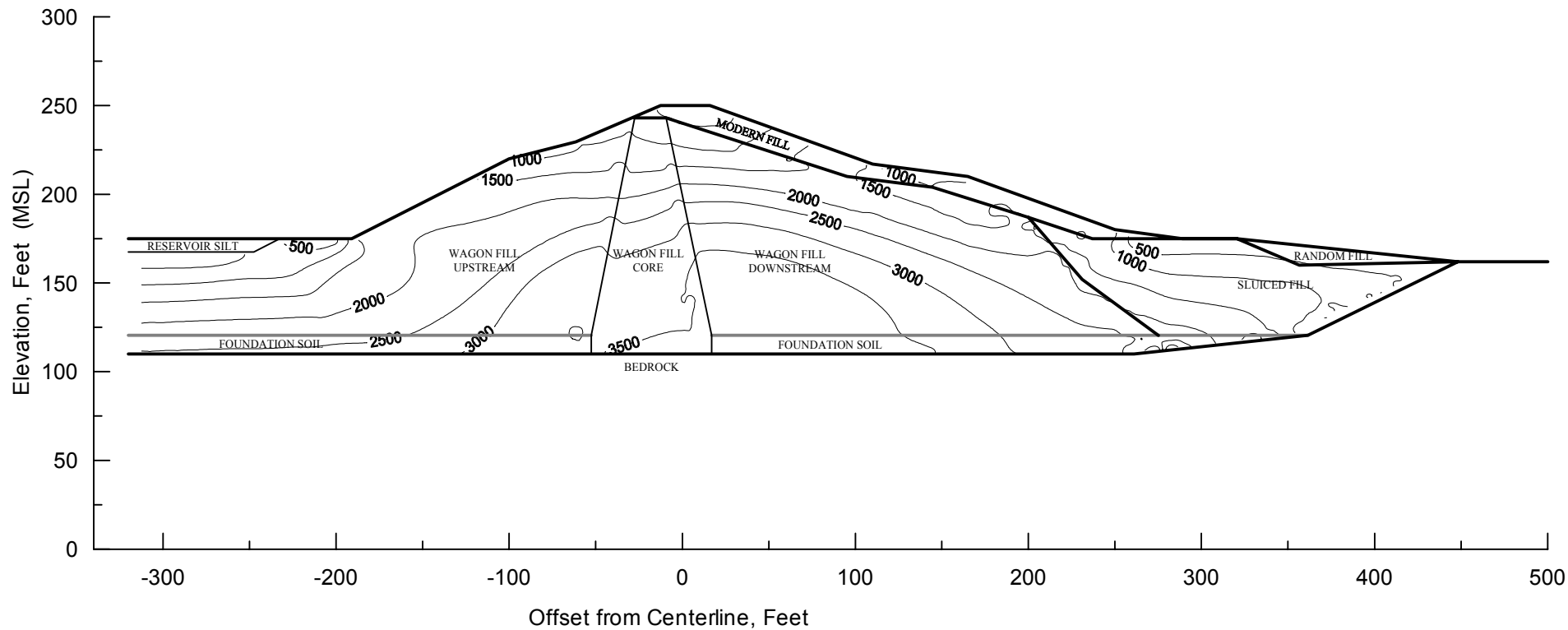


Project No. 26814536	Chabot Dam Seismic Stability Analysis	Cyclic Stress Ratio QUAD4M Analysis Hayward Fault MCE TH #1	Figure 10-21
URS			



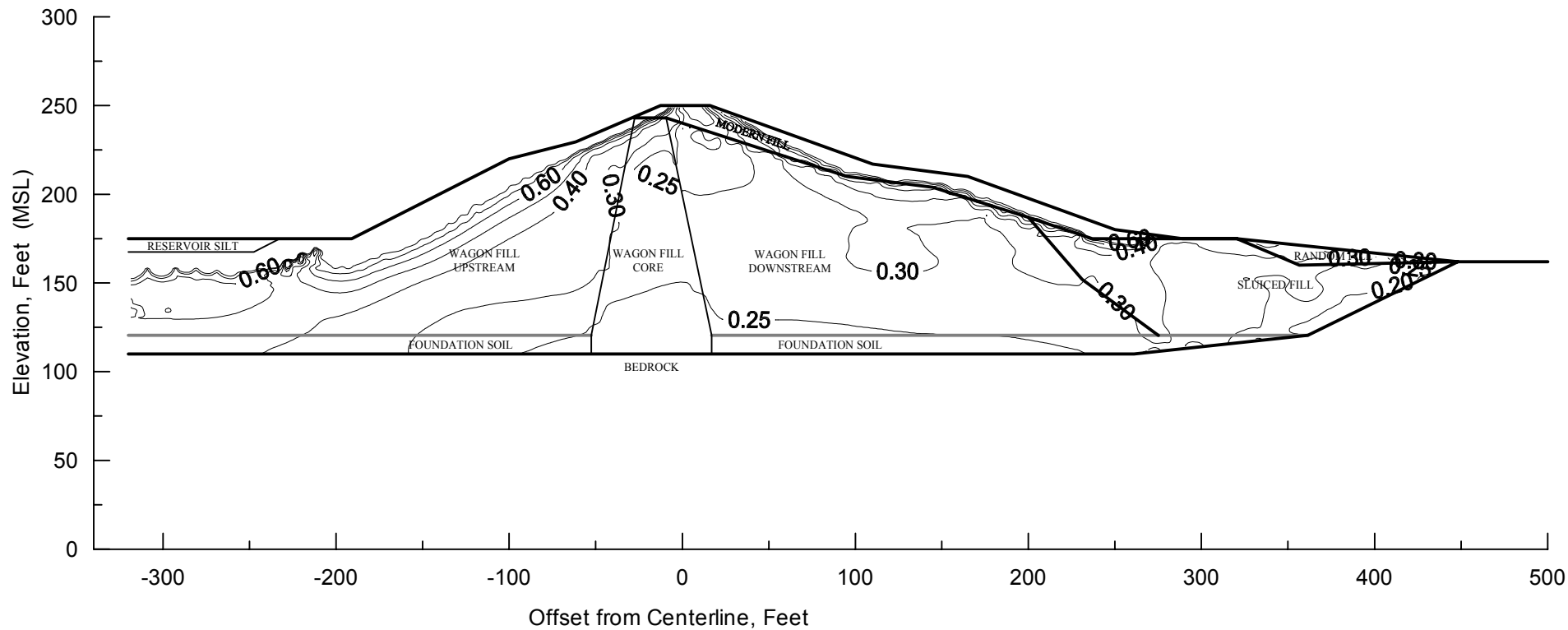
• 0.290 -- Peak horizontal acceleration in g.

Project No. 26814536	Chabot Dam Seismic Stability Analysis	Peak Horizontal Acceleration QUAD4M Analysis San Andreas Fault MCE	Figure
URS			10-22



Note: Peak shear stress contour values in pounds per square foot (psf).

Project No. 26814536	Chabot Dam Seismic Stability Analysis	Peak Shear Stress QUAD4M Analysis San Andreas Fault MCE	Figure 10-23
URS			



Project No. 26814536	Chabot Dam Seismic Stability Analysis	Cyclic Stress Ratio QUAD4M Analysis San Andreas Fault MCE	Figure 10-24
URS			

11.1 APPROACH

As described in Section 8, the approach to the seismic stability analysis of the dam consisted of using the results of the dynamic response analyses presented in Section 10 to evaluate the potential for liquefaction of the sluiced fill and for cyclic strength degradation of the wagon fill materials and foundation soils. The slope stability factors of safety and yield accelerations of potential sliding blocks were then evaluated using limit-equilibrium analyses and shear strengths appropriate for the materials subject to liquefaction or cyclic strength degradation. Together with the average mass accelerations of the sliding blocks obtained from the dynamic response analyses, the yield accelerations were used to calculate seismic displacements of the sliding blocks using a Newmark-type deformation analysis.

11.2 EVALUATION OF LIQUEFACTION POTENTIAL IN SLUICED FILL

11.2.1 Evaluation Procedures

The liquefaction resistance of the sluiced fill materials, and their residual strength after liquefaction, are best assessed based on available empirical correlations with in-situ test data. In this investigation, the liquefaction potential of the sluiced fill was evaluated from its estimated SPT blow count resistance using the correlations proposed by Youd et al. (2001). The factor of safety against liquefaction is calculated as:

$$FS = CRR / CSR$$

where: CRR = cyclic resistance ratio, and CSR = cyclic stress ratio induced by the earthquake. A FS of less than 1 indicates soil liquefaction, and vice versa.

The CSR was calculated from the dynamic response analyses as described in Section 10. The CRR values within the sluiced fill were calculated using the following expression:

$$CRR = K_{\sigma} \cdot K_{\alpha} \cdot MSF \cdot CRR_{7.5}$$

where: $CRR_{7.5}$ = cyclic resistance ratio defined as the cyclic stress ratio required to trigger liquefaction in fifteen loading cycles

MSF = magnitude scaling factor

K_{σ} = correction factor for effective overburden stress

K_{α} = correction factor for initial static shear stress.

The MSF factors for the sluiced fill were evaluated by using the following equation recommended by Youd et al. (2001):

$$MSF = 10^{2.24} / M_w^{2.56}$$

The magnitudes of the Hayward and San Andreas MCEs and of the 1989 Loma Prieta earthquake used for analysis were 7.25, 8.0 and 6.9, respectively.

The overburden correction factor (K_{σ}) for the sluiced fill was computed using the following equation recommended by Youd et al. (2001):

$$K_{\sigma} = (\sigma_{v0}' / Pa)^{(f-1)}$$

where: σ_{vo}' = initial effective overburden stress

Pa = atmospheric pressure (e.g. 2,000 psf)

f = empirical factor dependent on relative density. A value of 0.8 was selected for the sluiced fill based on its apparent relative density.

The K_α correction factor was evaluated based on several recently published relationships (e.g. Harder and Boulanger, 1997; Idriss and Boulanger, 2002). A constant K_α value of 1.0 was estimated for the sluiced fill based on the apparent relative density of the material and the range of applicable confining pressures.

11.2.2 SPT Blow Count Evaluation

The correlation between CSR required to cause liquefaction and normalized SPT blow count, $(N_1)_{60}$, shown in Figure 11-1 was used to estimate the liquefaction resistance of the sluiced fill. By definition, the CSR required to cause liquefaction corresponds to the CRR. The correlation is applicable to magnitude 7.5 earthquakes and therefore yields values of $CRR_{7.5}$.

For this investigation, a large number of SPT blow counts were obtained in rotary-wash borings drilled through the sluiced fill (borings WI-60, 63 and 65). SPT blow counts were recorded per inch of sampler penetration. The plots of cumulative SPT blow count versus sampler penetration are shown in Appendix A. Figure 11-2 shows a comparison between such blow counts and those obtained for the 1973 Woodward-Clyde study (Borings WI 37, 38, and 39). As shown, the two sets of data are consistent.

An attempt was made to adjust the SPT blow count for gravel effects in the sluiced fill, but it was found that such adjustment could not be reliably applied. Thus, it was judged that the SPT blow counts are likely biased toward the high side and do not provide a reliable measure of the liquefaction resistance of the sluiced fill materials. Accordingly, three BPT soundings were conducted in the sluiced fill zone for this investigation. The equivalent SPT resistance was estimated from the BPT resistance and used in the liquefaction potential evaluation as described below.

11.2.3 BPT Blow Count Evaluation

The BPT testing procedure is described in Section 4 and in Appendix B. Re-drive tests were performed to estimate the effects of casing friction on the BPT blow counts. These tests indicated that casing friction in soundings BPT-1 and 2 was negligible. A small amount of casing friction was observed in sounding BPT-3. The corresponding adjustments to the blow counts are shown in Figure 11-3.

The BPT blow count data were reduced using the approaches proposed by Harder and Seed (1986) based on the bounce chamber pressure measurements, and by Sy and Campanella (1994) based on the energy measurements. As illustrated for sounding BPT-1 in Figure 11-4, the equivalent SPT blow counts obtained using the two approaches were in excellent agreement in all cases.

Figures 11-5 through 11-7 compare the equivalent SPT blow counts obtained from the BPT soundings with the SPT blow counts measured in the rotary-wash borings. It may be seen that the blow counts from the SPT borings are significantly higher than those obtained from the BPT

soundings, as expected based on the gravel content of the materials. It is interesting to note that in zones where the gravel content is low, for example in BPT-3 between elevations 145 and 155, the SPT blow counts obtained by the two techniques are in good agreement.

Figures 11-8 through 11-10 show the equivalent normalized SPT blow count, $(N_1)_{60}$, of the materials. The $(N_1)_{60}$ values of the sluiced fill range from about 4 to 10 with an average representative value of about 6. Based on the SPT resistance and an average fines content of 15 percent for this material, the $CRR_{7.5}$ value is 0.10, according to the correlation shown in Figure 11-1.

11.2.4 Liquefaction Potential

The liquefaction potential of the sluiced fill, in terms of the calculated factor of safety against liquefaction, is presented in Figures 11-11 through 11-13. Figure 11-11 shows that, during the 1989 Loma Prieta earthquake, the factor of safety against liquefaction of the sluiced fill would have been well above 1.0 and that no liquefaction of the saturated sluiced fill would have been expected, which is in good agreement with the field observations after that earthquake. During the Hayward and San Andreas events, however, the calculated factors of safety against liquefaction in the sluiced fill are well below 1.0, as shown in Figures 11-12 and 11-13, indicating that these materials will liquefy early during the strong shaking phase of those earthquakes. No liquefaction or strength loss was assumed to occur in the sluiced fill or the random fill above the water table.

No evidence of liquefaction at the site was reported after the 1906 San Francisco earthquake, which occurred on the San Andreas fault. However, little information is available regarding the intensity of the ground motions at the site during that earthquake. Thus, the presumed performance of the dam during that earthquake cannot be compared directly with the results obtained for the San Andreas fault MCE, although such comparison might suggest that the liquefaction evaluation of the sluiced fill could be somewhat conservative.

11.2.5 Residual strength evaluation

The undrained residual strength, S_{ur} , of the sluiced fill after liquefaction (or post-liquefaction strength) is estimated to be between 150 and 200 psf based on a representative equivalent SPT blow count, $(N_1)_{60}$, of 6, an average fines content of 15 percent, and the correlations presented by Seed and Harder (1990) and by Idriss (2002). The latter correlation is shown in Figure 11-14. A S_{ur} value of 150 psf was used for the sluiced fill in the stability analyses.

11.3 EVALUATION OF POTENTIAL STRENGTH LOSS IN WAGON FILL AND FOUNDATION SOILS

11.3.1 Evaluation Procedures

The potential for strain and strength loss of the wagon fill and foundation soils was evaluated by comparing the earthquake-induced cyclic stress ratio with the cyclic strength of the materials. The cyclic strength of the materials was expressed in terms of the cyclic stress ratio required to develop a cyclic shear strain, γ , of 3.75%, which approximately corresponds to a cyclic axial

strain, ε , of 2.5% under undrained conditions and is commonly assumed to correspond to an excess pore pressure ratio, r_u , of 100%. Thus, this cyclic strength ratio (CSR) is adopted as the cyclic resistance ratio (CRR) of the materials. The CRR was estimated based on the results of the cyclic triaxial strength tests performed by WLA (1974). For a magnitude 7.5 earthquake, or about 30 cycles of loading in clayey soils (Boulanger and Idriss, 2004), the cyclic resistance ratio of the materials was estimated to be $CRR_{7.5} = 0.4$, for conditions of zero static shear stress ratio ($\alpha=0$) and effective overburden stress, (σ_v'), equal to 1 tsf. The estimated cyclic resistance curve for the materials for 1 to 100 cycles of loading is shown in Figure 11-15.

The factor of safety against development of shear strains of 3.75% was calculated as:

$$FS_{3.75} = CRR/CSR$$

where: CSR = earthquake-induced cyclic stress ratio and CRR is given by:

$$CRR = K_{\sigma} \cdot K_{\alpha} \cdot MSF \cdot CRR_{7.5}$$

where: $CRR_{7.5}$ = cyclic resistance ratio defined as the cyclic stress ratio required to produce a shear strain of 3.75% in thirty cycles of loading

MSF = magnitude scaling factor

K_{σ} = correction factor for effective overburden stress

K_{α} = correction factor for initial static shear stress ratio

The magnitude scaling factor was obtained from the following expression (Boulanger and Idriss, 2004):

$$MSF = 1.12 \exp(-M/4) + 0.828 ; MSF \leq 1.13$$

where: M is the moment magnitude of the earthquake. The overburden and shear stress correction factors were obtained from the following expressions, which were derived from the results of the cyclic strength tests:

$$K_{\sigma} = (\sigma_v')^{-0.3} ; K_{\sigma} \leq 1.2$$

$$K_{\alpha} = 1 + 3.29\alpha - 6.61\alpha^2 - 3.84\alpha^3 ; \alpha \leq 0.35$$

where: α = initial static shear stress ratio and σ_v' = effective vertical stress in tsf. The values of static stress ratio and vertical effective stress were obtained from the static stress analysis of the dam performed using the computer program FLAC (Section 12).

No reliable measurements of residual excess pore pressures were made during the cyclic strength tests by WLA (1974). Available measurements made upon completion of the tests suggest that a maximum residual excess pore pressure ratio (r_u) of about 95% generally developed during the tests. Thus, the excess pore pressures during shaking had to be estimated based on the results of cyclic tests with pore pressure measurements on similar materials (WCC, 1989), which yielded the following expression:

$$r_u = 1/FS_{3.75} ; r_u \leq 0.95$$

No laboratory test data are available on the post-cyclic strength of the wagon fill or foundation soils. Thus, limited data are available to evaluate the potential reduction in strength of the materials due to the calculated excess pore pressures. Accordingly, such reduction was estimated based on the available cyclic strength data and on published information for similar

materials (Thiers and Seed, 1969; Lee and Focht, 1976; Idriss, 1985; Mejia, 1989). Based on this information, the post-cyclic strength of the wagon fill and foundation soils was estimated from the following expression:

$$(\tau_{\max}) / (\tau_{\max})_{\text{static}} = (1 - r_u)^{0.16} ; (\tau_{\max}) / (\tau_{\max})_{\text{static}} \geq 0.6$$

where:

$$\begin{aligned} (\tau_{\max}) &= \text{Post-cyclic undrained shear strength} \\ (\tau_{\max})_{\text{static}} &= \text{Static undrained shear strength} \end{aligned}$$

11.3.2 Potential for Strength Loss

The calculated excess pore pressure ratios in the saturated wagon fill and foundation soils for the Loma Prieta earthquake are shown in Figure 11-16. These results indicate that low excess pore pressures (less than about 40%) would have developed in these materials during that earthquake, as was actually observed. As shown in Figure 11-15, the low calculated pore pressures are associated with a small reduction in post-cyclic undrained strength (less than about 10%).

The excess pore pressure ratios calculated for the Hayward-Rodgers Creek Fault MCE were about 95% throughout a large portion of the wagon fill and foundation soils (Figure 11-17). This corresponds to a reduction in the undrained strength of the materials of about 40% after the strong shaking phase of the earthquake.

The calculated excess pore pressure ratios for the San Andreas Fault MCE are shown in Figure 11-18. These ratios range from about 75 to 95% and correspond to a lower calculated degree of strength degradation for this event than for the Hayward Fault MCE.

11.4 POST-EARTHQUAKE SLOPE STABILITY

Limit equilibrium methods were used to check the post-earthquake stability of the dam. The analyses were performed assuming liquefaction of the saturated sluiced fill and reduction of the undrained strength of the wagon fill and foundation soils to their post-cyclic strength. The undrained residual strength of 150 psf was assigned to the liquefied sluiced fill. The post-cyclic undrained strengths of the saturated wagon fill and foundation soils were estimated as discussed above. The calculated post-earthquake factors of safety for the Hayward Fault MCE, for the sliding blocks shown in Figure 10-9, are summarized in Table 11-1. Because the Hayward Fault MCE induces the largest strength degradation of the wagon fill and foundation soils (up to 40%), the potential for post-earthquake instability will be highest after this event. The results shown in Table 11-1 indicate that the dam will be stable after that event. Greater margins of safety against post-earthquake instability are expected for the San Andreas Fault MCE since this event produces a lower degree of strength degradation in the materials.

To evaluate the potential for instability of the sluiced fill in the direction of the stream channel downstream of the dam, post-earthquake stability analyses for the Hayward Fault MCE were performed using composite section A-A". The results of these analyses are presented in Figure 11-19. The calculated factors of safety for sliding surfaces within the downstream sluiced fill zone are close to or below 1.0, indicating that calculation of a yield acceleration is not pertinent. These results indicate that there is a potential for downstream displacements of the sluiced fill during and after the Hayward Fault MCE. Because adequate factors of safety are

calculated for failure surfaces that reach into the wagon fill, it may be concluded that displacement of the sluiced fill is unlikely to result in gross instability of the wagon fill. This conclusion is corroborated by the deformation patterns calculated from the nonlinear analyses presented in Section 12.

11.5 DEFORMATION ANALYSES

11.5.1 Methodology

The seismic deformations of the dam were estimated with the Newmark sliding block method of analysis. The method is based on the assumption of rigid-perfectly plastic stress-strain behavior on a potential failure surface. Displacements of the sliding block are calculated by integrating twice with time the difference between the earthquake-induced average acceleration of the slide mass and its yield acceleration.

The results of the QUAD4M analyses were used to evaluate the earthquake-induced average mass accelerations of potential sliding blocks within the dam. Together with the yield accelerations obtained from the limit equilibrium analyses, the average mass accelerations were used to calculate seismic displacements of the sliding blocks. Double integration of the difference between the average mass and yield accelerations was performed with the computer program TNMN.

11.5.2 Yield Acceleration Evaluation

The yield accelerations, K_y , used in the analyses were calculated from pseudo-static limit-equilibrium analyses. The calculated K_y values for the selected sliding blocks are tabulated in Table 11-2 for various levels of strength degradation in the embankment and foundation materials. The K_y for the pre-earthquake condition corresponds to the yield acceleration of the sliding blocks prior to liquefaction of the sluiced fill or seismic strength degradation of the wagon fill and foundation soils. The K_y for post-cyclic conditions, assumes that the sluiced fill has liquefied and that the wagon fill and foundation soils have undergone strength loss.

Together with the results of the FLAC analyses presented in Section 12, the calculated shear stress time histories within the dam (Figures 10-19 and 10-20) were used to estimate the timing of strength reduction of the materials during the earthquake shaking. For the Hayward fault MCE, little strength reduction is expected during the first 10.8 seconds of shaking. A 20% reduction in strength is estimated between 10.8 and 12.2 seconds of shaking. The maximum reduction in strength of 40% is estimated thereafter. This timing of strength reduction was used to develop time histories of yield acceleration during the earthquake for the selected sliding blocks. For the San Andreas fault MCE little reduction in strength is calculated for the first 12 seconds of shaking and the maximum reduction shown in Table 11-3 is estimated to occur after 15 seconds.

11.5.3 Analysis Results

The Newmark-type deformation analyses results are presented in Figures 11-20 through 11-34. The calculated displacements are summarized in Table 11-3. These calculated displacements correspond to horizontal translation of the center of mass of each sliding block. The

corresponding vertical displacements can be obtained from the rotation of the block necessary to accommodate the horizontal displacements.

For the Loma Prieta earthquake, little strength degradation is expected during the earthquake and the peak mass acceleration for each block (see Figures 10-12 through 10-14) is less than the corresponding yield acceleration (see Figure 9-10). Thus, the calculated deformations are nil, and it may be concluded that the calculated dynamic response and seismic deformations from the Newmark-type analyses are in good agreement with the known performance of the dam during that earthquake.

The displacements calculated for Hayward event are shown in Figures 11-20 through 11-26. Horizontal displacements of 6 to 9 feet are calculated for upstream block No. 3. Based on the geometry of the block, such displacements would correspond to downward vertical displacements of the crest of 4 to 6 feet. Somewhat larger horizontal displacements (9 to 12 feet) are calculated for upstream block No. 1, but this block does not reach across the dam crest. Horizontal displacements of about 4 feet are calculated for downstream Block No. 4, which approximately encompasses the body of the sluiced fill. Horizontal displacements of less than 3 feet are calculated for other downstream blocks and for a deep-seated upstream block.

Parametric analyses were also performed based on the amount of strength degradation calculated from the FLAC analyses, which is discussed in Section 12. These latter analyses indicate that cyclic degradation will result in a reduction in strength of no more than about 10 percent over a large portion of the wagon fill. This reduction is expected to occur during the strong phase of shaking. Accordingly, the parametric analyses were performed for selected sliding blocks using time histories of yield acceleration that incorporate a 10 percent strength reduction (see Table 11-3) early in the strong phase of shaking. The results of these analyses are shown in Figures 11-27 through 11-29. As shown in Figures 11-27 and 11-28, the calculated horizontal displacements for upstream blocks Nos. 1 and 3 are less than about 5 feet. Such displacements correspond to a vertical downward displacement of the crest less than about 3.5 feet.

In summary, the Newmark analyses for the Hayward fault MCE result in calculated downward displacements of the crest less than about 6 feet, and likely less than about 3.5 feet. Horizontal displacements of up to about 12 feet are calculated for sliding blocks near the upstream face of the dam, but such blocks do not extend into the main body of the embankment and do not reach across the dam crest.

The displacements calculated for the San Andreas event are shown in Figures 11-30 through 11-34. It may be seen that the calculated dam deformations for the San Andreas event are lower than those for the Hayward event. Thus, the results of the analyses indicate that the San Andreas event is less critical than the Hayward event regarding the seismic stability of the dam.

11.5.4 Analyses of Alternative Cross-Sections

As discussed in Sections 7 and 9, there are uncertainties regarding the geometry of the embankment cross-section. Parametric analyses were performed for the Hayward Fault MCE to evaluate the effects of such uncertainties on the calculated deformations, as described below.

There is some uncertainty regarding the location of the downstream boundary between the wagon fill and the sluiced fill. Limited Newmark-type deformation analyses were performed on Modified Section A-A' (Figure 9-4) to examine the sensitivity of the calculated deformations to

the location of that boundary. The results of those analyses are illustrated in Figures 11-35 and 11-36 and are summarized in Table 11-4. They indicate that the calculated downstream deformations are not highly sensitive to the location of the wagon fill/sluced fill boundary.

As shown in the boring logs and in Figures 7-3 and 7-4, exploratory borings WI-66 and WI-67 encountered reservoir silt to depths of only about 6 feet. Between 6 and 15 feet, the materials in WI-67 may or may not be fill. The materials encountered in borings WI-66 and WI-67 below depths of 6 and 15 feet, respectively, have the characteristics of fill, similar to that encountered in borings at the crest and downstream bench. They do not appear to be landslide material and they are clearly not reservoir sediment. Nonetheless, to evaluate the effects of uncertainties in the characteristics of these materials, Alternative Section A-A' was developed and analyzed. This alternative section is shown in Figure 11-37. In this alternative section, the material overlying the upstream toe (at Elev. 120.5) is assumed to be reservoir silt. The results of Newmark-type deformation analyses to evaluate that assumption are illustrated in Figures 11-38 through 11-40 and are summarized in Table 11-4. Figures 11-38 and 11-39 illustrate the factors of safety and yield accelerations calculated for conditions of zero and 20% strength reduction. The latter condition is intermediate to the conditions of zero and the maximum reduction of 40% after strong shaking (see Section 11.5.2). Figure 11-40 shows the results of the time integration of slide mass displacement. As might be expected, the computed displacement for upstream block No. 2 increases somewhat from the value presented in Table 11-3, but is smaller than the values shown in that table for upstream blocks Nos. 1 and 3.

To evaluate the effects of potential liquefaction in the foundation soils beneath the sluced fill these soils were modeled with the same properties as the overlying sluced fill in alternative cross section A-A' (see Figure 11-37). The same change was also implemented in an alternative to modified section A-A', as shown in Figure 11-41. The results of Newmark-type deformation analyses to check those effects are shown in Figures 11-41 through 11-44, and are summarized in Table 11-4. The results indicate that the potential for liquefaction in the foundation soils beneath the sluced fill does not have a significant effect on the calculated deformations.

**Table 11-1
Post-Earthquake Factors of Safety for Hayward Fault MCE**

Sliding Block ⁽¹⁾	Calculated Factor of Safety
U/S 1	1.05
U/S 2	1.83
U/S 3	1.25
D/S 1	1.59
D/S 2	1.47
D/S 3	1.55
D/S 4	1.34

Note:

- (1) See Figure 10-9 for location and geometry of sliding blocks.
(2) Maximum strength reduction in saturated wagon fill is 40 percent.

**Table 11-2
Yield Acceleration Coefficients of Selected Sliding Blocks for Various Levels of Post-cyclic
Strength Reduction in Embankment and Foundation Materials**

Sliding Block ⁽²⁾	Pre-Earthquake Condition ⁽³⁾	Assumed Reduction in Post-cyclic Strength of Saturated Wagon Fill and Foundation Soils ⁽¹⁾		
		10% ⁽⁴⁾	20%	40%
U/S #1	0.29	0.22	0.14	0.01
U/S #2	0.37	0.31	0.26	0.15
U/S #3	0.28	0.21	0.14	0.06
D/S #1	0.37	0.29	0.23	0.14
D/S #2	0.40	0.30	0.21	0.12
D/S #3	0.39	0.27	0.16	0.11
D/S #4	0.50 ⁽⁵⁾	0.05	0.05	0.05

Note:

- (1) Saturated sluiced fill is assumed to have liquefied and its residual strength is used as its post-cyclic strength. No strength reduction is assumed in materials above the water table.
(2) See Figure 10-9 for location and geometry of sliding blocks.
(3) This condition applies to earthquake shaking period before strength degradation occurs.
(4) The yield acceleration coefficient, K_y , for 10% strength reduction was estimated by interpolation from the K_y values for pre-earthquake and post-cyclic earthquake conditions with 20% strength reduction.
(5) The K_y value is truncated at 0.5 and used in analysis.

Table 11-3
Calculated Horizontal Displacement in Newmark-type Analyses

Earthquake	Sliding Block ⁽¹⁾	Max. Strength Reduction ⁽²⁾	Displacement, ft	
			Standard Polarity	Reverse Polarity
Hayward Fault MCE	U/S 1	40%	9.3	11.8
	U/S 2	40%	0.0	0.6
	U/S 3	40%	5.6	8.9
	D/S 1	40%	0.9	2.9
	D/S 2	40%	0.3	1.7
	D/S 3	40%	0.8	2.8
	D/S 4	40%	1.1	4
	U/S 1	10 %	2.1	5.2
	U/S 3	10 %	2.2	5.4
	D/S 1	10 %	0.6	1.7
San Andreas Fault MCE	U/S 1	40%	8.3	10.2
	U/S 3	40%	3.3	4.2
	D/S 4	20%	1.8	1.8
	U/S 1	10 %	0.1	0.5
	U/S 3	10 %	0.1	0.6

Note:

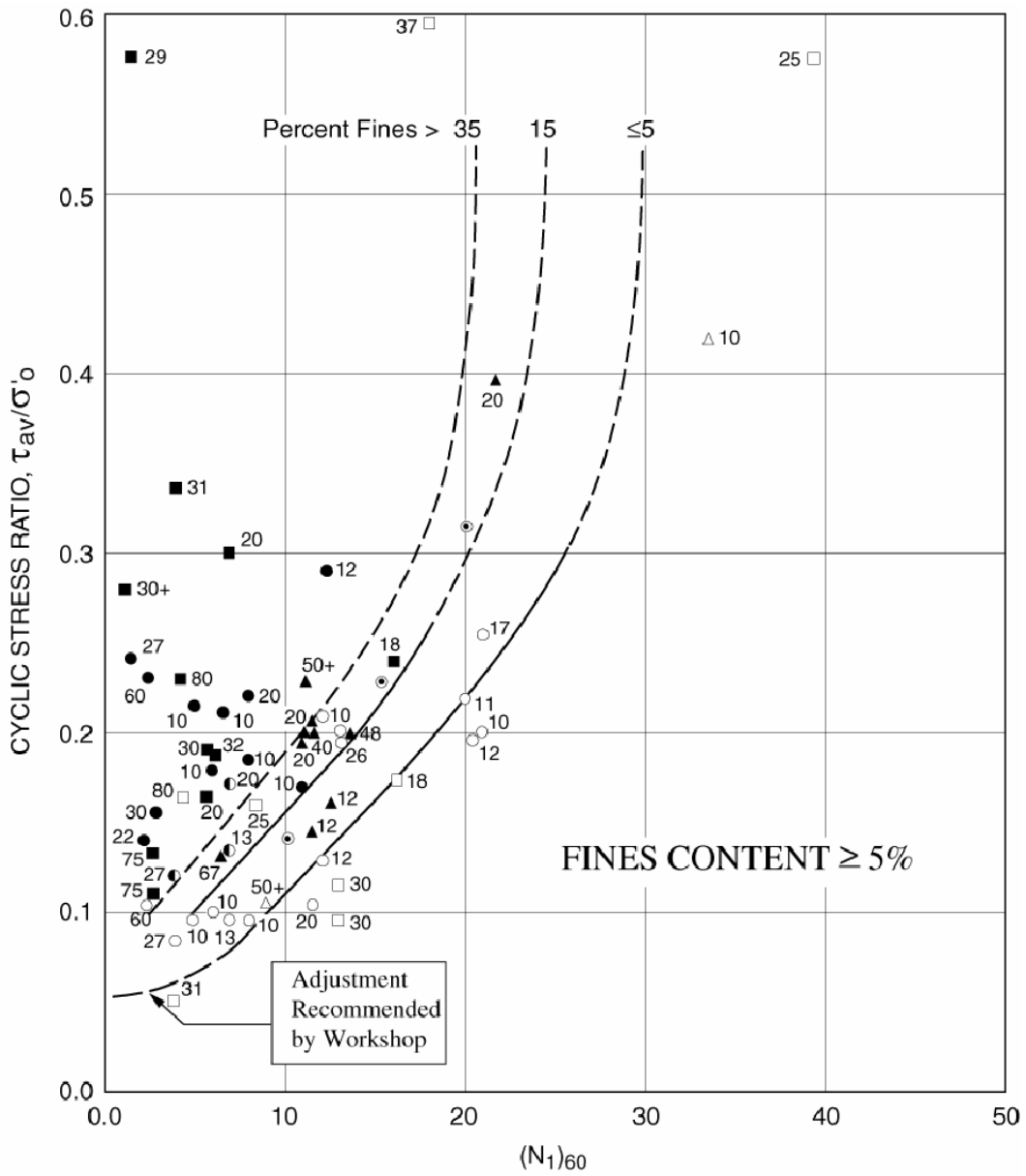
1. See Figure 10-9 for location and geometry of sliding blocks.
2. See report text for the assumed timing of strength reduction

Table 11-4
Sensitivity Analysis of Calculated Horizontal Displacement to Uncertainties in Embankment and Foundation Conditions - Hayward Fault MCE

Section	Sliding Block	Max. Strength Reduction	Displacement, ft	
			Standard Polarity	Reverse Polarity
Modified Section A-A' ⁽¹⁾	D/S 1	40%	1.4	4.4
	D/S 3	40%	1.4	5.1
Alternative Section A-A' ⁽²⁾	U/S 2	40%	0.1	1.2
	D/S 2	40%	0.4	2.6
Alternative Modified Section A-A' ⁽³⁾	D/S 2	40%	0.4	2.2

Note:

1. Obtained from Section A-A' by moving wagon fill/sluiced fill boundary upstream (Figure 9-4).
2. Obtained from Section A-A' by assuming upstream limit of wagon fill at 2:1 slope to top of foundation soil, and assuming foundation soil beneath sluice fill is liquefiable (Figure 11-37).
3. Combination of Modified Section A-A' and Alternative Section A-A' (Figure 11-41).



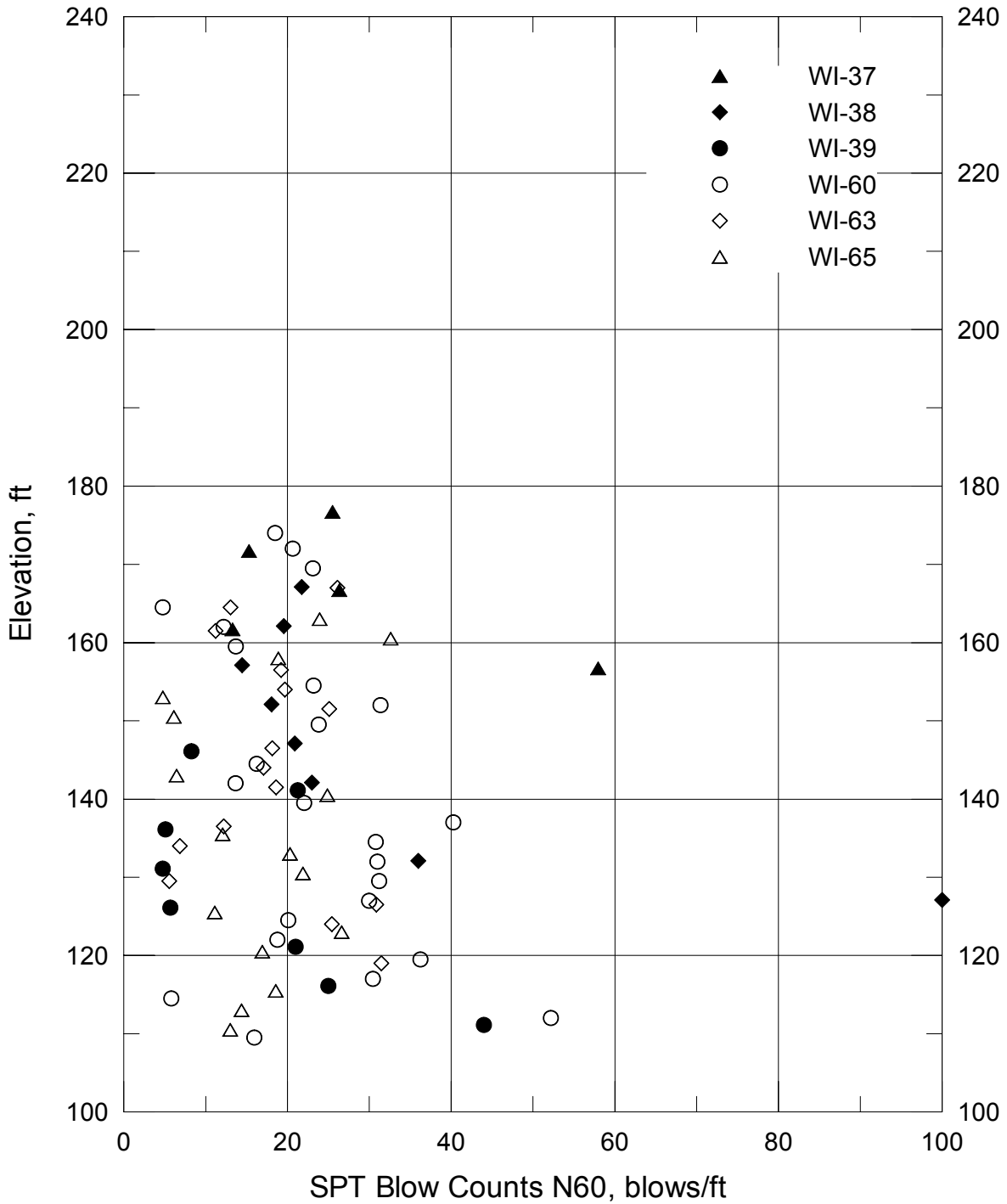
Project No. 26814536

Chabot Dam
Seismic Stability

**SPT-Based Liquefaction Triggering
Correlations for Mw 7.5 Earthquakes
(1996 and 1998 NCEER/NSF Workshops)**

Figure
11-1

Chabot Dam - SPT blow counts from borings WI-37, 38, 39, 60, 63, and 65

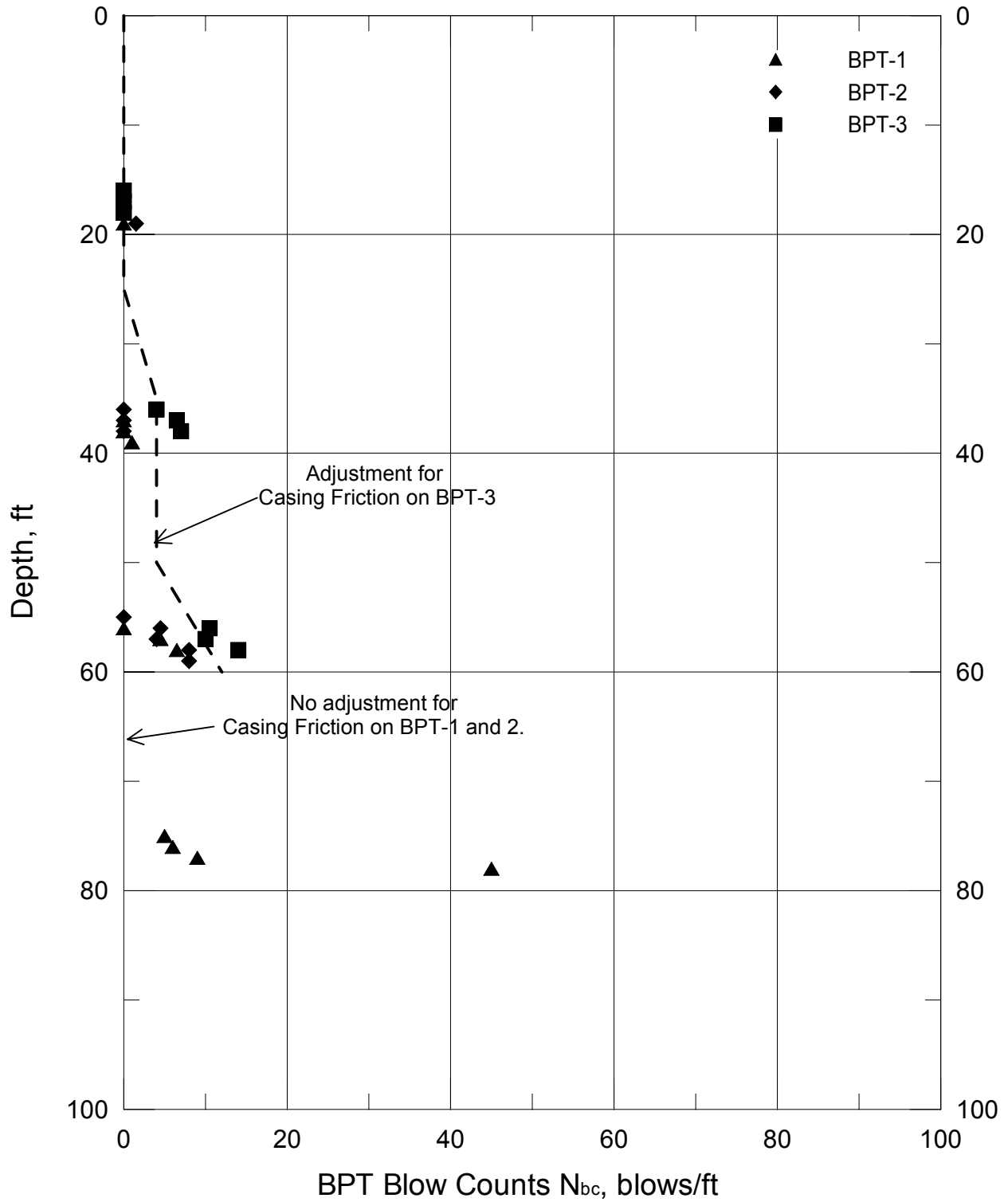


Note:

SPT blow counts in the bedrock, or affected by the bedrock, are excluded.

URS	Project No. 26814536	SPT Blow Counts N60 From Borings in Sluiced Fill Zone	Figure
	Chabot Dam Seismic Stability		11-2

Chabot Dam - Becker Hammer Penetration Test Redrives



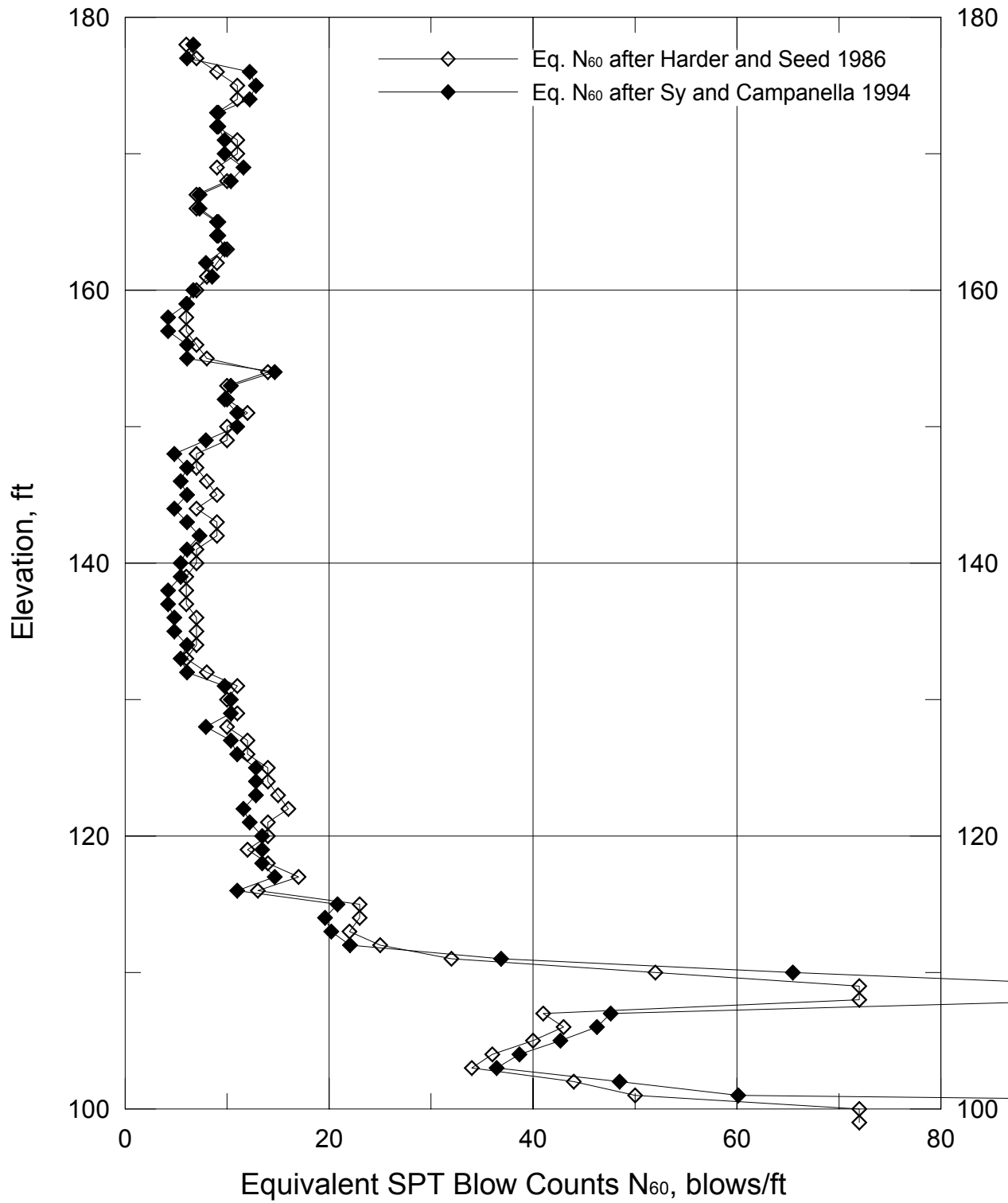
Project No. 26814536

Chabot Dam
Seismic Stability

**Adjustment of N_{bc} for Casing Friction
on BPT-1, 2 and 3**

Figure
11-3

Chabot Dam BPT-1 Blow Counts



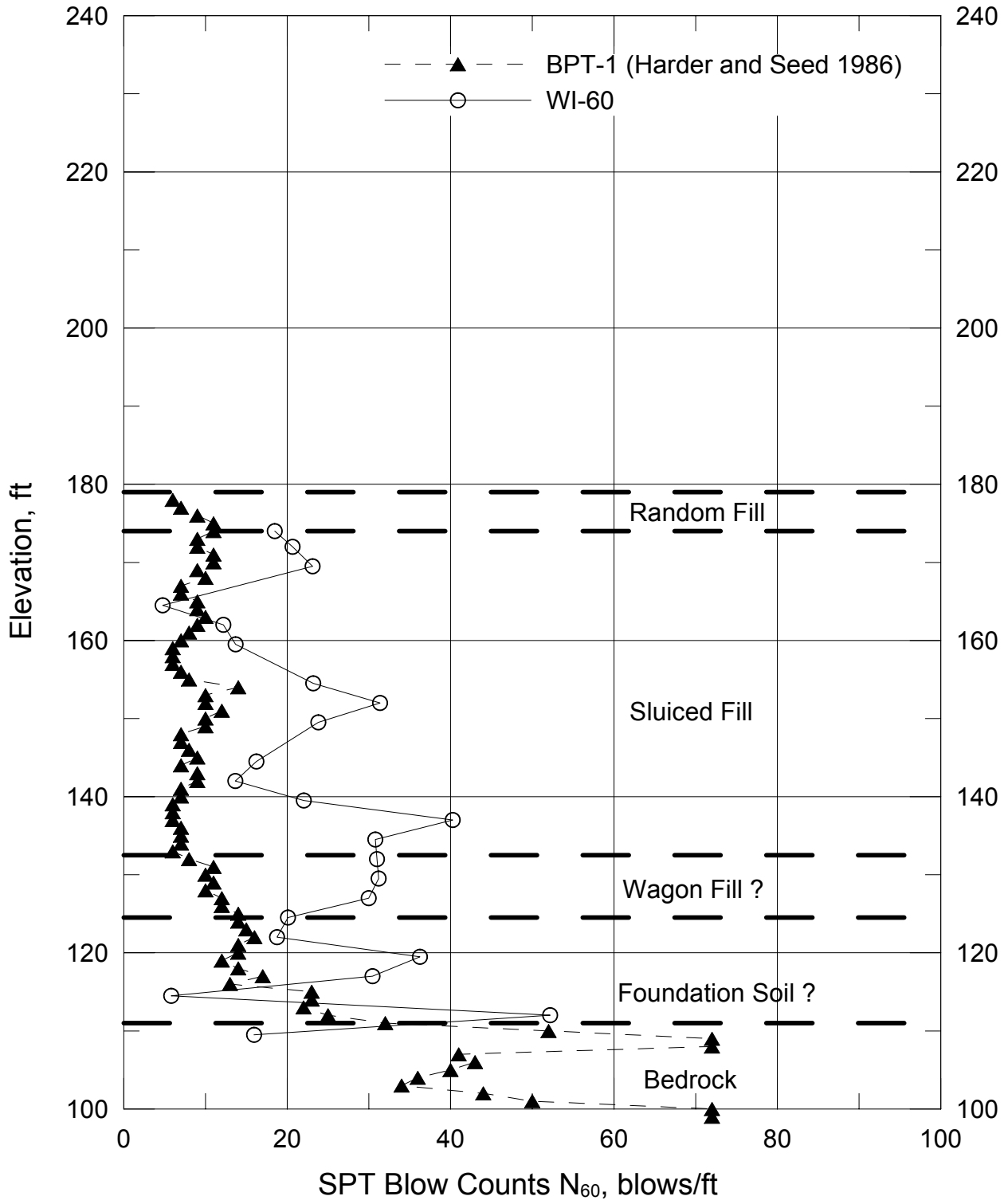
Project No. 26814536

Chabot Dam
Seismic Stability

**Becker Penetration Test
BPT-1**

Figure
11-4

Chabot Dam Borings WI-60 and BPT-1



Note:
Stratigraphy is inferred from BPT resistance and boring log of WI-60.



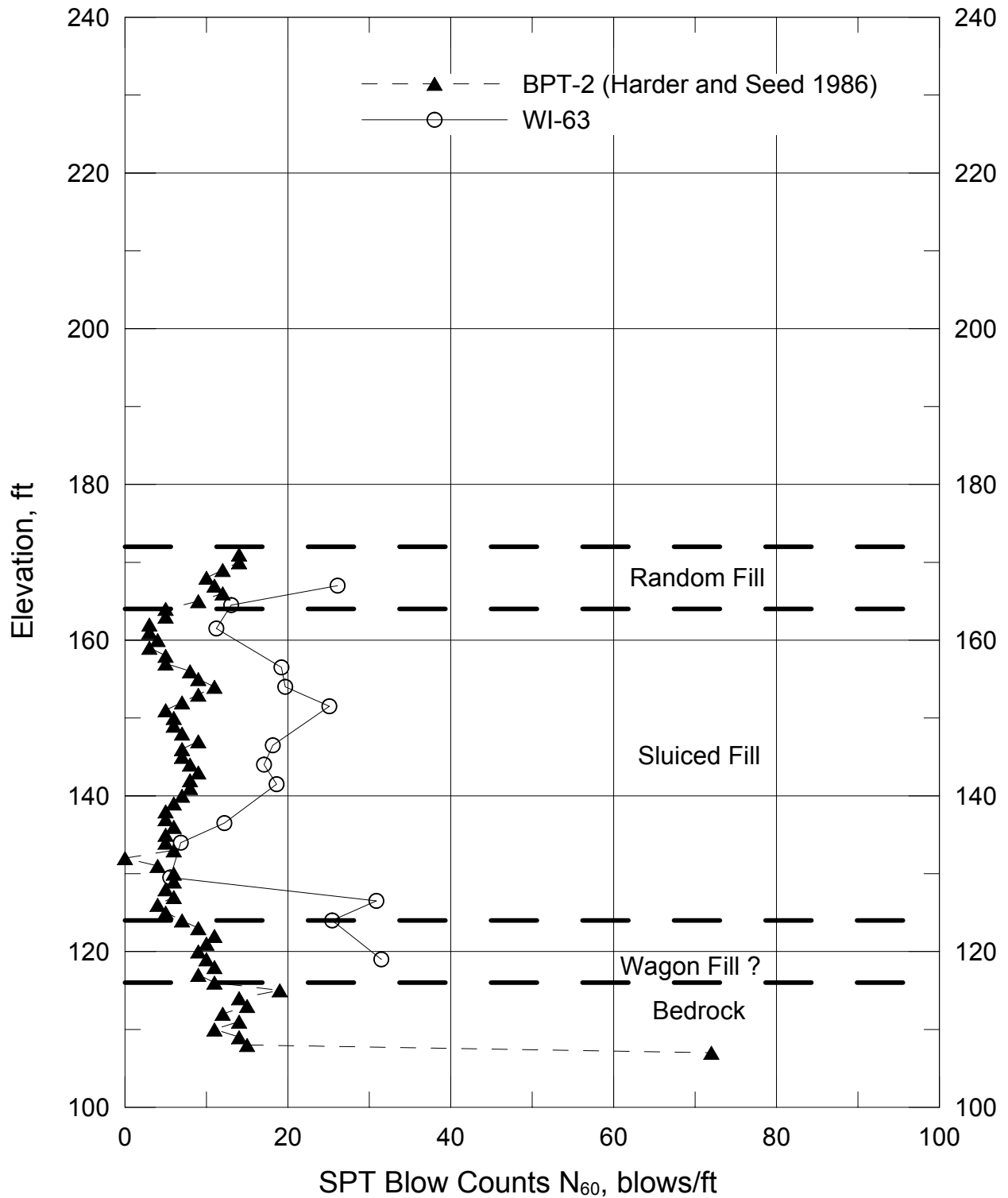
Project No. 26814536

Chabot Dam
Seismic Stability

**SPT Resistance N_{60} From
Borings WI-60 and BPT-1**

Figure
11-5

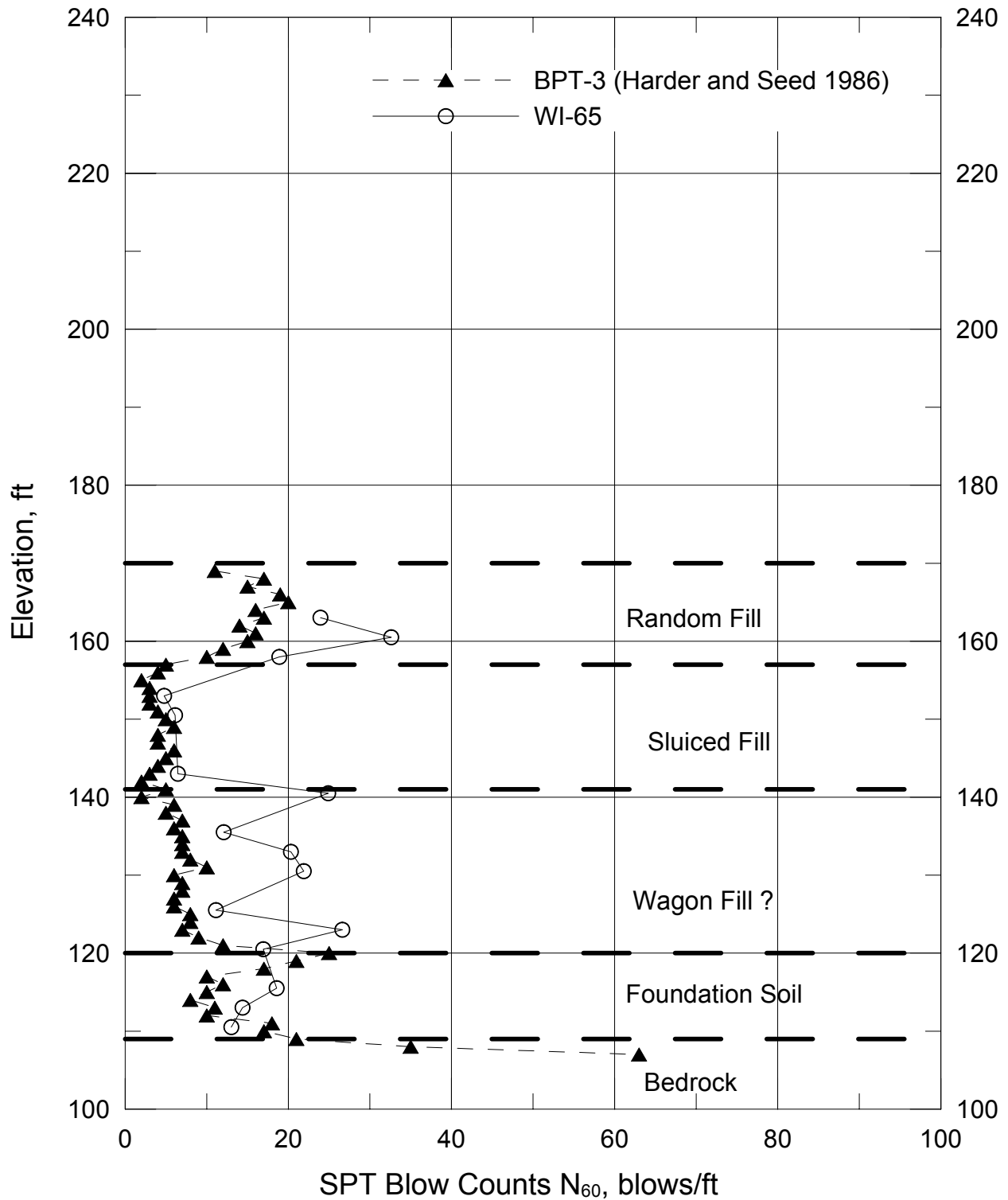
Chabot Dam Borings WI-63 and BPT-2



Note:
Stratigraphy is inferred from BPT resistance and boring log of WI-63

URS	Project No. 26814536	SPT Resistance N_{60} From Borings WI-63 and BPT-2	Figure
	Chabot Dam Seismic Stability		11-6

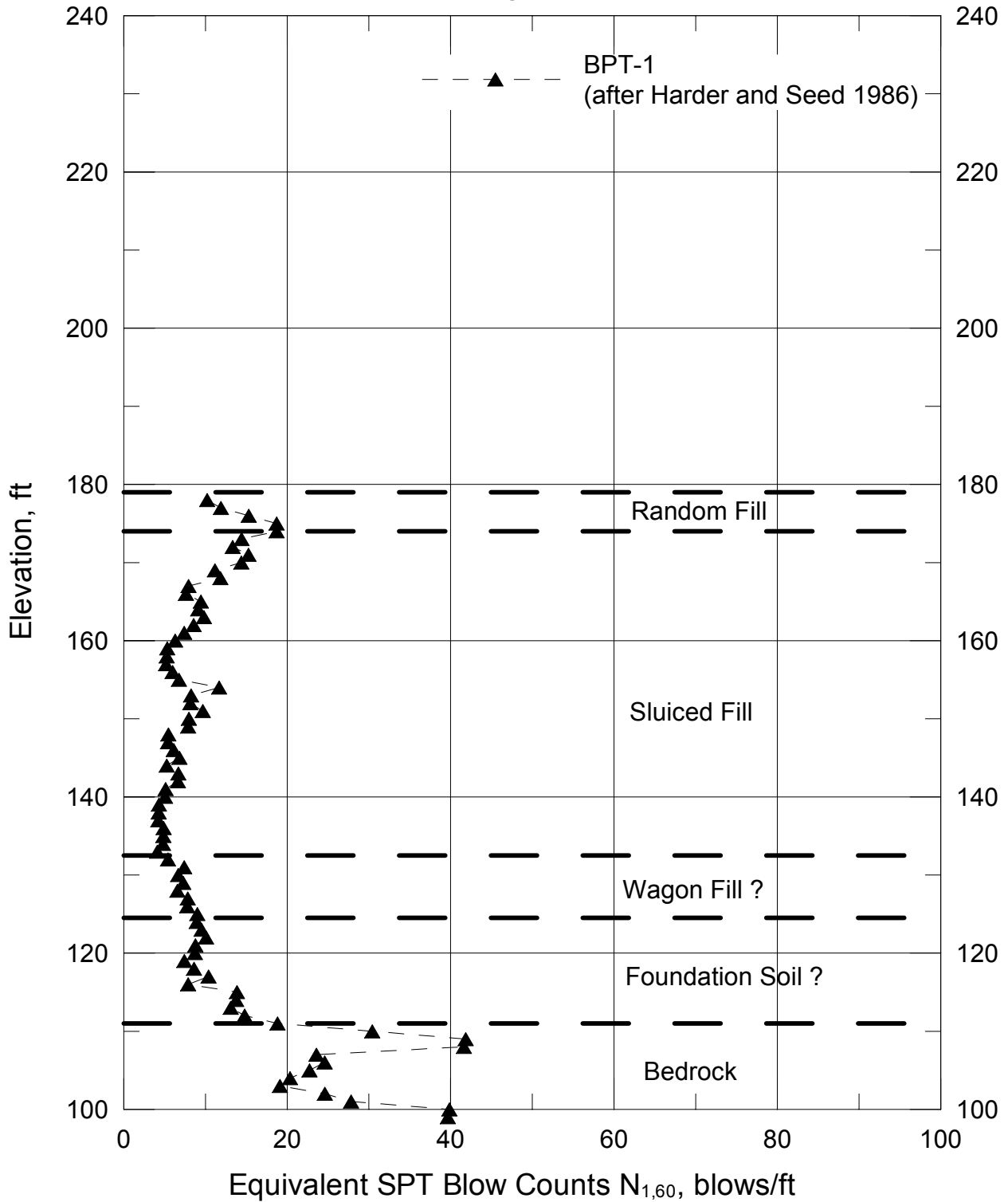
Chabot Dam Borings WI-65 and BPT-3



Note:
Stratigraphy is inferred from BPT resistace and boring log of WI-65.

URS	Project No. 26814536	SPT Resistance N_{60} From Borings WI-65 and BPT-3	Figure
	Chabot Dam Seismic Stability		11-7

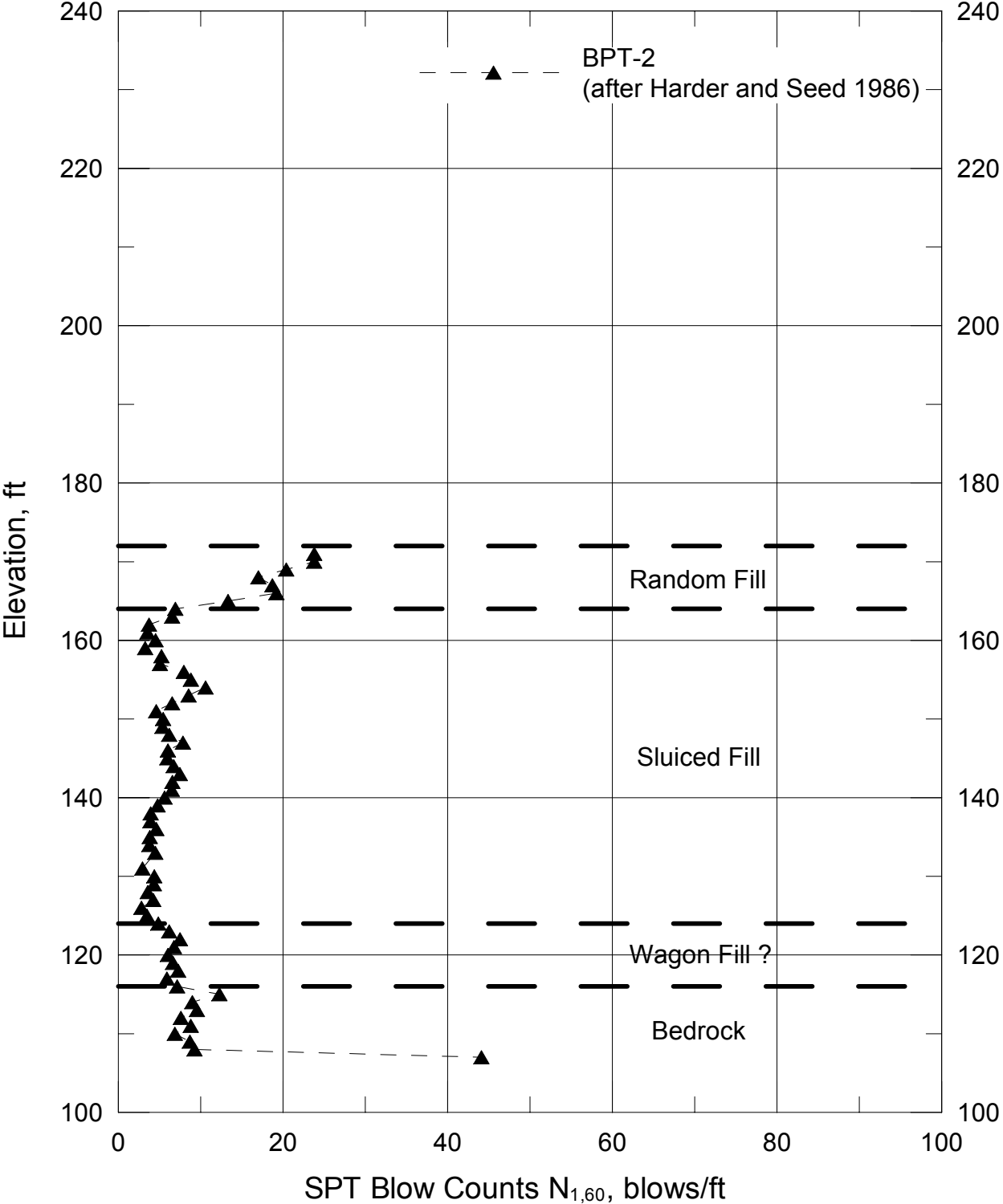
Chabot Dam Boring BPT-1



Note:
Stratigraphy is inferred from BPT resistance and boring log of WI-60.

URS	Project No. 26814536	Equivalent SPT $N_{1,60}$ and Stratigraphy From Boring BPT-1	Figure
	Chabot Dam Seismic Stability		11-8

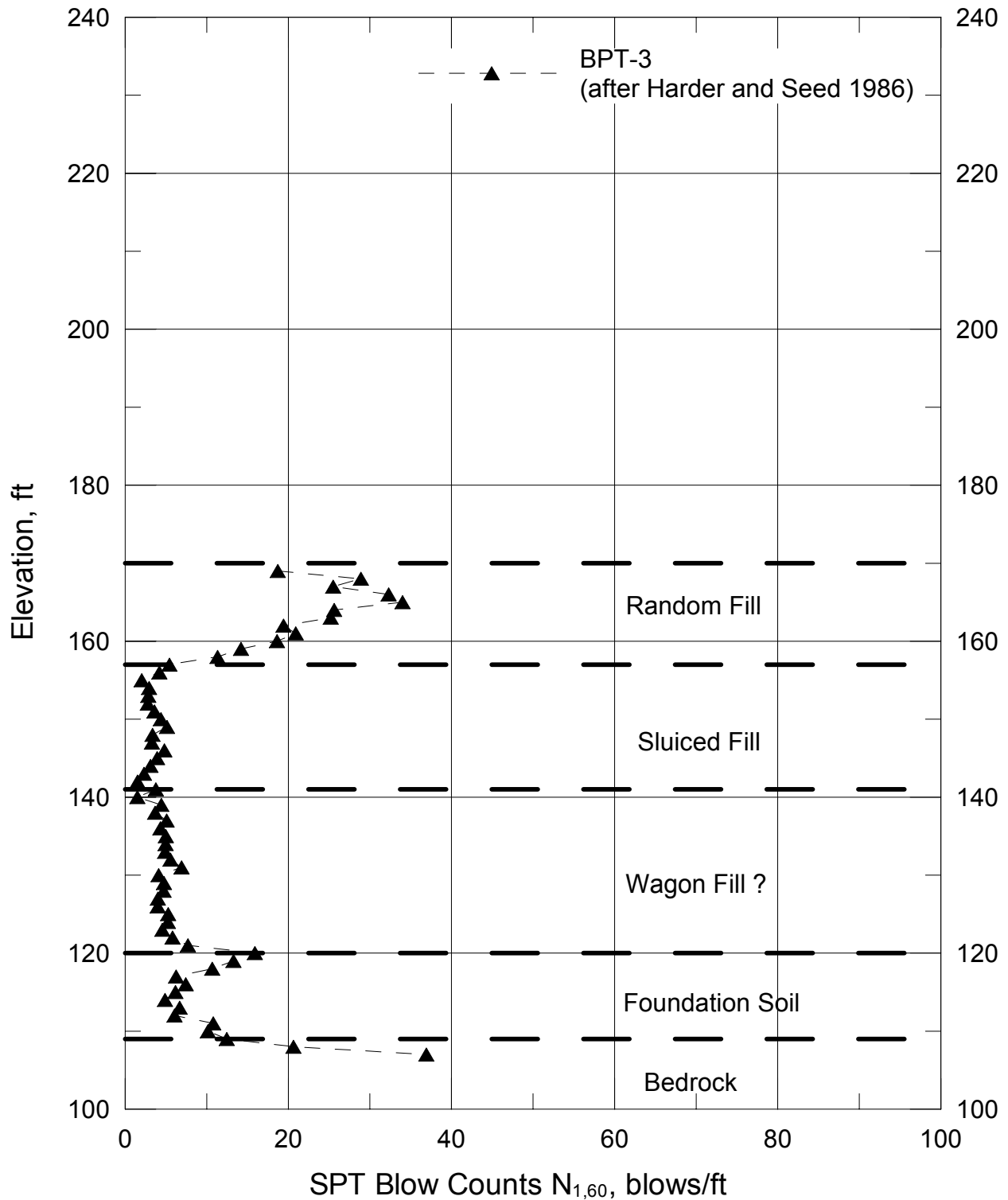
Chabot Dam Boring BPT-2



Note:
Stratigraphy is inferred from BPT resistance and boring log of WI-63

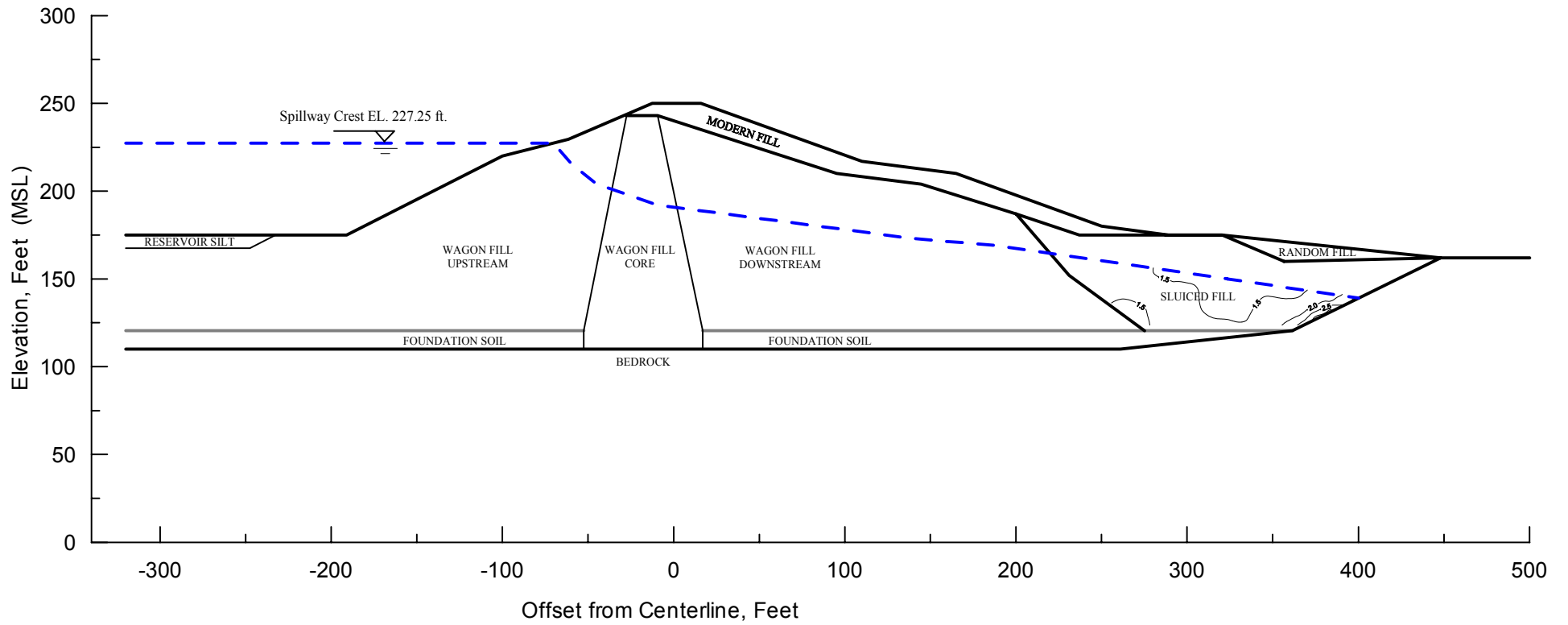
URS	Project No. 26814536	Equivalent SPT $N_{1,60}$ and Stratigraphy From Boring BPT-2	Figure
	Chabot Dam Seismic Stability		11-9

Chabot Dam Boring BPT-3

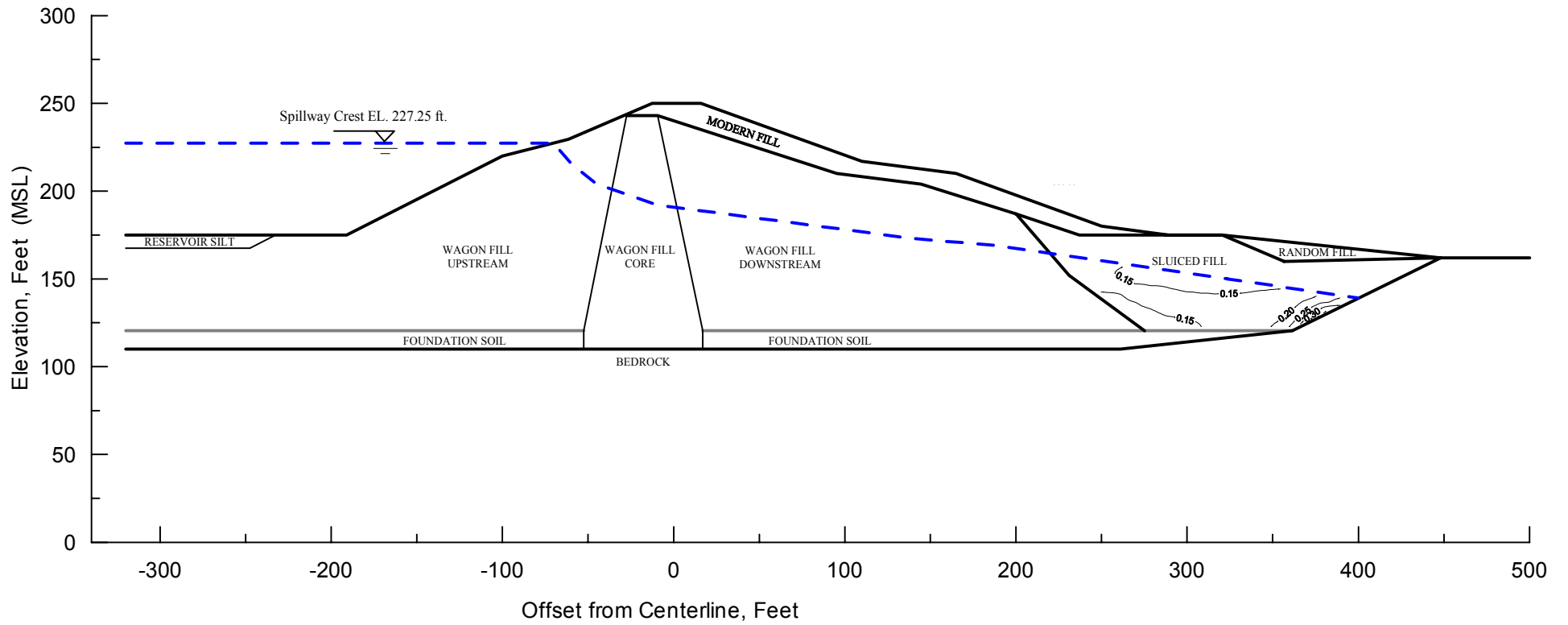


Note:
Stratigraphy is inferred from BPT resistance and boring log of WI-65.

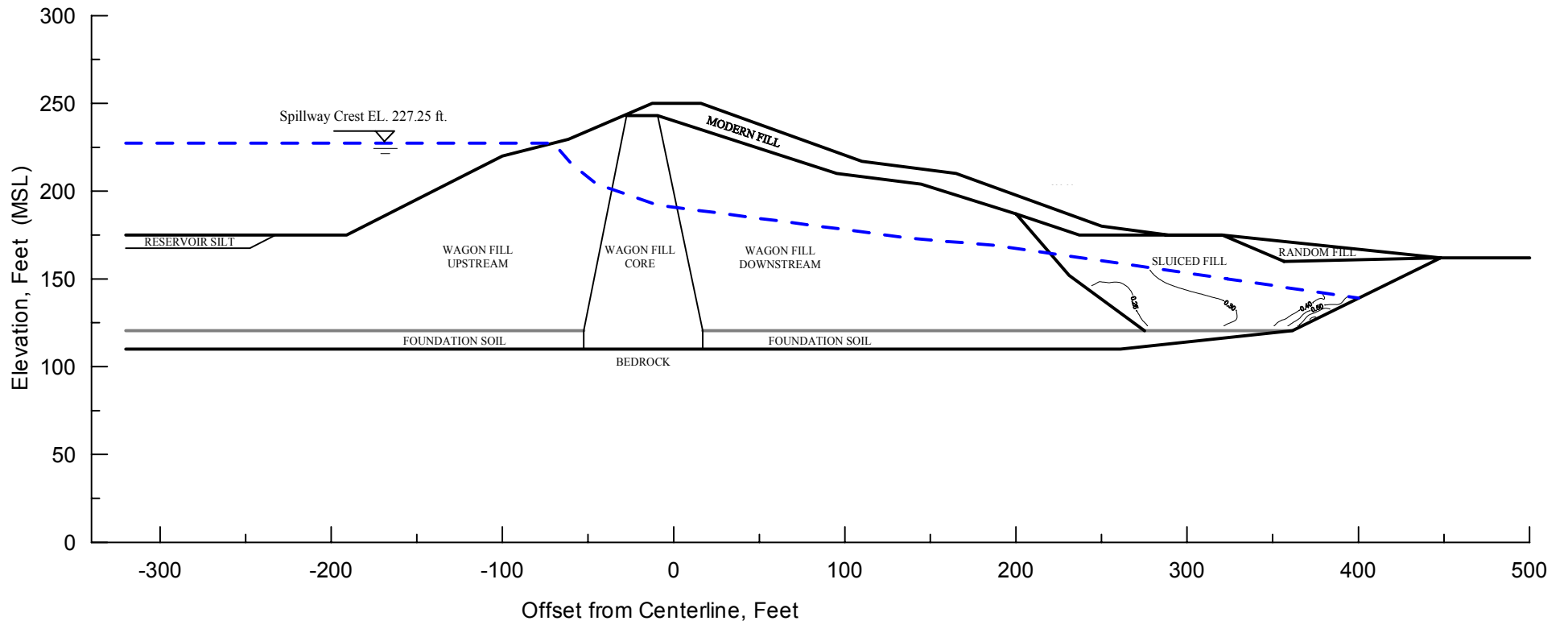
URS	Project No. 26814536	Equivalent SPT $N_{1,60}$ and Stratigraphy From Boring BPT-3	Figure
	Chabot Dam Seismic Stability		11-10



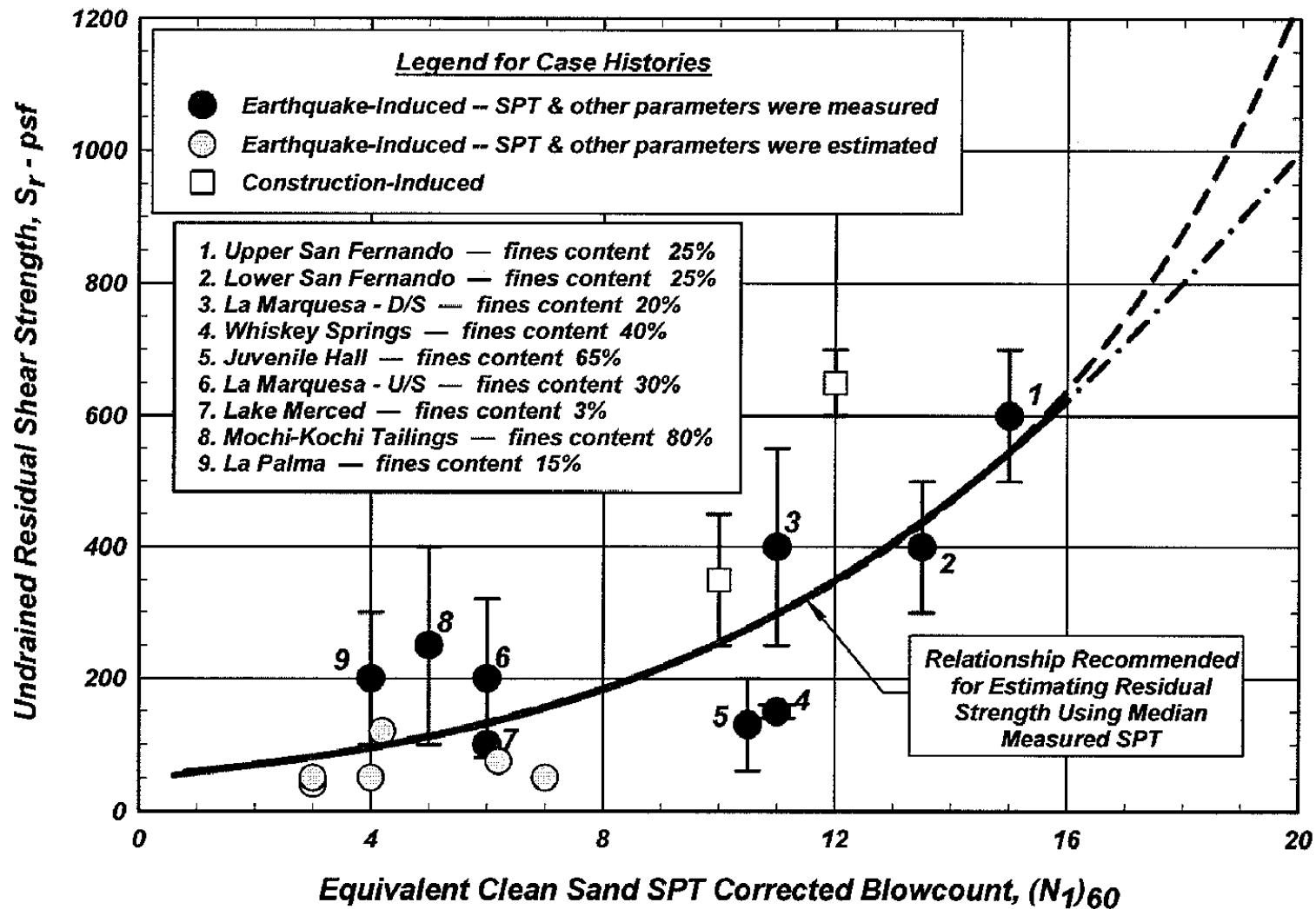
Project No. 26814536	Chabot Dam Seismic Stability Analysis	Factors of Safety against Liquefaction in Sluiced Fill 1989 Loma Prieta Earthquake	Figure
URS			11-11



Project No. 26814536	Chabot Dam Seismic Stability Analysis	Factors of Safety against Liquefaction in Sluiced Fill Hayward Fault MCE TH #1	Figure
URS			11-12



Project No. 26814536	Chabot Dam Seismic Stability Analysis	Factors of Safety against Liquefaction in Sluiced Fill San Andreas Fault MCE	Figure
URS			11-13



Dashed Curve:

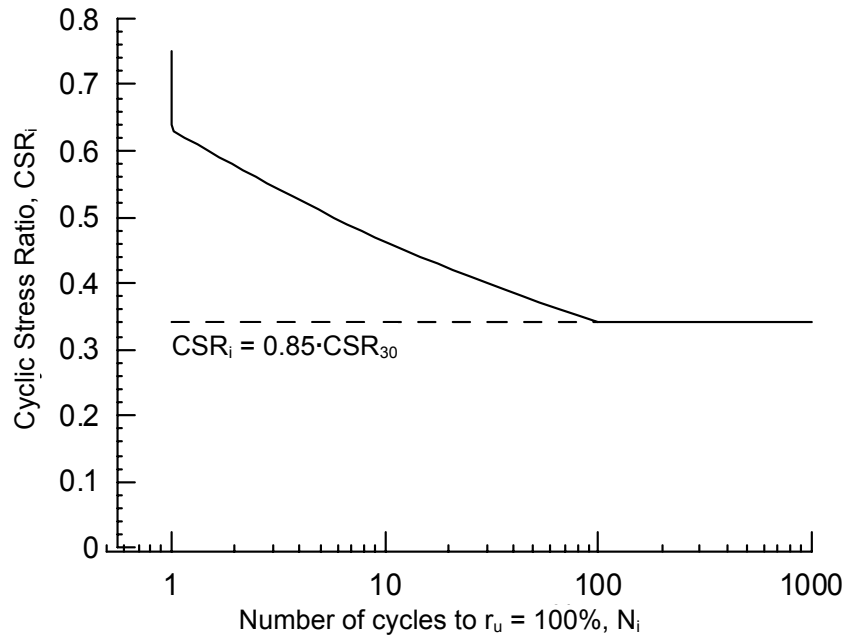
Solid & Dash-Dot Curve:

Curve Recommended by Hendron & Idriss in 1997

Curve Modified by Idriss in 2002

Project No. 26814536	Chabot Dam Seismic Stability	Correlation between Undrained Residual Strength and Equivalent Clean Sand SPT Corrected Blow Counts (Idriss, 2002)	Figure
URS			11-14

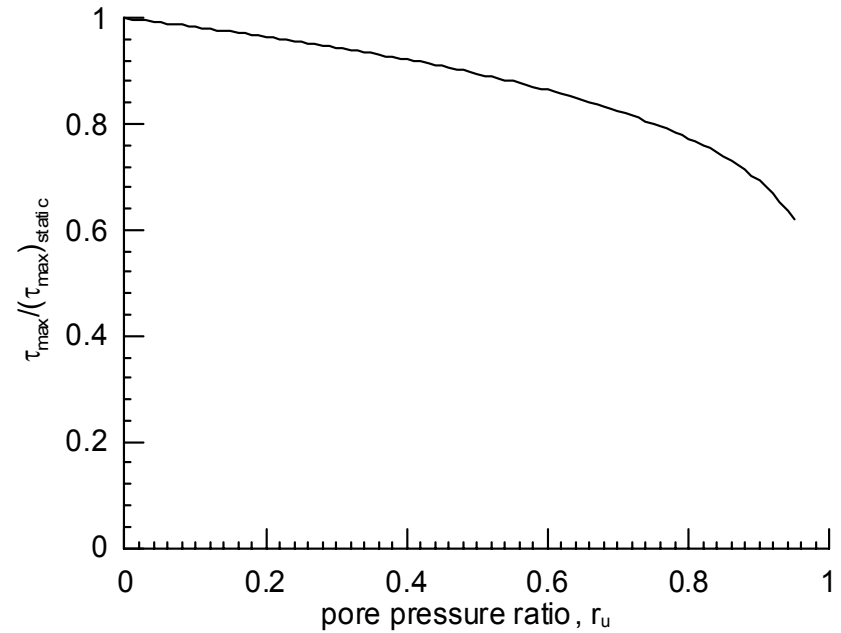
Cyclic Strength
 $CSR_{30} = 0.4$



$$N_i = 30 \left(\frac{CSR_{30}}{CSR_i} \right)^{7.41} \quad 1 \leq N_i \leq 100$$

where $CSR_{30} = 0.4$

Strength Degradation



$$\frac{\tau_{max}}{(\tau_{max})_{static}} = (1 - r_u)^{0.16}$$

Project No.
26814536

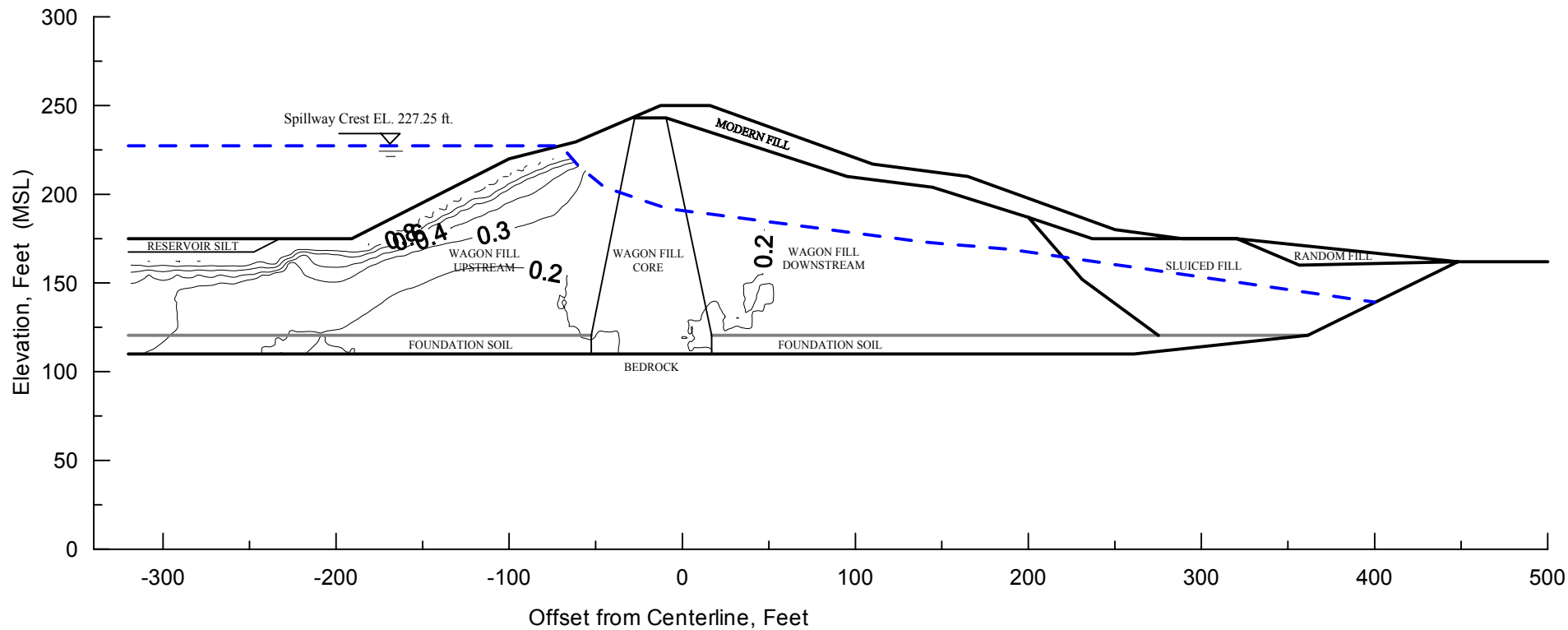
Chabot Dam
Seismic Stability Analysis

URS

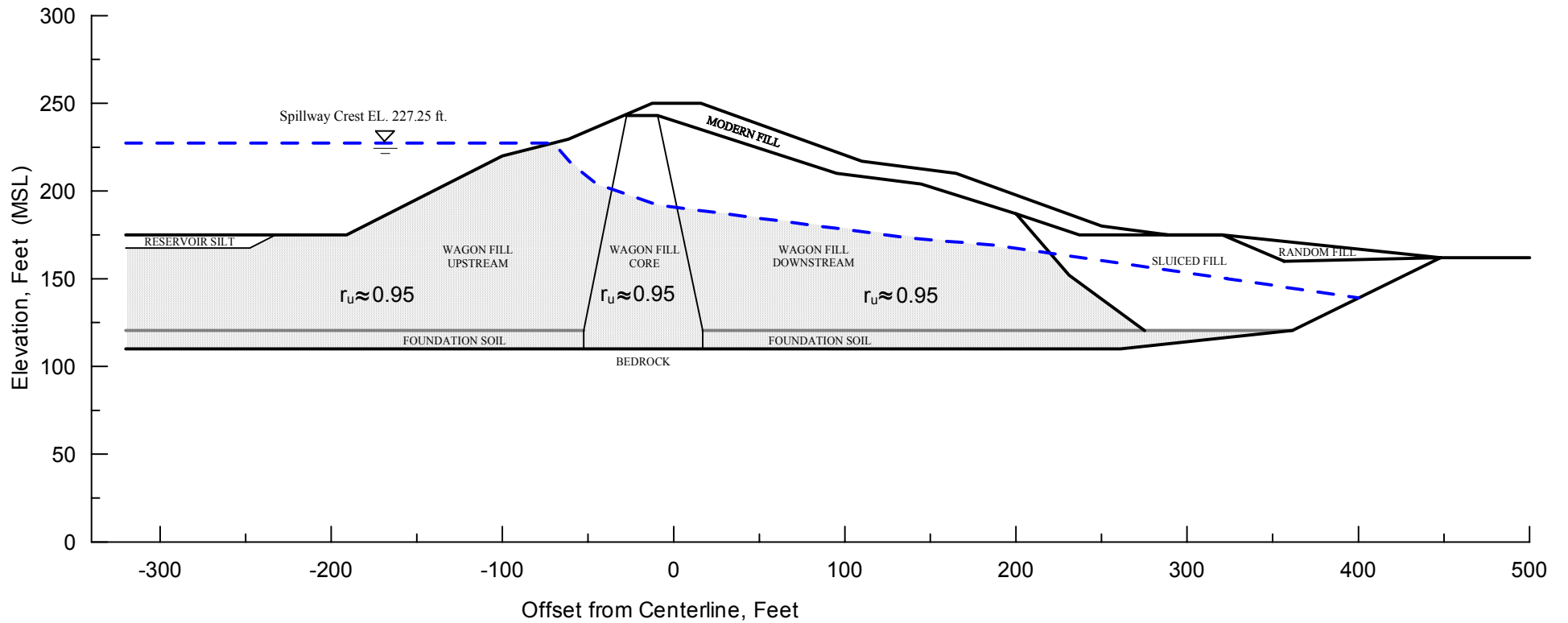
Cyclic Strength and Undrained
Strength Degradation of Saturated
Wagon Fill and Foundation Soils

Figure

11-15

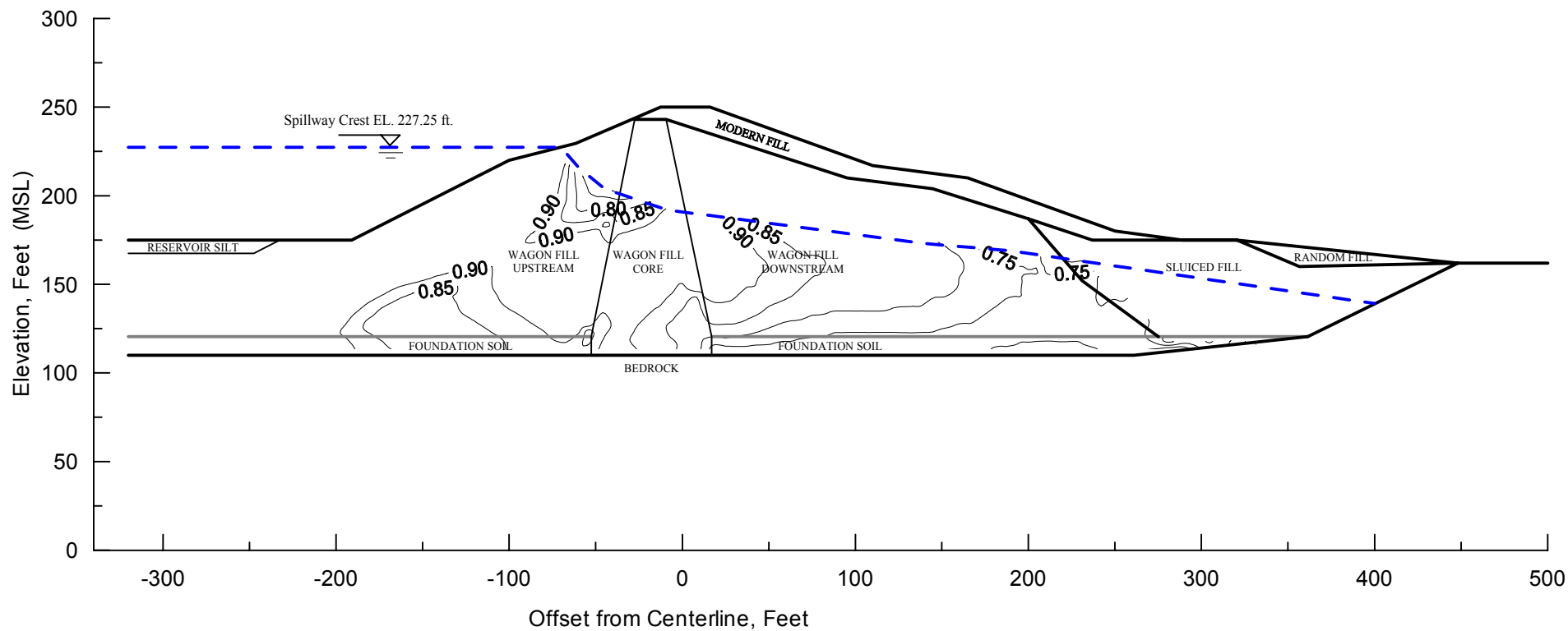


Project No. 26814536	Chabot Dam Seismic Stability Analysis	Excess Pore Pressure Ratio in Wagon Fill and Foundation Soils 1989 Loma Prieta Earthquake	Figure 11-16
URS			

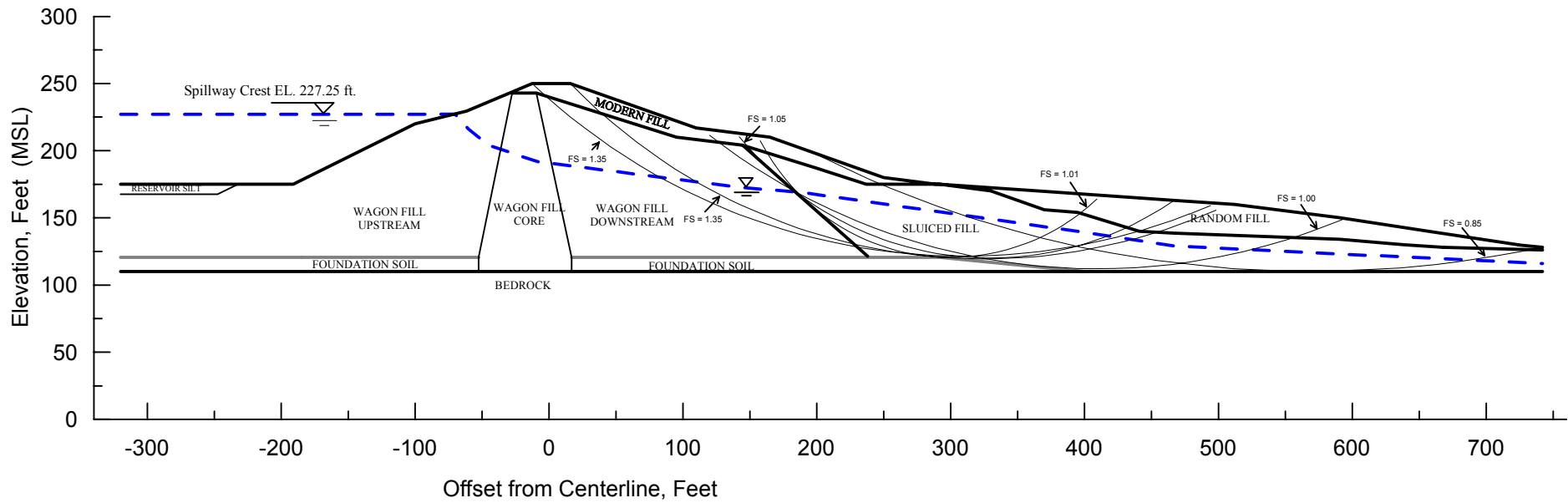


Note: Calculated excess pore pressure ratio in the shaded zone reaches the approximate maximum value estimated from the cyclic strength tests.

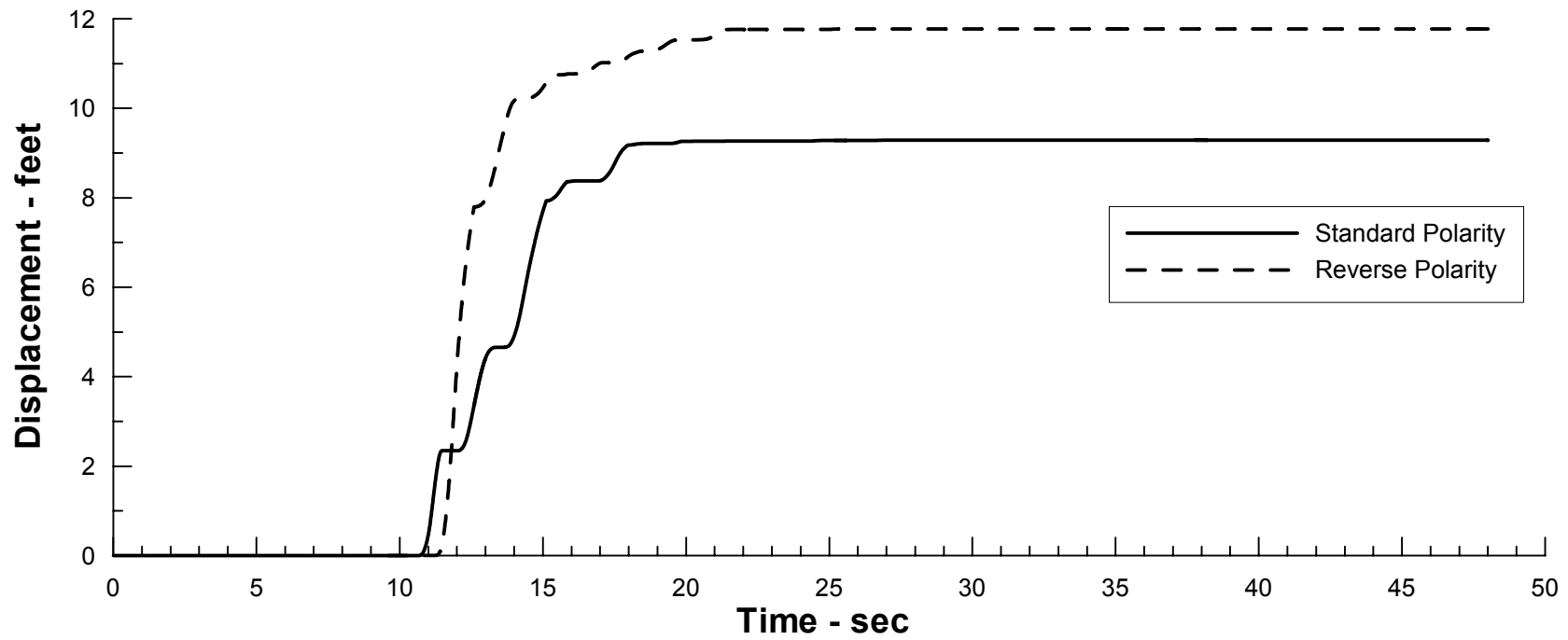
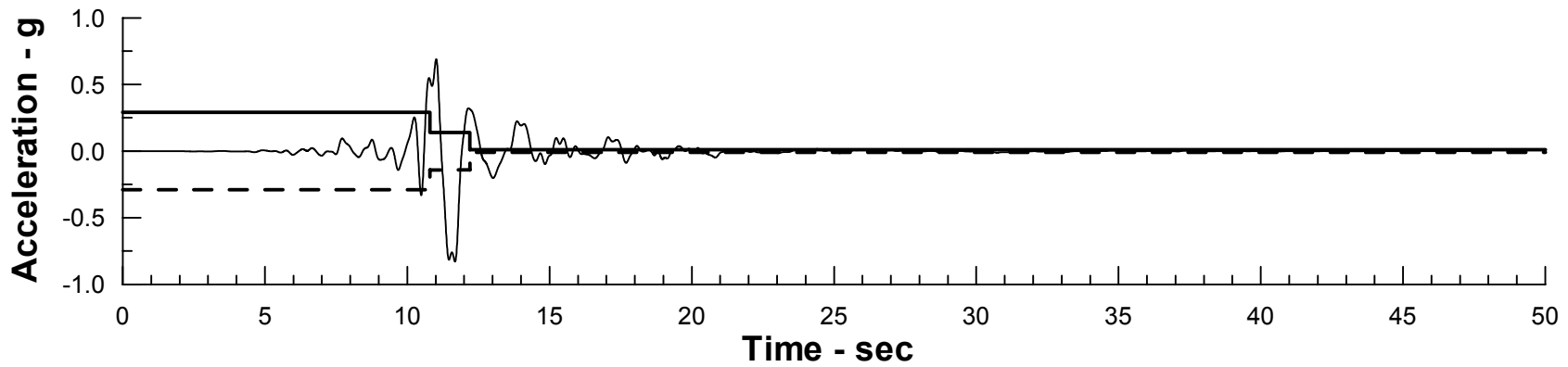
Project No. 26814536	Chabot Dam Seismic Stability Analysis	Excess Pore Pressure Ratio in Wagon Fill and Foundation Soils Hayward Fault MCE TH #1	Figure
URS			11-17



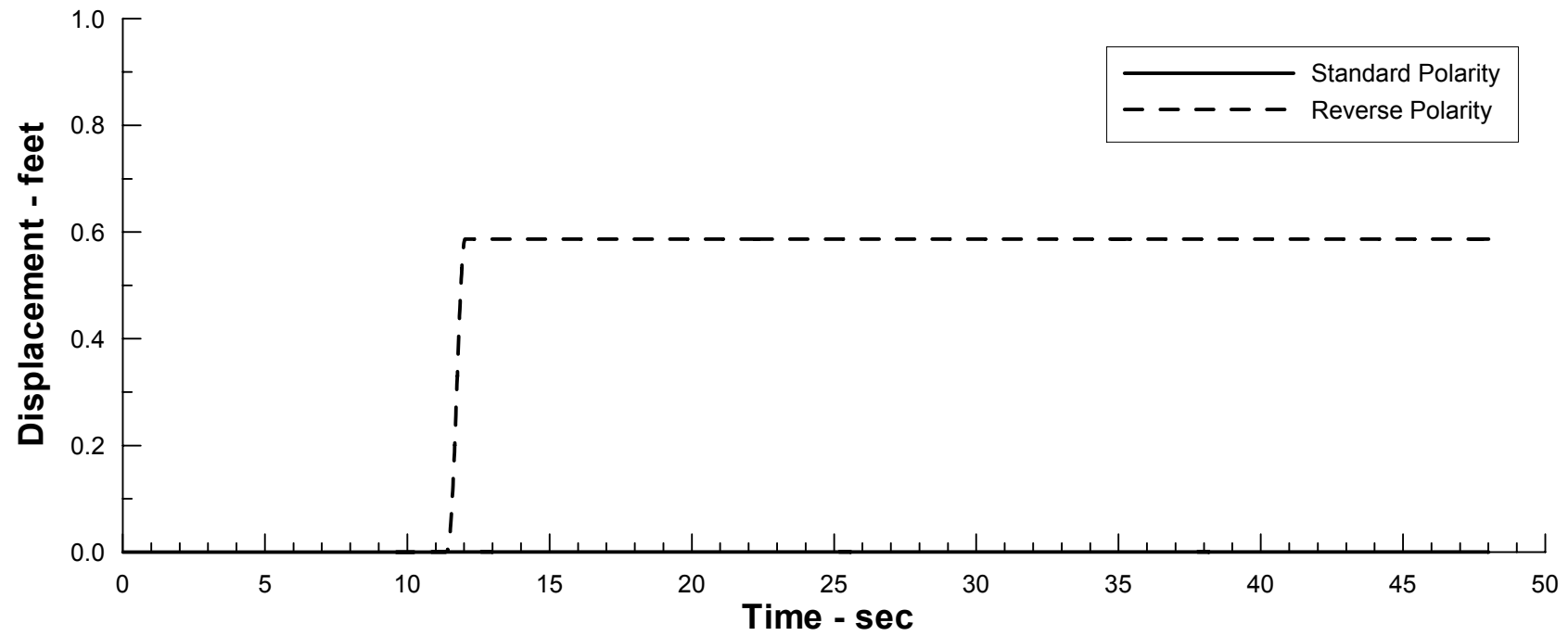
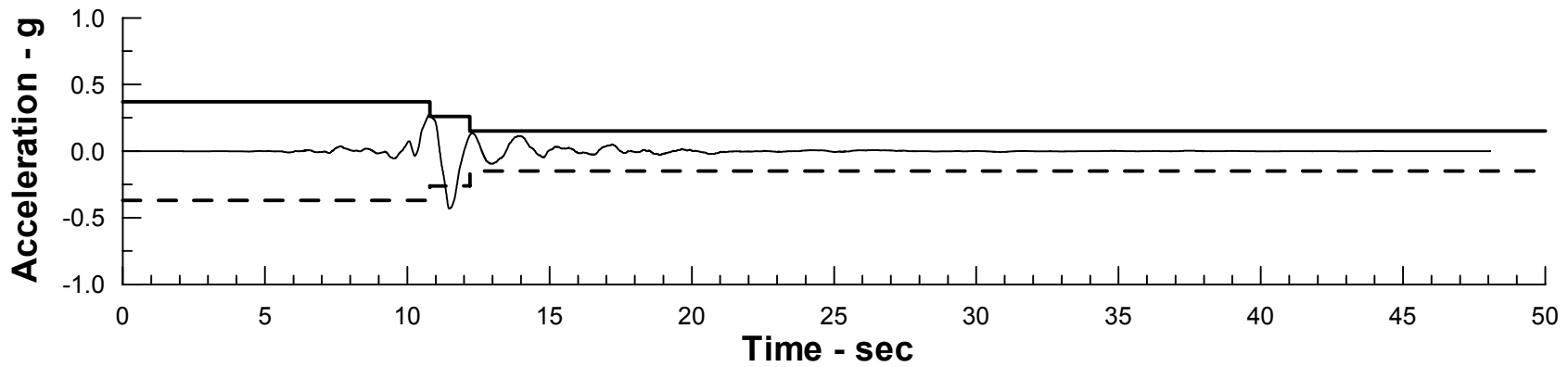
Project No. 26814536	Chabot Dam Seismic Stability Analysis	Excess Pore Pressure Ratio in Wagon Fill and Foundation Soils San Andreas Fault MCE	Figure
URS			11-18



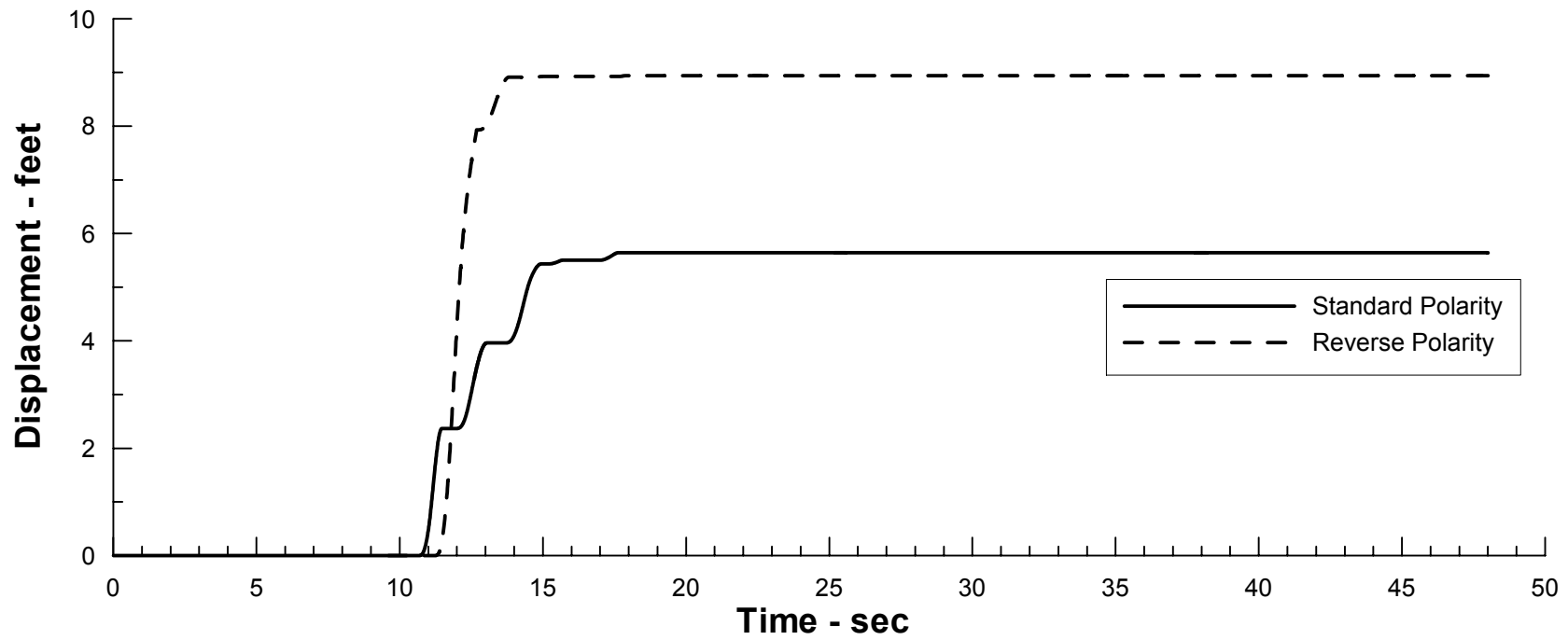
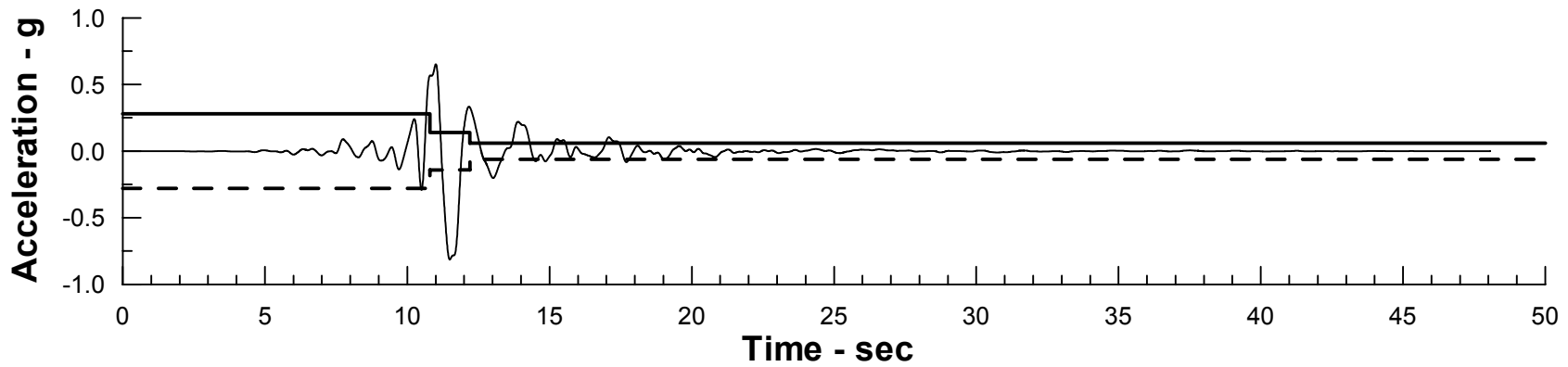
Project No. 26814536	Chabot Dam Seismic Stability Analysis	Seismic Stability Analysis Post-Earthquake Condition Downstream Section A-A" Hayward Fault MCE	Figure 11-19
URS			



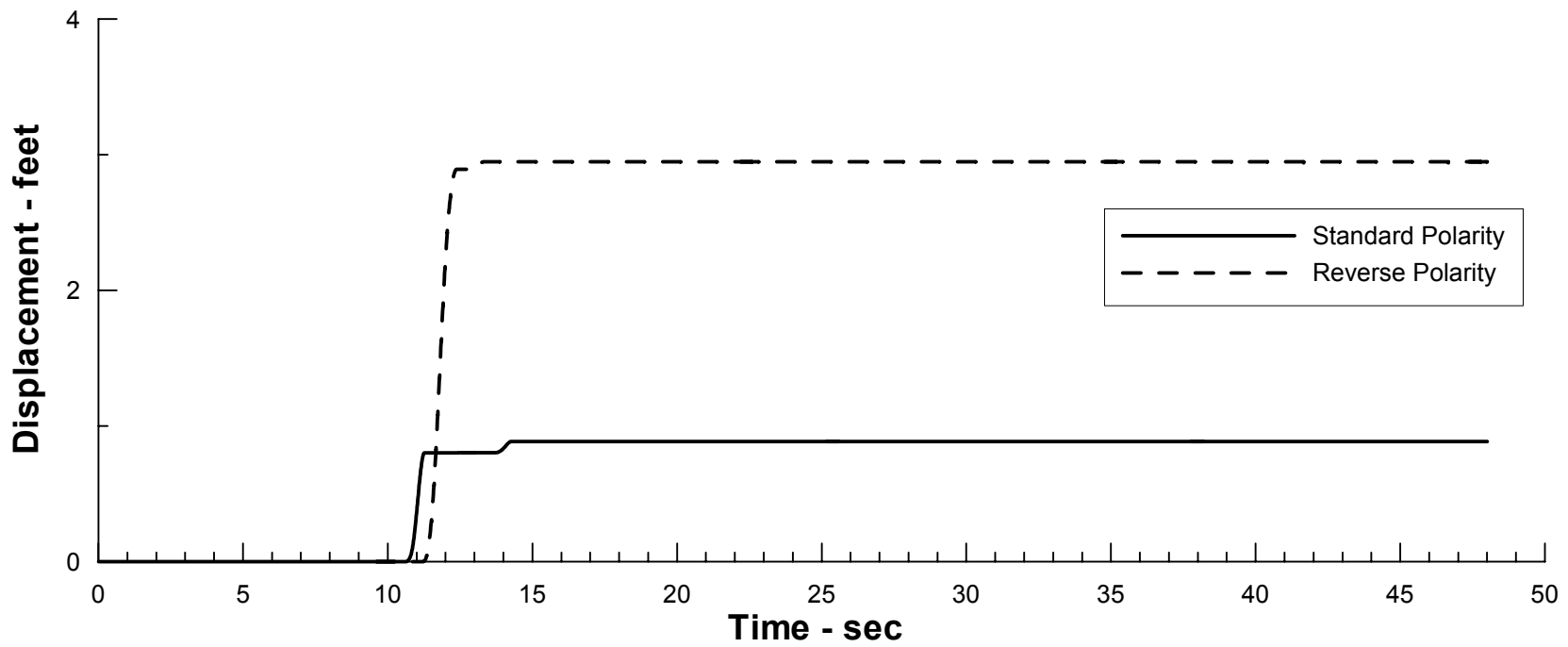
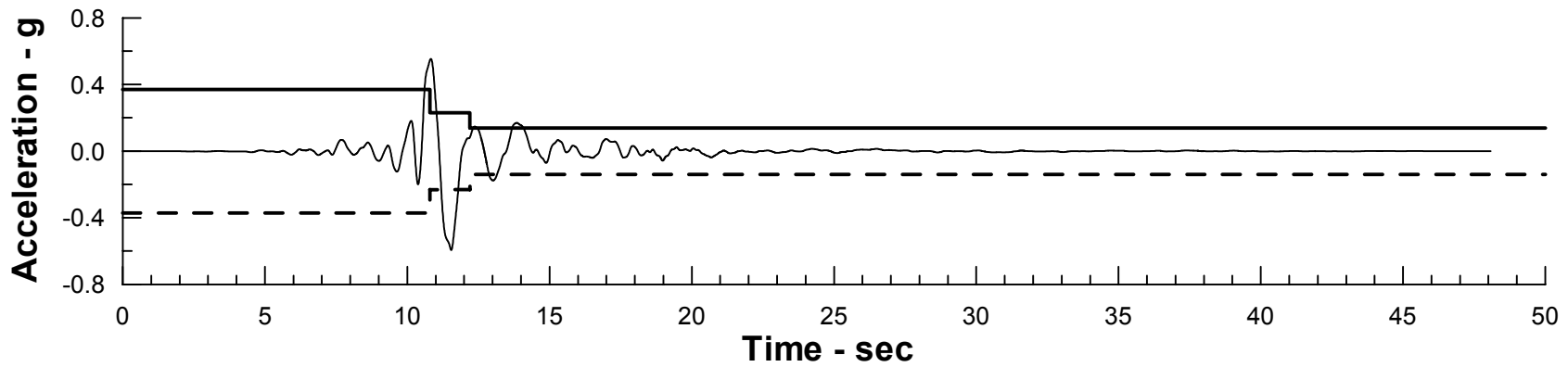
Project No. 26814536	Chabot Dam Seismic Stability Analysis	Newmark Deformation Analysis Calculated Displacement U/S Block #1 Hayward Fault MCE TH #1	Figure 11-20
URS			



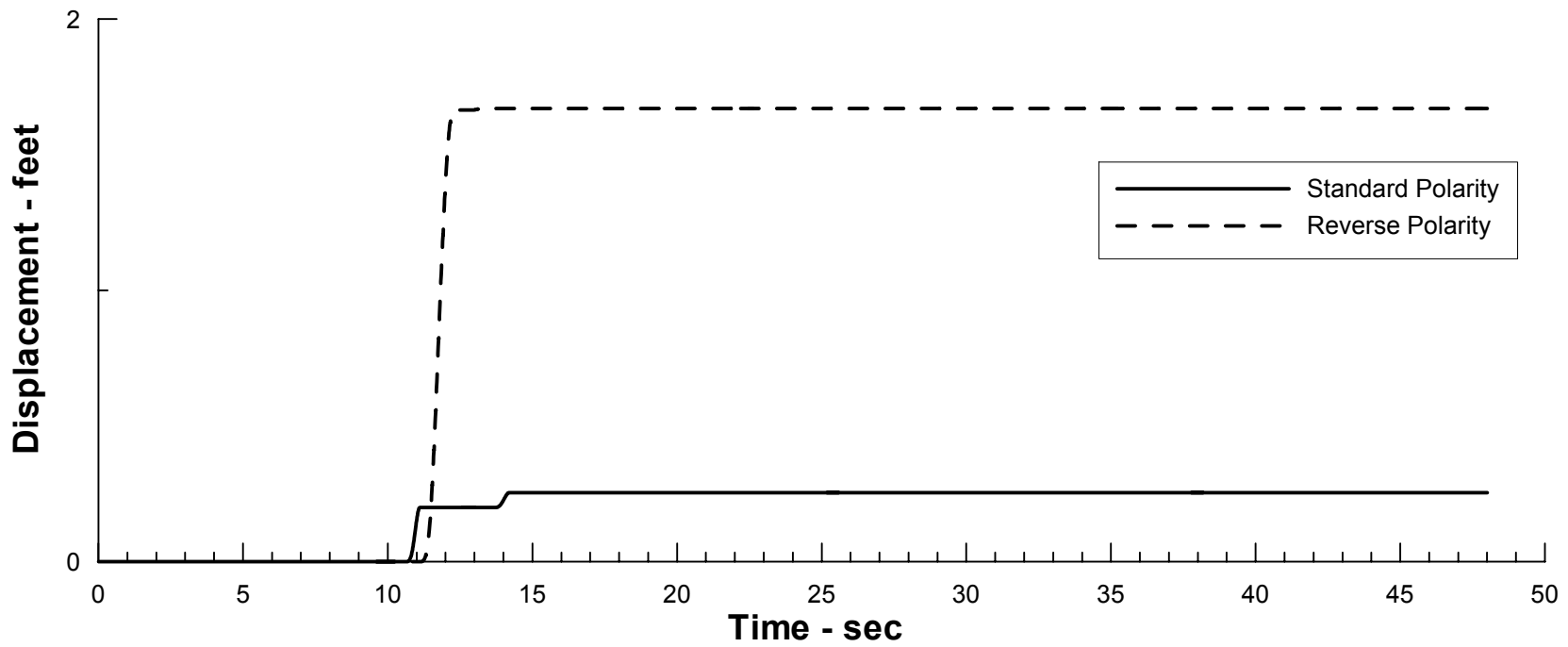
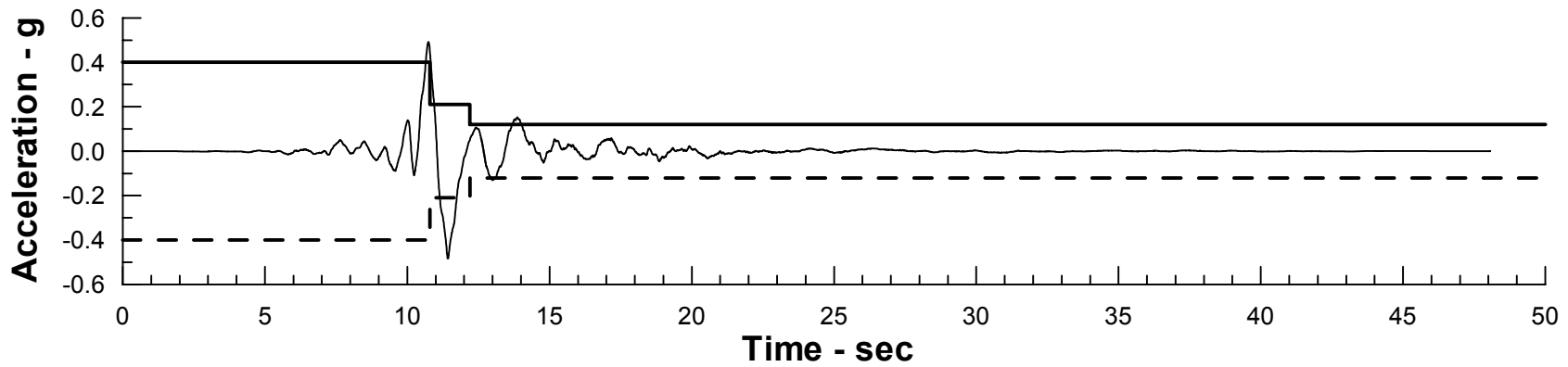
Project No. 26814536	Chabot Dam Seismic Stability Analysis	Newmark Deformation Analysis Calculated Displacement U/S Block #2 Hayward Fault MCE TH #1	Figure
URS			11-21



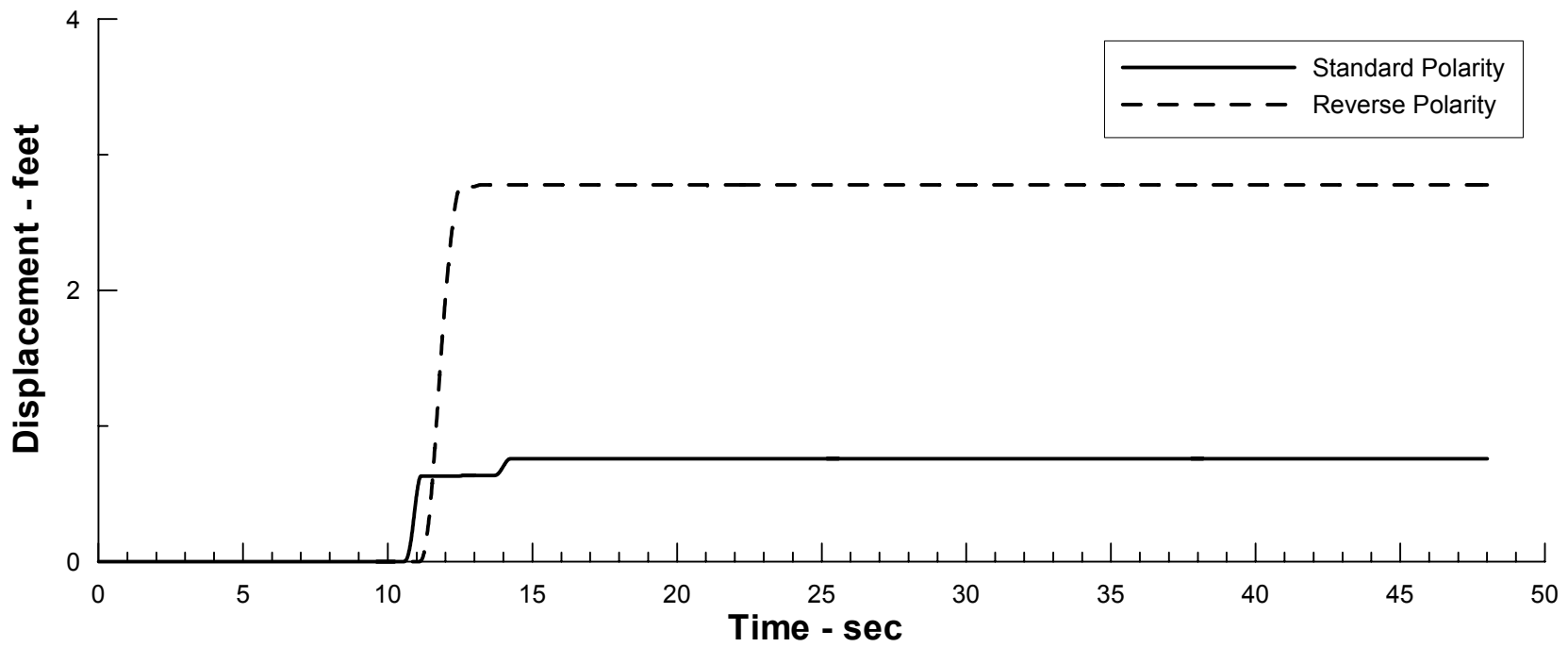
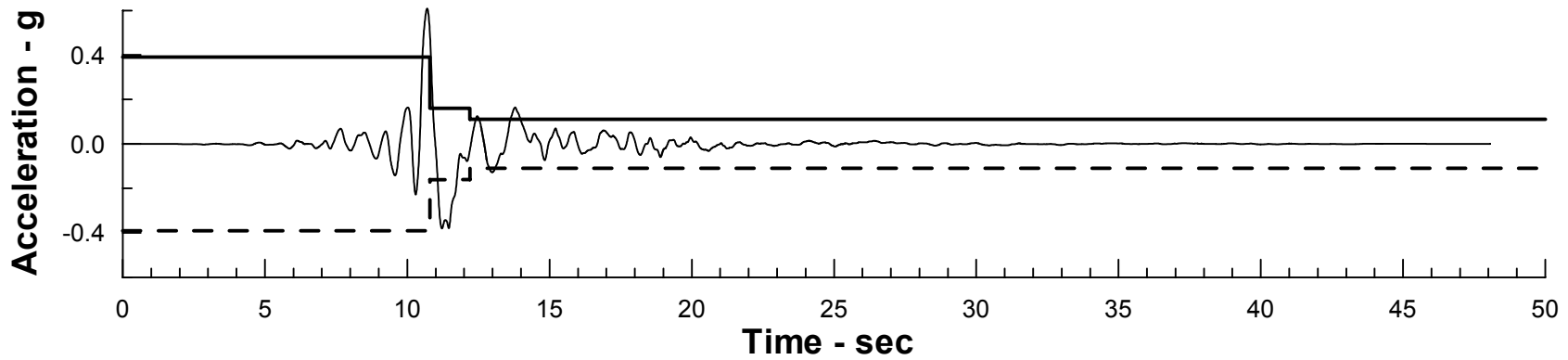
Project No. 26814536	Chabot Dam Seismic Stability Analysis	Newmark Deformation Analysis Calculated Displacement U/S Block #3 Hayward Fault MCE TH #1	Figure
URS			11-22



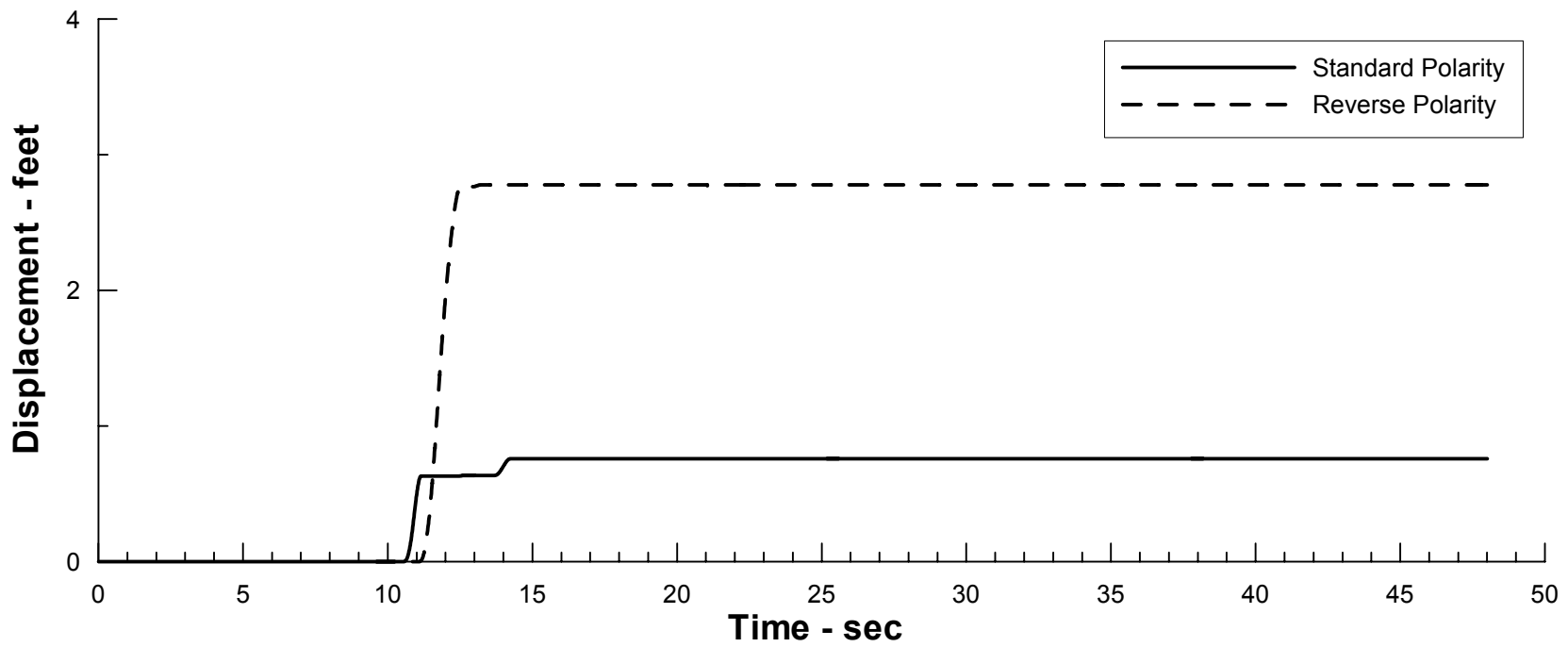
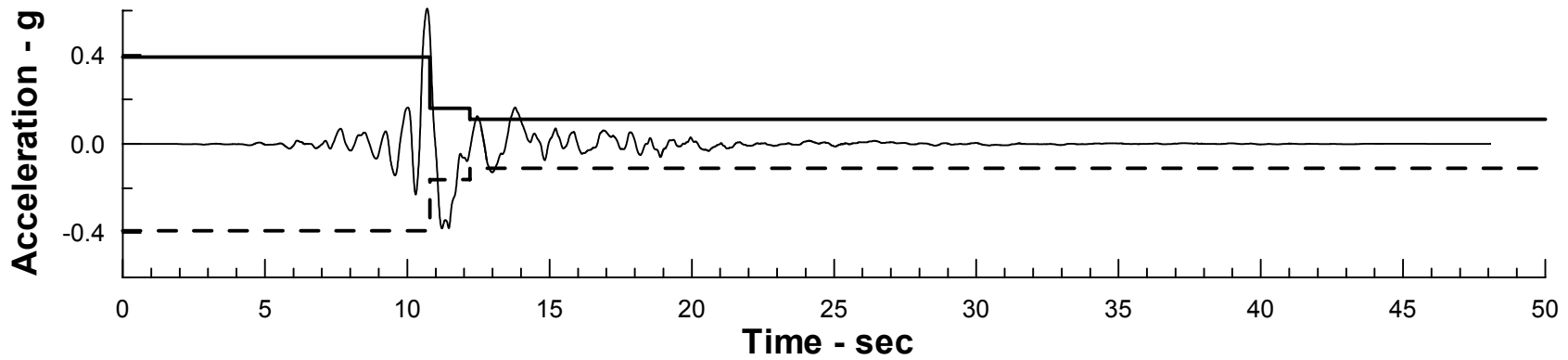
Project No. 26814536	Chabot Dam Seismic Stability Analysis	Newmark Deformation Analysis Calculated Displacement D/S Block #1	Figure 11-23
URS		Hayward Fault MCE TH #1	



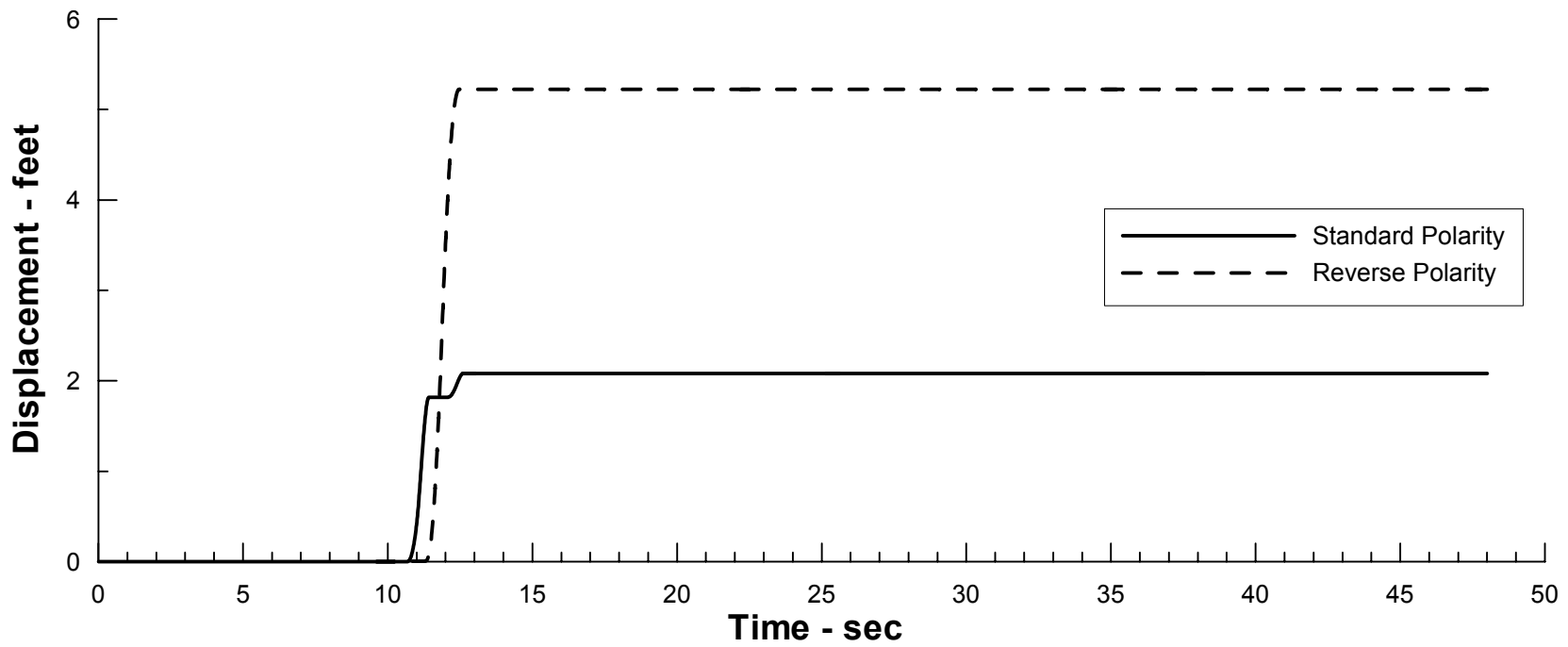
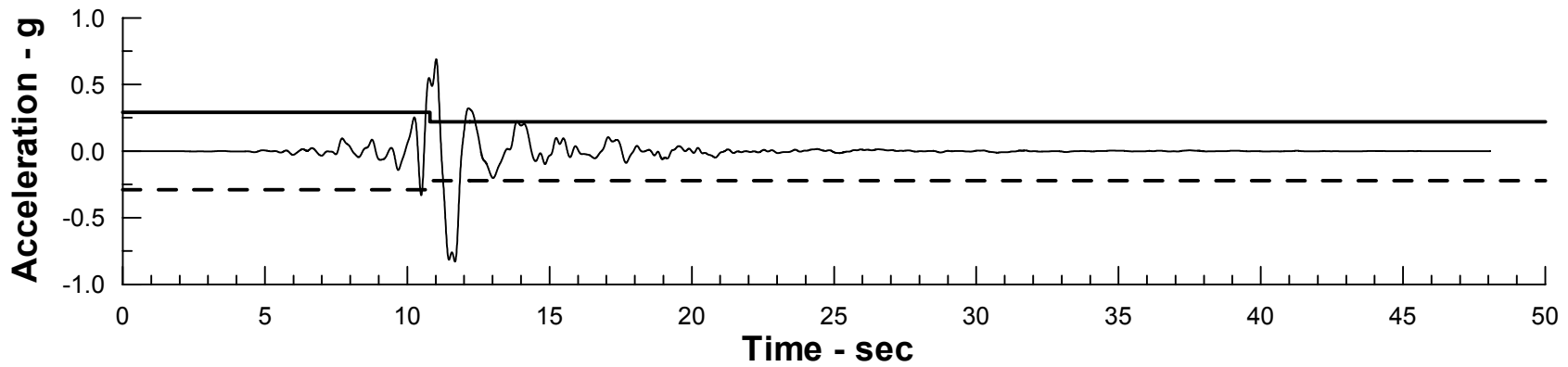
Project No. 26814536	Chabot Dam Seismic Stability Analysis	Newmark Deformation Analysis Calculated Displacement D/S Block #2 Hayward Fault MCE TH #1	Figure
URS			11-24



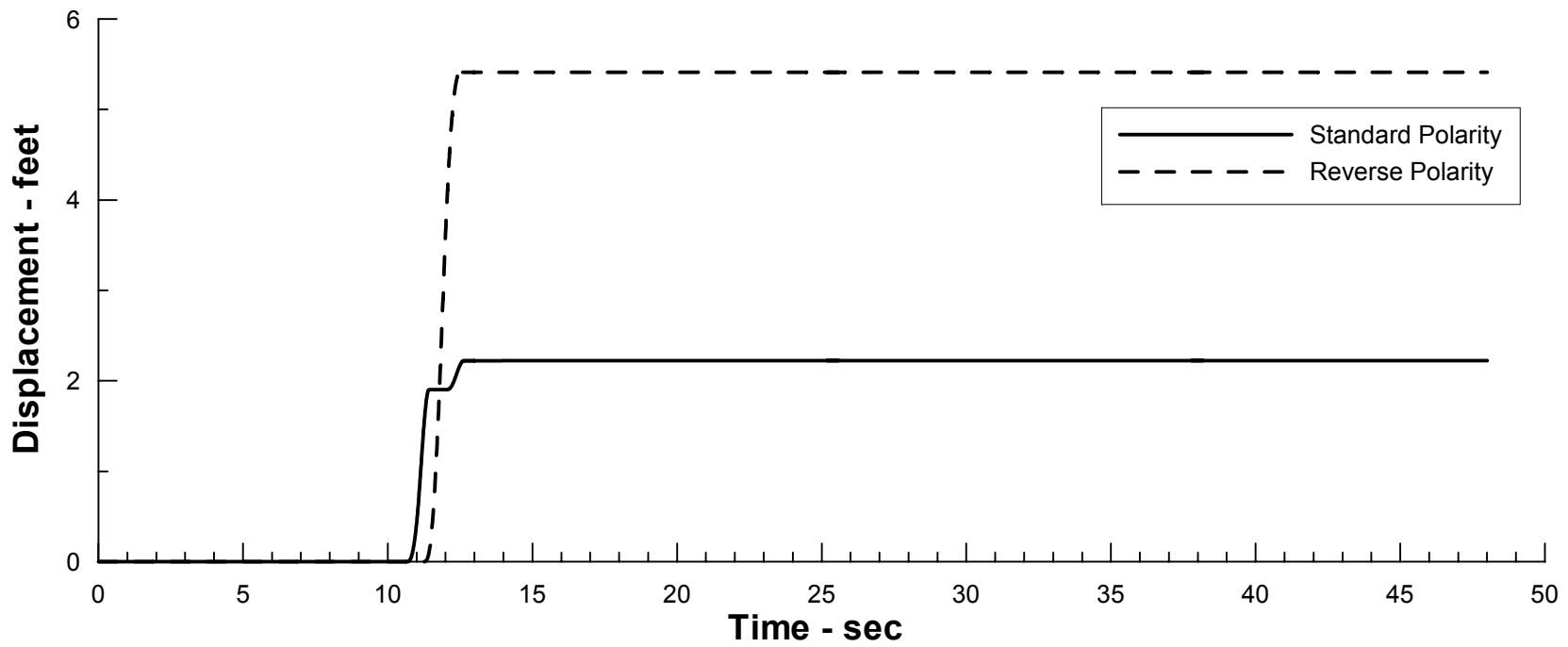
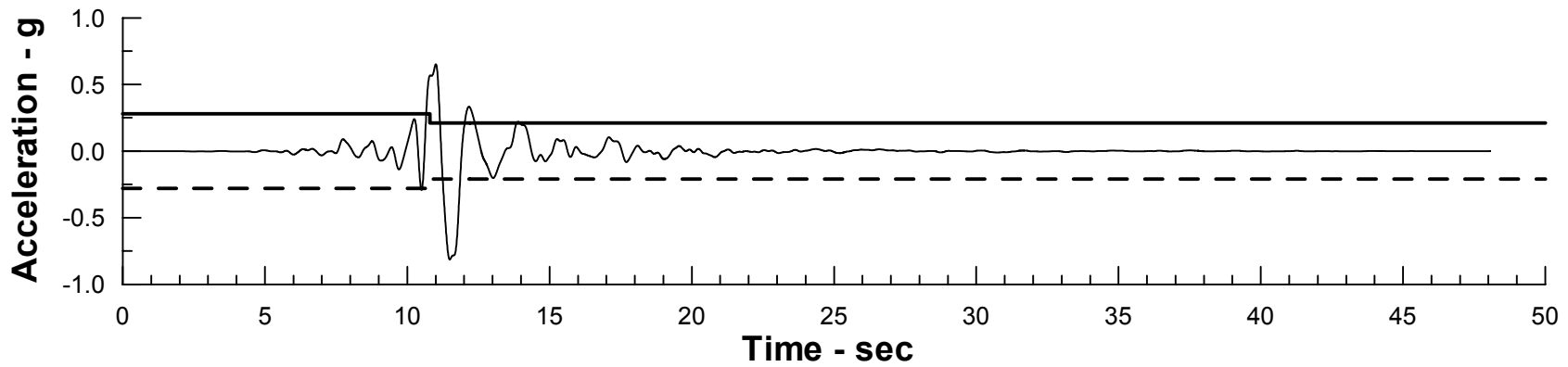
Project No. 26814536	Chabot Dam Seismic Stability Analysis	Newmark Deformation Analysis Calculated Displacement D/S Block #3	Figure 11-25
URS		Hayward Fault MCE TH #1	



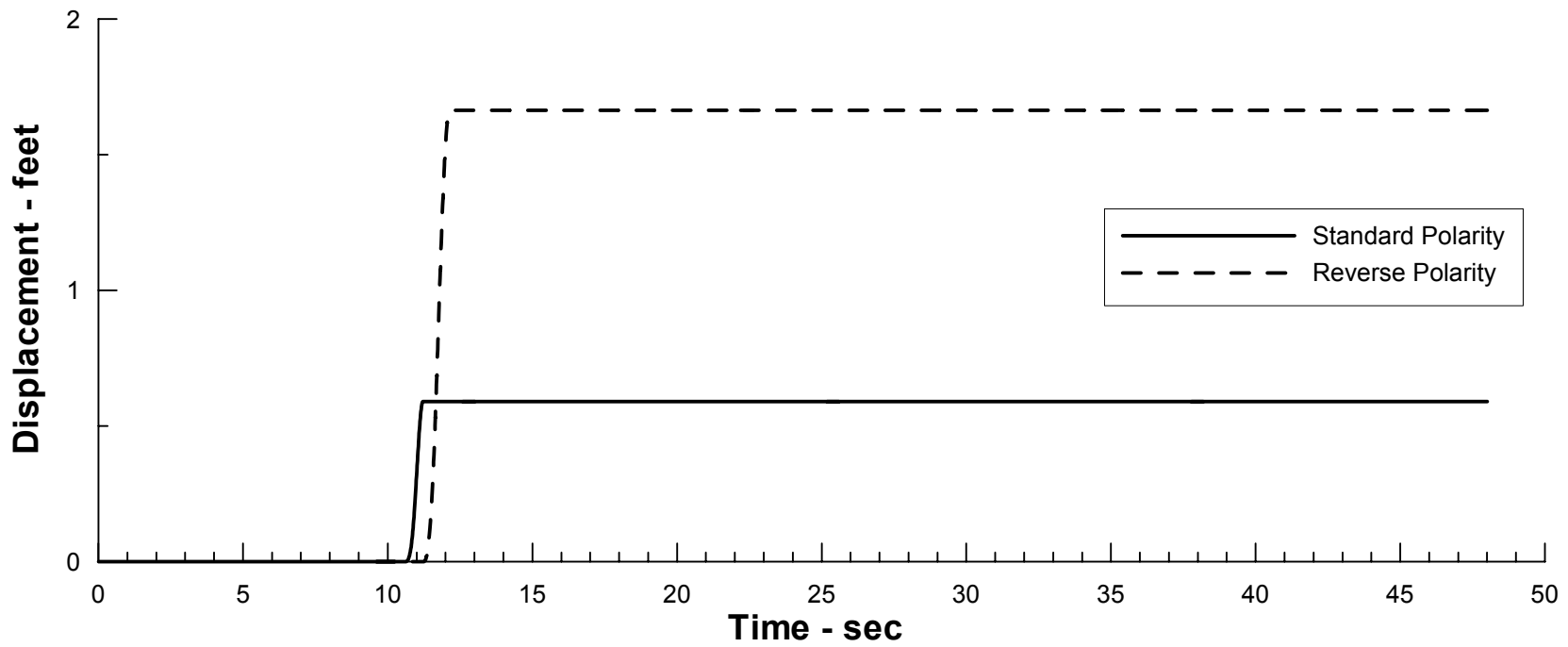
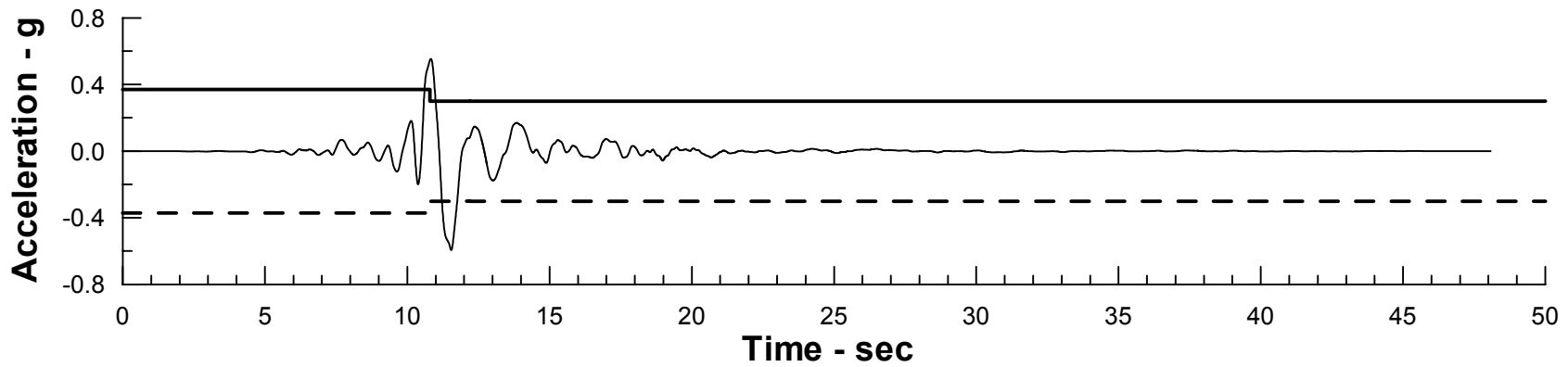
Project No. 26814536	Chabot Dam Seismic Stability Analysis	Newmark Deformation Analysis Calculated Displacement D/S Block #3 Hayward Fault MCE TH #1	Figure
URS			11-25



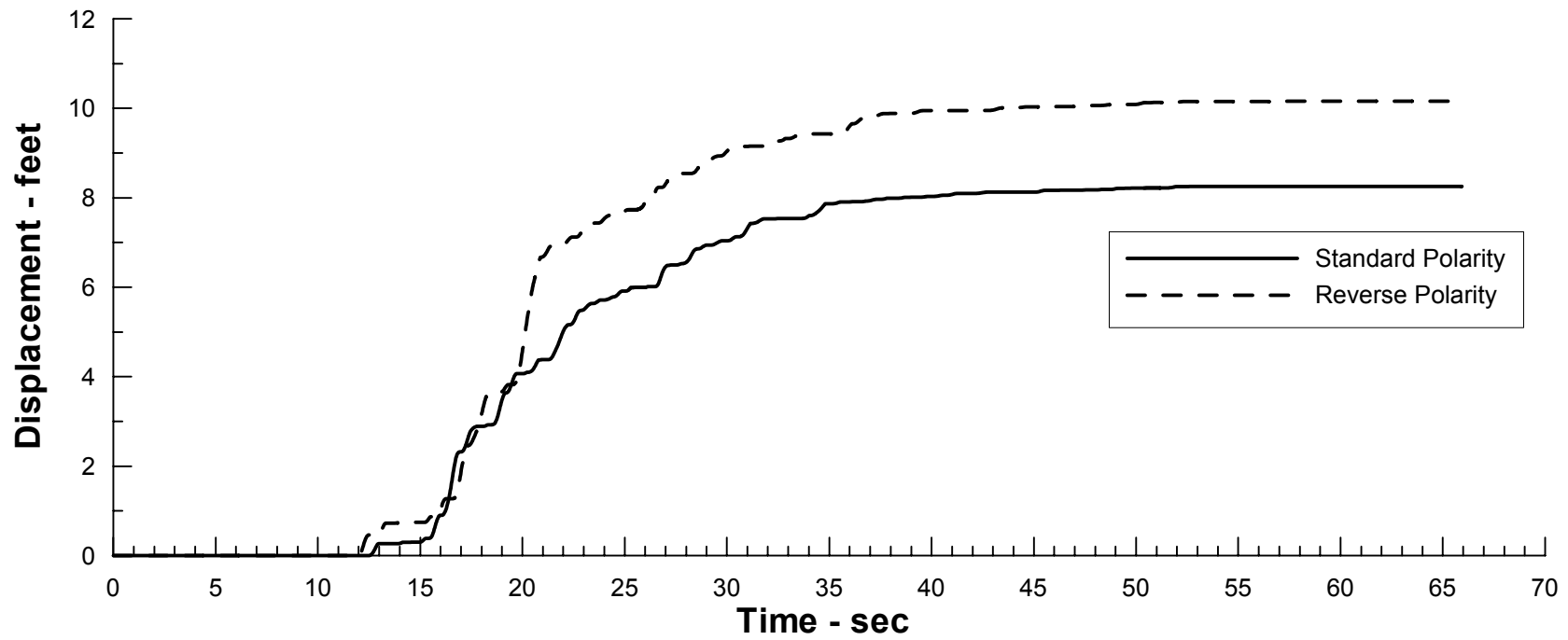
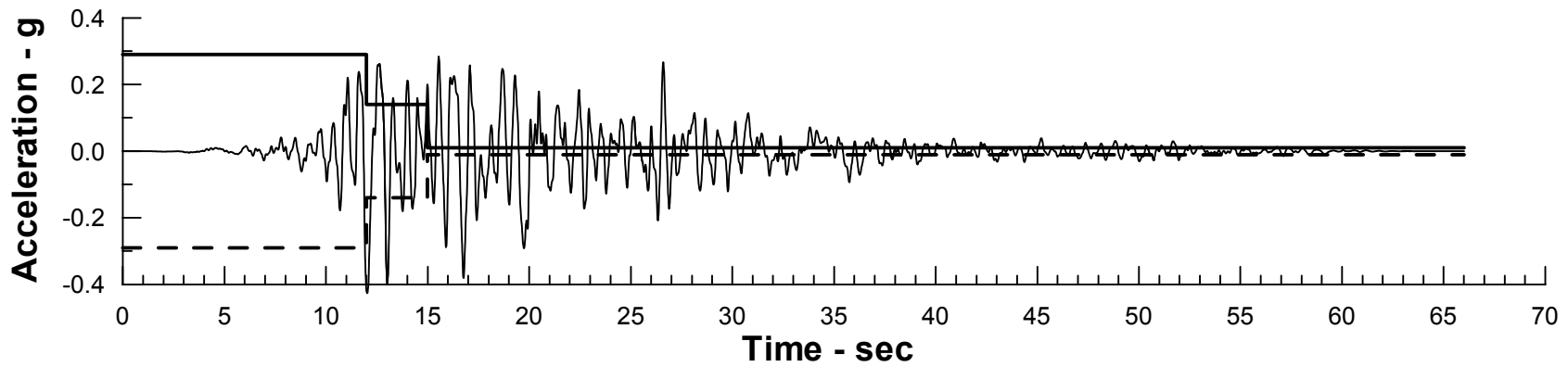
Project No. 26814536	Chabot Dam Seismic Stability Analysis	Newmark Deformation Analysis Calculated Displacement U/S Block #1	Figure 11-27
URS		Hayward Fault MCE TH #1 (10% Max. Strength Reduction)	



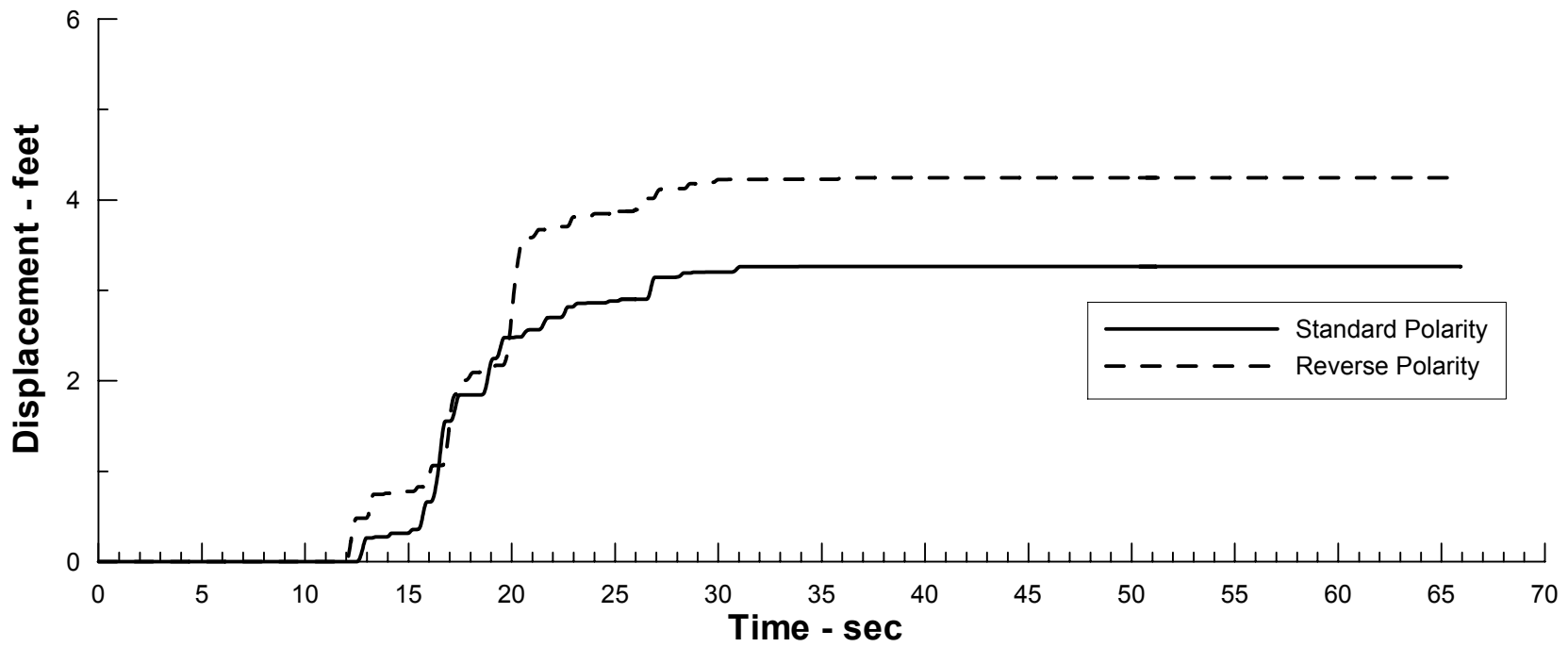
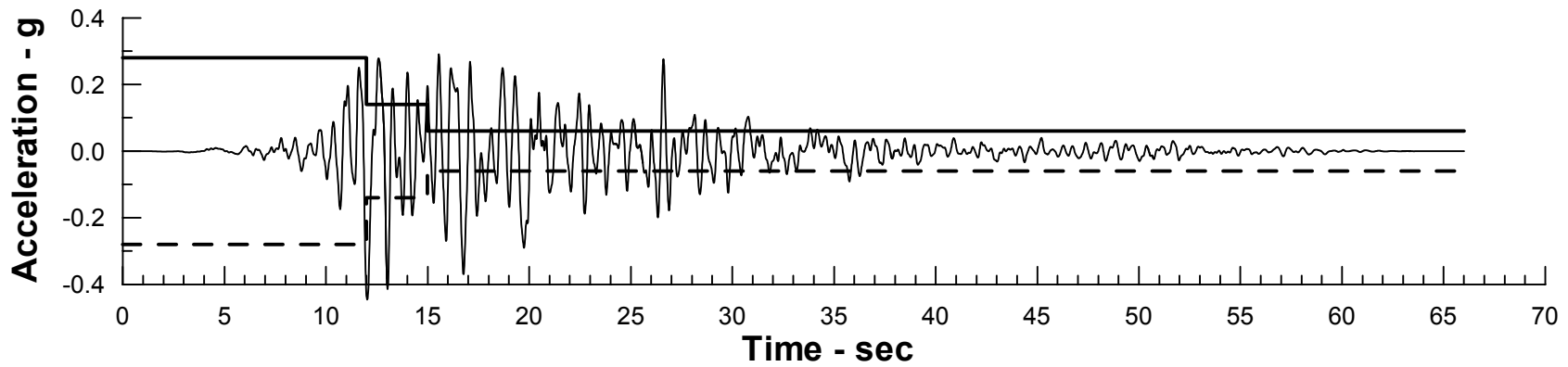
Project No. 26814536	Chabot Dam Seismic Stability Analysis	Newmark Deformation Analysis Calculated Displacement U/S Block #3 Hayward Fault MCE TH #1 (10% Max. Strength Reduction)	Figure
URS			11-28



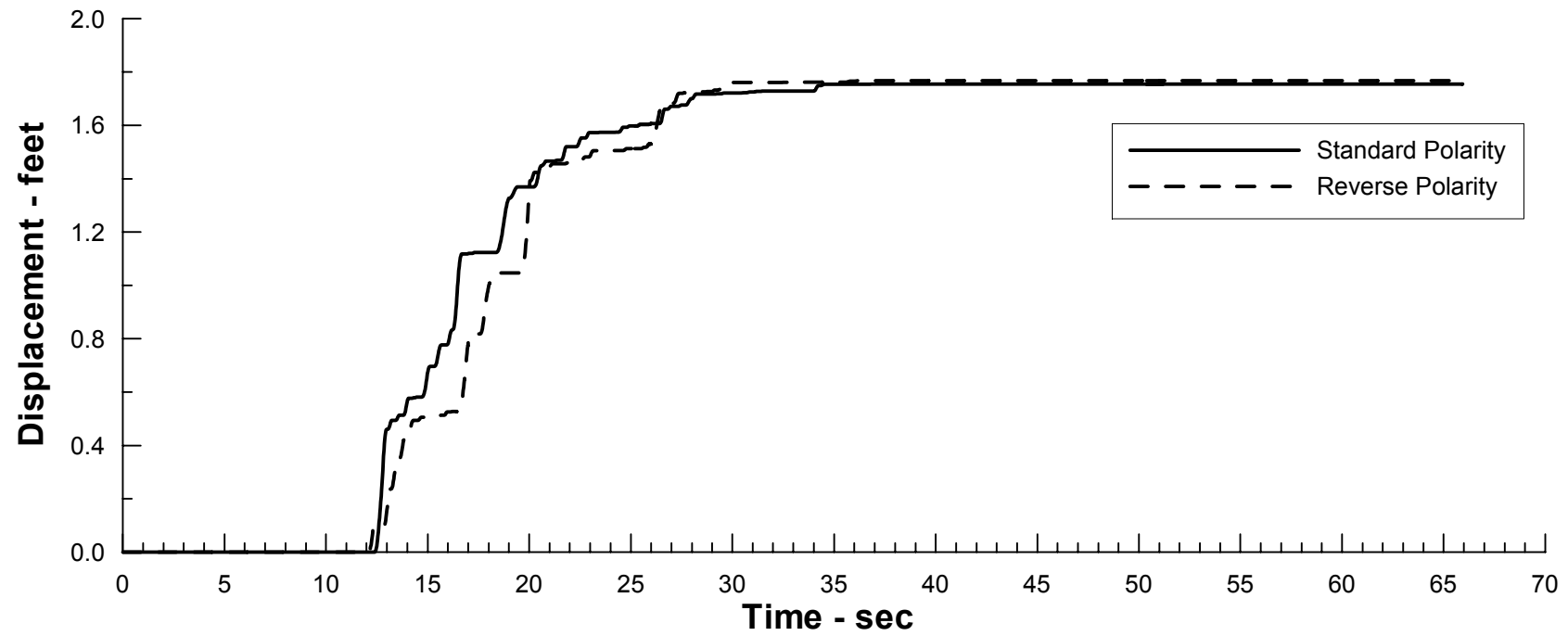
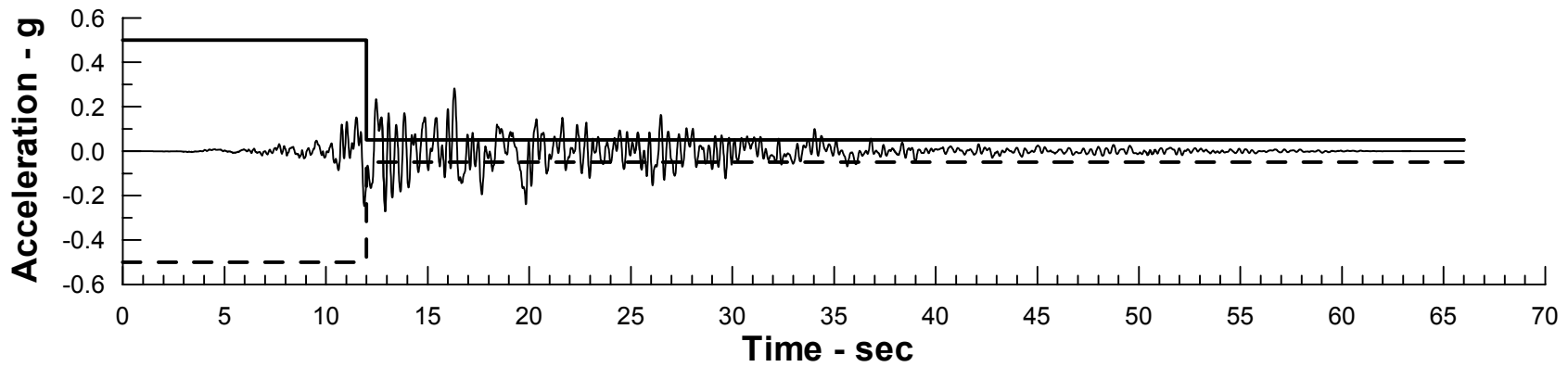
Project No. 26814536	Chabot Dam Seismic Stability Analysis	Newmark Deformation Analysis Calculated Displacement D/S Block #1 Hayward Fault MCE TH #1 (10% Max. Strength Reduction)	Figure
URS			11-29



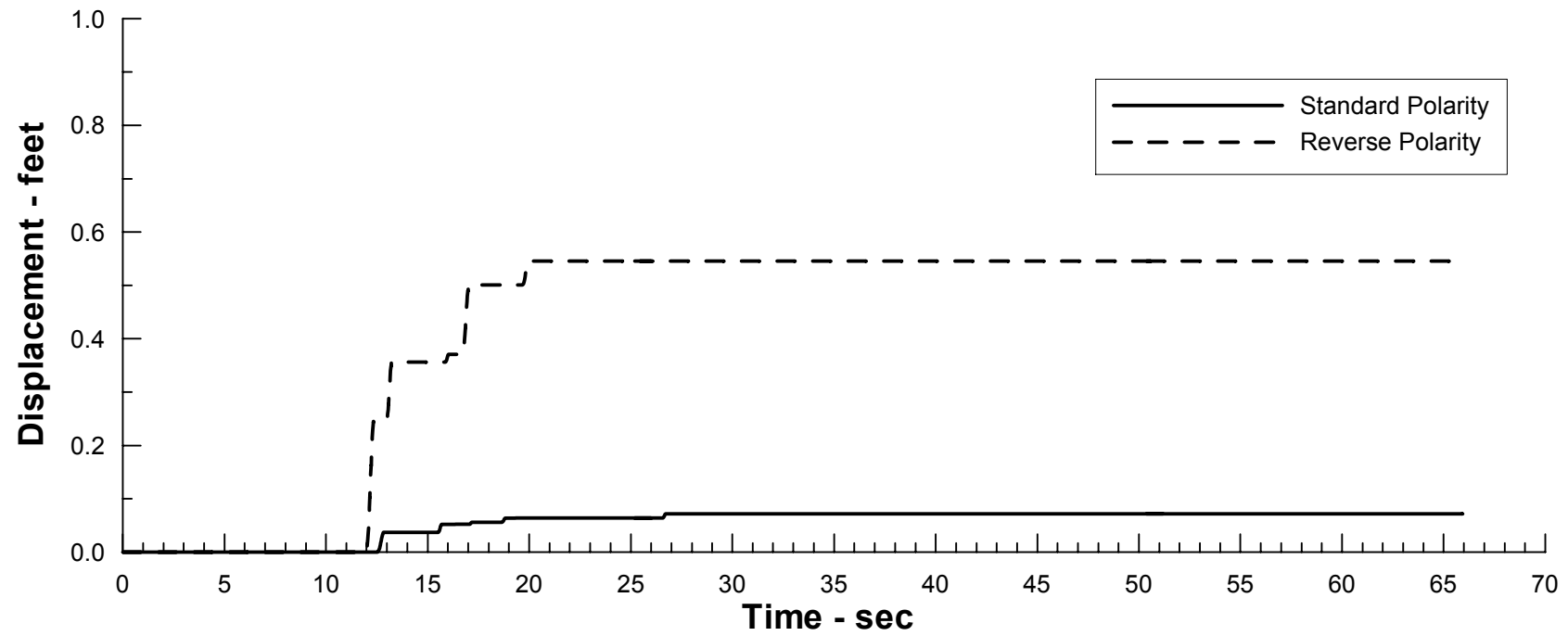
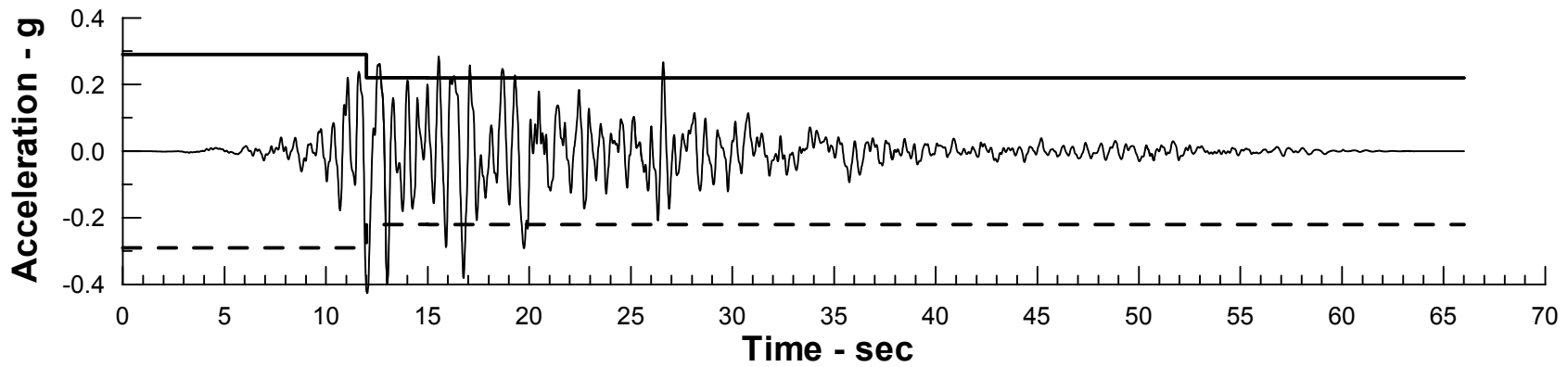
Project No. 26814536	Chabot Dam Seismic Stability Analysis	Newmark Deformation Analysis Calculated Displacement U/S Block #1 San Andreas Fault MCE	Figure 11-30
URS			



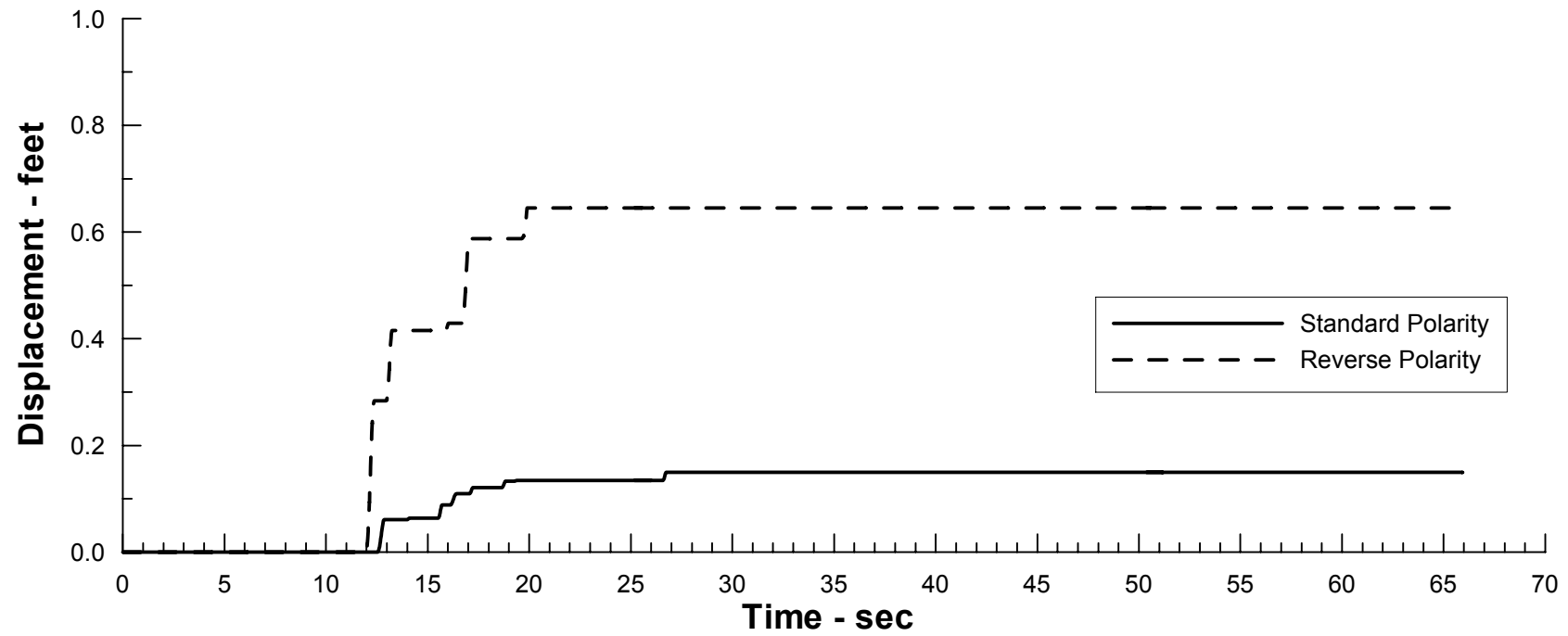
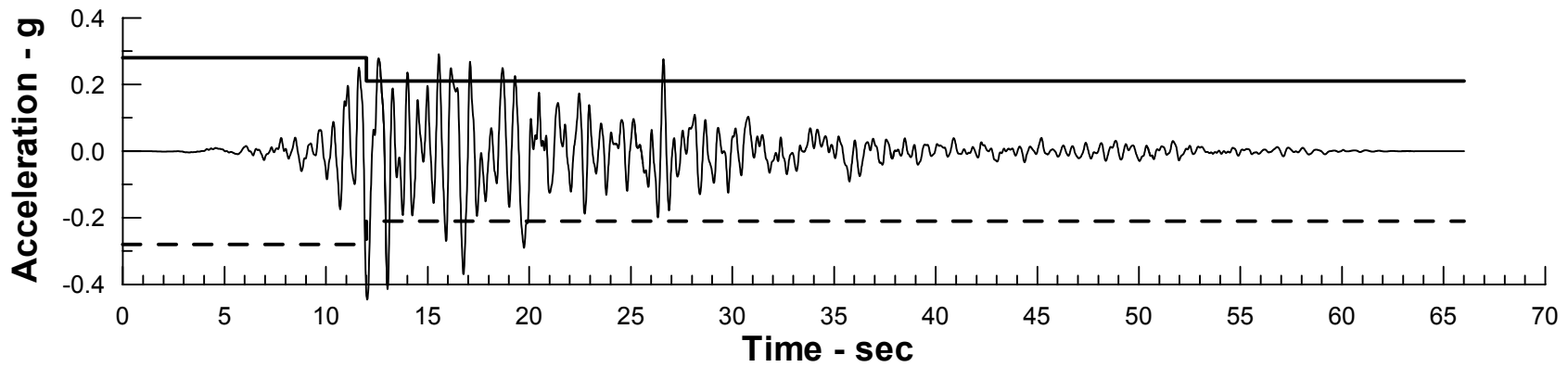
Project No. 26814536	Chabot Dam Seismic Stability Analysis	Newmark Deformation Analysis Calculated Displacement U/S Block #3 San Andreas Fault MCE	Figure
URS			11-31



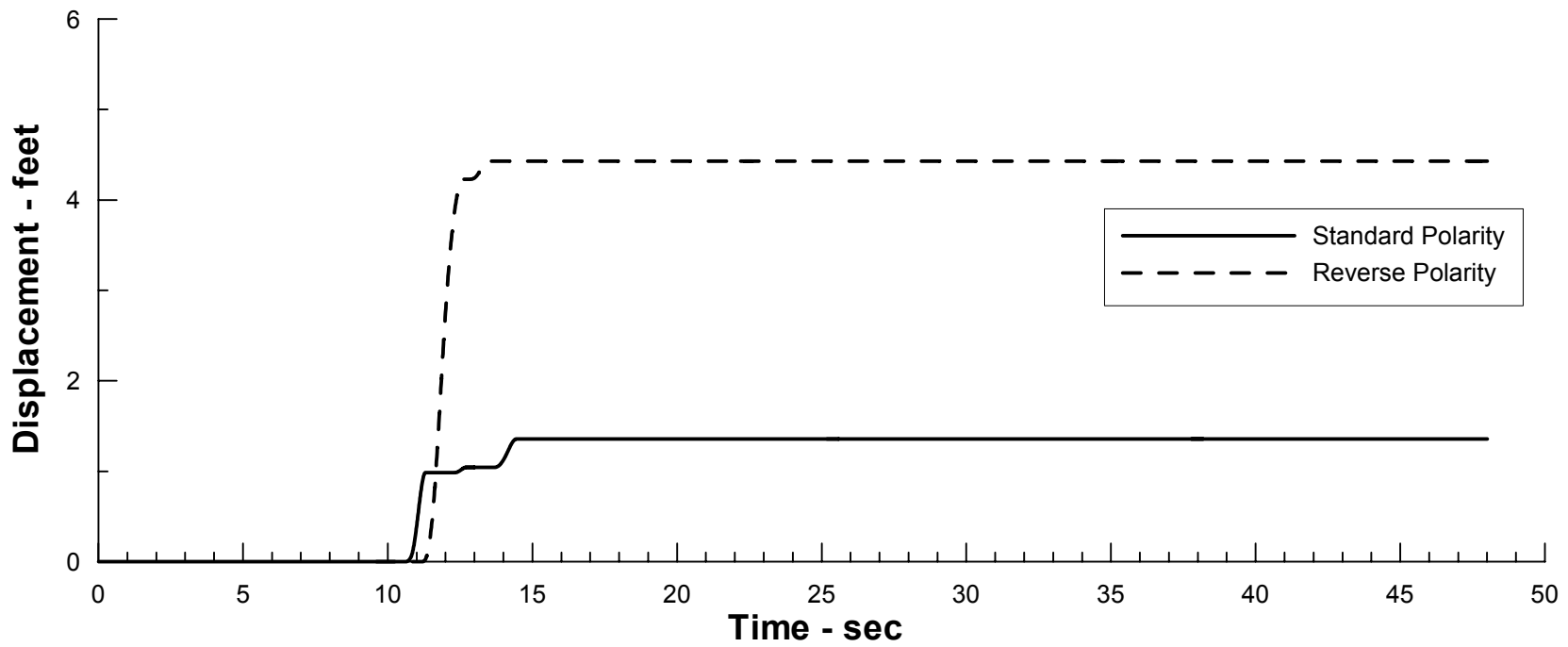
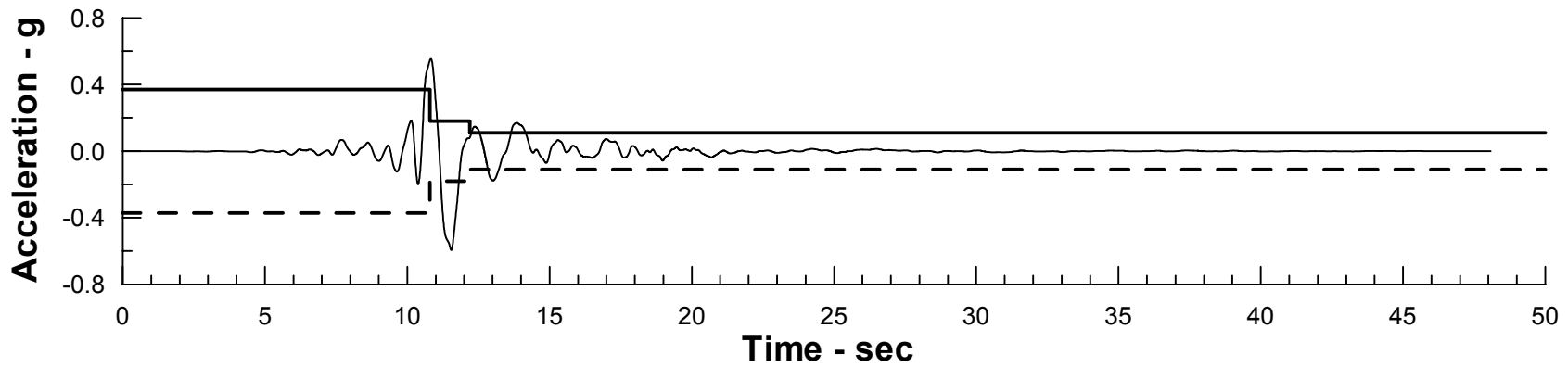
Project No. 26814536	Chabot Dam Seismic Stability Analysis	Newmark Deformation Analysis Calculated Displacement D/S Block #4 San Andreas Fault MCE	Figure 11-32
URS			



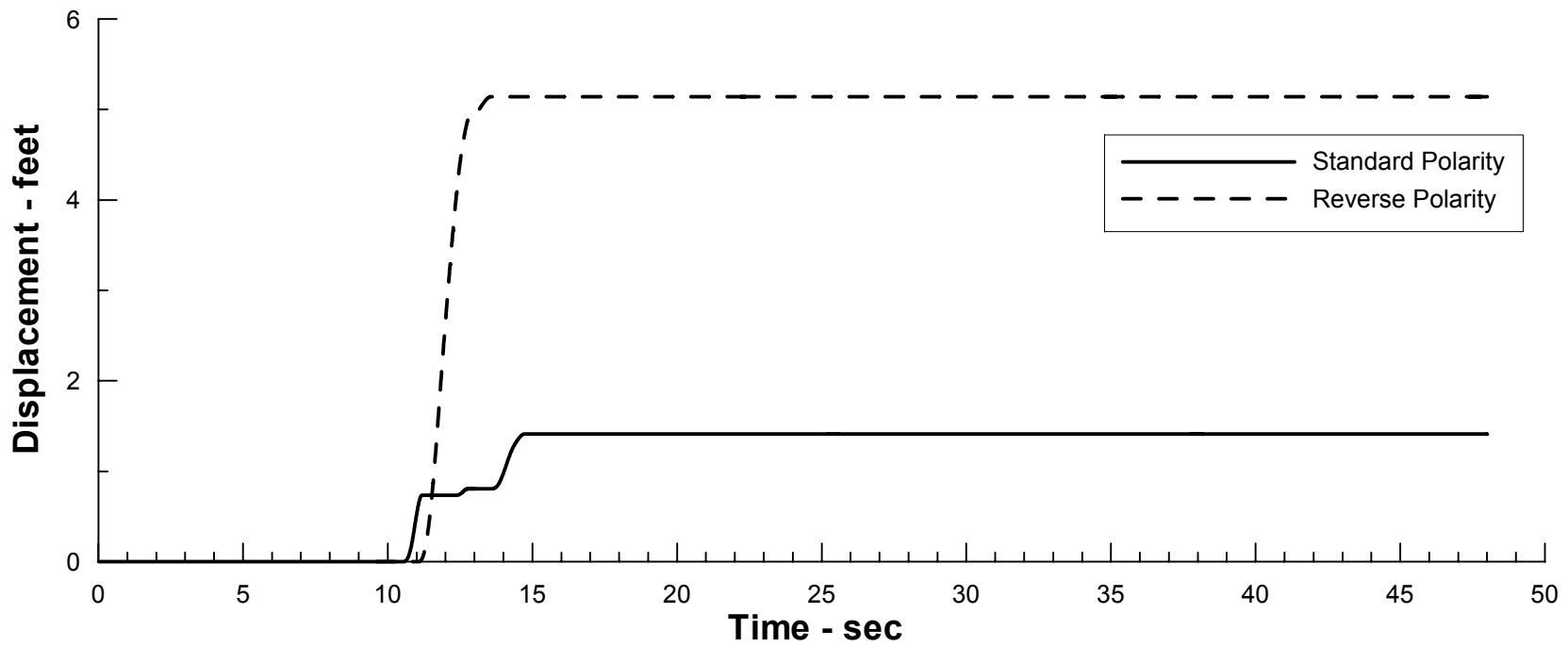
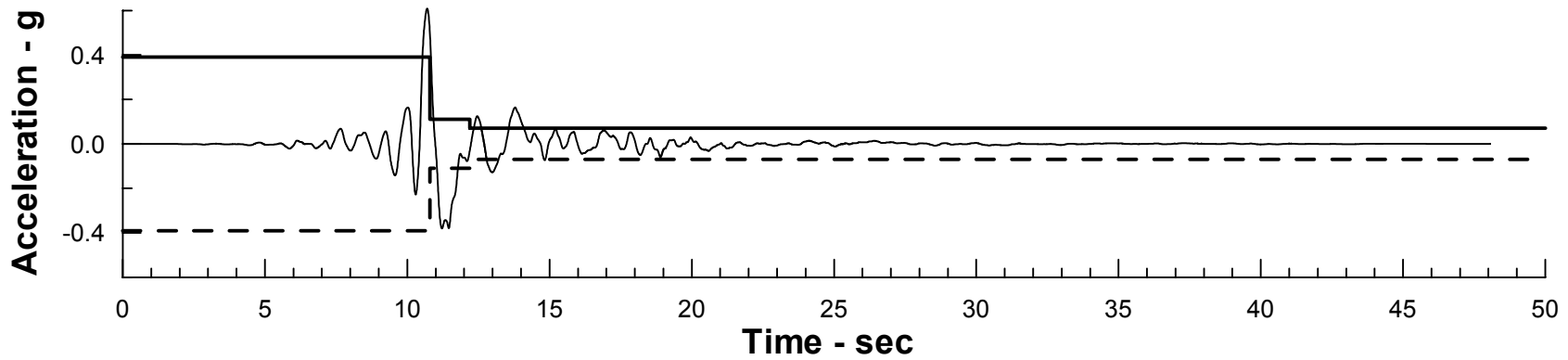
Project No. 26814536	Chabot Dam Seismic Stability Analysis	Newmark Deformation Analysis Calculated Displacement U/S Block #1	Figure
URS		San Andreas Fault MCE (10% Max. Strength Reduction)	11-33



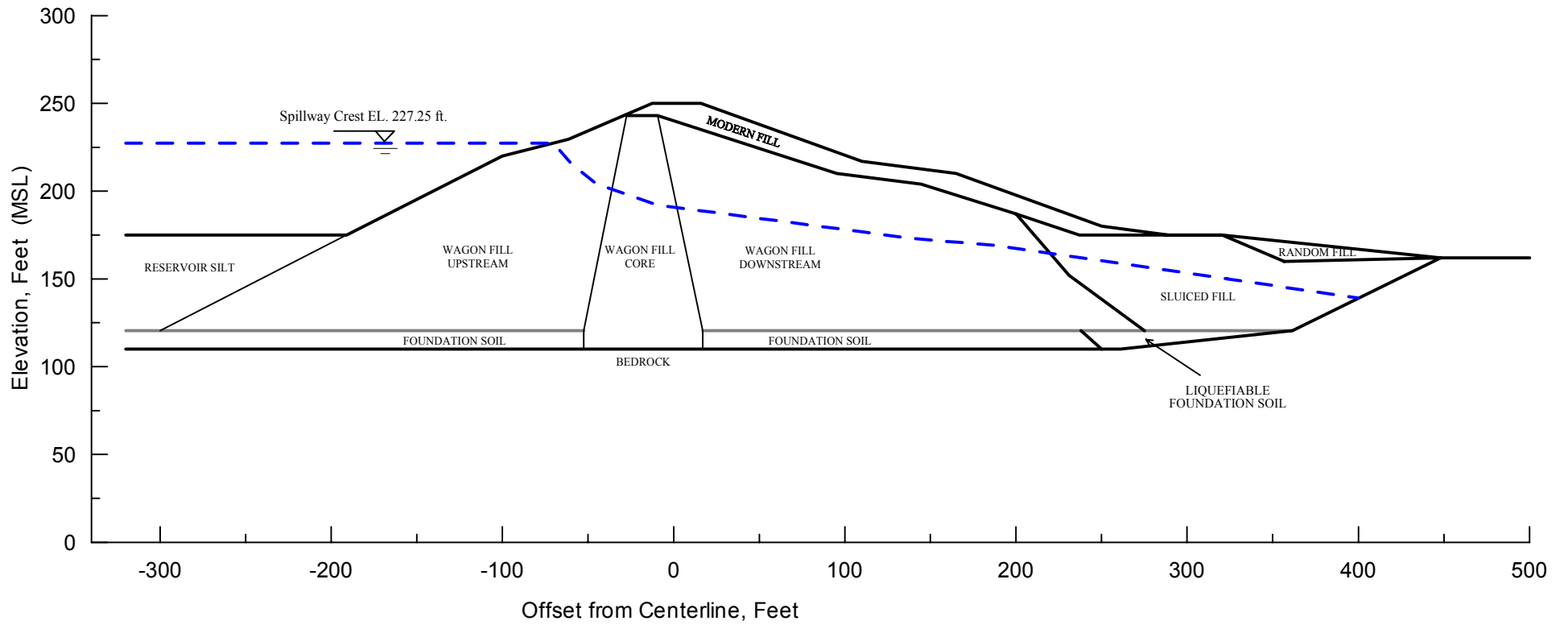
Project No. 26814536	Chabot Dam Seismic Stability Analysis	Newmark Deformation Analysis Calculated Displacement U/S Block #3 San Andreas Fault MCE (10% Max. Strength Reduction)	Figure
URS			11-34



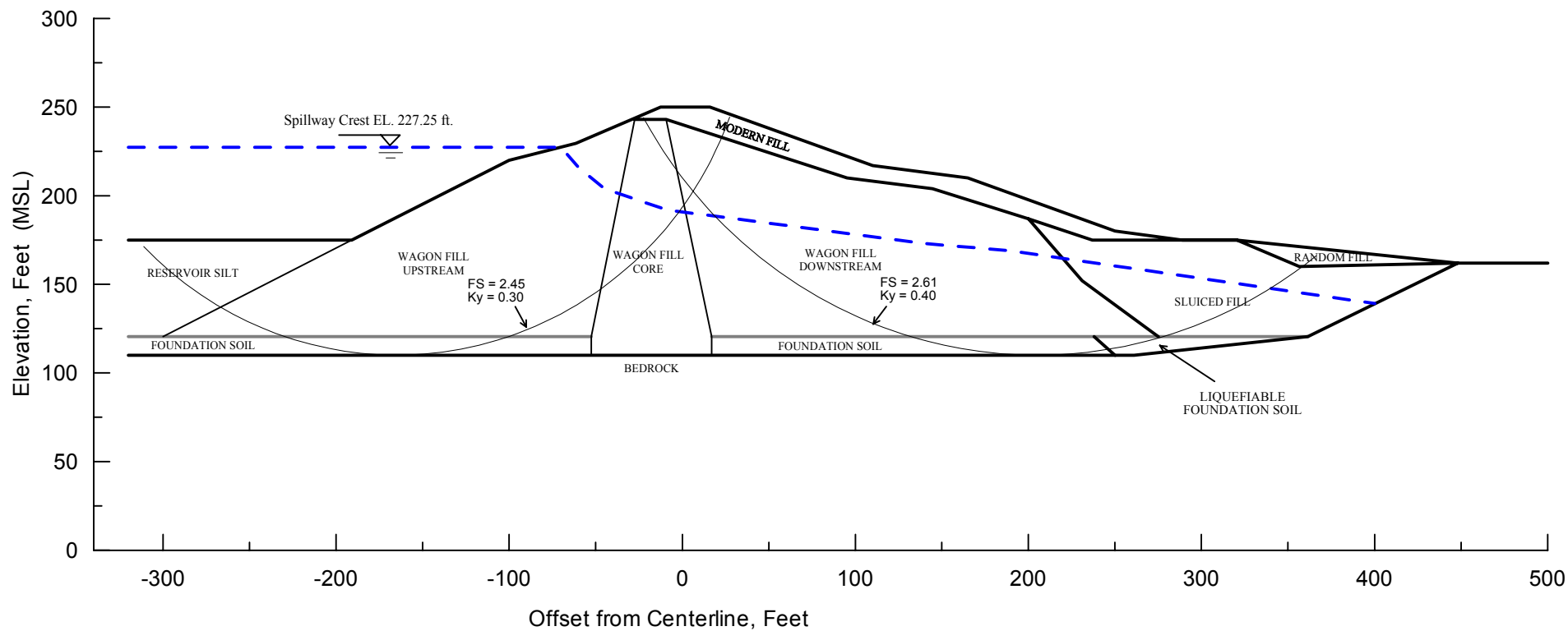
Project No. 26814536	Chabot Dam Seismic Stability Analysis	Newmark Deformation Analysis Calculated Displacement D/S Block #1 (Modified Section A-A') Hayward Fault MCE TH #1	Figure 11-35
URS			



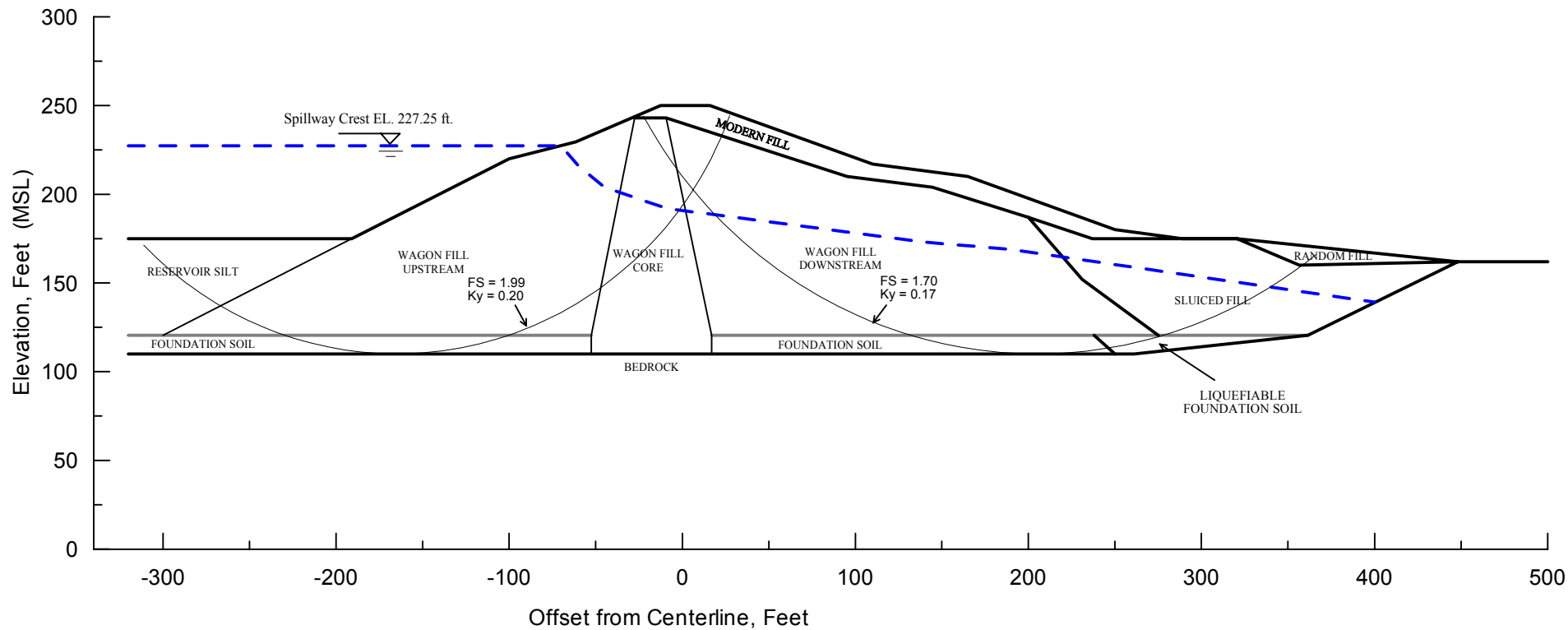
Project No. 26814536	Chabot Dam Seismic Stability Analysis	Newmark Deformation Analysis Calculated Displacement D/S Block #3 (Modified Section A-A') Hayward Fault MCE TH #1	Figure 11-36
URS			



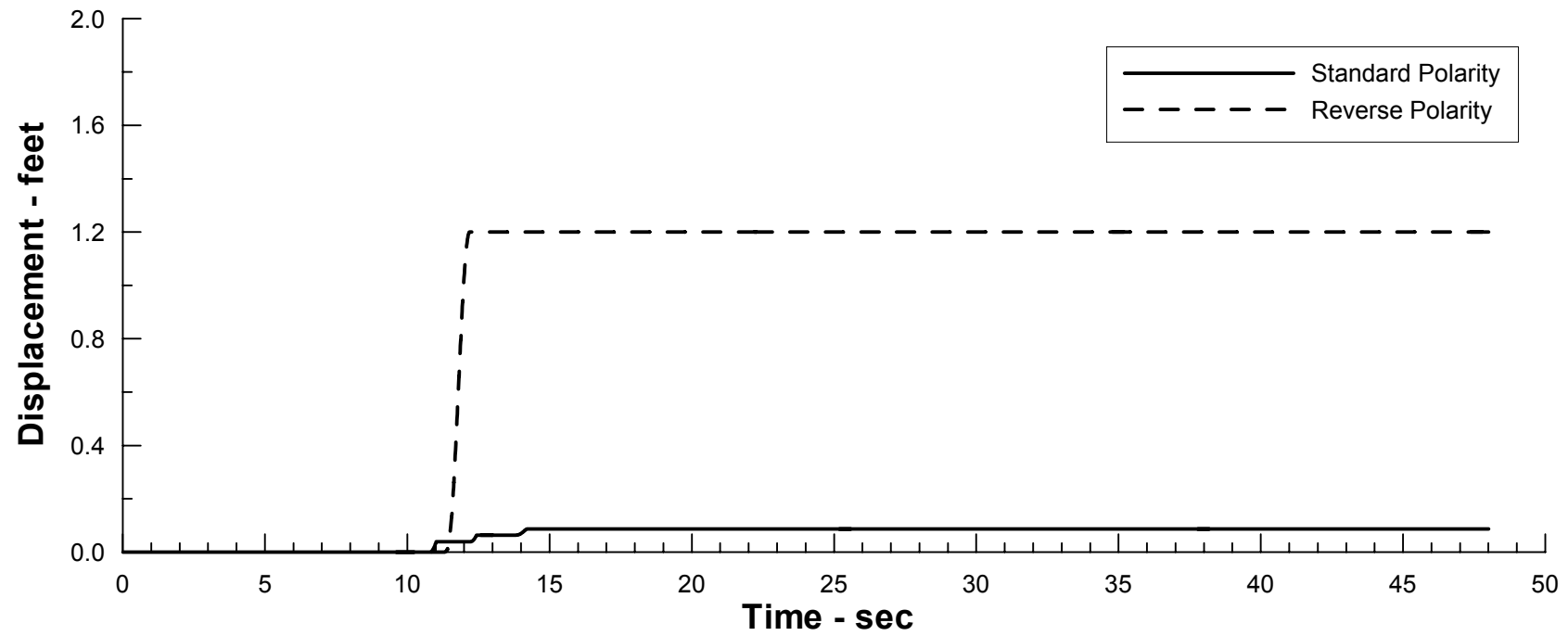
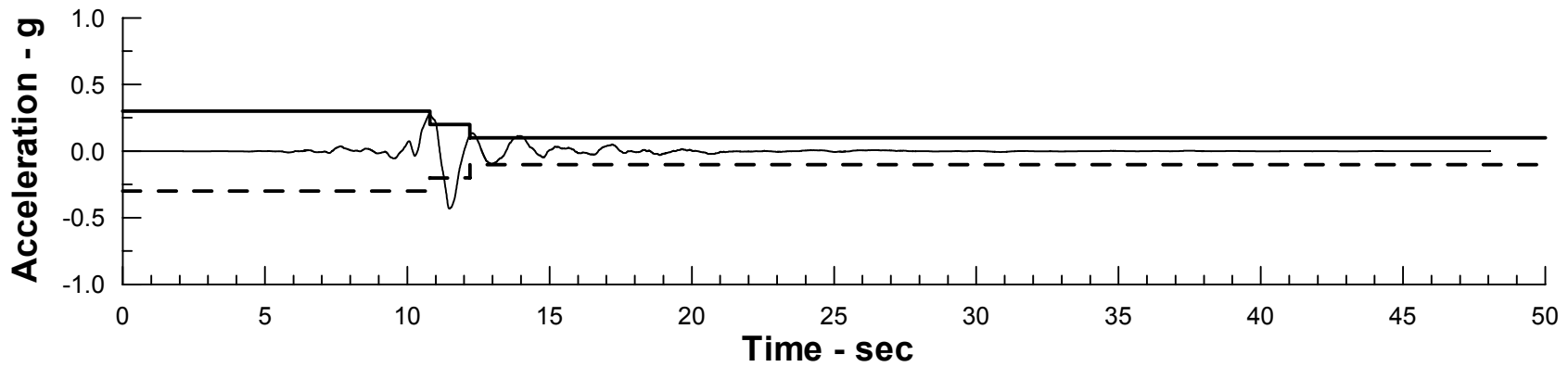
Project No. 26814536	Chabot Dam Seismic Stability Analysis	Alternative Cross Section A - A' for Stability Analysis	Figure
URS			11-37



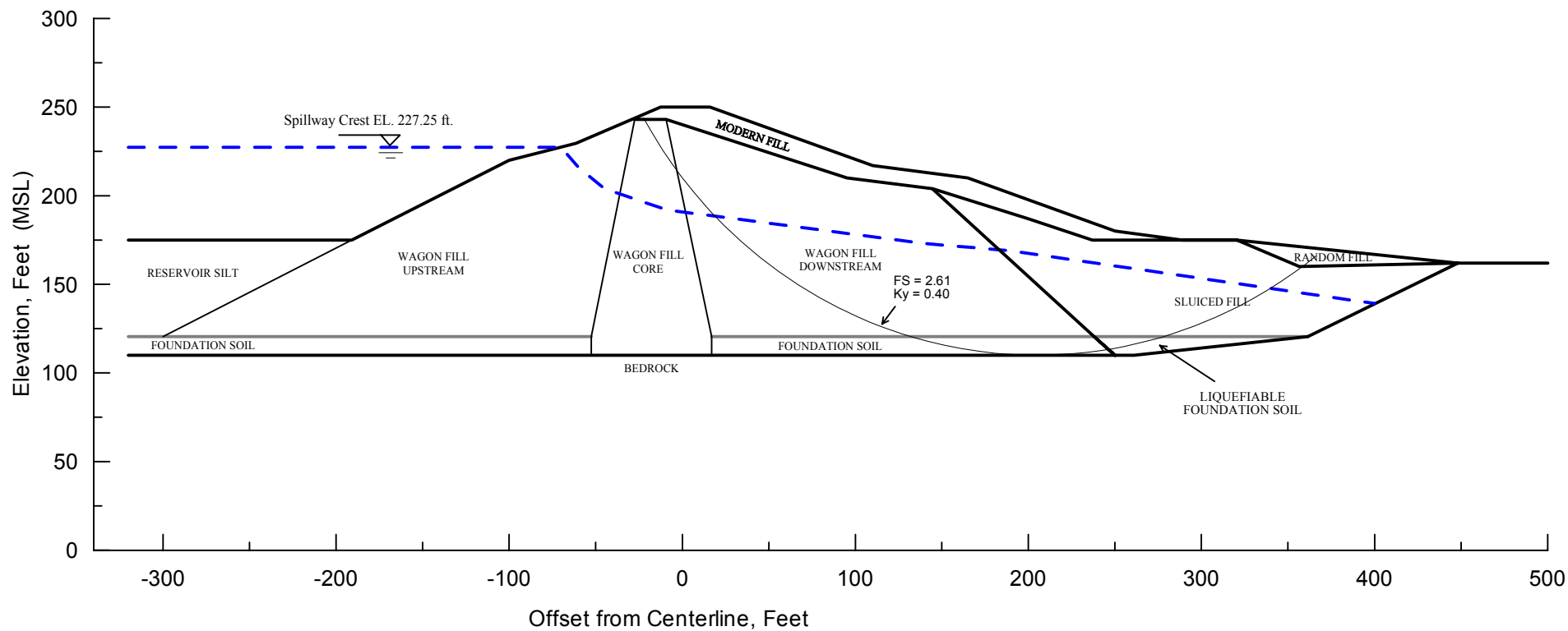
Project No. 26814536	Chabot Dam Seismic Stability Analysis	Seismic Stability Analysis Pre-Earthquake Condition Alternative Cross Section A - A'	Figure
URS			11-38



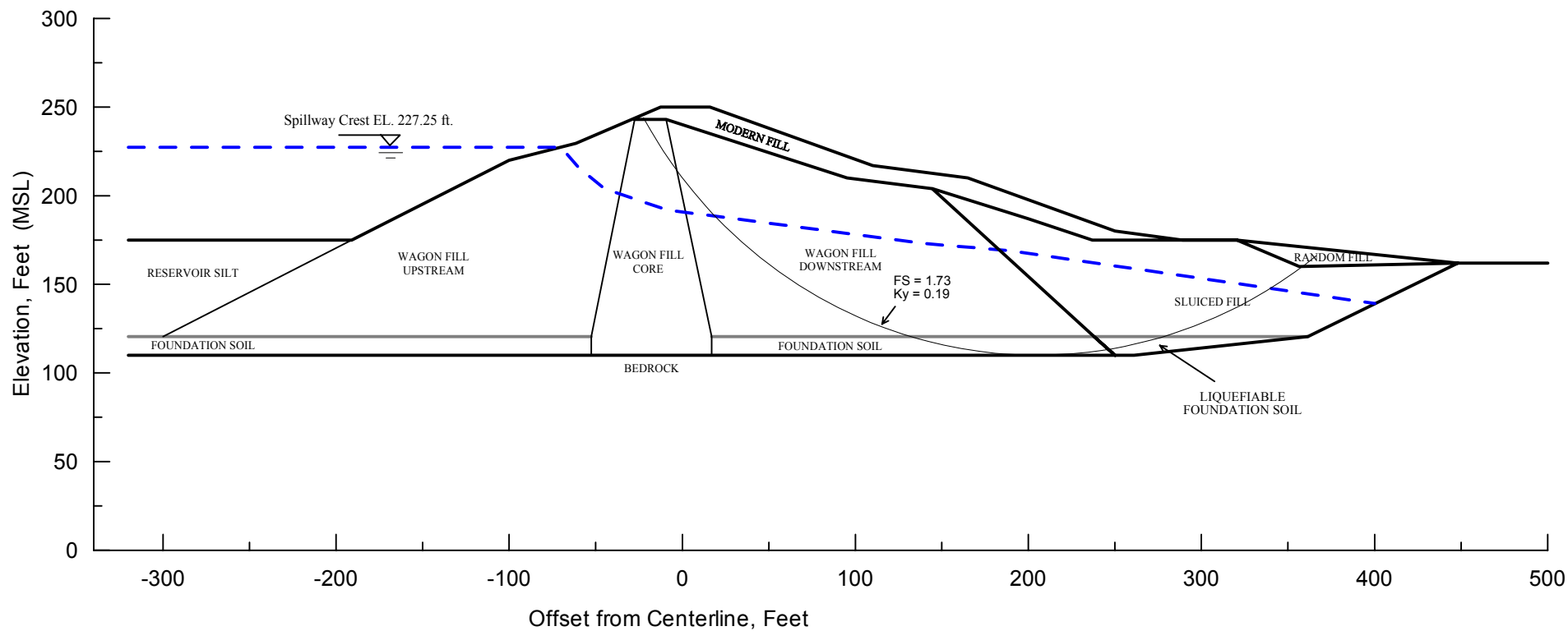
Project No. 26814536	Chabot Dam Seismic Stability Analysis	Seismic Stability Analysis Condition with 20% Strength Reduction Alternative Cross Section A - A'	Figure
URS			11-39



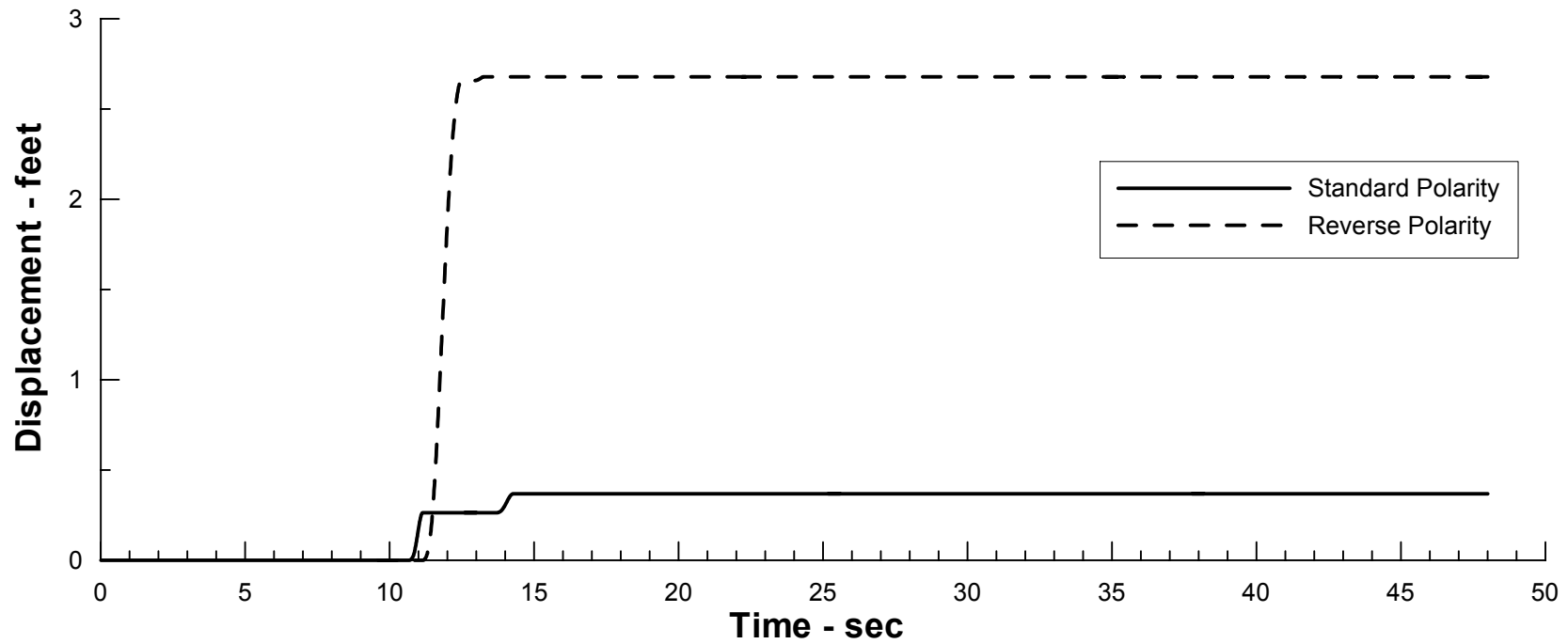
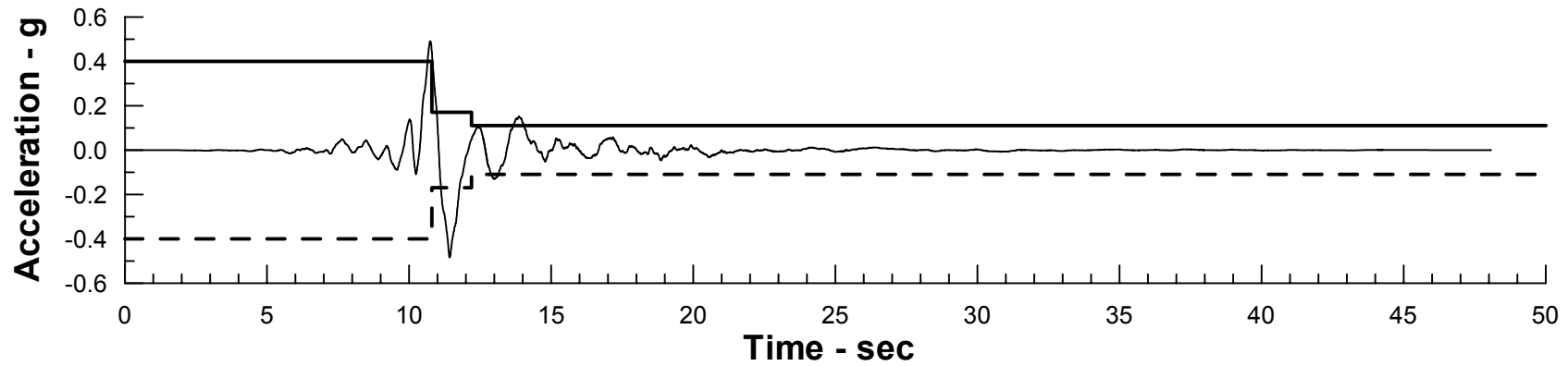
Project No. 26814536	Chabot Dam Seismic Stability Analysis	Alternative Cross Section A-A' Calculated Displacement U/S Block #2 Hayward MCE Time-history #1	FIGURE 11-40
URS			



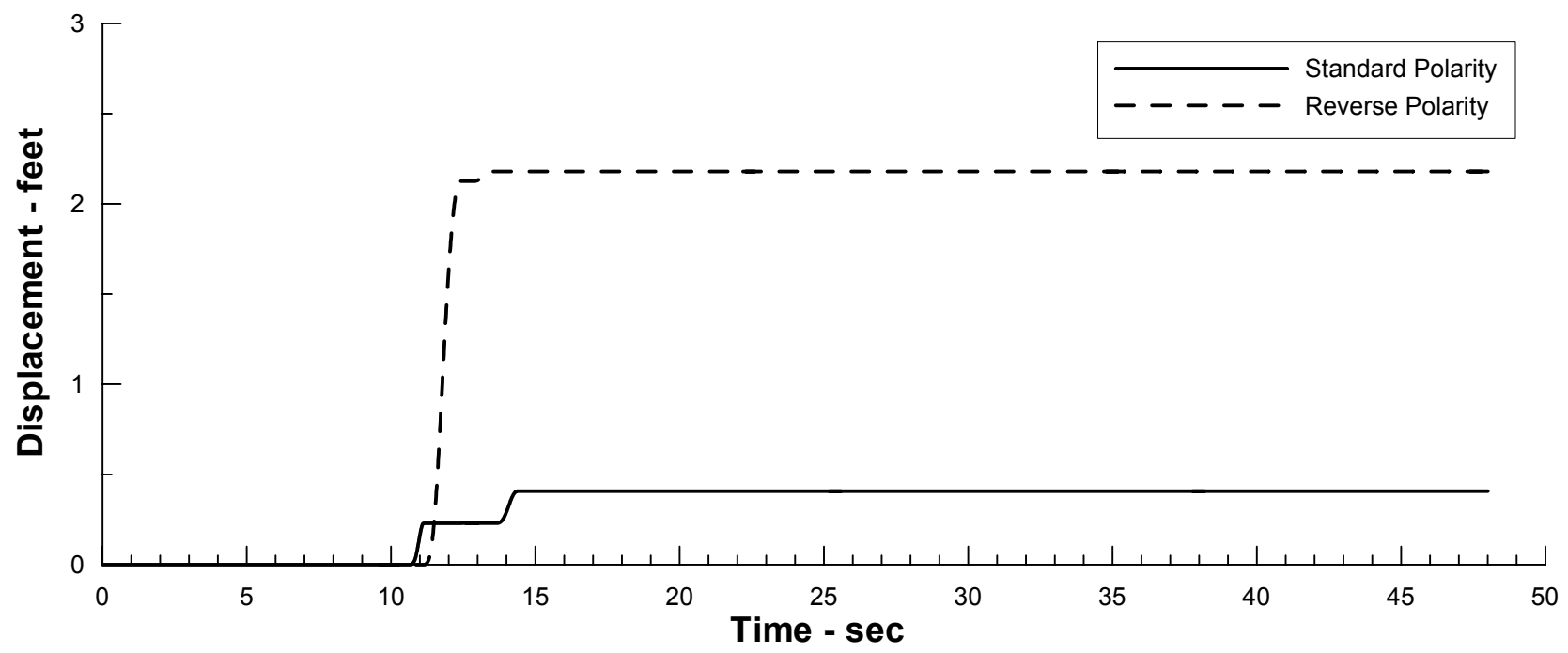
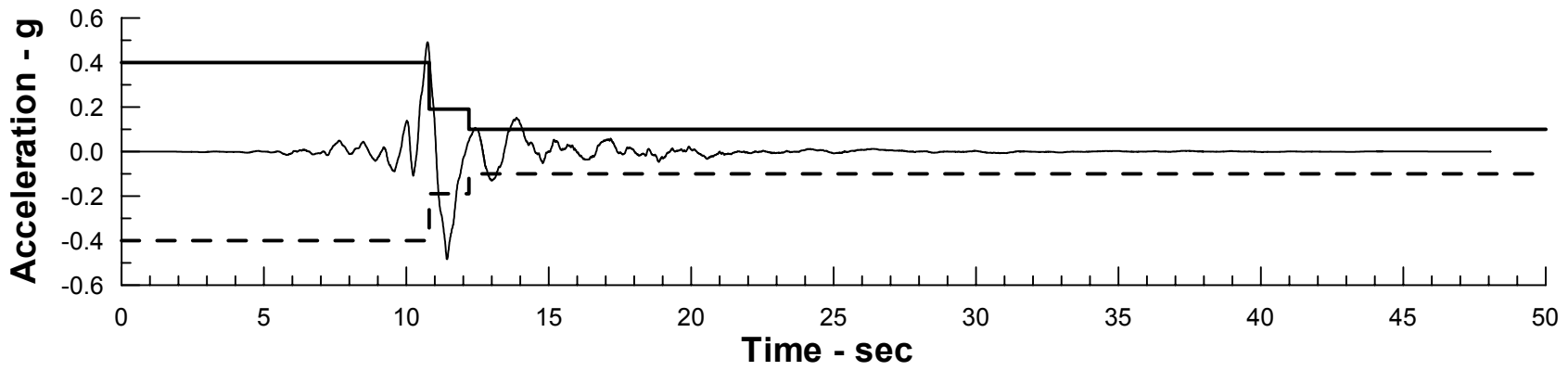
Project No. 26814536	Chabot Dam Seismic Stability Analysis	Seismic Stability Analysis Pre-Earthquake Condition Alternative Modified Section A - A'	Figure 11-41
URS			



Project No. 26814536	Chabot Dam Seismic Stability Analysis	Seismic Stability Analysis Condition with 20% Strength Reduction Alternative Modified Section A - A'	Figure 11-42
URS			



Project No. 26814536	Chabot Dam Seismic Stability Analysis	Alternative Cross Section A-A' Calculated Displacement D/S Block #2 Hayward MCE Time-history #1	Figure 11-43
URS			



Project No. 26814536	Chabot Dam Seismic Stability Analysis	Alternative Modified Section A-A' Calculated Displacement D/S Block #2	Figure 11-44
URS		Hayward MCE Time-history #1	

12.1 METHODOLOGY

The dynamic response and seismic deformations of the dam were directly calculated from fully nonlinear analyses with the computer program FLAC, Version 4.0 (Itasca, 2000). In these analyses, the calculation of seismic deformations is coupled with the calculation of dynamic response. Thus, the seismic deformations, excess pore water pressures, and cyclic degradation are calculated directly from the dynamic response analyses of the dam. To establish the state of stress in the dam prior to the earthquake, a seepage analysis and a static stress analysis were performed with FLAC. The resulting state of stress in the dam served as the initial state for the dynamic analysis. The initial state of stress calculated with FLAC was also used to develop the input for the dynamic response analyses with QUAD4M and the evaluations of potential for liquefaction and strength loss in the dam.

The FLAC analyses were performed for Section A-A'. The section was discretized using the same mesh used for the QUAD4M finite element analyses (Figure 10-1). A compliant boundary was specified along the base of the model to simulate the unbounded extent of the foundation bedrock beneath the dam. The earthquake motions are input as a stress time history at this boundary.

The Mohr-Coulomb elasto-plastic constitutive model in the basic FLAC code was used for the analyses. To evaluate the sensitivity of the calculated deformations to the choice of soil constitutive model, parametric analyses were also performed using a nested-yield surface plasticity model developed by URS. These analyses indicated that in the case of Chabot Dam the calculated deformations are not very sensitive to the choice of constitutive model. Only the results using the Mohr-Coulomb model are presented herein.

12.2 MATERIAL PROPERTIES

The material properties used for the seepage analysis are tabulated in Table 12-1. The hydraulic conductivity of the embankment and foundation materials, was first assumed based on the engineering characteristics of the materials and then adjusted by trial-and-error until a reasonable match was obtained between the calculated phreatic surface and the available piezometric data at the dam.

The material properties for the static stress analysis are summarized in Table 12-2. These parameters were selected based on the results of the laboratory tests reported herein, the values reported by WLA (1974), and published data for similar soils.

The FLAC dynamic analyses were conducted using the same material characterization used for the limit-equilibrium and QUAD4M dynamic response analyses, but adapted to the specific input requirements of FLAC. The material properties for dynamic analysis are listed in Table 12-3. For both the elasto-plastic and nested-yield surface constitutive models, the analyses were performed in terms of effective stresses by coupling the models with the pore pressure generation scheme shown in Figure 12-1. In this scheme, which is based on the cyclic stress approach proposed by Seed (1979), pore pressures are continuously updated for each element in response to shear stress cycles, and the effective stresses decrease with increasing pore pressure.

The strength of the materials was modeled to be consistent with that used in the limit equilibrium analyses. For the saturated sluiced fill, the soil model incorporates the post-liquefaction residual

strength of the material by using a bi-linear failure envelope as shown in Figure 12-2. The cyclic resistance of the saturated sluiced fill was modeled using the relationship shown in Figure 12-3. The models for cyclic strength and undrained strength degradation of the saturated wagon fill and foundation soils are illustrated in Figure 12-4. The strength degradation of those materials is expressed through the ratio of post-cyclic strength to pre-cyclic (i.e. static) strength as a function of excess pore pressure ratio (see Section 11).

12.3 ANALYSIS RESULTS

Dynamic analyses were performed for the 1989 Loma Prieta earthquake and the Hayward fault and San Andreas fault MCEs. As in the case of the decoupled analyses, the FLAC analyses show that the San Andreas event is less critical to the seismic stability of the dam. Only the results for the Loma Prieta and Hayward events are presented herein.

12.3.1 1989 Loma Prieta Earthquake

The analysis results for the 1989 Loma Prieta earthquake are presented in Figures 12-5 through 8. Figure 12-5 shows the calculated acceleration time histories at the crest and at the downstream rock surface together with the input time history. The maximum calculated excess pore pressure ratio in the sluiced fill is shown in Figure 12-6. The cyclic strength degradation of the wagon fill is shown in Figure 12-7. The calculated displacement vectors after the earthquake are presented in Figure 12-8. As shown in these figures, the analyses result in low excess pore pressures in the sluiced fill, little degradation of the wagon fill, and very small displacements of the dam. These results are in good agreement with the observed performance of the dam during the earthquake.

12.3.2 Hayward-Rogers Creek Fault MCE

For the Hayward fault MCE, analyses were performed for both standard and reversed polarities in the motion corresponding to acceleration time history No. 1. The results showed that the reverse polarity motions induce larger crest deformations of the dam. Thus, only the results for reversed polarity motions are presented herein.

The analysis results for the Hayward event are shown in Figures 12-9 through 12-16. Figure 12-9 shows the calculated acceleration time histories at the crest and at the downstream rock surface together with the input time history. Figure 12-10 shows calculated time histories of excess pore pressure ratio in the sluiced fill and of cyclic strength degradation in the wagon fill. These results indicate that the development of excess pore pressures in the sluiced fill will begin early during the shaking and that those materials will reach a state of initial liquefaction after about 10 seconds of shaking. Cyclic degradation of the wagon fill is calculated to occur during the strong phase of shaking between about 10.5 and 12 seconds. As shown in Figure 12-11, a maximum strength reduction of about 40% is calculated in the upstream zone beyond the toe of the embankment and in a small zone at the bottom of the core beneath the crest. However, the calculated amount of maximum cyclic strength degradation of the saturated fill over a large portion of the dam averages less than about 10%.

Figure 12-12 shows the calculated displacement vectors throughout the dam after the earthquake. Figures 12-13 and 12-14 show calculated time histories of horizontal and vertical displacements

at selected points on the dam slopes. As shown in these figures, the calculated downward vertical displacement of the dam crest is less than 1.5 feet. The calculated horizontal displacements of the upstream slope are less than 2 feet. The calculated horizontal displacements of the downstream slope are less than 1 foot, except in the sluiced fill where horizontal displacements of up to about 5 feet are calculated. Such displacements do not include potential movement of the sluiced fill along the downstream channel.

Figures 12-15 and 12-16 show the results of stability analyses with FLAC for the post-earthquake condition. These analyses result in adequate calculated factors of safety indicating that the dam slopes will remain stable after the earthquake, as was the case with the limit equilibrium post-earthquake stability analyses.

Table 12-1
Material Properties for Seepage Analysis

Property		Units	Modern Fill	Random Fill	Wagon Fill (U/S and Core)	Wagon Fill (D/S)	Sluiced Fill	Foundation Soils	Bedrock
Moist Density	ρ_m	pcf	134	130	133	133	130	133	140
Porosity	n	-	0.26	0.34	0.30	0.30	0.34	0.30	0.25
Vertical Hydraulic Conductivity	k_v	ft/sec	1.6E-06	1.6E-06	1.3E-06	3.3E-06	1.6E-05	1.3E-06	3.3E-09
Horizontal Hydraulic Conductivity	k_h	ft/sec	4.1E-07	4.1E-07	6.6E-07	1.6E-06	4.1E-06	6.6E-07	3.3E-09
Vertical Permeability Coefficient ⁽¹⁾	K_v	ft ² /(psf-sec)	2.6E-08	2.6E-08	2.1E-08	5.3E-08	2.6E-07	2.1E-08	5.3E-11
Horizontal Permeability Coefficient ⁽¹⁾	K_h	ft ² /(psf-sec)	6.6E-09	6.6E-09	1.1E-08	2.6E-08	6.6E-08	1.1E-08	5.3E-11

Notes:

(1) Also called 'mobility coefficient'. Used for specifying permeability for FLAC. $K = k / \gamma_{\text{water}}$.

Table 12-2
Material Properties for Static Stress Analysis

Property	Symbol	Modern Fill	Random Fill	Wagon Fill	Sluiced Fill	Foundation Soils	Bedrock
Modulus Number	K	400	400	400	400	400	-
Modulus Number	K_b	300	300	300	300	300	-
Modulus Exponent	m	0.4	0.4	0.4	0.4	0.4	-
Modulus Exponent	n	0.5	0.5	0.5	0.5	0.5	-
Elastic Bulk Modulus	B, psf	$K_b * Pa(\sigma_3' / Pa)^m$	-				
Youngs Modulus	E, psf	$K * Pa(\sigma_3' / Pa)^n$	-				
Poisson's Ratio	ν	$0.5 - E/(6*B)$	0.42				
Elastic Shear Modulus	G, psf	$E/(2+2\nu)$	$E/(2+2\nu)$	$E/(2+2\nu)$	$E/(2+2\nu)$	$E/(2+2\nu)$	3.17E+07
Cohesion	c', psf	0	0	0	0	0	100,000
Friction Angle	$\phi', degree$	35	33	30	33	30	0

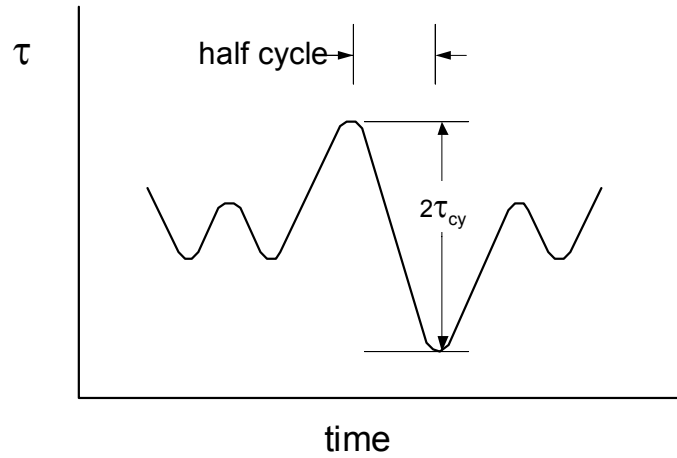
**Table 12-3
Material Properties for Dynamic Analysis**

Property	Symbol	Units	Modern Fill	Random Fill	Wagon Fill (D/S and U/S)	Wagon Fill (Core)	Sluiced Fill	Foundation Soils	Bedrock
Poisson's Ratio ⁽¹⁾	ν	-	0.36	0.36	0.37, 0.45	0.40, 0.45	0.36, 0.48	0.46	0.42
Shear wave velocity ⁽²⁾	V_s	fps	1,200	$695 \cdot \sigma'_m{}^{0.38}$ and > 500	$650 \cdot \sigma'_m{}^{0.43}$ and > 1,000	$600 \cdot \sigma'_m{}^{0.43}$ and > 900	$695 \cdot \sigma'_m{}^{0.38}$ and > 500	1300	2,700
Maxim Shear Modulus	G_{max}	psf	5.99E+06	$\rho \cdot V_s^2$	$\rho \cdot V_s^2$	$\rho \cdot V_s^2$	$\rho \cdot V_s^2$	6.98E+06	3.17E+07
Shear Modulus	G	psf	$0.7 \cdot G_{max}$	$0.7 \cdot G_{max}$	$0.7 \cdot G_{max}$	$0.7 \cdot G_{max}$	$0.7 \cdot G_{max}$	$0.7 \cdot G_{max}$	G_{max}
Rayleigh Damping	ε_{min}	-	3%	3%	3%	3%	3%	3%	0.5%
Rayleigh Damping Center Frequency	f_{min}	Hz	3	3	3	3	3	3	3
Hysteretic Damping	-	-	see note 3	see note 3	see note 3	see note 3	see note 3	see note 3	-
Cohesion	c	psf	0	0	540	540	0	540	100,000
Friction Angle	ϕ	degree	35	33	26.4	26.4	33	26.4	0

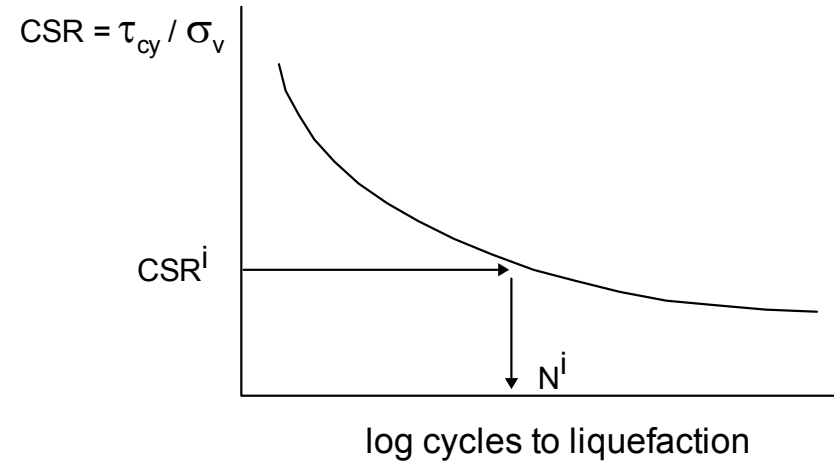
Notes:

- (1). Dual values correspond to unsaturated and saturated conditions, where applicable.
- (2). $\sigma'_m = (\sigma_1' + \sigma_2' + \sigma_3')/3$, in ksf
- (3). Hysteretic damping is automatically generated and added to the Rayleigh damping in FLAC analyses when materials yield.

Shear Stress Time History



Cyclic Strength

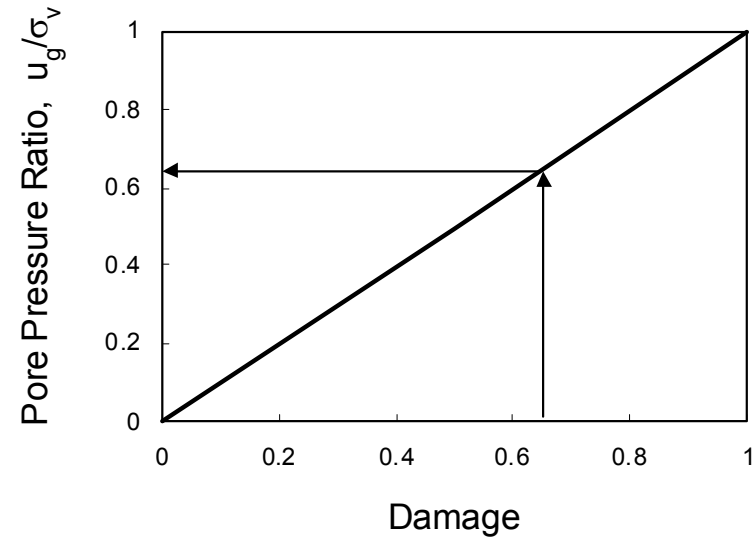


Damage Increment

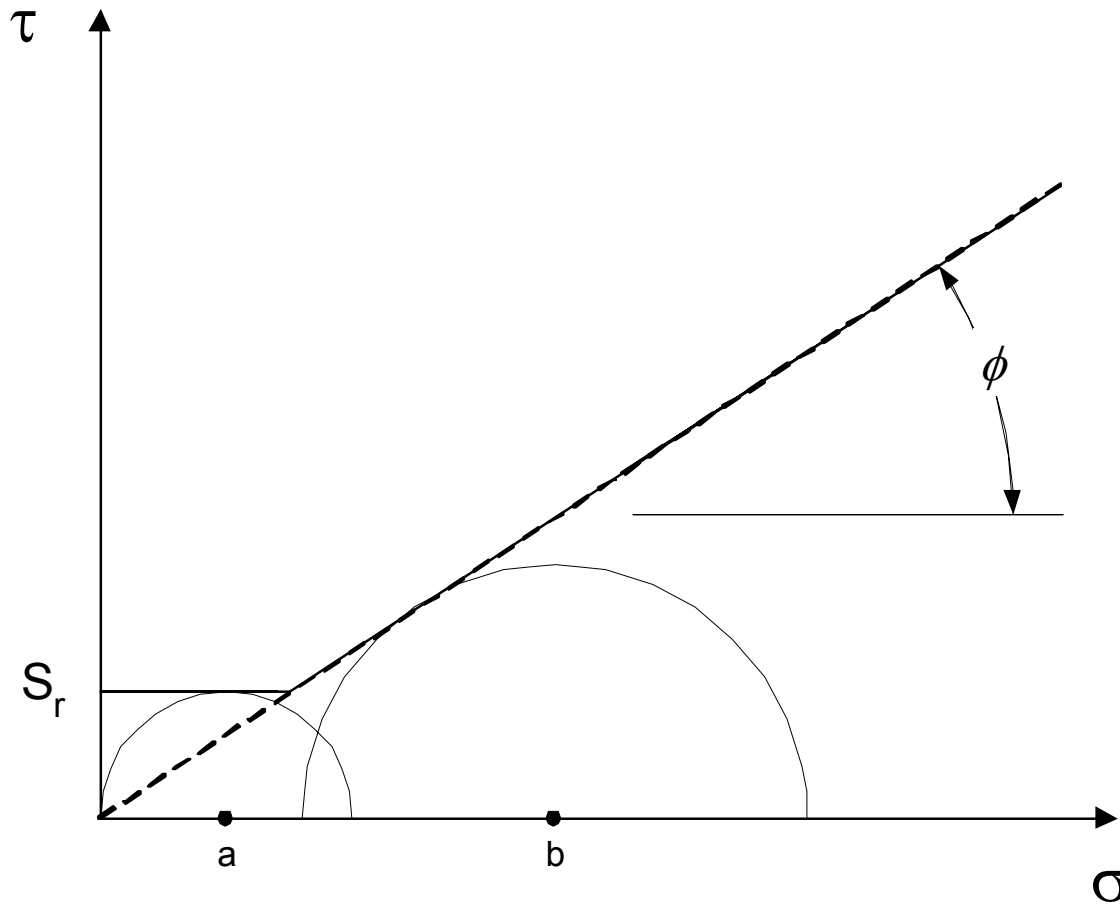
$$\Delta D^i = 0.5 / N_L^i$$

Cumulative Damage

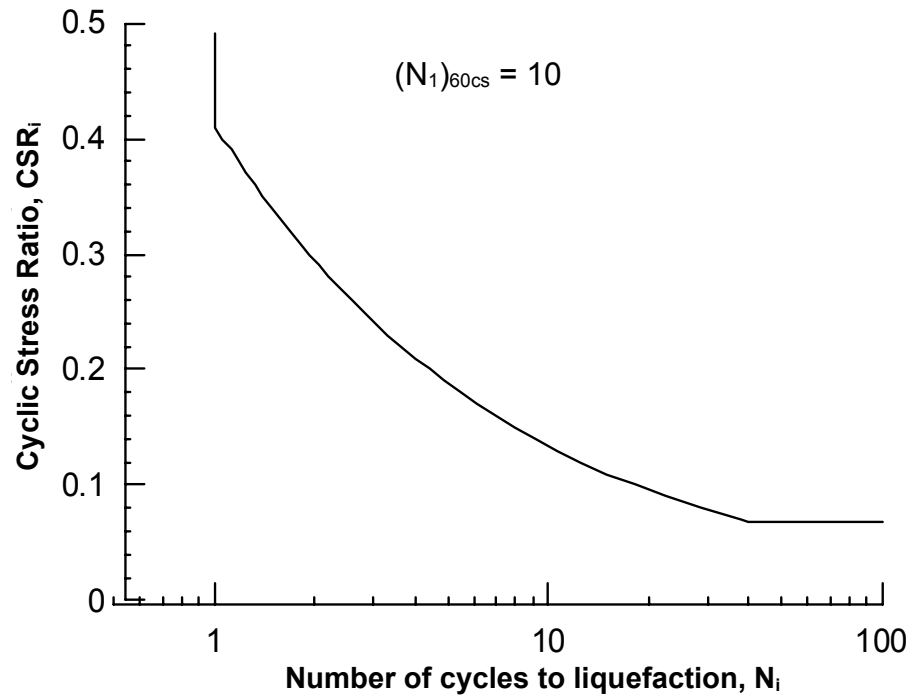
$$D = \sum \Delta D^i$$



Project No. 26814536	Chabot Dam Seismic Stability Analysis	FLAC Analysis Pore Pressure Generation Model	Figure 12-1
URS			



Project No. 26814536	Chabot Dam Seismic Stability Analysis	Mohr-Coulomb and Residual Strength Envelope	Figure
URS			12-2

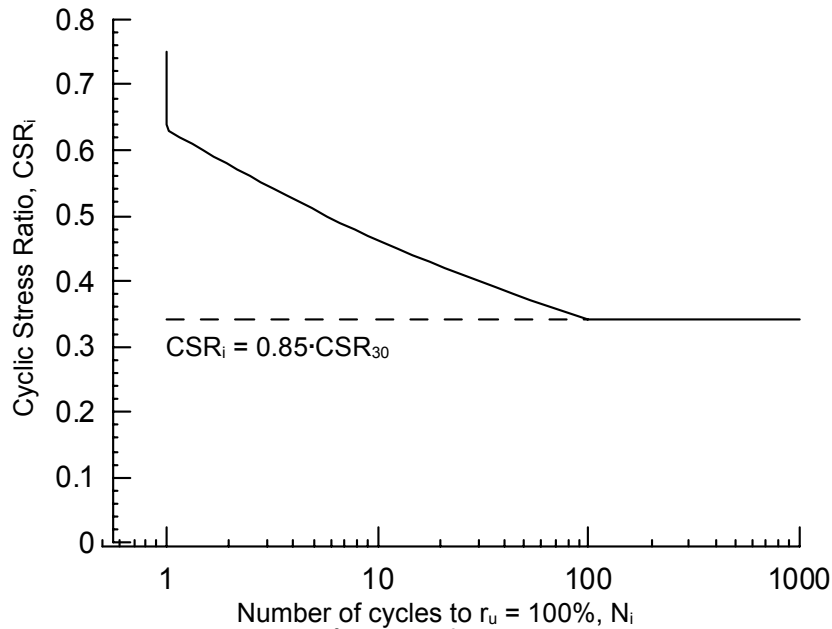


$$N_i = 15 \left(\frac{CSR_{15}}{CSR_i} \right)^{2.05} \quad 1 \leq N_i \leq 40$$

where $CSR_{15} = 0.11$

Project No. 26814536	Chabot Dam Seismic Stability Analysis	Cyclic Strength of Saturated Sluiced Fill	Figure
URS			12-3

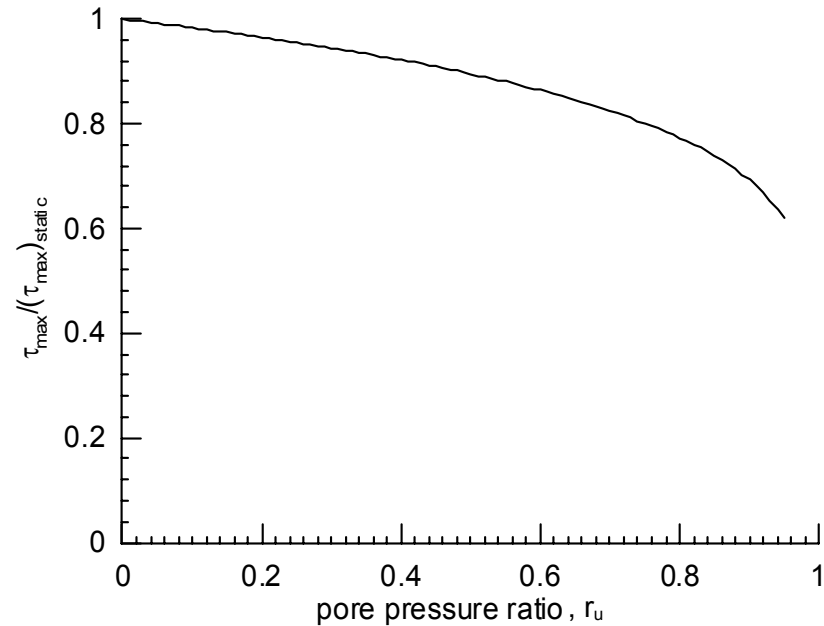
Cyclic Strength
 $CSR_{30} = 0.4$



$$N_i = 30 \left(\frac{CSR_{30}}{CSR_i} \right)^{7.41} \quad 1 \leq N_i \leq 100$$

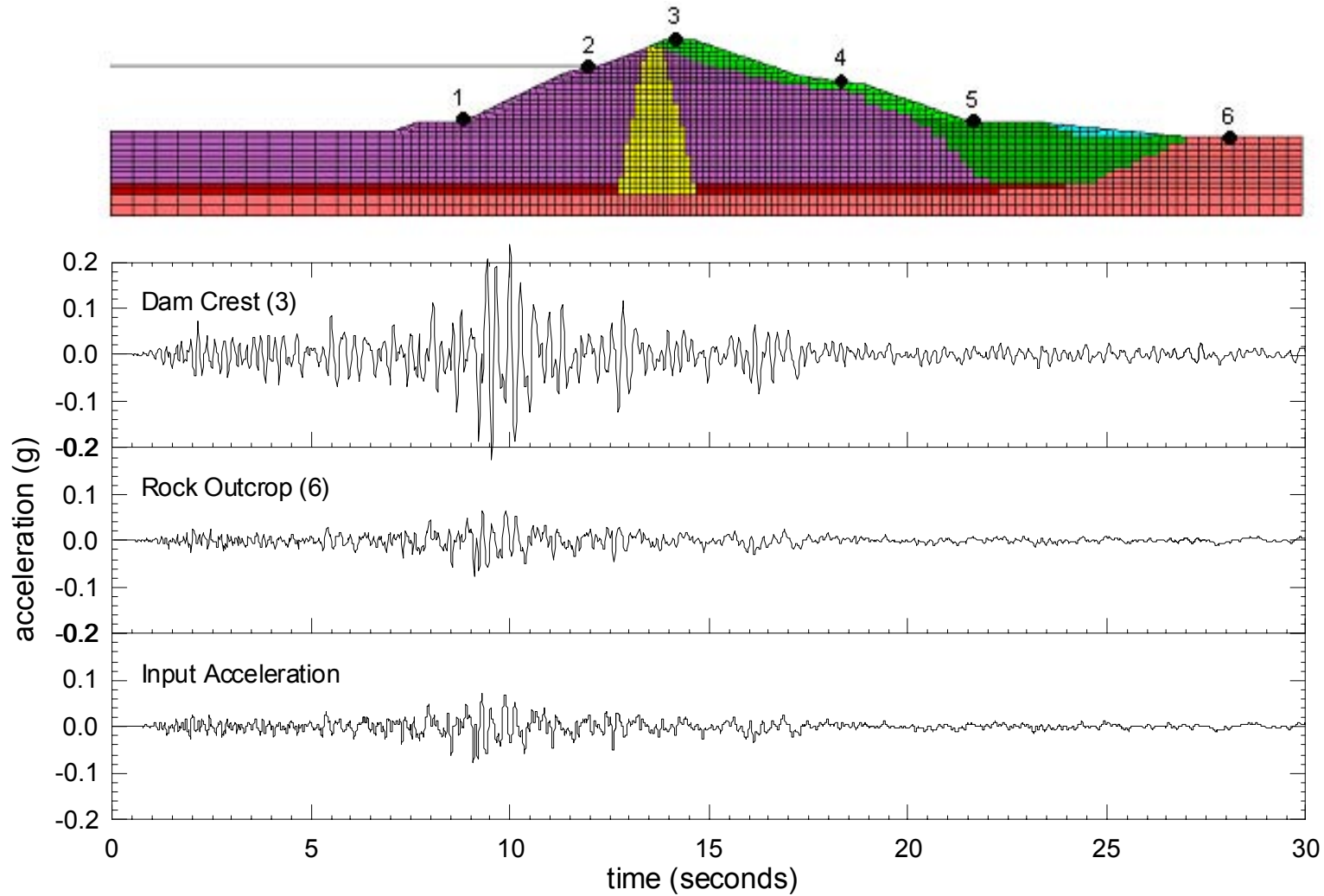
where $CSR_{30} = 0.4$

Strength Degradation



$$\frac{\tau_{max}}{(\tau_{max})_{static}} = (1 - r_u)^{0.16}$$

Project No. 26814536	Chabot Dam Seismic Stability Analysis	Cyclic Strength and Undrained Strength Degradation of Saturated Wagon Fill and Foundation Soils	Figure 12-4
URS			



Project No. 26814536	Chabot Dam Seismic Stability Analysis	Acceleration at Dam Crest and Rock Outcrop 1989 Loma Prieta Earthquake	Figure 12-5
URS			

JOB TITLE : Chabot Dam Non-linear Dynamic Response Analysis

(*10^2)

FLAC (Version 4.00)

LEGEND

16-Jan-05 18:43

step 868525

Cons. Time 6.2628E+08

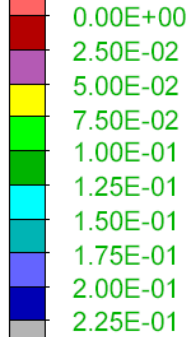
-5.583E+02 <x< 6.083E+02

-4.133E+02 <y< 7.533E+02

Grid plot



sd_pore_pres

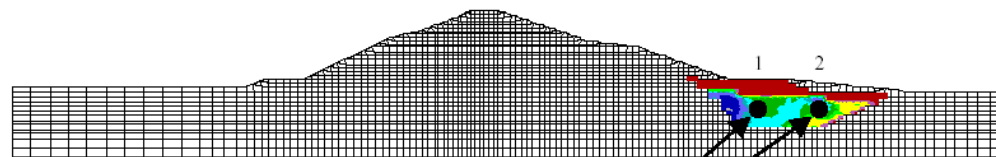


Contour interval= 2.50E-02

URS
Oakland

Pore Pressure Ratio

Max $r_u = 0.23$



pore pressure
recording points

-4.000 -2.000 0.000 2.000 4.000 6.000
(*10^2)

7.000
5.000
3.000
1.000
-1.000
-3.000

Project No.
26814536

Chabot Dam
Seismic Stability Analysis

Excess Pore Pressure Ratio
in Sluiced Fill
1989 Loma Prieta Earthquake

Figure
12-6



JOB TITLE : Chabot Dam Non-linear Dynamic Response Analysis

FLAC (Version 4.00)

LEGEND

16-Jan-05 18:43

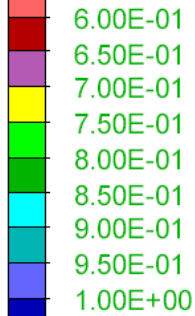
step 868525

Cons. Time 6.2628E+08

-5.583E+02 <x< 6.083E+02

-4.133E+02 <y< 7.533E+02

cd_degradati



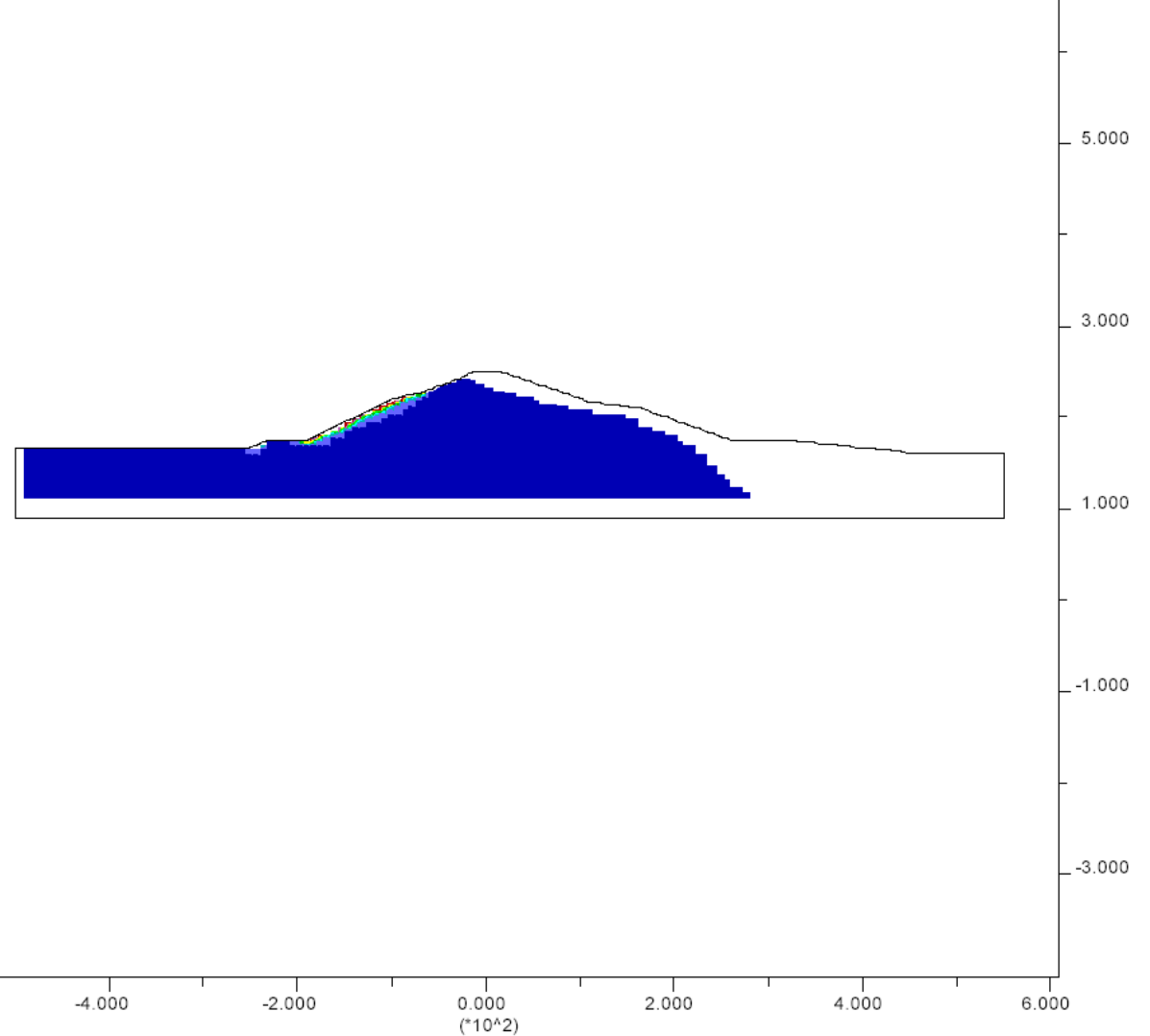
Contour interval= 5.00E-02

Boundary plot



URS
Oakland

Cyclic Degradation of Wagon Fill



Project No. 26814536	Chabot Dam Seismic Stability Analysis	Cyclic Degradation of Wagon Fill and Foundation Soils 1989 Loma Prieta Earthquake	Figure 12-7
URS			

FLAC (Version 4.00)

LEGEND

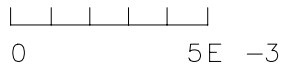
16-Jan-05 18:43
 step 868525
 Cons. Time 6.2628E+08
 -5.583E+02 <x< 6.083E+02
 -4.133E+02 <y< 7.533E+02

User-defined Groups

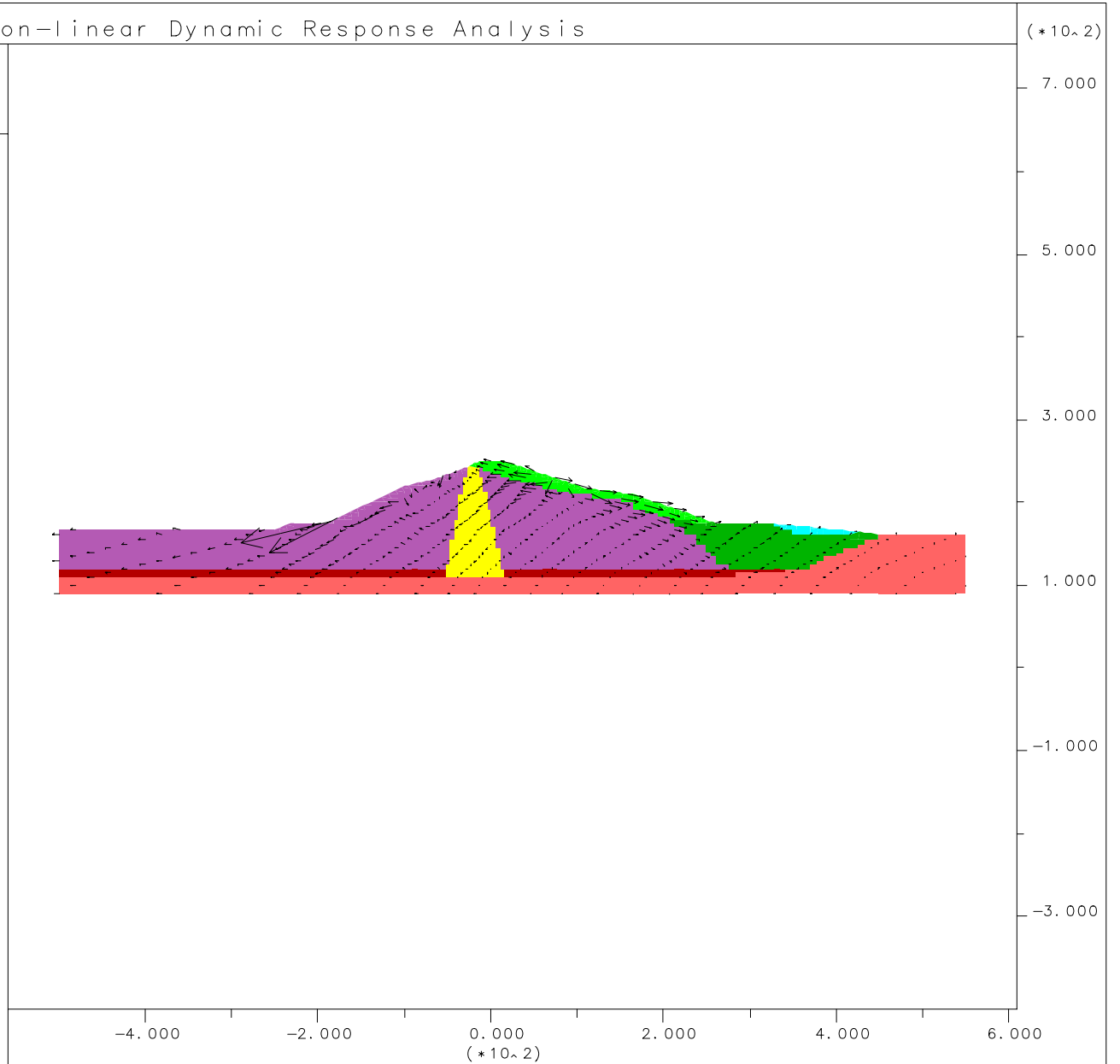
- Bedrock
- Foundation_Soils
- Wagon_Fill
- Wagon_Fill_Core
- Modern_Fill
- Sluiced_Fill
- Random_Fill

Displacement vectors

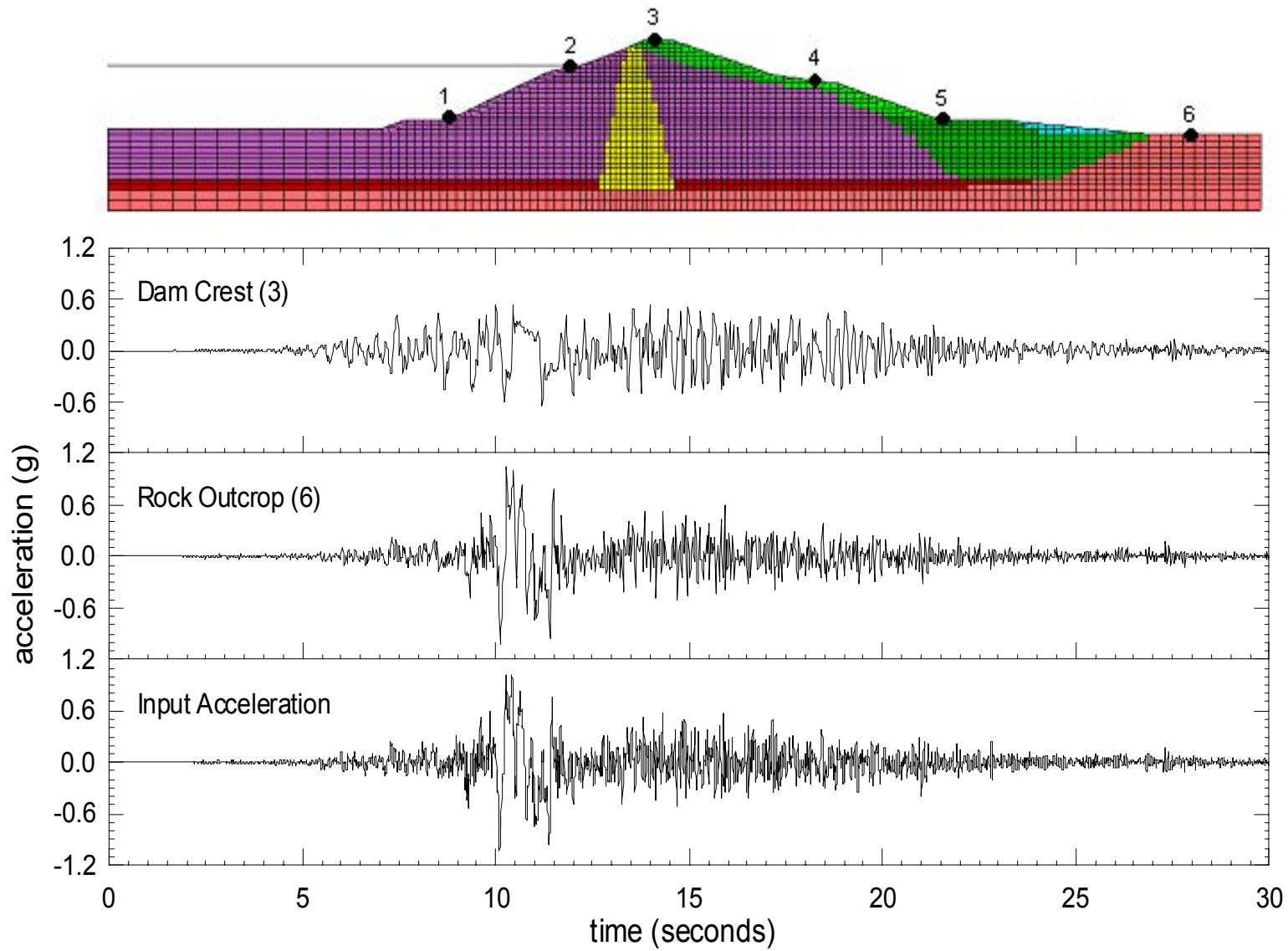
Max Vector = 2.737E-03



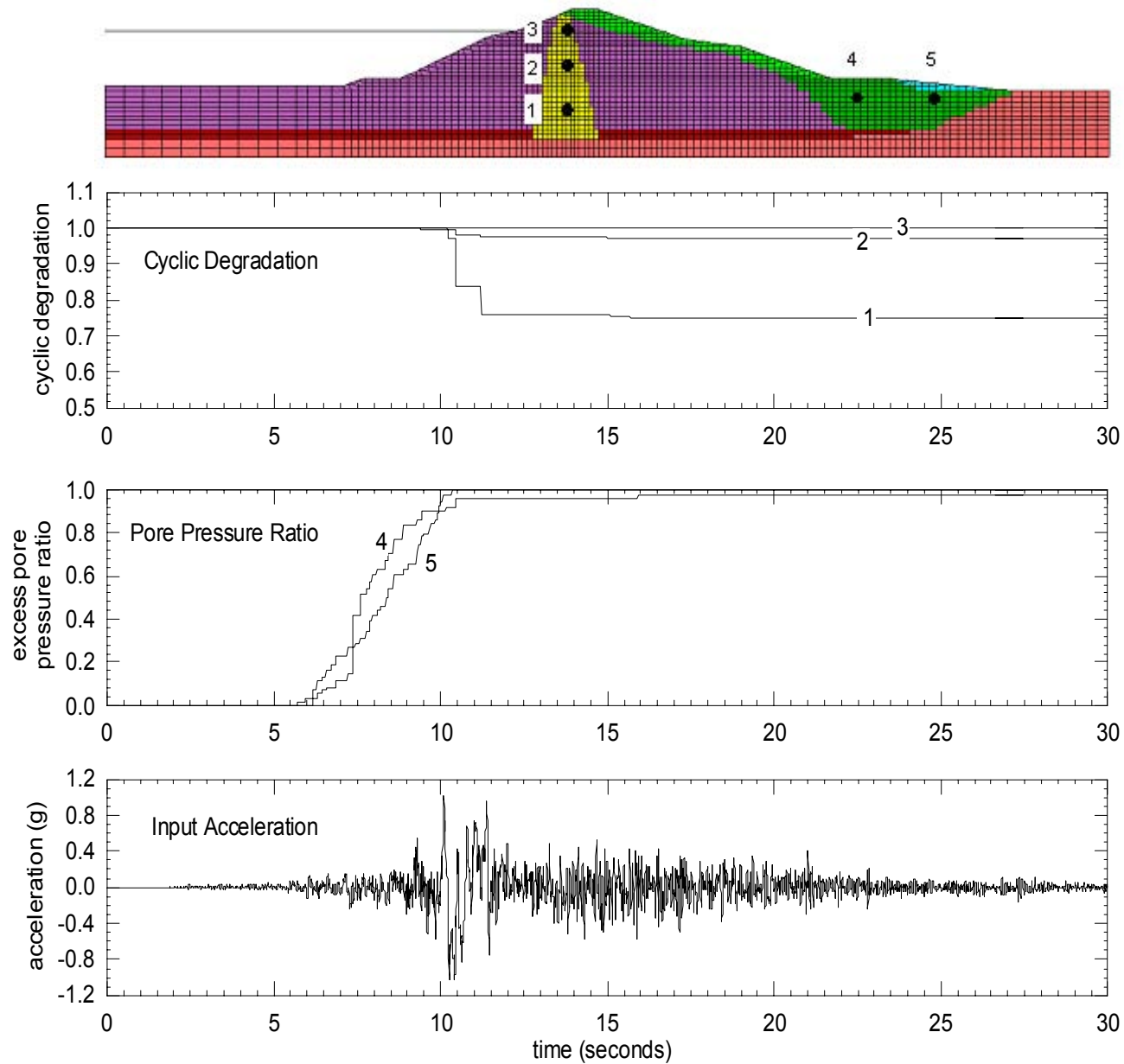
URS
 Oakland



Project No. 26814536	Chabot Dam Seismic Stability Analysis	Calculated Displacement Vectors 1989 Loma Prieta Earthquake	Figure 12-8
URS			



Project No. 26814536	Chabot Dam Seismic Stability Analysis	Acceleration at Dam Crest and Rock Outcrop Hayward Fault MCE TH #1	Figure
URS			12-9



Project No. 26814536	Chabot Dam Seismic Stability Analysis	Time Histories of Cyclic Degradation and Pore Pressure Ratio Hayward Fault MCE TH #1	Figure 12-10
URS			

JOB TITLE : Chabot Dam Non-linear Dynamic Response Analysis

(*10^2)

FLAC (Version 4.00)

LEGEND

1-Feb-05 1:45

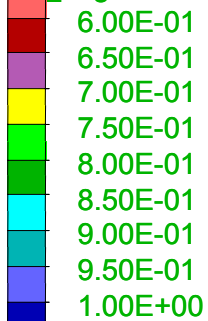
step 868525

Cons. Time 6.2628E+08

-5.583E+02 <x< 6.083E+02

-4.133E+02 <y< 7.533E+02

cd_degradati



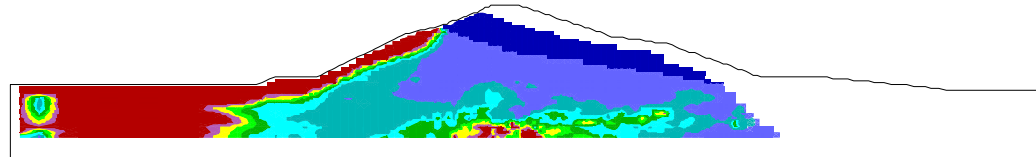
Contour interval= 5.00E-02

Boundary plot



URS
Oakland

Cyclic Degradation of Wagon Fill



-4.000 -2.000 0.000 2.000 4.000 6.000 (*10^2)

7.000
5.000
3.000
1.000
-1.000
-3.000

Project No. 26814536	Chabot Dam Seismic Stability Analysis	Cyclic Degradation of Saturated Wagon Fill and Foundation Soils Hayward Fault MCE TH #1	Figure 12-11
URS			

FLAC (Version 4.00)

LEGEND

1-Feb-05 1:45
 step 868525
 Cons. Time 6.2628E+08
 -5.583E+02 <x< 6.083E+02
 -4.133E+02 <y< 7.533E+02

User-defined Groups

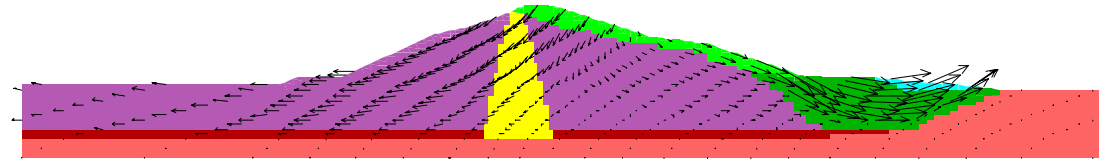
- Bedrock
- Foundation_Soils
- Wagon_Fill
- Wagon_Fill_Core
- Modern_Fill
- Sluiced_Fill
- Random_Fill

Displacement vectors

Scaled to Max = 1.000E+01
 Max Vector = 4.749E+00

 0 2E 1

URS
 Oakland



-4.000 -2.000 0.000 2.000 4.000 6.000 (* 10^-2)

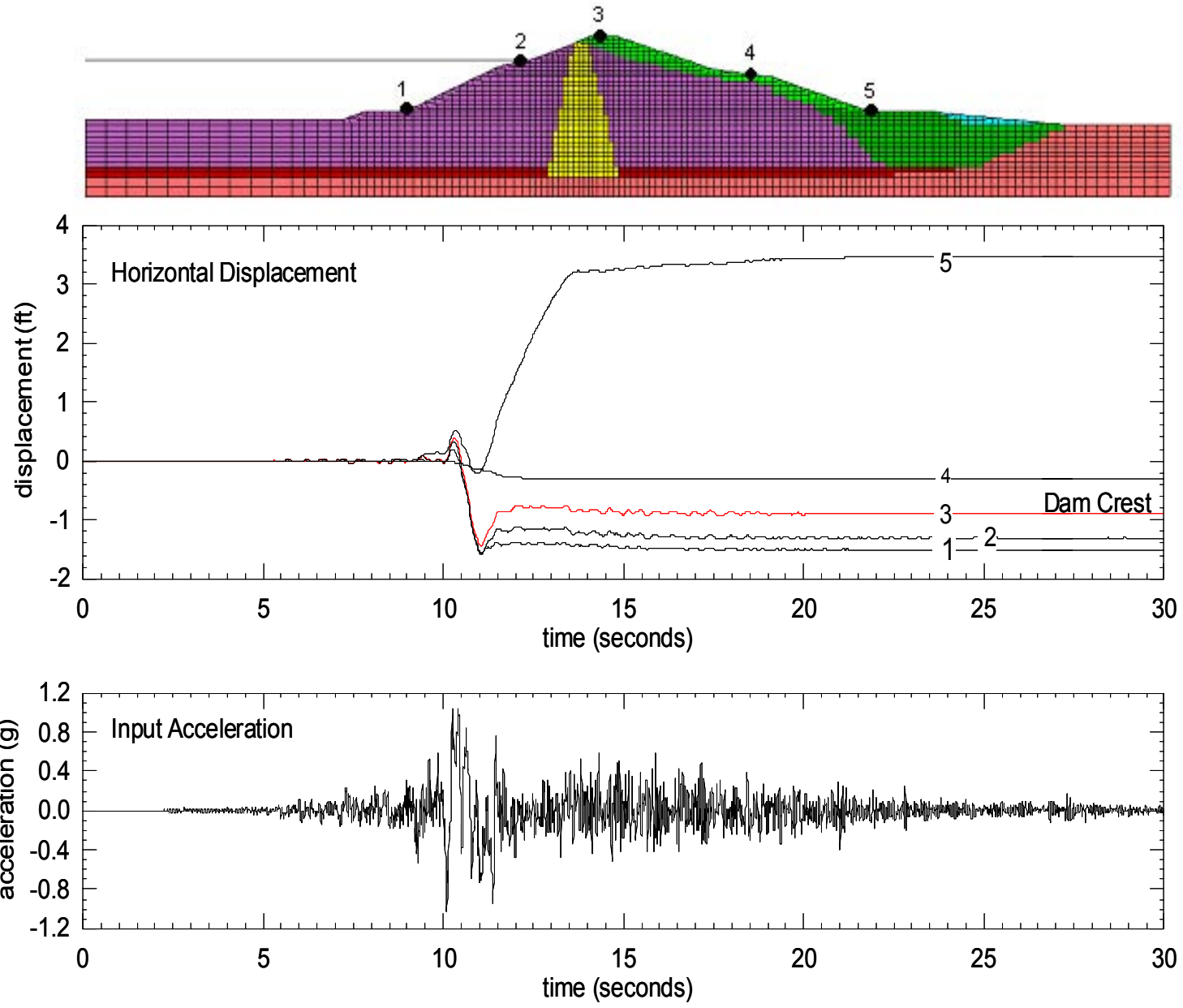
Project No.
26814536

Chabot Dam
Seismic Stability Analysis

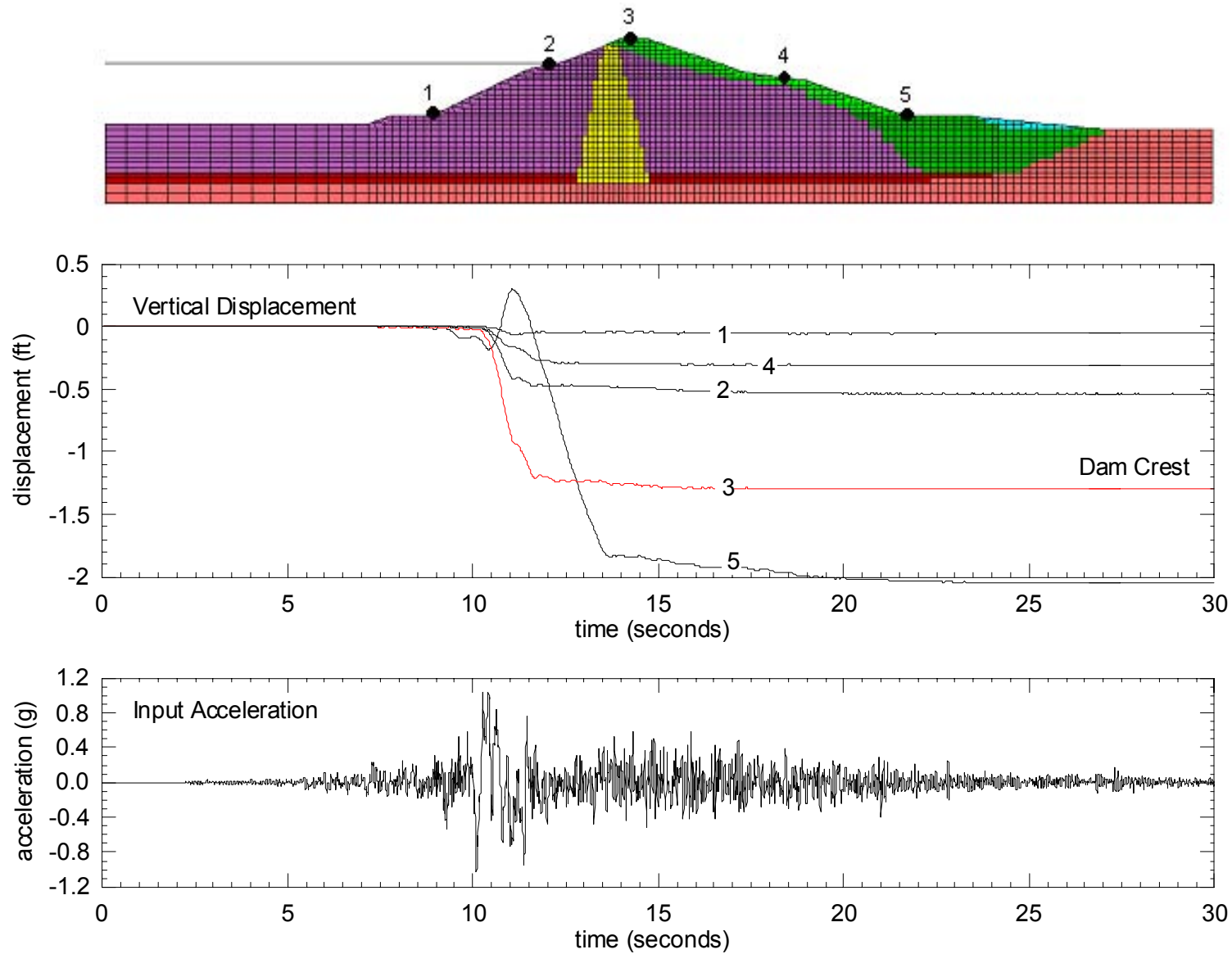
Calculated Displacement Vectors
Hayward Fault MCE TH #1

Figure
12-12





Project No. 26814536	Chabot Dam Seismic Stability Analysis	Calculated Horizontal Displacement Time Histories Hayward Fault MCE TH #1	Figure 12-13
URS			



Project No. 26814536	Chabot Dam Seismic Stability Analysis	Calculated Vertical Displacement Time Histories Hayward Fault MCE TH #1	Figure 12-14
URS			

JOB TITLE : Contours of Shear Strain Rate

(*10^-2)

FLAC (Version 4.00)

LEGEND

12-Jan-05 12:52

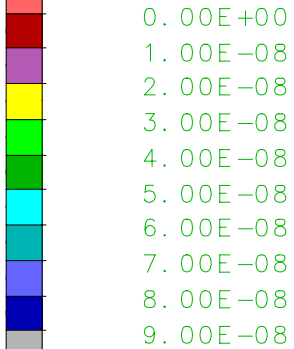
step 919635

Cons. Time 6.2628E+08

-5.583E+02 <x> 6.083E+02

-4.133E+02 <y> 7.533E+02

Max. shear strain-rate



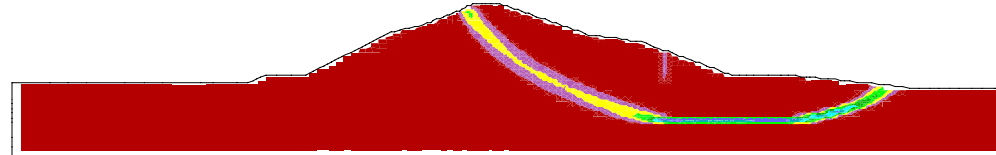
Contour interval = 1.00E-08

Boundary plot



URS
Oakland

Post-Shaking Stability Analysis (downstream)
FOS = 1.81



-4.000 -2.000 0.000 2.000 4.000 6.000
(*10^-2)

7.000
5.000
3.000
1.000
-1.000
-3.000

Project No.
26814536

Chabot Dam
Seismic Stability Analysis

Post-Earthquake Stability of
Downstream Slope
Hayward Fault MCE TH #1

Figure
12-15

URS

JOB TITLE : Contours of Shear Strain Rate

(*10^-2)

FLAC (Version 4.00)

Post-Shaking Stability Analysis (upstream)
FOS = 2.08

LEGEND

12-Jan-05 12:18
step 1024949
Cons. Time 6.2628E+08
-5.583E+02 <x< 6.083E+02
-4.133E+02 <y< 7.533E+02

Max. shear strain-rate

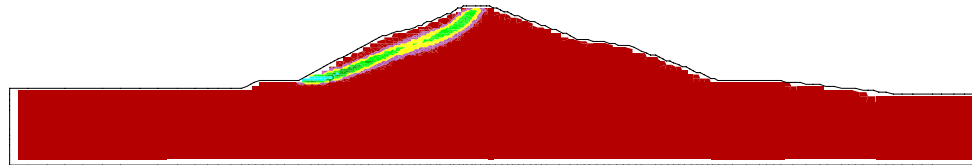


Contour interval = 5.00E-08

Boundary plot



URS
Oakland



-4.000 -2.000 0.000 2.000 4.000 6.000 (*10^-2)

7.000
5.000
3.000
1.000
-1.000
-3.000

Project No.
26814536

Chabot Dam
Seismic Stability Analysis

Post-Earthquake Stability of
Upstream Slope
Hayward Fault MCE TH #1

Figure
12-16



The expected performance of the dam during the design earthquake was evaluated based on the analyses presented in Sections 11 and 12. Overall, the analyses indicate that the dam will experience deformations during such earthquake, but will remain stable. No liquefaction of the wagon fill is expected because of its overall clayey nature, but the earthquake is likely to induce high excess pore pressures in these materials with accompanying strength reduction. Likewise, no liquefaction of the foundation soils is expected, except possibly in isolated pockets of sands and gravels. Such pockets appear to be confined primarily to near the stream channel and are unlikely to affect the overall stability of the dam. The sluiced fill at the downstream toe of the dam is expected to liquefy early in the strong shaking phase of the earthquake and to deform subsequently.

The Newmark analyses for the Hayward fault MCE result in calculated downward displacements of the crest less than about 6 feet. The FLAC analyses result in downward crest displacements less than 1.5 feet. Considering the limitations of the methods of analysis, the best estimate of the maximum crest vertical displacements is between 1.5 and 3.5 feet. These settlements correspond to about 1.1% to 2.5% of the structural dam height. Such settlement estimates are generally consistent with the past seismic performance of embankment dams (URS, 2001), considering the age of Chabot Dam and the methods used for its construction.

Horizontal displacements of up to about 12 feet are calculated from the Newmark analyses for sliding blocks near the upstream face of the dam, but such blocks do not extend into the main body of the embankment and do not reach across the dam crest. Horizontal displacements of less than 2 feet are calculated from the FLAC analyses. The best estimate of horizontal displacements of the upstream slope is less than 5 feet. Because the calculated displacements are limited and the blocks will remain stable, progressive sliding of the dam and instability of the crest are not expected to occur.

Except for the sluiced fill, horizontal displacements of the downstream slope are expected to be less than 2 feet. Horizontal displacements of about 4 feet are calculated for a sliding block that primarily encompasses the sluiced fill. However, displacements of several feet may occur in the sluiced fill in the direction of the downstream channel. The stability analyses indicate that such displacements, however, are unlikely to lead to instability of the main body of the embankment.

Because the dam has a freeboard of about 23 feet, the estimated crest settlements will not lead to overtopping of the embankment. The dam deformations are also not expected to affect the structural integrity of the spillway since it is founded on rock. Likewise, they will not affect the outlet works. However, the estimated settlements and horizontal deformations will likely result in cracking of the dam embankment.

Based on the calculated deformations and the observed performance of similar embankment dams during past earthquakes, cracking is expected to develop primarily near the crest. Longitudinal cracks can be expected to form at the crest in response to the tendency for spreading caused by lateral deformation of the embankment. Settlements of the embankment may also lead to transverse cracking at the crest. Transverse cracking is most likely to develop near the abutments because of their steep nature, although it can develop elsewhere along the crest in response to possible differential settlements. Transverse cracking is of particular concern as it could provide a mechanism for leakage, if it were to extend below the reservoir level and to be continuous from the reservoir to the downstream slope or to be interconnected with longitudinal cracking in pathways across the dam crest.

The extent and depth of cracking are difficult to estimate accurately, although they can be roughly assessed by comparison with the past performance of other embankment dams. Published compilations of the past seismic performance of embankment dams (e.g. Fong and Bennett, 1995) suggest that the depth of transverse cracking is roughly correlated to the maximum amount of crest settlement. However, the maximum depth of cracking will be constrained by the nature and strength of the embankment materials near the crest and their ability to support open cracks.

The performance of Austrian Dam during the 1989 Loma Prieta earthquake is a relevant case history to the assessment of potential cracking at Chabot Dam during the design earthquake. Austrian Dam, a 185-foot-high embankment, experienced transverse and longitudinal cracking during the Loma Prieta earthquake, a magnitude 6.9 event. That dam was subjected to ground motions with a peak horizontal acceleration of about 0.6 g and experienced crest settlements of up to 2.9 feet. Fong and Bennett (1995) report that transverse cracking developed across the crest at the dam abutments to a depth of about 16 feet. USCOLD (1992) reports that a transverse crack was traced 30 feet down the left abutment, where the dam had been constructed on highly fractured rock, and that transverse cracking and embankment separation from the spillway structure occurred to a depth of 23 feet on the right abutment.

The potential for developing through-going transverse cracks at Chabot Dam will be tempered by the considerable width of the embankment (about 150 feet at the elevation of the spillway crest). In addition, the likelihood of leakage will be a function of the reservoir level at the time of the earthquake (over the last 5 years, EBMUD readings show that reservoir levels have remained 1 to 6 feet below spillway crest elevation). Nonetheless, transverse cracking that extends below the reservoir elevation, even if not fully continuous across the embankment, would increase seepage and the potential for leakage immediately after the earthquake. On this basis and given that the dam lacks an internal filter and drainage system to safely control possible leakage and its consequent effects, it may be concluded that the potential for transverse cracking represents a risk regarding the safety of the structure.

No active faults underlie the dam and the potential for sympathetic movement on faults passing beneath the dam is judged to be very small. Nonetheless, previous studies have concluded that if sympathetic movement were to occur on those faults in response to a large earthquake on the Hayward fault, such movement would be less than 1 foot (Marliave, 1978; WCC, 1978), and the dam would be able to safely withstand the effects of such movement (EBMUD, 1978). Those earlier conclusions seem reasonable in light of the investigations reported herein.

The analyses for the San Andreas fault MCE result in a dynamic response of the embankment lower than that calculated for the Hayward fault MCE. Nonetheless, liquefaction and deformations of the sluiced fill are also expected to occur during the San Andreas fault MCE. The calculated dam deformations for the San Andreas event are lower than those for the Hayward event. Thus, the results of the analyses indicate that the San Andreas event is less critical than the Hayward event regarding the seismic stability of the dam.

In summary, the results of the seismic stability analyses indicate that the dam is likely to undergo deformations, including crest settlements of a few feet, during the Hayward fault MCE. However, the dam is expected to remain stable after the earthquake. Gross instability of the main embankment is unlikely to occur, although displacements of several feet may develop in the sluiced fill downstream of the dam. Likewise, horizontal displacements of up to about 5 feet

may occur in the near-surface upstream slope. The expected displacements will be associated with damage and cracking of the embankment but will not affect the integrity of the spillway or the outlet works.

The purpose of this study was to evaluate the seismic stability of Chabot Dam. The study included a review of previous engineering investigations and geologic studies of the dam, geologic mapping of the site, field exploration and laboratory testing of the embankment and foundation materials, evaluation of the design earthquake ground motions, analyses of seismic stability and deformations, and assessment of the overall expected seismic performance of the dam. The main conclusions from the study are summarized as follows.

The main body of the dam is composed of so-called “wagon fill,” which consists predominantly of clayey sands and sandy clays with gravel, placed and compacted by teams of horses and wagons. The wagon fill is buttressed at the downstream toe with “sluiced fill” consisting primarily of clayey and silty sands with gravel, with interspersed lenses of clays and gravelly sands. Modern engineered fill was placed in 1980 on the crest and downstream slope of the embankment to raise the dam by 7 feet to its current configuration.

The thickness of foundation soils near the stream channel is generally less than 10 feet. A wedge of foundation soils 20 to 25 feet thick underlies the embankment east of the stream channel. A similar wedge underlies the downstream toe area on the west side. The materials consist primarily of clayey sands and sandy clays with gravel, similar to the wagon fill materials. Occasional pockets of sand and gravels are encountered primarily near the stream channel.

The site is underlain by Mesozoic rocks consisting of shale and siltstone beneath the dam upstream shell; rhyolite beneath the midsection of the dam; and basalt, serpentinite, and gabbro beneath the downstream shell. Faults within and between these rocks formed prior to the late Cenozoic and are no longer active. No weaknesses that could affect the stability of the dam have been previously mapped in the bedrock, and from a stability viewpoint the rock mass is much stronger than the embankment and foundation soils.

The dam is located within 0.5 km of the Hayward fault and 30 km of the San Andreas fault. The Hayward-Rodgers Creek fault is judged capable of generating a maximum earthquake of magnitude M_w 7¼. The San Andreas fault is judged capable of a M_w 8 earthquake. In accordance with DSOD guidelines, the ground motions from these earthquakes were estimated at the 84th-percentile level. The ground motions for the MCE on the Hayward fault are associated with a peak horizontal ground acceleration (PGA) of 1.05 g whereas those for the San Andreas fault MCE correspond to a PGA of 0.33 g. No active faults underlie the dam and the potential for sympathetic movement on faults passing beneath the dam is judged to be very small.

Because of their clayey nature, the wagon fill materials will exhibit cohesive behavior under earthquake shaking and are not susceptible to liquefaction. However, they may develop excess pore pressures and undergo strength loss under strong earthquake shaking. Pockets of sands and silty sands within the wagon fill are of limited extent and will not affect the strength of the overall zone. The sluiced fill is likely to exhibit cohesionless behavior and is likely to liquefy under strong earthquake shaking. Its liquefaction resistance is best assessed in terms of its SPT resistance. Because of their clayey nature, the foundation soils are also not susceptible to liquefaction, except for interspersed pockets of sands and gravels. However, such pockets seem confined primarily to the stream channel, and are unlikely to affect the overall stability of the dam.

The results of the analysis indicate adequate factors of safety for the upstream and downstream slopes under long-term static conditions, in good agreement with the known long-term stability

of the dam. The dam should perform satisfactorily during relatively minor earthquakes that do not trigger liquefaction of the sluiced fill or generate high pore pressures within the wagon fill.

The dam is likely to undergo deformations, including crest settlements of a few feet, during the Hayward fault MCE. However, the dam is expected to remain stable after the earthquake. Gross instability of the main embankment is unlikely to occur, although displacements of several feet may develop in the sluiced fill downstream of the dam. Likewise, horizontal displacements of up to about 5 feet may occur in the near-surface upstream slope.

Crest settlements induced by the Hayward fault MCE are likely to be less than about 6 feet. The best estimate of the maximum settlements is between 1.5 and 3.5 feet. Such settlements correspond to about 1.1% to 2.5% of the structural dam height. Except for the sluiced fill, horizontal displacements of the downstream slope are expected to be less than 2 feet.

Because the dam has a freeboard of about 23 feet, the estimated crest settlements will not lead to overtopping of the embankment. However, the expected deformations will be associated with damage and cracking of the embankment and may require drawdown of the reservoir immediately after the earthquake. The estimated dam deformations are not expected to affect the structural integrity of the spillway or outlet works.

Transverse cracking of the crest is most likely to develop near the abutments and could provide a mechanism for leakage, if it were to extend below the reservoir level and be continuous across the dam embankment. The potential for developing through-going transverse cracks will be tempered by the width of the embankment. Nonetheless, transverse cracking that extends below the reservoir elevation, even if not continuous across the embankment, would increase seepage and the potential for leakage immediately after the earthquake. Because the dam lacks an internal filter and drainage system, the potential for transverse cracking represents a risk regarding the safety of the dam.

Liquefaction and deformations of the sluiced fill are also expected to occur during the San Andreas fault MCE. The calculated dam deformations for the San Andreas event are lower than those for the Hayward event. Thus, the San Andreas event is less critical than the Hayward event regarding the seismic stability of the dam.

The calculated response of the dam for motions representative of those expected to have occurred at the site during the 1989 Loma Prieta earthquake is in good agreement with the known performance of the dam during that earthquake.

- Abrahamson, N.A. (1993). "Non-Stationary Spectral Matching Program RSPMATCH," Unpublished Report, July.
- Abrahamson, N.A. and Silva, W.J. (1997). "Empirical response spectral attenuation relations for shallow crustal earthquakes," *Seismological Research Letters*, v. 68, p. 94-127.
- Abrahamson, N.A. (2000) "Effects of rupture directivity on probabilistic seismic hazard analysis," *Proceedings of the 6th International conference on Seismic Zonation*, Palm Springs, California.
- Andrews, D. and Martin, G.R. (2000) "Criteria for liquefaction susceptibility of silty soils," *Proc. 12th World Conference on Earthquake Engineering*, Auckland, New Zealand.
- Boore, D.M., Joyner, W.B., and Fumal, T.E. (1997). "Equations for estimating horizontal response spectra and peak acceleration from western North American earthquakes: A summary of recent work," *Seismological Research Letters*, v. 68, p. 128-153.
- Boulanger, R.W. and Idriss, I.M. (2004). "Evaluating the potential for liquefaction or cyclic failure of silts and clays," *Center for Geotechnical Modeling, Report No. UCD/CGM-04/01*, University of California, Davis, December.
- Bray, J.D. et al. (2001) "Ground failure in Adapazari, Turkey," *Proc., Earthquake Geotechnical Engineering Satellite Conference of the XVth International Conference on Soil Mechanics and Geotechnical Engineering*, Istanbul, Turkey, August.
- Duncan, J.M., Wright, S.G. and Wong, K.S. (1990) "Slope stability during rapid drawdown," *Proc., H.B. Seed Memorial Symp., BiTech, Vancouver, B.C., (2)*, 253-272.
- EBMUD (1978) "Chabot Dam and sympathetic fault movement," Letter to J. Doody of DSOD from D. Larkin of EBMUD, dated October 31.
- Fong, F.C. and Bennett, W.J. (1995) "Transverse cracking on embankment dams due to earthquakes," presented at the Association of State Dam Safety Officials (ASDSO) Western Regional Seminar and Conference, Red Lodge, Montana, May.
- Fraser, W.A. and Howard, J.K. (2002), "Guidelines for use of the Consequence-Hazard Matrix and selection of ground motion parameters," *The Resources Agency, Department of Water Resources, Division of Safety of Dams*.
- Fumal, T.E. (1978). "Correlations between seismic wave velocities and physical properties of near-surface geologic materials in the southern San Francisco Bay region, California," *Open-file Report 78-1067*, National Center for Earthquake Research, United States Department of the Interior Geological Survey.
- Itasca, (2000). "FLAC, fast lagrangian analysis of continua, version 4.0, user's guide," Itasca Consulting Group, Inc., Thrasher Square East, 708 South Third Street, Suite 310, Minneapolis, Minnesota.
- Hudson M., Idriss, I.M. and Beikae, M. (1994) "User's manual for QUAD4M," *Department of Civil and Environmental Engineering, University of California, Davis, California*, May.

- Harder, L.F. and Seed, H.B. (1986) "Determination of penetration resistance of coarse-grained soils using the Becker hammer drill," Earthquake Engineering Research Center, Report No. UCB/EERC-86/06, University of California, Berkeley.
- Harder, L.F. and Boulanger, R.W. (1997) "Application of K_{σ} and K_{α} Correction Factors," Proceedings of the NCEER Workshop on Evaluation of Liquefaction Resistance of Soils, Report NCEER-97-0022, National Center for Earthquake Engineering Research, SUNY Buffalo, N.Y., pp. 41-87.
- Idriss, I.M. (1985) "Evaluating seismic risk in engineering practice," Proceedings 11th International Conference on Soil Mechanics and Foundation Engineering, San Francisco, August.
- Idriss, I.M. (2002) "Evaluation of liquefaction potential during earthquakes," personal communication.
- Idriss, I.M. and Boulanger, R.W. (2002) "Estimating K_{α} for use in evaluating cyclic resistance of sloping ground," Proceedings of the 8th U.S.-Japan Workshop on Earthquake Resistance Design of Lifeline Facilities and Countermeasures Against Liquefaction, Tokyo, Japan, December.
- Lee, K.L. and Focht, J.A. (1976) "Strength of clay subjected to cyclic loading," Marine Geotechnology, Vol 1, No. 3, pp 165-185.
- Lilhanand, K. and Tseng, W.S. (1988). "Development and application of realistic earthquake time histories compatible with multiple-damping design spectra," Proceeding of the 9th World Conference on Earthquake Engineering, Tokyo-Kyoto, Japan, August.
- Lienkaemper, J.J. (1992) "Map of recently active traces of the Hayward fault, Alameda and Contra Costa Counties, California," USGS Miscellaneous Field Studies Map MF-2196.
- Marliave, C. (1933) "Geological report on chabot dam situated on San Leandro Creek in Alameda County," report prepared for State of California, Department of Public Works, Division of Water Resources, August.
- Marliave, B. H. (1978), "Chabot dam and sympathetic movement on the Hayward fault," letter report to EBMUD, September.
- Mejia, L.H. (1989) "Three-dimensional stability of an old dam," Proceedings 12th International Conference on Soil Mechanics and Foundation Engineering, Rio de Janeiro, August.
- Sadigh, K., Chang, C.Y., Egan, J.A., Makdisi, F., and Youngs, R.R. (1997). "Attenuation relationships for shallow crustal earthquakes based on California strong motion data," Seismological Research Letters, v. 68, p. 180-189.
- Schnabel, P.B., Lysmer, J. and Seed, H.B. (1982) "SHAKE: A computer program for earthquake response analysis of horizontally layered sites," Report No. UC/EERC-72/12, Earthquake Engineering Research Center, University of California, Berkeley, December.
- Seed, H.B., and Idriss, I.M, (1970). "Soil moduli and damping factors for dynamic response analyses," Report No. EERC 70-10, Earthquake Engineering Research Center, University of California, Berkeley.

- Seed, H.B. (1979) "Soil liquefaction and cyclic mobility evaluation for level ground during earthquakes," *Journal of the Geotechnical Engineering Division, ASCE*, Vol. 105 No. GT2, pp 201-255.
- Seed, H.B. (1979) "Considerations in the earthquake-resistant design of earth and rockfill dams," *Geotechnique*, 29(3), Sept., pp 215-263.
- Seed, H.B. and Idriss, I.M. (1982) "Ground motions and soil liquefaction during earthquakes," EERI Monograph, Earthquake Engineering Research Institute.
- Seed, R.B., Cetin, K.O., Moss, R.E.S., Kammerer, A., Wu, J., Pestana, J., Riemer, M., Sancio, R.B., Bray, J.D., Kayen, R.E. and Faris, A. (2003) "Recent advances in soil liquefaction engineering: a unified and consistent framework," Report No. EERC 2003-06, (originally presented at 26th Annual ASCE Los Angeles Geotechnical Spring Seminar, Keynote Presentation, H.M.S. Queen Mary, April 30, 2003, Long Beach, CA), Earthquake Engineering Research Center, University of California, Berkeley, June.
- Shannon & Wilson, Inc. (1965) "Review of stability, Chabot Dam," report prepared for EBMUD, September.
- Somerville, P.G., Smith, N.F., Graves, R.W., and Abrahamson, N.A. (1997). "Modification of empirical strong ground motion attenuation relations to include the amplitude and duration effects of rupture directivity," *Seismological Research Letters*, V. 68, n.1, pp. 199-222.
- Sy, A. and Campanella, R.G. (1994) "Becker and standard penetration tests (BPT-SPT) correlations with consideration of casing friction", *Canadian Geotechnical Journal*, V. 31, 343-356.
- Thiers, G.R. and Seed, H.B. (1969) "Strength and stress-strain characteristics of clays subjected to seismic loads," *Symposium on Vibration Effects of Earthquakes on soils and Foundations, ASTM STP 450*, pp 3-56.
- URS (2001) "Seismic safety assessment and prioritization studies of Waitaki hydroelectric system dams, Phase 2, Task 31100 – Updated review of embankment dam seismic performance," Client report prepared for Meridian Energy Ltd., March.
- USCOLD (1992) "Observed Performance of Dams During Earthquakes," Report prepared by USCOLD Committee on Earthquakes, United States Committee on Large Dams, July.
- Wells, D.L. and Coppersmith, K.J., (1994) "New empirical relationships among magnitude, rupture length, rupture width, rupture area, and surface displacement," *Bulletin of the Seismological Society of America*, v. 84, p. 974-1002.
- Woodward-Lundgren & Associates (1974) "Evaluation of the seismic stability of Chabot Dam," report prepared for EBMUD, May.
- Woodward-Clyde Consultants (1977) "Evaluation of seismic stability of Chabot Dam modification," Client report prepared for EBMUD, August.
- Woodward-Clyde Consultants (1978) "Potential for sympathetic fault displacement, Chabot fault and cross fault traces," Letter report submitted to EBMUD, dated October 5.

- Woodward-Clyde Consultants (1979) "Geologic inspection, Chabot Dam, Alameda County, California," letter report prepared for EBMUD, September.
- Woodward-Clyde Consultants (1989) "Seismic Safety Evaluation, Lake Madigan Dam, Solano County, California," Client report prepared for City of Vallejo, July.
- Wright, S.G. (1991) "UTEXAS3, a computer program for slope stability calculations," Shinoak Software, Austin, Texas.
- Youd, T.L., Idriss, I.M., Andrus, R.D., Arango, I., Castro, G., Christian, J.T., Dobry, R., Finn, W.D., Harder, L.F., Hynes, M.E., Ishihara, K., Koester, J.P., Liao, S., Marcuson, W.F., Martin, G.R., Mitchell, J.K., Moriwaki, Y., Power, M.S., Robertson, P.K., Seed, R.B., and Stokoe, K.H. (2001) "Liquefaction resistance of soils: Summary report from the 1996 NCEER and 1998 NCEER/NSF workshops on evaluation of liquefaction resistance of soils," *Journal of Geotechnical and Geoenvironmental Engineering*, ASCE, 124(10).